MICROCOPY RESOLUTION TEST CHART
NATIONAL BUREAU OF STANDARDS-1963-A

LEVEL II

EFFECTS OF OIL SLICK PROPERTIES ON THE DISPERSION OF FLOATING OIL INTO THE SEA

Jerome H. Milgram
Richard G. Donnelly
Robert J. Van Houten
John M. Camperman

DDC

DEC 29 1978

F

340 p.

Sep 76-Jul 78,

Prepared for

U.S. DEPARTMENT OF TRANSPORTATION

NOTICE

This document is disseminated under the sponsorship of the Department of Transportation in the interest of information exchange. The United States Government assumes no liability for its contents or use thereof.

The contents of this report do not necessarily reflect the official view or policy of the Coast Guard; and they do not constitute a standard, specification, or regulation.

This report, or portions thereof may not be used for advertising or sales promotion purposes. Citation of trade names and manufacturers does not constitute endorsement or approval of such products.

1. Report No. CG-D-64-78	2. Government Accession No.	3. Recipient's Catalog No.
4. Title and Subtitle EFFECTS OF OIL SLICK PROPERTIES ON THE DISPERSION OF FLOATING OIL INTO THE SEA		5. Report Date August 1978
		6. Performing Organization Code
7. Author's) Milgram, Donnelly, Van Houten, Camperman		8. Performing Organization Report No.
9. Performing Organization Name and Address Massachusetts Institute of Technology 77 Massachusetts Avenue Cambridge, MA 02139		10. Work Unit No. (TRAIS)
		11. Contract or Grant No.
12. Sponsoring Agency Name and Address Office of Research and Development United States Coast Guard Washington, DC 20590		13. Type of Report and Period Covered Final Report September 1976 to July 1978
		14. Sponsoring Agency Code USCG

15. Supplementary Notes

16. Abstract

The salient physical effect causing initial dispersion of oil into the sea is breaking waves. Subsequent behavior of the dispersed oil, including droplet trajectories and droplets rejoining the slick are strongly influenced by oceanic turbulence caused by breaking waves and other sources as well. All the aspects of dispersion are related to oil slick properties, the most important being physical and chemical properties of the oil as well as the slick thickness distribution. This report does not give a way of making a quantitative prediction of the extent of dispersion of an oil slick of prescribed properties inasmuch as there is not yet sufficient knowledge to do this. Rather, the report deals with the fundamentals of the dispersing processes and reports the results of a group of laboratory experiments relating to them. These results can ultimately be used in a model for predicting dispersion and also lead to some immediate conclusions. One of them is that the most important slick property influencing dispersion by breaking waves is the oil slick thickness. Thick slicks are much more resistant to dispersion than thin slicks.

17. Key Words oil spills, oil dispersion, pollution studies, ocean turbulence, wave breaking, waves	18. Distribution Statement

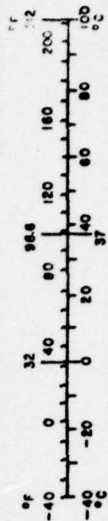| 19. Security Classif. (of this report) Unclassified	20. Security Classif. (of this page) Unclassified	21. No. of Pages 26	22. Price

Form DOT F 1700.7 (8-72)   Reproduction of completed page authorized

METRIC CONVERSION FACTORS

Approximate Conversions to Metric Measures

Symbol	When You Know	Multiply by	To Find	Symbol
		LENGTH		
in	inches	*2.5	centimeters	cm
ft	feet	30	centimeters	cm
yd	yards	0.9	meters	m
mi	miles	1.6	kilometers	km
		AREA		
in²	square inches	6.5	square centimeters	cm²
ft²	square feet	0.09	square meters	m²
yd²	square yards	0.8	square meters	m²
mi²	square miles	2.6	square kilometers	km²
	acres	0.4	hectares	ha
		MASS (weight)		
oz	ounces	28	grams	g
lb	pounds	0.45	kilograms	kg
	short tons (2000 lb)	0.9	tonnes	t
		VOLUME		
tsp	teaspoons	5	milliliters	ml
Tbsp	tablespoons	15	milliliters	ml
fl oz	fluid ounces	30	milliliters	ml
c	cups	0.24	liters	l
pt	pints	0.47	liters	l
qt	quarts	0.95	liters	l
gal	gallons	3.8	liters	l
ft³	cubic feet	0.03	cubic meters	m³
yd³	cubic yards	0.76	cubic meters	m³
		TEMPERATURE (exact)		
°F	Fahrenheit temperature	5/9 (after subtracting 32)	Celsius temperature	°C

*1 in = 2.54 (exactly). For other exact conversions and more detailed tables, see NBS Misc. Publ. 286, Units of Weights and Measures, Price $2.25, SD Catalog No. C13.10:286.

Approximate Conversions from Metric Measures

Symbol	When You Know	Multiply by	To Find	Symbol
		LENGTH		
mm	millimeters	0.04	inches	in
cm	centimeters	0.4	inches	in
m	meters	3.3	feet	ft
m	meters	1.1	yards	yd
km	kilometers	0.6	miles	mi
		AREA		
cm²	square centimeters	0.16	square inches	in²
m²	square meters	1.2	square yards	yd²
km²	square kilometers	0.4	square miles	mi²
ha	hectares (10,000 m²)	2.5	acres	
		MASS (weight)		
g	grams	0.035	ounces	oz
kg	kilograms	2.2	pounds	lb
t	tonnes (1000 kg)	1.1	short tons	
		VOLUME		
ml	milliliters	0.03	fluid ounces	fl oz
l	liters	2.1	pints	pt
l	liters	1.06	quarts	qt
l	liters	0.26	gallons	gal
m³	cubic meters	35	cubic feet	ft³
m³	cubic meters	1.3	cubic yards	yd³
		TEMPERATURE (exact)		
°C	Celsius temperature	9/5 (then add 32)	Fahrenheit temperature	°F

Temperature scale:
°F -40   0   32   80   98.6   120   160   200   212
°C -40 -20   0   20   37   40   60   80   100

TABLE OF CONTENTS

LIST OF TABLES

NOTATION

C_D - drag coefficient

C_g - group velocity

C_p - phase velocity

D   - coefficient of eddy diffusivity

d   - particle or droplet parameter

$E(k)$ - energy spectrum of turbulence

$F(k)$ - wave-number spectrum of ocean waves

$F(\omega)$ - frequency spectrum of ocean waves

g   - acceleration due to gravity

$H(\omega)$ - transfer function of a filter

h   - oil layer thickness

k   - wavenumber

L   - Eulerian integral length of turbulence (isotropy assumed)

L_z - vertical Eulerian integral length of turbulence

m   - mass; or as subscript referring to mixture properties

p   - probability density function

R   - Reynolds number

$R(r)$ - Eulerian spatial velocity correlation of turbulence

$R_e(\theta)$ - Eulerian temporal velocity correlation of turbulence

$R_L(\theta)$ - Lagrangian temporal velocity correlation of turbulence

$R_p(\theta)$ - particle-based velocity correlation of turbulence

r   - spatial difference variable

$S_{o/w}$ - spreading pressure of oil on water

$S(k)$ - Eulerian wavenumber spectrum of turbulence

$S_e(\omega)$ - Eulerian frequency spectrum of turbulence

$S_p(\omega)$ — particle-based spectrum of turbulence

T — surface or interfacial tension

T_e — Eulerian integral time of turbulence

T_L — Lagrangian integral time of turbulence

T_{oa} — oil-air surface tension; "a" subscript sometimes deleted

T_{ow} — oil-water interfacial tension

T_p — particle-based integral time of turbulence

T_{wa} — water-air surface tension; "a" subscript sometimes deleted

t — time variable

U — free-stream velocity

u — RMS velocity of isotropic turbulence

u_f — turbulent velocity in direction of interest

$\overline{u_f}$ — vectoral turbulent velocity

u_R — relative velocity between particle and fluid

u_x — turbulent velocity in x-direction

u_z — turbulent velocity in z-direction

v — voltage

W — terminal velocity of particle in calm fluid

We — Weber number

x,z — horizontal and vertical Cartesian coordinates

x_i — mole fraction of i in liquid phase

δ — "delta" or "impulse" function

Δ — density difference ratio

ε — specific energy dissipation rate

η — Kolmogorov microscale of turbulence

θ — time difference variable

λ_e - Eulerian spatial Taylor microscale of turbulence

λ_p - particle-based Taylor temporal microscale of turbulence

μ - viscosity

ν - kinematic viscosity

ρ_f - density of fluid

ρ_o - density of oil

ρ_p - particle density

ϕ - volume fraction

σ - standard deviation, or concentration in a dispersion

τ - dummy time variable

$\tau*$ - most probable coalescence time

ω - radian frequency

1.0 INTRODUCTION

It is known that in calm weather most spilled oil floats on the surface of the sea. In rough weather much of the oil can be dispersed into submerged droplets. The degree to which the oil is dispersed by natural effects has been observed to depend on the properties of the oil slicks. Some slicks are readily dispersed, whereas others are resistant to dispersion.

The principle purpose of the work described here was to determine how oil slick properties affect the dispersion of the oil into the water. We hasten to point out that a consideration of the beneficial and detrimental effects of dispersing oil is not part of the work. Although the results of our work may be useful to those making such a consideration, our direct efforts have been aimed at evaluating how slick properties affect dispersion.

The work we have done has centered on a group of laboratory experiments. Detailed experiments related to determining how oil slick properties affect dispersion have not been done in significant amounts in the past. However, a great deal of related work has been done so that in order to plan our work properly this related work was studied. In addition, to plan and carry out our experimental program effectively it was necessary to do a considerable amount of theoretical analysis. This analysis was generally aimed at determining the most important dispersing mechanisms at sea and at gaining an understanding of how our experimental results, obtained from a small size laboratory apparatus, could be related to results at sea, where typical lengths and speeds are much greater than in our experiments.

We found, both by our initial theoretical considerations and by preliminary experiments, that the predominant effect causing initial dispersion of oil into the form of submerged droplets is that of breaking waves. In the absence of breaking waves at sea the very small amount of dispersion of oil that occurs is expected to be insignificant as far as cleanup operations are concerned. Some explanation of this insignificance is appropriate here. When oil is spilled, even under most ideal circumstances, not all of the oil is collected and recovered because of

small leakage past containment devices and the fact that rapid oil spreading frequently makes complete containment impossible. Thus, in general, some oil from a spill remains in the sea or pollutes shorelines. Effective containment and cleanup, however, can reduce the amount of this oil to a small fraction of the amount that was spilled. However, since some oil will inevitably remain, effects which disperse an amount of oil that is small in comparison to what could not be cleaned up even without dispersion can be considered insignificant insofar as they affect the salient results of cleanup efforts. These effects may not be insignificant as regards polluting vulnerable coastal areas or biota. On the other hand, the large amounts of oil that can be dispersed by breaking waves can have a major influence on spill cleanup efforts and their results.

Since consideration of containment and cleanup must focus on most, but necessarily not all, of the oil, the effects of breaking waves must be considered paramount in the initial natural dispersion of oil into small droplets. Once the oil is dispersed into droplets, the subsequent motion of these droplets is largely influenced by the turbulent flow in the water. This turbulence can be generated by winds, currents, and also by breaking waves. All droplets of oil which are less dense than water tend to rise. The large droplets rise relatively rapidly and the small droplets rise relatively slowly. In completely calm water, the rise time for a droplet of any specific size starting out at any specific depth could be easily calculated. However, in the presence of turbulence some droplets rise more quickly than they would in calm water and some droplets rise more slowly. The condition that occurs depends on the turbulent velocities experienced by the droplet during its rise. Thus, the time that some of the oil droplets remain submerged can be increased by the presence of turbulence. When a dispersed oil droplet does rise to the surface it generally encounters the floating oil slick, and if it remains against the slick it will eventually recoalesce with the slick. Its oil could then be dispersed again only by another breaking wave. However, during the time that the droplet is against the slick, but before recoalescence has occurred, turbulent motion in the water can easily

-2-

resubmerge the droplet. Hence the recoalescence time of oil droplets with slicks is of importance.

As a result of our literature survey, theoretical studies, and preliminary experiments, our main test program was oriented toward a study of the effect of oil slick properties on the dispersion of oil by breaking waves, the fundamentals of the effect of turbulence on small rising droplets, and the recoalescence of oil droplets with slicks. These subjects were studied experimentally by a number of individual sets of experiments. In the case of the effect of turbulence on droplet rise, it seemed most important to us to determine whether or not the direct application of the statistical theory of turbulence to small rising droplets gave correct answers when the instantaneous vertical velocity of the droplet was taken as the sum of the calm water rise velocity and the vertical component of the turbulent velocity. We carried out this experiment by measuring the statistics of the rise times of small, slightly buoyant plastic spheres and comparing these statistics with predictions based on an analysis of the statistical theory of turbulence using the measured turbulence velocities from our experiments as an "input". We confirmed that the predicted results were indeed correct. This means that theories for the rise of oil droplets in a turbulent field can be based on the assumption that the vertical velocity of a droplet is its terminal rise velocity plus the vertical component of the turbulence velocity with statistical theory then applied.

Three sets of experiments related to the effects of breaking waves were carried out. One set used no oil and was done for the purpose of determining the intensities of the turbulence beneath a breaking wave. In another set, breaking waves were generated in a wave channel, and these breaking waves dispersed floating oil. The amount of oil at various depths and at various times following the passage of a breaking wave was measured. These experiments were carried out with a variety of oils having a variety of physical properties and with two different oil slick thicknesses in order to determine the effect of slick thickness on the dispersion of oil by breaking waves. This was a particularly important part of our experimental program and in order to make its results most

-3-

useful for predicting effects at sea, we carried out a theoretical analysis concerned with how the results should be "scaled" for conditions at sea. An interesting result of this part of our experimental program was that the most important oil slick property for relating the amount of oil dispersed into the water after the passage of a breaking wave was the oil slick thickness. Generally, more oil is dispersed from a thin slick than a thick one. This shows that if oil is spilled and one wants ultimately to collect it, it is important to contain the oil and keep it in a thick pool as quickly as possible to minimize the amount of oil that is dispersed.

For our experiments on the dispersion of oil by breaking waves, a wave was generated at one end of the wave channel and the height of this wave was increased by means of a contraction in the channel width. When the wave became large enough breaking began. Although the same size wave was generated for all experiments, the actual size of the breaking wave varied slightly from slick to slick because of the effects that the different oil types and thicknesses had on the wave growth and wave breaking phenomena. Since the actual breaking waves did have differences from case to case, we carried out another set of experiments in which all the different oil slicks encountered identical dispersing influences at the local level. In these experiments, the dispersing influence was a thin falling "sheet" of water impacting on the upper surface of a floating oil slick. This falling water dispersed oil into a tank of water beneath the slick. With this dispersing influence, the rate of dispersion of oil into the water for each oil type and thickness was measured.

The effect of oil properties on recoalescence rates was measured by measuring the recoalescence time for a droplet against the slick with a variety of oil types and droplet sizes. Since the oil properties were found to be dependent on the aging of oils, especially with crude oils, we also carried out a group of experiments in which the changes in oil properties that occurred as the oils aged were measured.

The next section of this report, §2, presents the results of our literature survey and the following section, §3, presents that part of our theoretical analysis related to the turbulence caused by waves and

how this affects scaling laws relating laboratory work to oceanic conditions. The subsequent seven sections describe the details of our experimental studies along with the theoretical considerations appropriate to each one. The concluding summary, §11, is written in a way that permits readers who are only interested in an overview of the results and their meanings to proceed from this point directly to the concluding summary.

2.0 A SURVEY OF LITERATURE CONCERNING THE DISPERSION OF OIL IN THE OCEAN

The dispersion of spilled oil in the ocean is a complex phenomenon. In order to understand it, one must consider the relevant physical aspects of the ocean environment, such as the existence of ocean waves and turbulence. In this way one may hope to predict the strength of the dispersing forces under varying sea conditions. Furthermore, since many different types of oil are spilled at sea, it is imperative to consider the chemical phenomena involved, so that the chemical properties of a particular oil can be related to its tendency to disperse when subjected to the physical environment. This is particularly true in light of the fact that the properties of a given oil will change once it is subjected to weathering. What follows is a review of literature concerning both the physical and chemical aspects of the oil dispersion problem.

2.1 Physical Phenomena
Direct Empirical Evidence

Although many investigators have mentioned that the existence of waves, particularly breaking waves, worsens the entrainment problems encountered in containing oil spills, there is little documentation of the entrainment and vertical dispersion of uncontained oil due to waves. MacIntyre (1974)[*] reported that the presence of whitecaps limited the growth of an oil slick, due to the "dissipation" of the slick near its edges. We have also observed this effect at sea. As a whitecap enters a "patch" of oil, dispersion of the oil takes place. However, the wave then usually stops breaking so less oil is dispersed from the interior of the patch than from the "upwind edge". Forrester (1971) investigated the existence of small oil droplets in the water column following the grounding of the tanker ARROW. He found drops ranging in size from 5 micrometers to 1 millimeter, and found that the total volume of entrained oil was evenly distributed with respect to drop diameter. As expected, the largest drops were generally found higher in the water column than were the

---

[*] MacIntyre, W.G., C.L. Smith, J.C. Munday, V.M. Gibson, J.L. Lake, J.G. Windsor, J.L. Dupuy, W. Harrison, and J.D. Oberholtzer (1974).

smaller drops. The source of these oil droplets was postulated to be surface slicks in the presence of waves and the surf zone of oil coated beaches. Forrester postulated a steady state model which related the distribution of oil sizes to the turbulent energy spectrum. An analysis of this model is made subsequently in this section.

The areas of research which have a bearing on the physical aspects of the problem of predicting the extent of entrainment of an oil slick lie in three general areas: (1) wave breaking, (2) ocean turbulence, and (3) the behavior of dispersed droplets in a turbulent field. A review of these areas of research follows.

Wave Breaking

Efforts to estimate the extent of wave breaking can be divided into two areas: (1) those which formulate an energy balance for the wave field and infer therefrom the extent of wave breaking, and (2) those which predict from probabilistic models of the sea surface the probability that any given wave will break. Each of these areas of research is reviewed below.

Extent of Wave Breaking - Energy Balance

Phillips (1969) summarizes and integrates the various wave generation mechanisms and postulates that the nonlinear transfer of energy from one wave component to another, as studied by Hasselmann (1962, 1963), is weak compared with the energy input into each component by the wind. Consequently, in the saturated portion of the spectrum, the energy lost in wave breaking could be calculated from the energy input from the atmosphere into these wave components.

Phillips (1963), Longuet-Higgins (1969b) and Hasselmann (1971) all have looked at nonconservative wave interaction, specifically the case where small waves break on waves with wave lengths much larger than those of the breaking waves themselves. Although the first two investigators discovered a mechanism for significant energy exchange between the two wavenumber components, Hasselmann noted the existence of an opposing effect which exactly cancelled this energy transfer to

-7-

first order, leaving a net energy transfer of very small magnitude. No studies have been made of energy exchange during breaking of two wave components of the same order of magnitude.

The JONSWAP study (Hasselmann, 1973[*]) resulted in the development of a general five parameter ocean wave spectrum which essentially added a peak enhancement factor to the Pierson-Moskowitz spectrum (1964). Mean values were given for those parameters defining the peak enhancement factor, and the two scale parameters (peak frequency, ω_m, and Phillips' constant, α) were given as power law functions of nondimensional fetch $X = gx/U^2$, where x is the actual fetch, g is the gravitational acceleration, and U is the wind speed 10 meters above the ocean surface. It was shown that conservative nonlinear interactions, which can be computed directly from a given spectrum, were quite important near the spectral peak, and were largely responsible for the growth of wave components of frequencies smaller than the peak frequency. The JONSWAP study did not establish the relative magnitude of nonlinear momentum transfer compared with momentum flux from the atmosphere and momentum lost in breaking for the higher frequency region due to lack of knowledge about these latter processes - specifically, the amount of overlap of these processes in wavenumber space. The nonlinear source term is three-lobed, being negative in the center of the spectrum, and positive at each end. The momentum transferred to the low frequency lobe and responsible for low frequency wave growth is relatively small and is advected away by these fast moving waves. The momentum input from the atmosphere must be at least as large as the momentum which passes out of the central region, and similarly the momentum lost in dissipation must be at least as large as the amount of momentum which is transferred to the higher wave numbers, since the amount of energy at the high frequency end of the spectrum does not increase with fetch. These values for momentum input and dissipation are lower bounds, however. The upper bound is the drag force on the water surface by the wind, which can be determined from boundary-layer measurements in the atmosphere. The difference

---

* Hasselmann, K., T.P. Barnett, E. Bouws, H. Carlson, D.E. Cartwright, K. Enke, J.A. Ewing, H. Gienapp, D.E. Hasselmann, P. Kruseman, A. Meerburg, P. Müller, D.J. Olbers, K. Richter, W. Sell, and H. Walden (1973).

and this drag force presumably is accounted for by direct viscous
shear and such small scale processes as capillary wave growth. On the
basis of wave generation theories, Phillips estimated that the
momentum flux to waves whose phase velocities are greater than five
times the friction velocity of the air is at most 10% of the total
momentum flux. The JONSWAP study, however, determined that at small
values of fetch ($X = 10^2$) the lower bound for momentum lost by the wave
field was 90% of the upper bound, showing that the minimum dissipation
model, where there is very little overlap in wavenumber space between
the energy input region and the dissipation region, is very nearly
correct at this value of fetch. At $X = 10^3$, however, this figure was
down to 20%, and it was further reduced to 5-10% at $X = 10^4$.

In a later report (1974), Hasselmann surmised that the atmospheric
input source function has the form $S_{in} = \beta F(k)$, where β is a function
of the wavenumber, k, and U, and F is the energy density spectrum.
This relationship would correspond to a linear energy feedback
mechanism. If this form is correct, and if the high frequency end of
the spectrum were invariant with fetch, then increasing the fetch could
not reduce the amount of energy or momentum entering the wave field
since it has been found that $F(k)$ increases with fetch for low
frequencies. Since the total drag coefficient is roughly constant
with fetch, and almost all the air-water momentum transfer enters the
gravity wave field at small fetches, then this would also be true at
larger fetches. Actually, the Phillips constant, α, which is propor-
tional to the wave energy of the high frequency end of the spectrum,
has been observed to decrease with fetch somewhat. Hasselmann
attributed this to the fact that some of the total momentum transfer
must directly enter the center frequency wave components under the
central lobe of the nonlinear source function. He judged it unlikely
that the reduction in α is sufficient to allow for significant air-
water momentum transfer other than through the gravity wave field.

Also in his 1974 report, Hasselmann showed that since wave
breaking is weak in the mean, it is quasi-linear, and can be represented
by a damping factor γ:

$$\frac{\partial F_k}{\partial t} = -\gamma F_k \tag{2-1}$$

where F is the energy at the discrete wave number k. Furthermore, if
the space and time scales of the whitecaps are small compared to the
length and period of the waves, the damping factor is quadratic in
frequency: $\gamma = \eta\omega^2$, where η is a function of the wave propagation
direction and the overall properties of the wave field. By assuming
an input source function which satisfies the condition that all the
momentum transferred to the water enters the wave field, Hasselmann
obtained the following approximate value for η:

$$\eta = \omega_m^{-1}\{2.2 \times 10^{-4}(1 - .3g/\omega_m U) + 2\alpha^2\lambda\} \tag{2-2}$$

where ω_m is the peak frequency of the spectrum, and λ is a non-
dimensional shape factor, equal to 0.12 for the Pierson-Moskowitz
spectrum, and 0.16 for the mean JONSWAP spectrum.

Extent of Wave Breaking - Kinematic Approach

Another approach to the problem of estimating the amount of energy
dissipated by wave breaking has been taken by Longuet-Higgins (1969a)
Nath and Ramsey (1976), and Houmb and Overvik (1976). Longuet-Higgins
hypothesized that a useful criterion for wave breaking was that the
acceleration of fluid particles equals one-half the acceleration due
to gravity, as in the case of a progressive Stokes wave of maximum
amplitude. He furthermore assumed that in the case of irregular waves,
described by the spectral density $F(\omega)$, the acceleration of water
particles could be taken to be $\overline{\omega}^2 a$ where

$$\overline{\omega}^2 \int_0^\infty F(\omega)d\omega = \int_0^\infty \omega^2 F(\omega)d\omega \tag{2-3}$$

and a is the amplitude of the wave. Assuming that the spectrum is
narrow, and therefore that the probability density of wave amplitude can
be described by a Rayleigh distribution, he could calculate the proba-
bility that any given wave would break:

$$P_b = \exp\left(-\frac{a_o^2}{a^2}\right) \qquad (2\text{-}4)$$

where $a_o = g/2\overline{\omega}^2$ and $\overline{a}^2$ is the mean square surface elevation. By assuming that the wave energy lost is equal to the difference between actual wave energy and that of the largest nonbreaking wave, he could calculate the mean loss of energy per wave cycle:

$$E_\ell = E \exp(-E_o/E) \qquad (2\text{-}5)$$

where $E = \rho g \overline{a}^2$ and $E_o = \rho g a_o^2$. Performing the necessary calculations for an assumed equilibrium spectrum,

$$F(\omega) = \begin{cases} \alpha g^2 \overline{\omega}^5, & \omega > \omega_1 \\ \\ 0, & \omega < \omega_1 \end{cases} \qquad (2\text{-}6)$$

Longuet-Higgins obtained an estimate for the proportion of energy lost per cycle:

$$E_\ell/E = \exp^{-1/8\alpha} \qquad (2\text{-}7)$$

Making an independent estimate for energy supplied by the wind to a fully developed sea, he then calculated the value of α necessary to yield agreement between the calculations. He found this value to be a constant with respect to wind speed, and to be close to experimentally obtained values of α. Furthermore, he argued that as fetch is decreased, E_ℓ/E will increase, as will α. This trend is supported by experimental evidence.

Banner and Phillips (1974) determined the effect of wind drift on the limiting wave height. They gave the following expression for maximum wave elevation:

$$\zeta_{max} = \frac{c_p^2}{2g} \left(1 - \frac{q}{c_p}\right)^2 \qquad (2\text{-}8)$$

-11-

where q is the wind drift velocity where the wave profile intersects
the mean water level, and c_p is the phase speed of the wave. They found
that in the presence of wind drift incipient breaking was characterized
by the existence of a stagnation point near the wave crest but not a
discontinuity in wave slope.

In 1976, Nath and Ramsey made a calculation similar to that of
Longuet-Higgins but with a slightly different criterion for wave
breaking. They assumed that a wave would break when $H = H_o = \nu T^2$,
where ν is a dimensional constant, H is waveheight, and T is the period
between zero upcrossings. ν was chosen equal to its value for a
progressive wave (from Dean, 1965): $\nu = 0.267$ m/sec^2 $= 0.875$ ft/sec^2.
Longuet-Higgins' criterion, in comparison, gives:

$$\overline{\omega}^2 a_o = \frac{g}{2} \tag{2-9}$$

$$\left(\frac{2\pi}{T}\right)^2 \frac{H_o}{2} = \frac{g}{2} \tag{2-10}$$

$$H_o = \frac{g}{(2\pi)^2} \overline{T}^2 \tag{2-11}$$

$$H_o = \nu' \overline{T}^2 \tag{2-12}$$

where $\nu' = 0.817$ ft/sec^2. More important than the difference in the
value of the constant is the fact that where Longuet-Higgins used a
mean period defined by

$$\overline{T} = 2\pi \sqrt{\int F(\omega)\, d\omega / \int \omega^2 F(\omega)\, d\omega} \tag{2-13}$$

Nath and Ramsey proposed that the period for the individual wave be
used. Presumably this criterion is better than that of Longuet-Higgins.
However, this added complication requires that the joint probability
density be known for wave height and period. In 1975, Longuet-Higgins
gave that density as:

$$p(\xi, \eta) = \frac{\xi^2}{(2\pi)^{\frac{1}{2}}} \exp\left[-\xi^2(1 + \eta^2)/2\right] \tag{2-14}$$

-12-

where $\xi = a/\mu_o^{\frac{1}{2}}$, $\mu_o \equiv \bar{a}^2$ is the mean square wave amplitude, and
$\eta = (t - <t>)/w<t>$, where $<t>$ is the mean wave period and w is propor-
tional to the width of the energy spectrum: $w = (\mu_2/\mu_o)^{\frac{1}{2}} \cdot (<t>/2\pi)$.
The calculation of the probability of breaking and the mean energy
loss according to the Nath and Ramsey criterion would require numerical
integrations. To avoid this, Nath and Ramsey assumed that the wave
amplitude and period squared were independent random variables, both
with Rayleigh distributions. They found the probability of a wave's
breaking in one period to be:

$$P_b = k^2/(k^2 + 1) \qquad (2-15)$$

where $k = \bar{a}/\nu\tau^2$ is the so-called steepness parameter, τ^2 is the RMS
squared period, and $\bar{a}$ is the RMS wave height. Using their assumed
probability density for period, Nath and Ramsey showed that
$\bar{T} = \tau\Gamma(5/4)$, where Γ represents the gamma function. The above
expression for P_b can therefore be compared with that obtained by
Longuet-Higgins, which can be posed as:

$$P_b = e^{-(1/k')^2} \qquad (2-16)$$

where $k' = 2\bar{a}/\nu'\bar{T}^2 \sim 1.30k$.

The Pierson-Moskowitz spectrum for a fully developed sea gives
0.29 as the value of k' for all wind speeds. For this value of k',
Longuet-Higgins' model gives $P_b = 7 \times 10^{-6}$, whereas Nath and Ramsey's
gives $P_b = 0.046$. The reason for this large discrepancy lies in the
fact that in integrating over all periods, the weighting factor used
is the probability that the wave breaks given that the period is
known,

$$P_b = \int_0^\infty e^{-(\nu t^2/\bar{a})^2} d[p(t)] \qquad (2-17)$$

where p(t) is the probability density function for period. This
weighting function dies off very rapidly at large periods, so the

effective period is much less than τ or $\overline{T}$ and the resulting P_b is much greater than would be obtained by using either of these other two measures of average period.

Houmb and Overvik (1976) used Longuet-Higgins' joint density for wave height and period to calculate the percentage of waves that break. Figure 2-1 shows their results for a typical spectral width, in addition to the corresponding results of Nath and Ramsey and Longuet-Higgins. That figure demonstrates that Nath and Ramsey's results follow a realistic trend with sea state but underestimate the extent of breaking significantly. For the abovementioned value of steepness parameter, $k' = 0.29$, Houmb and Overvik calculated the breaking probability to be between 9% and 10%, rather than the 5% predicted by Nath and Ramsey. Houmb and Overvik also calculated the short and long term distributions of the heights of breaking waves.

It should be pointed out that even the work of Houmb and Overvik is subject to severe theoretical limitations. The large-height region of the Rayleigh distribution of wave height and the joint density for wave height and period developed by Longuet-Higgins are realistic only in the absence of wave breaking. The probability of wave breaking calculated by all of the authors mentioned above is the percentage of waves at a given time which, given that they follow these distributions, would be higher than the various breaking criteria allow. In other words, if the wave breaking mechanism could be turned on at a given time, P_b is the number of waves which would break over the next wave period. This model ignores the effect of previous wave breaking on the underlying distribution of wave height, which, although possibly small for small breaking probabilities (small steepness parameter), is bound to be significant for large breaking probabilities. The wave breaking process constantly reduces all wave heights to the maximum allowable height, H_o, so that one would expect there to exist a relatively large number of waves of height H_o, and none higher. This condition would result in more breaking events, each of less intensity than predicted by the theories presented here.

It is interesting to note that the models proposed by Longuet-

-14-
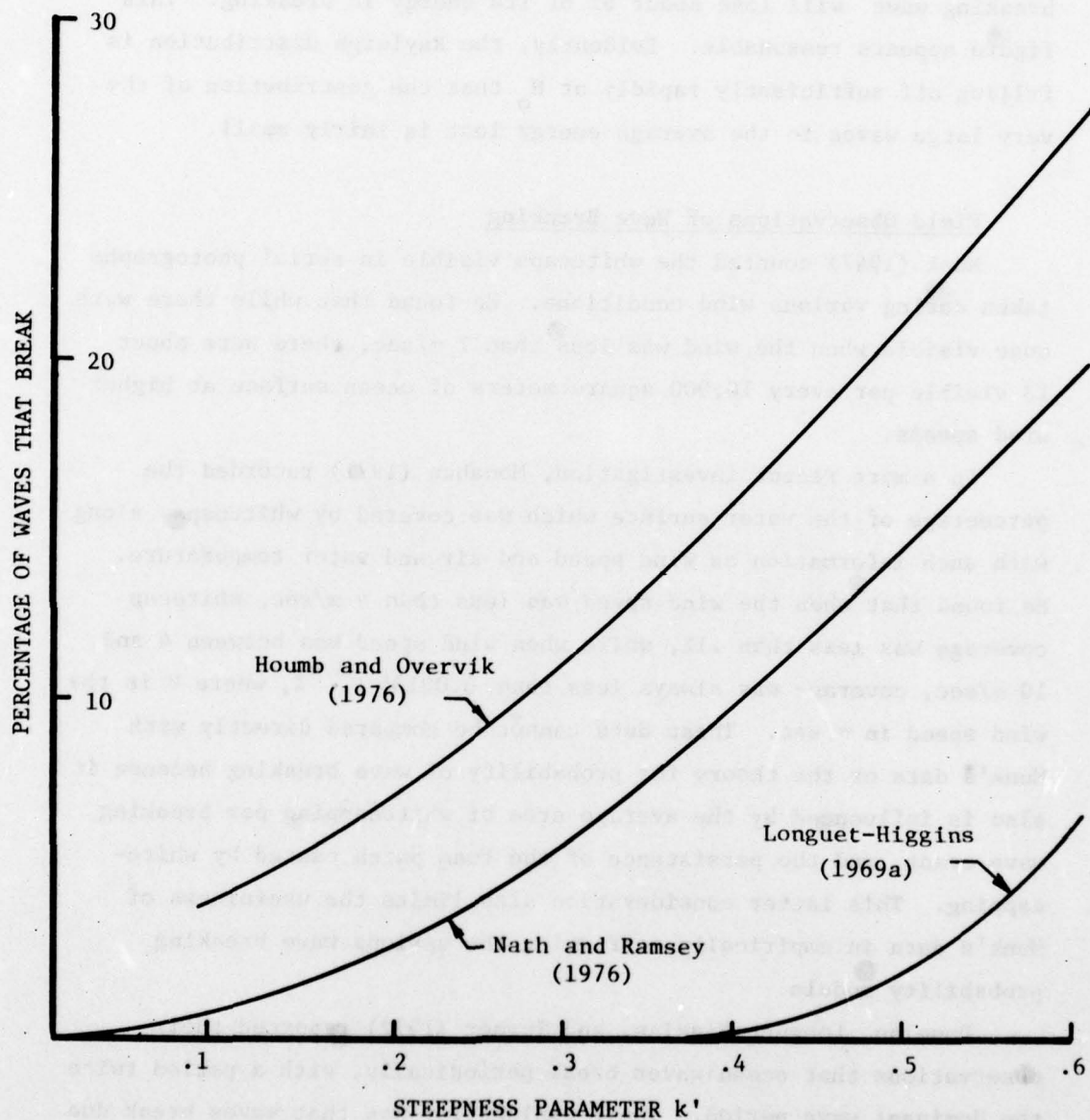
FIGURE 2-1   A Comparison of Theories for Predicting the Percentage of Waves that Break

Higgins and Nath and Ramsey predict that the average amount of energy lost per wave breaking event is equal to the average wave energy per wavelength. Thus, for a steepness parameter of 0.29, the average breaking wave will lose about 8% of its energy in breaking. This figure appears reasonable. Evidently, the Rayleigh distribution is falling off sufficiently rapidly at H_o that the contribution of the very large waves to the average energy lost is fairly small.

Field Observations of Wave Breaking

Munk (1947) counted the whitecaps visible in aerial photographs taken during various wind conditions. He found that while there were none visible when the wind was less than 7 m/sec, there were about 13 visible per every 10,000 square meters of ocean surface at higher wind speeds.

In a more recent investigation, Monahan (1971) recorded the percentage of the water surface which was covered by whitecaps, along with such information as wind speed and air and water temperature. He found that when the wind speed was less than 4 m/sec, whitecap coverage was less than .1%, while when wind speed was between 4 and 10 m/sec, coverage was always less than $0.00135 \ U^{3.4}$%, where U is the wind speed in m/sec. These data cannot be compared directly with Munk's data or the theory for probability of wave breaking because it also is influenced by the average area of whitecapping per breaking wave event, and the persistence of the foam patch caused by white-capping. This latter consideration also limits the usefulness of Munk's data in empirically confirming the various wave breaking probability models.

Donelan, Longuet-Higgins, and Turner (1972) reported their observations that ocean waves break periodically, with a period twice the dominant wave period. Their explanation was that waves break due to their propagation into a region, or wave group, with a high energy density. Since the wave group moves with a velocity equal to half the phase velocity of the dominant waves, the time interval between breaking events is twice the significant wave period.

-16-

Experimental Observations of Wave Breaking

Most experimental investigations of wave breaking phenomena have been concerned with that form of breaking which occurs in shoaling waters. Shoaling breakers are often of the plunging type, and are quite different from the spilling breakers found at sea. Only in recent years have experimentalists turned their attention to spilling breakers.

Banner and Phillips (1974) studied experimentally a breaking wave on a moving stream and reported the existence of a turbulent wake behind the breaker. Although they reported that this wake is only as deep as the breaker itself, their time of observation was limited by the length of their flume.

Longuet-Higgins (1974) reported on some experiments performed in the wake of a towed body, in which turbulence intensity and Reynold's stress were measured in the neighborhood of a breaking wave. He found that the x-momentum flux was downward above the level of the wave trough, and upward below the wave trough. The largest turbulent velocities were on the order of 10% of the phase speed.

Van Dorn and Pazan (1975) conducted a comprehensive experimental program to investigate the breaking of waves in deep water. Regular progressive deep water waves were generated by a wavemaker at one end of a wave channel. One side of the channel converged linearly, so that the tank lost one foot of width for every ten feet of length. Each wave generated by the wavemaker would gain energy due to the convergence until it eventually broke. The growth rate was smallest near the wavemaker and largest where the channel was at its narrowest, since the amount of energy added was a constant whereas the crest length of the wave to which it was added decreased with longitudinal position in the channel. The relative growth rate $(\lambda(\partial w/\partial x)/w$, where λ is the wavelength, w is the width, and x is the dimension along the length of the tank) ranged from 0.165 to 0.75. By varying the initial wave amplitude, the position along the channel at which the wave broke, and therefore its pre-breaking growth rate, could be adjusted. It was found that breaking intensity and wave steepness during breaking were

-17-

larger for waves which underwent a larger growth rate prior to breaking. After breaking, the energy loss rates were roughly in equilibrium with the energy input by the convergence. An attempt was made to apply these results to wave breaking at sea, where the growth rate is determined by the narrow bandedness of the spectrum. Van Dorn and Pazan also measured fluid velocities, surface elevations, and phase velocities for growing waves.

The Structure of a Breaking Wave

Longuet-Higgins (1973) and Longuet-Higgins and Turner (1974) modeled a spilling breaker as a turbulent gravity current which rides down the front of a breaking wave, entraining air from above and water from below. The entrainment of air causes the density of the gravity current to be less than that of the water beneath, providing the current with buoyancy, and thereby limiting the entrainment of water from below. This latter process contributes to a tangential Reynolds stress at the interface between the gravity current and the irrotational fluid beneath it. Longuet-Higgins and Turner obtained a similarity solution wherein the height of the current (away from the leading edge) increases linearly with distance from the crest.

Turbulence in the Ocean

Turbulence in the ocean is due to various causes. Shear flows of large Reynolds number such as those due to strong tidal currents will obviously be turbulent. Grant, Stewart, and Moillet (1962) measured the turbulence in a tidal flow of Reynolds number over 10^8 and found that there exists an inertial subrange over several decades of wave number, wherein the energy spectrum can be represented as

$$E(k) = K\varepsilon^{2/3}k^{-5/3} \tag{2-18}$$

where ε is the specific energy dissipation rate, and K is a constant. They found the value of K to be 1.44 over a range of dissipation rates between 0.0015 and 1.02 cm^2/sec^3. They further determined the behavior

-18-

of E(k) at wave numbers larger than those of the inertial subrange.

In most areas of the ocean, the strongest turbulence occurs due to the breaking of waves on the surface. The Reynolds number of these waves is much less than that of the tidal flow investigated by Grant, et.al. In 1962, Stewart and Grant published the results of their field investigation of turbulence under breaking waves. They fit the function $E(k;\varepsilon)$, which was previously determined from tidal flow measurements, to measured velocity fluctuations near the free surface under breaking waves. They found that an inertial subrange could be identified, although it was considerably smaller than that found at higher Reynolds numbers. At a distance of 1.5 meters below waves with wavelengths of 5 meters and heights of .4 meters and a wind speed of 6 meters per second, the inertial subrange existed over the decade of wave numbers from 10^{-1} cm^{-1} to 10^{0} cm^{-1}, or scales of 6 to 60 cm. The computed value of ε for this depth was 0.023 cm^2/sec^3. The Kolmogorov hypothesis states that if an equilibrium exists, the viscous length scale η is given by $\eta = (\nu^3/\varepsilon)^{1/4}$, where ν is the kinematic viscosity. For the case of breaking waves mentioned above, η equals .08 cm. Therefore, the wave number corresponding to the viscous (or "Kolmogorov") length scale, k_o, is about 80 cm^{-1}. Assuming that the turbulence level in the area of the ARROW's grounding is not too dissimilar to that found by Stewart and Grant, it appears that the largest of the droplets detected by Forrester (1971) are the same size as the viscous length scale.

An empirical relation which states that the decay time of the energy is the period of the large scale eddies is (Batchelor, 1953) $\varepsilon \sim U^3/L$, where L is the size and U the velocity of the largest size eddies. Assuming that L can be approximated by the significant wave height, one can compute the velocity of these eddies to be approximately 1 cm/sec. Thus, the large scale turbulent velocities are quite small compared to the phase speed, C_p, of the predominant waves, which is about 300 cm/sec, and also small compared with the velocity achieved after falling a distance equal to the wave height, which is $\sqrt{2gh}$, or 300 cm/sec. Unfortunately, Stewart and Grant did not publish the significant wavelengths

-19-

corresponding to the rest of their data, so the universality of this result cannot be tested.

The above data were recorded at a distance below the free surface of almost 4 wave heights. Indeed, the closest that Stewart and Grant approached the surface in obtaining any of their published data was 2 wave heights. It's quite possible that the turbulence intensity is significantly higher above this level, and Stewart and Grant concluded that this was in fact the case. However, the basis for their conclusion was the assumption that the total energy input equaled $\tau_w \cdot C_p$, where τ_w is the total wind stress. As explained earlier, this is an upper bound on the energy associated with breaking waves, and the correct result may in fact be smaller by an order of magnitude. If the turbulence is significantly more intense above the depth where Stewart and Grant took their measurements, the values of η and U derived above may be too large and too small, respectively.

Belyaev, et.al. (1975) reported field values of ε obtained in the Atlantic Ocean at depths of 36 to 140 meters. Values obtained by the method of Stewart and Grant ranged from 0.037 to 0.39 cm^2/sec^{-3}, although other methods of calculation yielded somewhat smaller values.

Other sources of turbulence near the free surface of the open seas are the wind stress and nonbreaking waves. The latter source was considered by Phillips (1961), who, by equating the vorticity generation due to the stretching of vortex lines to the dissipation of vorticity by viscosity determined that

$$\overline{\Omega^2}^{1/2} \sim a^2 k^2 \omega \exp(kz) \qquad (2\text{-}19)$$

where Ω is turbulent vorticity, k is the wave number of the waves, ω is their frequency, and a is their amplitude. Since $\varepsilon = -\nu\overline{\Omega^2}$, this is equivalent to

$$\varepsilon \sim -\nu(ak)^4 \omega^2 \exp(2kz) \qquad (2\text{-}20)$$

For the wave field discussed above, this value of ε is at most

-20-

4×10^{-4} cm^2/sec^3 – about one percent of the value measured by Stewart and Grant. It can therefore be assumed that the dominant sources of near surface turbulence are breaking waves and (possibly) wind stress.

Oil Droplets in a Turbulent Field

Splitting

Both Kolmogorov (1949) and Hinze (1955) considered the problem of the breakup of neutrally buoyant droplets in a homogeneous, isotropic turbulent field. For droplets of a viscous liquid which are large compared to the viscous length scale of the turbulence, the relevant parameters determining maximum stable drop size are the Weber and Reynolds numbers:

$$We = \frac{T}{v_d^2 d \rho_w} \qquad (2\text{-}21)$$

$$R = \frac{v_d d}{\nu_o} \qquad (2\text{-}22)$$

where T is the interfacial surface tension, d is the diameter of the drop, v_d is the RMS velocity difference over distance d, ρ_w is the density of water, and ν_o is the kinematic viscosity of the oil. In the limit of large Reynolds number, the Weber number alone determines this size:

$$We_{crit} = \frac{T}{v_d^2 d_{max} \rho_w} = const. \qquad (2\text{-}23)$$

Since $v_d^2 \sim (\epsilon d)^{2/3}$ in the inertial subrange,

$$d_{max} \sim \left(\frac{T}{\rho_w}\right)^{3/5} \epsilon^{-2/5} \quad \text{for } d_{max} \gg \eta \qquad (2\text{-}24)$$

For not so large Reynolds numbers (or smaller oil drops), this relationship must be modified to include the Reynolds number effects. The Reynolds number used by Hinze is:

-21-

$$R^* = \frac{\mu_o}{\sqrt{\rho_o T d}}$$ (2-25)

where ρ_o is the oil density and $\mu_o = \nu_o \rho_o$. R^* is the ratio of viscous to surface tension forces in the case of natural oscillation of the drop. Kolmogorov also considered drops much smaller than η. The non-dimensional parameters influencing the behavior of these drops are Weber number and ν_o / ν_w, where ν_w is the kinematic viscosity of water. The most complicated case is that where the drops are of the same order of magnitude as the viscous length scale. Here an additional parameter, d/η, must be considered.

The splitting of droplets solely due to a density difference was studied by Hu and Kintner (1955). They assumed that drops break up at a constant value of the ratio of drag force to surface tension force. From experimental results, they determined the following relationship:

$$d_c = [1.452 \times 10^{-2} (\frac{T}{\Delta \rho_w})]^{1/2} \qquad \text{(CGS units)} \qquad (2\text{-}26)$$

where Δ is the density difference ratio $(\rho_w - \rho_o)/\rho_w$. Substituting likely values of T and Δ for the ARROW's cargo of Bunker C (24 dynes/cm, and 0.06, respectively), this equation predicts a maximum stable drop size of approximately 2.4 cm.

Forrester (1971) proposed that the probability that an oil drop will split in a turbulent field is proportional to the ratio of turbulent energy density to d^2, or

$$P(d) \sim \frac{E'(d)}{d^2} \qquad (2\text{-}27)$$

where

$$E'(d) \, \delta d = E(k) \delta k \qquad (2\text{-}28)$$

He then assumed that the dispersed oil was in a steady state - that is, oil was removed from the small size end of the distribution as fast as

-22-

it was added at the large size end. Using the fact that the distribution of oil volume with respect to particle size was found to be a constant, he concluded that the turbulent energy spectrum responsible for the dispersion was proportional to k^{-3}. He then claimed that this behavior was in agreement with the trend shown by the spectrum of ocean turbulence found by Grant et.al.

Two elements of Forrester's analysis appear to be questionable. The most obvious is the assumption without substantiation of the existence of a steady state. The leakage of oil from the ARROW was slow (about 1 ton per week after the initial spillage), but the entrainment no doubt occurred during relatively short periods of storm waves and heavy surf action, whereas the biodegradation of the oil was probably a very slow process. Certainly in the case of most spills, a non-steady state is more appropriate.

The other questionable aspect of Forrester's analysis is his proposed P(d). The largest particles generated by wave breaking are probably the size of turbulent motion in the inertial subrange, where

$$E(k) \sim k^{-5/3} \tag{2-29}$$

Therefore,

$$E'(d) \sim k^2 \, E(k) \sim k^{1/3} \tag{2-30}$$

so that Forrester's assumed P(d) behaves as $k^{7/3}$. This says that the probability of the largest drops' splitting is small, which is opposite the expected behavior. P(d) should, as shown by Kolmogorov, depend on Weber number for particles of a size not comparable to the viscous length scale η. The simplest model is one where P(d) is inversely proportional to Weber number.

$$P(d) \sim \frac{\rho_w v_d^2 d}{T} \sim \frac{\rho_w}{T} E(d) d^2 \tag{2-31}$$

-23-

This model predicts a large probability for the splitting of large drops, and a small probability for the splitting of small drops, as expected intuitively.

Rise of Droplets

In 1927, Bond showed the effect of viscosity on the terminal velocity of a droplet moving in the Stokes regime to be:

$$V_{\infty} = \frac{1}{k} \left\{ \frac{1}{18} \frac{(\rho' - \rho)gd^2}{\mu} \right\} \qquad (2-32)$$

$$k = \frac{2/3 + \mu'/\mu}{1 + \mu'/\mu} \qquad (2-33)$$

Here primed symbols denote characteristics of the droplet, and unprimed symbols those of the surrounding fluid. In 1928, Bond and Newton investigated the effect of surface tension on the terminal velocity and showed that for small droplets, where surface tension is relatively important, the drops behave like solid spheres ($\mu' \rightarrow \infty$). Landau and Lifshitz (1959) postulated that this behavior was due to the presence of an adsorbed film at the droplet interface.

The more complicated case where inertial effects cannot be ignored was investigated experimentally by Hu and Kintner (1955). They obtained a correlation between $Y = C_d P^{0.15} We$ and $X = Re/P^{0.15} + 0.75$ where $P = T^3 \rho_w / g \mu_w^4 \Delta$, and C_d is the drag coefficient, for 10 organic liquids falling through water. That correlation is:

$$Y = \frac{4}{3} X^{1.275} \qquad\qquad 2 < Y \leq 70$$

$$\qquad\qquad\qquad\qquad\qquad\qquad\qquad\qquad (2-34)$$

$$Y = .045 X^{2.37} \qquad\qquad Y \geq 70$$

They found no dependence on drop viscosity. The one liquid with very low values of interfacial surface tension (T = 2.8 dynes/cm) and

-24-

density difference ($\Delta = 0.02$) did not behave according to the correlation which fitted all other liquids. Upon closer examination, it appears that all of the liquids which did obey the correlation had sufficient surface tension to behave essentially as solid spheres, as found by Bond and Newton in the case of low Reynolds number. The correlation therefore seems to account only for viscous and inertial effects, and not those of surface tension.

Friedlander (1957) calculated the mean square velocity of a particle relative to the turbulent water around it. He restricted his analysis to those directions perpendicular to the gravity force. He assumed that the particle was smaller than the microscale of the stationary, homogeneous turbulence and such that the relative velocity was in the Stokes regime. He also assumed that viscous terms could be neglected in relating pressure gradients to turbulent accelerations. His result was:

$$\overline{u_R^2} = (1-\gamma)^2 \left[\overline{u_f^2} - \beta \int_0^\infty e^{-\beta\theta} R(\theta) d\theta \right] \tag{2-35}$$

where γ is the density ratio ρ_f/ρ_p, where the f and p subscripts denote fluid and particle properties respectively. u_f is the fluid velocity, and $\beta = 18\nu/d^2$, where ν is the kinematic viscosity of the fluid and d is the particle diameter. $R(\theta)$ is the temporal correlation of velocities seen by the particle. For very small particles, Friedlander showed that

$$\overline{u_R^2} \sim 2(1-\gamma)^2 \frac{\overline{u_f^2}}{\lambda^2\beta^2} \tag{2-36}$$

where λ is the temporal Taylor microscale seen by the particle. This expression is valid for $\lambda\beta$ much greater than 1. Thus, small, neutrally buoyant droplets are carried along by the turbulence, as expected intuitively.

The ability of a turbulent fluid to entrain buoyant particles in opposition to a gravity force is a well researched field. Most of the work done (e.g., Rouse, 1939) has assumed the existence of

-25-

a steady state. This steady state may exist when the turbulence itself can entrain sediment from a riverbed, for instance, but it is unlikely in the case of an oil slick, since it appears that typical quasi-steady state oceanic turbulence is insufficient to tear droplets off an intact slick. Instead, the oil is entrained during the short intervals of very strong turbulence caused by the passage of a breaking wave. It is possible that droplets previously entrained by breaking waves which have reached the slick but have not yet recoalesced may become re-entrained by the relatively mild steady state turbulence, although this has not been observed. The typical result for the concentration C of sediment in a steady dispersion is:

$$C = \overline{C}_o \exp\{-W \int_0^z \frac{1}{D} \, dz\} \qquad (2-37)$$

where $\overline{C}_o$ is the concentration at z=0, D is an eddy diffusivity, and W is the terminal velocity of the particles in calm water.

Leibovich (1975) presented a simple model of vertical dispersion which predicted the concentration of oil droplets at various depths as a function of the original depth to which they were entrained, the vertical velocity correlation of the turbulence, and the terminal velocity of the droplets of oil in calm water. This model made the assumption that the instantaneous deviation of an oil droplet's rise velocity from its terminal velocity in calm water is the local vertical turbulent velocity. Using this model, Leibovich obtained the rather surprising result that in a wind speed of 23 knots, fifty percent of the oil would be greater than 1 meter deep. He obtained this result by finding the probability density for the position of an oil drop released from some depth z_o in the absence of a free surface, and accounting for the existence of the free surface by taking the conditional density given that the oil drop is below the position of the free surface. In other words, he ignored the oil which was in fact on the free surface, which is likely to be the bulk of the oil. He did not consider the actual entrainment process, which must be known in order to predict the amount of oil dispersed in the water column.

-26-

Leibovich's probability density function $p(z,t)$ for the position at time t of a drop released at $z = z_o$, with terminal velocity $(-W)$, in the absence of a free surface, is

$$p(z,t) = [2\pi t \, D(t)]^{-\frac{1}{2}} \exp[-(z + Wt - z_o)^2/2t \, D(t)] \qquad (2\text{-}38)$$

where

$$D(t) = 2 \int_0^t (1 - \frac{\tau}{t}) \; \overline{u_z(t+\tau)u_z(\tau)} \; d\tau \qquad (2\text{-}39)$$

Here, u_z is the turbulent velocity in the z direction, and z is taken to be positive downward. Thus, the proportion of oil on the free surface would be

$$\int_{-\infty}^0 p(z,t)dz = 1 - \frac{1}{2} \, \text{erfc}\left[\frac{Wt - z_o}{\sqrt{2t \, D(t)}}\right] \qquad (2\text{-}40)$$

The large time limit of the probability density of the depth of oil, given that it is below the free surface, is:

$$P_{t\to\infty}(z; \, z \geq 0) = \nu e^{-\nu z} \qquad (2\text{-}41)$$

where $\nu = W/D(\infty)$. Leibovich stated that $D(\infty)$ could be approximated by K_ν where K_ν is the vertical eddy viscosity, estimated by Ekman (Sverdrup, et.al., 1942) to be $4.3 \times 10^{-4} \, U^2$ sec and by Ichiye (1967) to be $.028 \, H^2 \, T^{-1} \, E^{-2kz}$, where k, H, and T are the significant wave number, height, and period respectively. Leibovich noted the similarity between this result and that obtained by assuming a steady state dispersion.

Droplet Collisions and Recoalescence

Levich (1954) and Saffman and Turner (1956) have considered the coalescence of droplets in a turbulent field. Both assume that the droplets are small compared with the internal scale of the

-27-

turbulence, η. It has been shown that some distance below the free surface the larger droplets entrained in the water column in the case of the ARROW grounding were of the same order of magnitude as η, whereas the smaller droplets are at least as small as 1/2 of 1 percent of this size. These smaller droplets are therefore of the type considered by these authors.

In the case of neutrally buoyant drops, Saffman and Turner obtained the following expression for the rate of collision, N:

$$N = 1.30(r_1 + r_2)^3 \, n_1 n_2 (\varepsilon/\nu)^{1/2} \qquad (2\text{-}42)$$

where r_i and n_i are the radius and concentration of drops of ith size. This expression is valid only for r_1/r_2 between 1 and 2, since it assumes a collision efficiency of unity. The authors went on to develop an approximate expression for the collision rate of non-neutrally buoyant drops:

$$N = 2(2\pi)^{1/2} \, R^2 n_1 n_2 \left[(1 - \frac{\rho_w}{\rho_o})^2 (\tau_1 - \tau_2)^2 \, \overline{(\frac{Du}{Dt})^2} \right.$$

$$\left. + \frac{1}{3} (1 - \frac{\rho}{\rho_o})^2 (\tau_1 - \tau_2)^2 \, g^2 + \frac{1}{9} R^2 \frac{\varepsilon}{\nu} \right]^{1/2} \qquad (2\text{-}43)$$

where $R = r_1 + r_2$, $\tau_i = 2r_i^2 \rho_o / 9\mu_w$, g is the acceleration due to gravity, and u is the turbulent velocity. The first term considers the collisions due to the accelerations of the turbulent eddies. The authors quoted Batchelor (1951), who showed that

$$\overline{(\frac{Du}{Dt})^2} \simeq 1.3\nu^{-1/2}\varepsilon^{3/2} \qquad (2\text{-}44)$$

when the Reynolds number of the turbulence is large. The second term accounts for gravitational acceleration, whereas the third term corresponds to that already considered for neutrally buoyant drops.

-28-

Although the relative magnitudes of the second and third terms are comparable for the case of oil in the ocean, the second term clearly dominates the first term except possibly in the strong turbulence immediately under a breaking wave. Using the largest value of ϵ found by Grant, et.al. in a tidal channel, the ratio of the magnitude of the second term to that of the first is 2.5×10^4.

2.2 Chemical Phenomena

The chemical phenomena which have the greatest bearing on the dispersion of oil at sea are those involving surface chemistry. A survey of the relevant aspects of this field will be presented here, following a brief summary of the primary components of petroleum. Previous work on the use of surface films to contain oil slicks and chemical dispersants to disperse oil will be discussed, as will the literature dealing with natural spreading and weathering of oil at sea.

Composition of Petroleum (Nelson, 1958)

Most of the compounds found in petroleum are composed of hydrogen and carbon. In addition to these hydrocarbons, other compounds containing small amounts of sulfur, oxygen, and nitrogen are also present. Certain naphthene-base oils contain relatively large amounts of oxygen. The oxygen is often combined in the form of naphthenic acids. Nitrogen is most often found in naphthene-base oils and is generally in the form of basic compounds. Sulfur may be present as dissolved free sulfur, hydrogen sulfide, or as organic compounds, such as the thiophenes, sulfonic acids, mercaptans, alkyl sulfates, and alkyl sulfides.

Many series of hydrocarbons are found in crude petroleum (see Figure 2-2). Among the series that have been identified in petroleum are those having the type formulas $C_n H_{2n+2}$, $C_n H_{2n}$, $C_n H_{2n-4}$, $C_n H_{2n-6}$, $C_n H_{2n-8}$, $C_n H_{2n-10}$, etc. The paraffin series (type formula $C_n H_{2n+2}$) is characterized by relative chemical inertness. The lower members have been identified in most crude petroleums. The higher members of

-29-
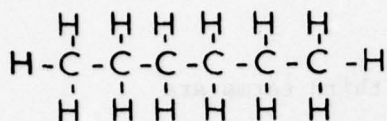
(a) Normal Hexane C$_6$H$_{14}$
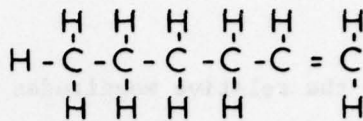
(b) Normal Hexene, C$_6$H$_{12}$
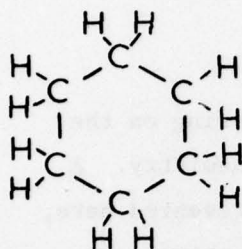
(c) Cyclohexane, C$_6$H$_{12}$
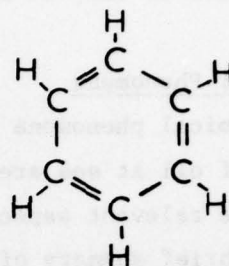
(d) Benzene, C$_6$H$_6$
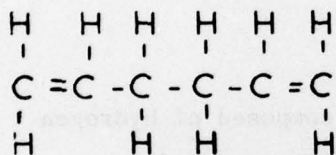
(e) Hexadiene -1,5, C$_6$H$_{10}$
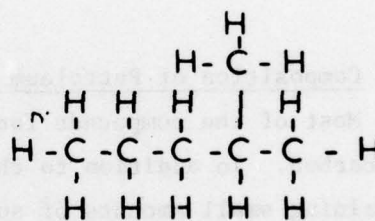
2 Methylpentane C$_6$H$_{14}$
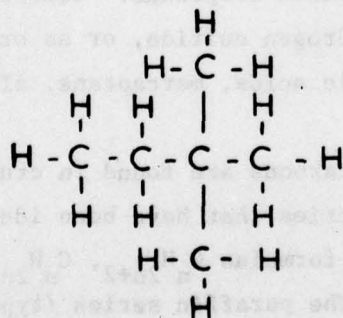
(f) Isomeric Isopar- affin Compounds

2-2 Dimethyl butane C$_6$H$_{14}$

FIGURE 2-2 Structural Formulas of Hydrocarbons
(After Nelson, 1958)

the paraffin series are probably present in most petroleums, although
crude oils that are entirely free from wax may contain no high-boiling
paraffin hydrocarbons. The olefin or ethylene series (type formula C_nH_{2n})
is composed of unsaturated hydrocarbons. The names of these hydro-
carbons end in -ene, as ethene (ethylene), propene (propylene), and
butene (butylene). The low-boiling olefins are probably not present
in crude petroleum. The naphthene series (type forumla C_nH_{2n}) has
the same type formula as the olefin series but the members are ring
or cyclic compounds, whereas the olefins are straight-chain compounds
in which a double bond connects two carbon atoms. The preferred
names are cyclobutane, cyclopentane, and cyclohexane. As an example
of the relation of this series to other cyclic series, consider
benzene and cyclohexane. Both compounds contain six carbon atoms
per molecule, but six hydrogen atoms must be added to benzene to
produce cyclohexane. Naphthenes have been found in almost all crude
oils. The aromatic series (type formula C_nH_{2n-6}), often called
the benzene series, are particularly susceptible to oxidation
with the formation of organic acids. Only a few petroleums contain
more than a trace of the low-boiling aromatics such as benzene and
toluene. The cyclic series such as those having type formulas
C_nH_{2n-2}, C_nH_{2n-4}, C_nH_{2n-8}, etc., predominate in the higher boiling
point oils.

Adsorption and Orientation at Interfaces (Shaw, 1970)

Some of the molecular species present in petroleum--those which
are predominantly composed of hydrogen and carbon, but which contain
the heteroatoms oxygen, nitrogen and sulfur--tend to collect at the
oil/water or air/water interface. For example, oxygen-containing
species such as short-chain fatty acids and alcohols are soluble
in both water and organic solvents. The hydrocarbon part of the
molecule is responsible for its solubility in oil, while the polar
-COOH or -OH group has sufficient affinity to water to drag a short-
length non-polar hydrocarbon chain into aqueous solution with it.
If these molecules accumulate at an air-water or oil-water interface,
they are able to locate their hydrophilic head groups in the aqueous

-31-

phase and their lipophilic hydrocarbon chains in the vapor or oil phase. (See Fig. 2-3). This situation is energetically more favorable than complete solution in either phase.

The strong adsorption of such materials at surfaces or interfaces in the form of an orientated monomolecular layer (or monolayer) is termed surface activity. Surface-active materials (or surfactants) consist of molecules containing both polar and non-polar parts (amphiphilic). Surface activity is a dynamic phenomenon, since the final state of a surface or interface represents a balance between this tendency towards adsorption and the tendency towards complete mixing due to the thermal motion of the molecules. Figure 2-4 shows the effect of lower members of the homologous series of normal fatty alcohols on the surface tension of water. The longer the hydrocarbon chain, the greater is the tendency for the alcohol molecules to adsorb at the air-water surface and, hence, lower the surface tension.

The hydrophilic part of the most effective soluble surfactants (e.g. soaps, synthetic detergents and dyestuffs) is often an ionic group. Ions have a strong affinity for water owing to their electrostatic attraction to the water dipoles and are capable of pulling fairly long hydrocarbon chains into solution with them. For example, palmitic acid, which is virtually nonionized, is insoluble in water, whereas sodium palmitate, which is almost completely ionized, is soluble. Surfactants are classified as anionic, cationic or nonionic according to the charge carried by the surface-active part of the molecule. Some common examples are given in Table 2-1.

The formation of an adsorbed surface layer is not an instantaneous process but is governed by the rate of diffusion of the surfactant through the solution (through the oil in the case of natural surfactants present therein) to the interface. It might take several seconds for a surfactant solution to attain its equilibrium surface tension, especially if the solution is dilute in surfactant and the solute molecules are large and unsymmetrical, as may be the case for natural surfactants in oil.

-32-
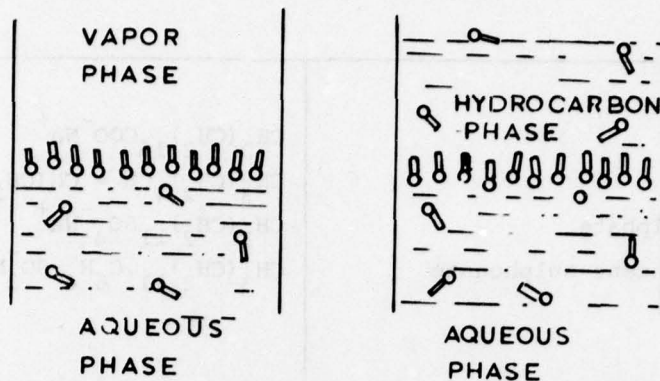
FIGURE 2-3 Adsorption of Surface-Active Molecules as an
Orientated Monolayer at Air-Water Interfaces.
The Circular Part of the Molecules Represents
the Hydrophilic Polar Head Group and the Rectangular
Part Represents the Nonpolar Hydrocarbon Tail
(After Shaw, 1970)
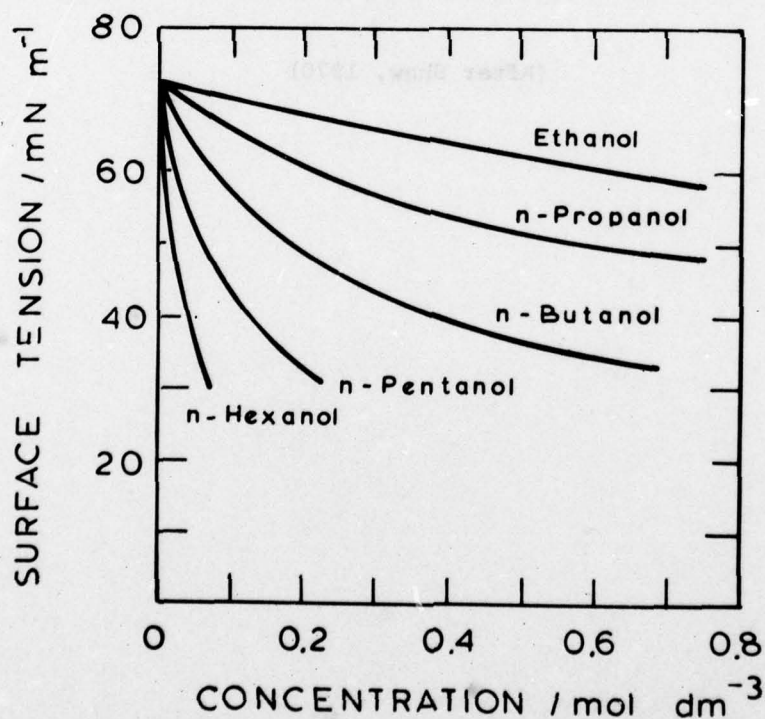
FIGURE 2-4 Surface Tension of Aqueous Solutions of Alcohols
at 20°C (After Shaw, 1970)

-33-

TABLE 2-1 Surface-Active Agents

Anionic	
Sodium stearate	$CH_3(CH_2)_{16}COO^-Na^+$
Sodium oleate	$CH_3(CH_2)_7CH = CH(CH_2)COO^-Na^+$
Sodium dodecyl sulphate	$CH_3(CH_2)_{11}SO_4^-Na^+$
Sodium dodecyl benzene sulphonate	$CH_3(CH_2)_{11}\cdot C_6H_4\cdot SO_3^-Na^+$
Cationic	
Laurylamine hydrochloride	$CH_3(CH_2)_{11}NH_3^+Cl^-$
Cetyl trimethyl ammonium bromide	$CH_3(CH_2)_{15}N(CH_3)_3^+Br^-$
Non-ionic	e.g.
Polyethylene oxides	$CH_3(CH_2)_7\cdot C_6H_4\cdot(O.CH_2.CH_2)_8OH$
Spans (sorbitan esters)	
Tweens (polyoxyethylene sorbitan esters)	

(After Shaw, 1970)

-34-
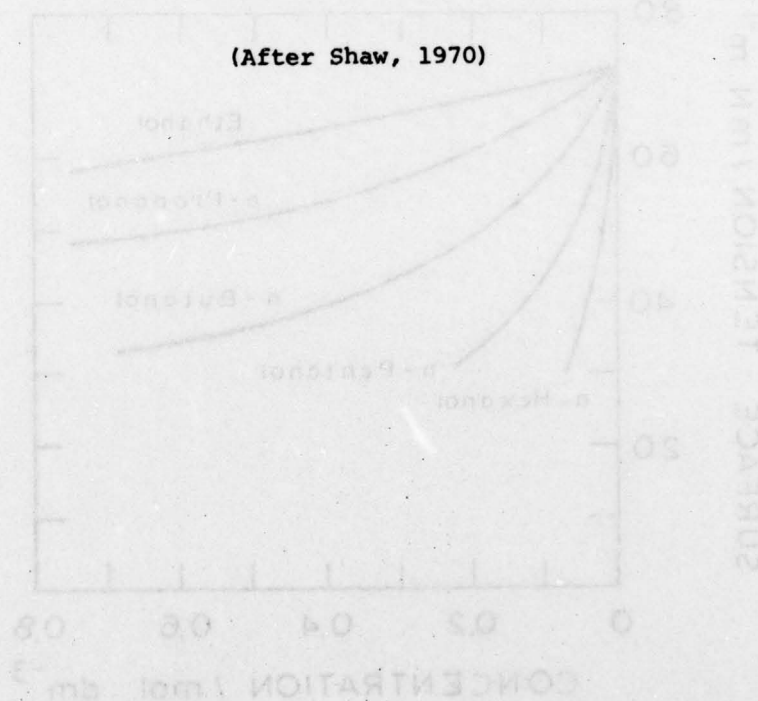
Spreading: Surface Films of Insoluble Substances
(Overbeek, Mayr and Donnelly, 1971)

When a drop of liquid 2 (say, a hydrocarbon) is placed on the surface of another liquid 1 (say, water), as shown in Figure 2-5, one of three things may happen:

(a) <u>Dissolution</u> - This might be interpreted as a situation in which the interfacial tension T_{12} is negative.

(b) <u>Spreading</u> - From Figure 2-5, one can see that spreading occurs when $T_1 > T_2 + T_{12}$. Here T_1 and T_2 represent the surface tension between the gaseous phase and liquids 1 and 2, respectively. The tendency of one liquid to spread over another is described by the <u>spreading coefficient</u> for 2 on 1, $S_{2/1}$, defined as:

$$S_{2/1} \equiv T_1 - T_2 - T_{12} \tag{2-45}$$

Liquid 2 will therefore spread over liquid 1 when $S_{2/1}$ is positive. One concludes that spreading can only occur when a low surface tension liquid is placed on a high surface tension surface. (This is a necessary, but by no means sufficient, condition, as will be shown below.)

(c) <u>Lens formation</u> - If $S_{2/1}$ is negative, spreading will not occur and the droplet will assume an equilibrium position in the form of a lens, the shape of which is dictated mainly by the relative magnitude of the three surface tension forces shown.

The phenomenon of spreading of one liquid over another is complicated by the fact that mutual dissolution of liquids 2 and 1 can significantly alter the values of the surface and interfacial tensions, so that one must carefully distinguish between the <u>initial</u> and <u>final</u> spreading coefficients. For example, benzene (b) initially spreads over water, but a lens is formed after the water surface is saturated with benzene. Calculation of the initial and final spreading coefficients indicates that this is the expected behavior:
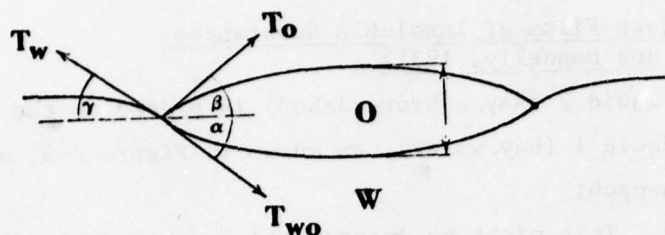
FIGURE 2-5: Profile of an oil lens on water

Direction of
Deformation

Air   Low T   High T   Low T

Vertically Oriented
Adsorbed Surfactant
Molecules

Water
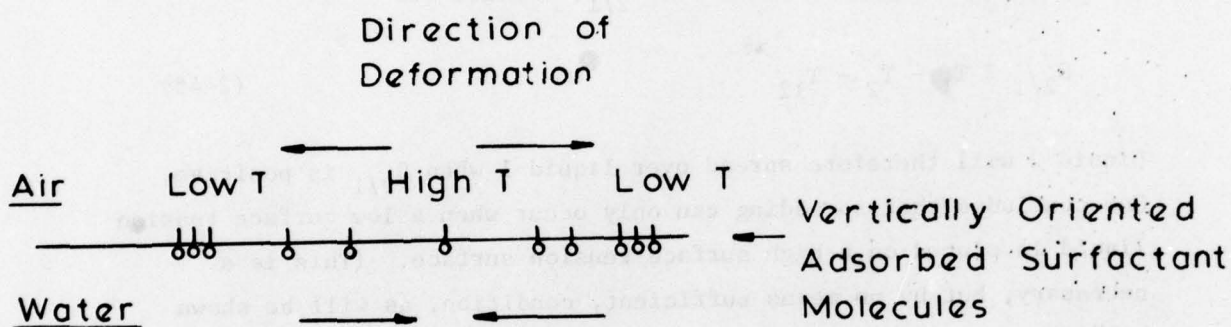
Opposing Surface Tension Force

FIGURE 2-6 Elasticity of Surface Films.

Initially:

$$T_{wa} = 72.8 \text{ dynes/cm}$$
$$T_{ba} = 28.9$$ $$S_{bw \text{ (initial)}} = +8.9 \text{ dynes/cm}$$
$$T_{bw} = 35.0$$ (spreads)

After Saturation:

$$T_{w(\text{sat'd with } b),a} = 62.2 \text{ dynes/cm}$$
$$T_{b(\text{sat'd with } w),a} = 28.8$$ $$S_{bw \text{ (final)}} = -1.5 \text{ dynes/cm}$$
$$T_{bw} = 35.0$$ (lens)

The substantial lowering of the surface tension of water by the
benzene (from 72.8 to 62.0 dynes/cm) is the reason for the final
negative spreading coefficient. This is typical of all aqueous
systems. In many cases, however, even the <u>initial</u> spreading is nega-
tive. An example of such a system is carbon disulfide on water.

If a surface active solute is dissolved in the benzene or carbon
disulfide (e.g., 0.1% oleic acid), T_2 is only slightly affected, but
T_{12} is lowered considerably. Consequently, the initial spreading
coefficient is positive for both the benzene-water and CS_2-water
systems, and <u>rapid</u> spreading occurs. This causes a monolayer of
surfactant to be formed on the water, so that T_1 is appreciably
lowered and $S_{2/1}$ again becomes negative.

Monolayer (one molecule thick) surface films of virtually
insoluble surfactants, such as the higher fatty acids (stearic,
lauric, oleic acid) and higher fatty alcohols (cetyl alcohol), easily
form on water. The adsorbed layer in the form of a monolayer lowers
the surface tension of water, or conversely can be considered to exert
a <u>surface pressure</u>, Π, defined as

$$\Pi = T_0 - T \tag{2-46}$$

where T_0 is the surface tension of pure water and T is the surface
tension of water with surfactant. The amount by which the surface
tension is lowered, Π, depends upon the surface concentration of the

surfactant. A portion of the surface which is deforming (expanding) as a result of some perturbation will exhibit momentarily higher surface tension which opposes deformation of the surface. Thus, such a layer displays surface elasticity. This is illustrated schematically in Figure 2-6. The adsorbed layer will prevent ripples from forming (or damp them strongly), and this may in part explain the apparent phenomenon of oil calming ocean waves. Such oil must, of course, be polar or contain surfactants.

Emulsion Chemistry and Stability (Overbeek, Mayr and Donnelly, 1971)

When one liquid is dispersed in another, the mixture is termed an emulsion. Emulsions are of the type water-in-oil (W/O) with the water found in the form of extremely fine droplets and the oil as the continuous phase, or of the type oil-in-water (O/W) where oil is dispersed as droplets in water. If the interfacial tension between two liquids is reduced to a sufficiently low value in the presence of a surfactant, emulsification will readily take place because only a relatively small increase in the surface free energy of the system is involved. As noted above, petroleum may contain a number of natural materials which are surface active and which can, therefore, promote emulsion formation.

Emulsion chemistry relates to the chemical nature of the interface between the oil phase and aqueous phase. These interfaces are often charged, usually as a result of the preferential adsorption of positive or negative ions at the interface. To satisfy the requirements of local electroneutrality, the counter-charge must be nearby. The charged interface and the adjacent region of counter charge form what is called the electrical double layer. The presence of such a double layer leads to a repulsive interaction between droplets which can, if sufficiently large, provide the necessary stability to prevent aggregation and coalescence.

An O/W emulsion is generally not stable, however, even though a natural double layer is often present. The double layer will be of the double-diffuse type with most of the potential drop occurring in the oil phase due to the low electrolyte strength in, and low dielectric constant of the oil. The charge densities will be low--in

-38-

water because of the low potential and in oil because of the very much extended double layer (see Figure 2-7). The repulsive double layer energy will then also be small, too small to counteract the attractive physical forces.

The O/W emulsion could be stabilized if a suitable surface-active substance were present at the interface. Figure 2-7 shows the influence of the adsorption of negative soap ions on the potential distribution (dotted curve).

For droplets larger than about 1 to 10 μm in diameter there is a strong tendency for separation under the influence of gravity. In this case oil droplets will rise to the surface and may form a concentrated but stable emulsion. When the repulsion is not strong enough to keep the oil droplets apart, they may flocculate (aggregate) without coalescing, or they may coalesce (flow together to form a continuous oil phase).

It is also possible to disperse water in oil, but again in order to obtain stability a strong double layer must be formed in the oil phase, and this requires an increased electrolyte content. Inorganic electrolytes are usually very poorly soluble in oil, and, if soluble, they are much less dissociated than in water. Some organic electrolytes, however, have large ions and can dissociate in oil. Crude oils often do have substantial electrical conductivity. Even in the presence of dissociated organic electrolytes, however, the double layer remains extended. In concentrated W/O emulsions of 50%/50%, for example, there is a considerable overlap of double layers, and the repulsion is largely overcome of necessity because the droplets are so close together. This explains the ability of organic electrolytes to stabilize dilute W/O emulsions, but not concentrated ones.

The effects of the surface active species which may be naturally present in crude oils or which may be added during chemical dispersing are to facilitate emulsification and promote emulsion stability. The emulsifying agent forms an adsorbed film around the dispersed droplets which helps to prevent flocculation and coalescence. The stabilizing mechanism is complex and may vary from system to system. In general,

-39-

Oil   Water

Untreated

$\Delta\phi$

ϕ_o

0

Negative Soap
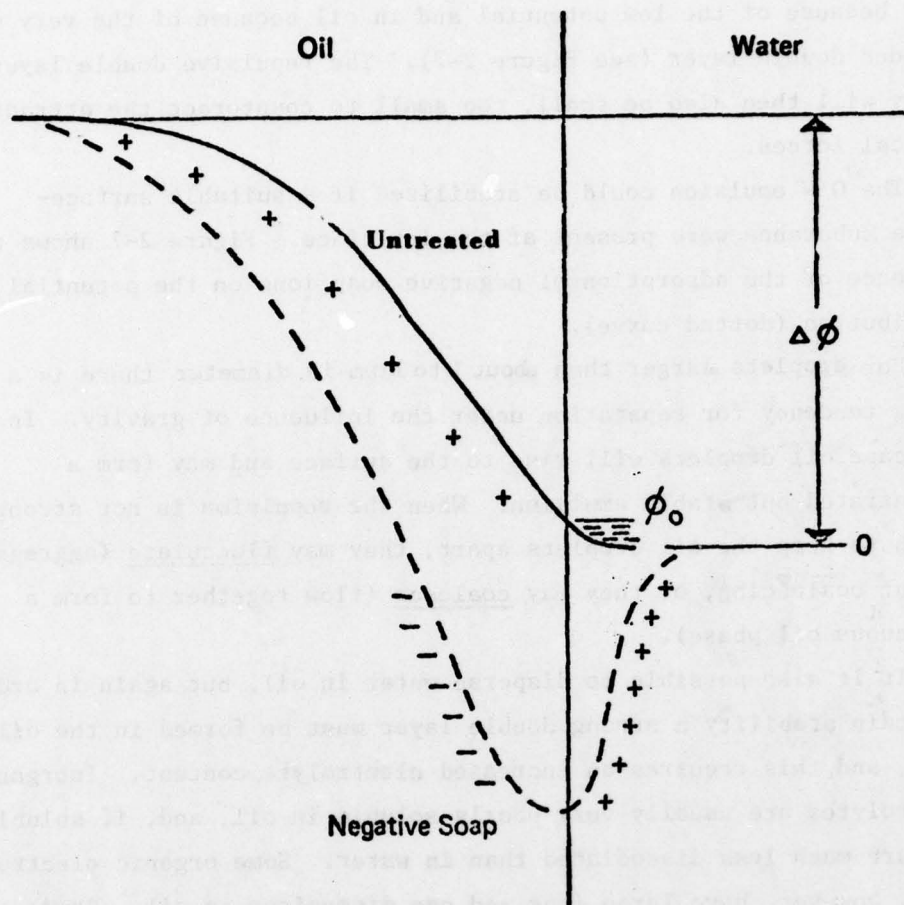
FIGURE 2-7 Schematic of Potential Distribution in Double
Layer at Oil/Water Interface

-40-

however, the factors which control droplet flocculation are electro-
static in nature as discussed above, whereas stability against droplet
coalescence depends mainly on the mechanical properties of the
interfacial film. In addition to those already discussed, the
following factors (which depend on the nature of the surface-active
agent and/or on the fluid dynamical conditions leading to the emulsion)
favor emulsion stability:

Low interfacial tension - The adsorption of surfactant at the
oil-water interfaces causes a lowering of interfacial energy,
thus facilitating the development and enhancing the stability
of the large interfacial areas associated with emulsions.

A mechanically strong interfacial film - The stability of
emulsions stabilized by various long-chain stabilizers arises
from the mechanical protection given by the adsorbed films
around the droplets, rather than from a reduction of interfacial
tension. Surfactants can also stabilize in the mechanical
sense. Coalescence involves droplet flocculation followed by
a squeezing of film material from the region of droplet contact,
and the latter is more favored with an expanded film than with
a close-packed film. For example, very stable hydrocarbon O/W
emulsions can be prepared with sodium cetyl sulphate plus
cetyl alcohol as emulsifier (a condensed mixed film being formed
at the interface), whereas the identical emulsions prepared with
sodium cetyl sulphate plus oleyl alcohol (which gives an
expanded mixed film) are much less stable.

High viscosity - A high viscosity simply retards the rates of
droplet migration, coalescence, etc. This is a major factor in
the stability of W/O emulsions typical of chocolate mousse.

A completely different mechanism of stabilizing emulsions which
has relevance to seawater emulsions is the adsorption of solid
particles at the oil/water interface. If the particulates are hydro-
philic, the contact angle on the water side is small, and the particles
reside on the water side of the oil/water interface, stabilizing the
O/W emulsion. Oleophilic particles with a small contact angle on the
oil side would lead to stabilization of the W/O emulsion. The solid
particles act as mechanical barriers to coalescence. If the
continuous phase is water, small quantities of electrolyte enhance
emulsion stability because the particles are permitted to come closer
together. However, larger amounts of electrolyte lead to flocculation
and to rapid gravity separation of the emulsion, although coalescence

-41-

may remain prevented. Emulsions stabilized by solid particles are called Pickering emulsions.

Whether an emulsion is of the O/W or W/O type will be mainly determined by the stabilizing mechanism. However, in some cases, the phase-volume ratio is also of some influence, the phase present in larger volume forming the continuous phase. Many O/W emulsions may be inverted into W/O emulsions by addition of suitable chemicals.

Use of Surface Films to Contain Oil Slicks

Some of the newest and most interesting technology is the use of water-insoluble monomolecular surface films in the control of oil slicks. The most appropriate application of this technology is in condensing a very thin oil film into a thicker, more collectable lens. A surface film used in the vicinity of a boom and skimmer or absorber arrangement may be used to "push" the oil towards the collector, eliminating a need for towing. Since the material will spread to achieve a thickness of only one molecule, very little is needed to contain a good-sized slick. It has been determined that liquid water-insoluble compounds with high film pressures and low oil solubility display optimum containment characteristics (Garrett and Barger, 1970). Other important characteristics of a suitable compound are the mono-layer spreading velocity, ability to spread against wind, and the maximum lens thickness which the monolayer will support. Compounds which generally meet these requirements are liquids with high spreading pressures and low oil and water solubilities. Oleyl alcohol (9-octadecen-1-ol) meets the above requirements and was tested by Garrett and Barger. However, the alcohol has a comparatively low spreading pressure (33.8 dynes/cm), and thus other compounds with higher spreading pressures are being tested. Solid saturated fatty alcohols and the fatty esters of sorbitol and glycerol are being investigated. Their drawbacks, since they are solids, are a slow spreading velocity and possible monolayer collapse with wave action. Liquid monolayers will readily respread over an area where wave-induced surface dilations have disrupted the film (Garrett and

Barger, 1970). Suggested areas for use are harbors, rivers, between shore and a slick to prevent land contamination, and for driving oil out of inaccessible locations under piers and between ships.

Dispersing

Dispersing oil via detergent application accomplishes two things: first, it allows the oil to form discrete droplets which do not readily "wet" or cling to a solid surface. Secondly, it increases the surface area available to bacterial attack; the oil is then available to a larger population for degradation. When applied properly, detergents may increase the rate at which oil is removed from the ecosystem.

Pure hydrocarbons, for example a refined white mineral oil, will form a lens rather than spread on a water surface and will not form a stable emulsion. Natural crudes, however, contain surface active agents (surfactants) which enhance spreading by reducing the oil-water interfacial tension and/or which stabilize emulsions. It is the oil-in-water (O/W) emulsion which is sought in the application of dispersion technology. To achieve the desired oil-in-water (O/W) emulsion, Bancroft's law states that surfactants added to the oil must be principally water soluble (Sherman, 1968). These surfactants have generally been in the form of nonionic emulsifiers carried in a solvent. Especially effective dispersants are nonylphenolethyleneoxide condensates, according to two English laboratories (Smith, 1962). They have also determined that effective diluents and concentrations are 10-20% of the emulsifier in an aromatic solvent with a boiling range between 170 and 220°C. Laboratory experiments demonstrate that less than 10% of such a solvent/emulsifier mixture is needed to obtain a stable dispersion.

In practice, the use of dispersants presents several problems. Both emulsifier and diluent can be toxic, the organic diluents possibly extremely so. Investigations are continuing in an attempt to find less toxic dispersants. Satisfactory results have been achieved by several changes. Where the emulsifying agent

-43-

is water compatible, water is used as the diluent in application.
When organic solvents must be used as diluents (due primarily to
emulsifier nature), high-boiling point saturated hydrocarbons have re-
placed the low-boiling point aromatics, because of their similarity to
the types of hydrocarbons occurring naturally in the ocean (Canevari, 1971).
A further reduction in toxicity in emulsifier-diluent systems is
achieved by the use of surfactants from generic types which are not
considered chemically toxic. Changes in toxicity levels are
illustrated by some Torrey Canyon dispersant and post-Torrey Canyon
dispersant data. The data are presented as the ppm of dispersant
product necessary to kill 50% of the test organism crangon crangon
(brown shrimp) in 48 hours (called an LC_{50}). The Torrey Canyon
dispersants killed the shrimp at levels of 6 - 9 ppm. More
recently developed surfactant systems require 3,300 to 10,000 ppm
before reaching the same toxicity levels (Canevari, 1971).
COREXIT 7664, developed by Exxon Research and Engineering Company,
is an effective nonionic dispersant which has less than a 50%
mortality rate when applied to test species for 96 hours at a level
of 10,000 ppm. Planktonic species, barnacles, and mussels are among
those organisms investigated in conjunction with COREXIT 7664
(Canevari, 1969a).

By a careful choice of dispersant and the use of short-term
exposures, acute toxicity can be greatly reduced. Long range
contaminant effects of the finely dispersed surfactant-oil composite
are unknown. Possible effects are changes in organism behavioral
patterns (i.e., interference in metabolic processes, mating signals)
or the accumulation of trace persistent hydrocarbons (Canevari,
1971).

There are two other major difficulties encountered in trying to
disperse an oil slick. The first problem is that of application.
Water-compatible surfactants can be educted into a system (usually
a fire hose) and sprayed over the oil surface, either directly
through the hose or through a boom spray apparatus which can cover
up to 50' laterally per boat pass. The water eduction system
cannot be used to apply emulsifiers in organic diluents. The organic
systems must be applied neat (undiluted by water), otherwise a stable
diluent-in-water dispersion will form upon eduction into the water
stream. The surfactant will be in a thermodynamically stable state
at the diluent-water interface and will not transfer to the oil-water
interface (Canevari, 1969a, b). A related applications problem
is that on the open sea the solution required may be as much as
100% of the amount of oil to be dispersed due to losses in application
and water dilution (Smith, 1968).

The second problem stems from the energy input needed for
dispersion. Work is required to increase the oil-water interfacial
surface area. Explicitly stated,

$$W = A_{ow}T_{ow} \tag{2-47}$$

where W is the mixing energy or work input (ergs), A_{ow} is the inter-
facial area (cm^2), and T_{ow} is the interfacial tension (dyne/cm). Addition

-45-

of a surfactant will reduce T_{ow}, but some mixing energy will still
be required to form fine oil droplets. For example, the energy
required to disperse one gallon of gasoline into 150 µ drops is
7.2×10^7 ergs. For the same work input drops of 57 µ can be
produced after the addition of a small amount of surfactant such
as sodium oleate. The system's surface tension is reduced from
48 dyne/cm to 7 dyne/cm. The surfactant addition also aids in the
dispersion stability, since the ratio of the rise time of the
smaller droplets to that of the larger droplets is 0.0215. The slower
the rise velocity, the better the chances are that the dispersed
particle will be convected away from the slick, rather than recoalescing
with it (Canevari, 1969b). Minimum dispersion coalescing times of
1 1/2 to 2 hours may be acceptable (Blacklaw, Strand and Walkup, 1971).

Although theoretically applicable, Eq. (2-47) has the following
practical limitation: a significant amount of mixing energy is
lost to the sea, i.e., only a portion of the mixing energy applied
in the field is applied to the oil-water interface. Water solvent
systems have the added limitation that energy must be supplied while
the immediate water environment is surfactant-rich. Failure to
apply energy before dilution in the ocean means a loss of surfactant
to the environment (Canevari, 1969a). On the open ocean agitation
is typically supplied first by the hoses or nozzles used in applica-
tion and then also by the vessel's bow wave and wake.
The limiting step in oil slick dispersion is currently the need
for agitation of the oil-water-surfactant mixture after application.
A typical working vessel can cover about 35 acres/hour. For a
1,000 ton spill, then, approximately 180 working hours would be
required to provide agitation over the area of the spill (Canevari, 1973).
This working time is irrespective of the time lost to obtain supplies,
more fuel or dispersant. The dispersion technique for cleaning
up spills might ideally be used when oil impingement on a coastline
is imminent. However, in such cases the required time for dispensing
and mixing dispersant is excessive. Furthermore, working boats
cannot be used in shallow areas or around piers effectively.

Obviously, the way to overcome both the time constraint and the inability to supply dispersant to shallow areas is to develop dispersants which spontaneously form o/w dispersions upon application without mixing.

Dispersions are formed without mixing via the "diffusing and stranding" mechanism. The surfactant used is predominantly oil-soluble and is thus compatible with the bulk oil. However, when it comes in contact with the water interface the surfactant is placed under a large driving force to diffuse into the water. At the interface a three component system is formed; oil, water and surfactant. As the surfactant diffuses out of the oil and into the water phase, the oil associated with the surfactant oil is dragged out of solution and into the water phase. An example of this behavior is the ethanol-toluene-water system. When ethanol diffuses into the water fine droplets of toluene are entrained and end up dispersed in water (Canevari, 1973). So far, only a preliminary study has been done, and research is continuing in this area, which seems promising.

Natural Dispersion and Weathering

There are a number of natural mechanisms related to the chemical and physical properties of the oil which result in the final degradation of a slick. These include spreading, evaporation and aerosolization, dissolution, adsorption and removal by particulates, atmospheric oxidation, microbial digestion and the formation of o/w and w/o emulsions. Figure 2-8, from Parker, Freegarde and Hatchard (1971), presents an overview of the weathering mechanism, showing the major pathways (wide arrows) and the minor pathways (dotted arrows). All the individual mechanisms are interrelated and interdependent.

Spreading

The first mechanism leading toward the ultimate degradation of oil which is spilled is spreading. P.C. Blokker (1964) derived an equation for spreading kinetics for the period beginning after at least 90% of the potential energy of the oil is dissipated by

-47-
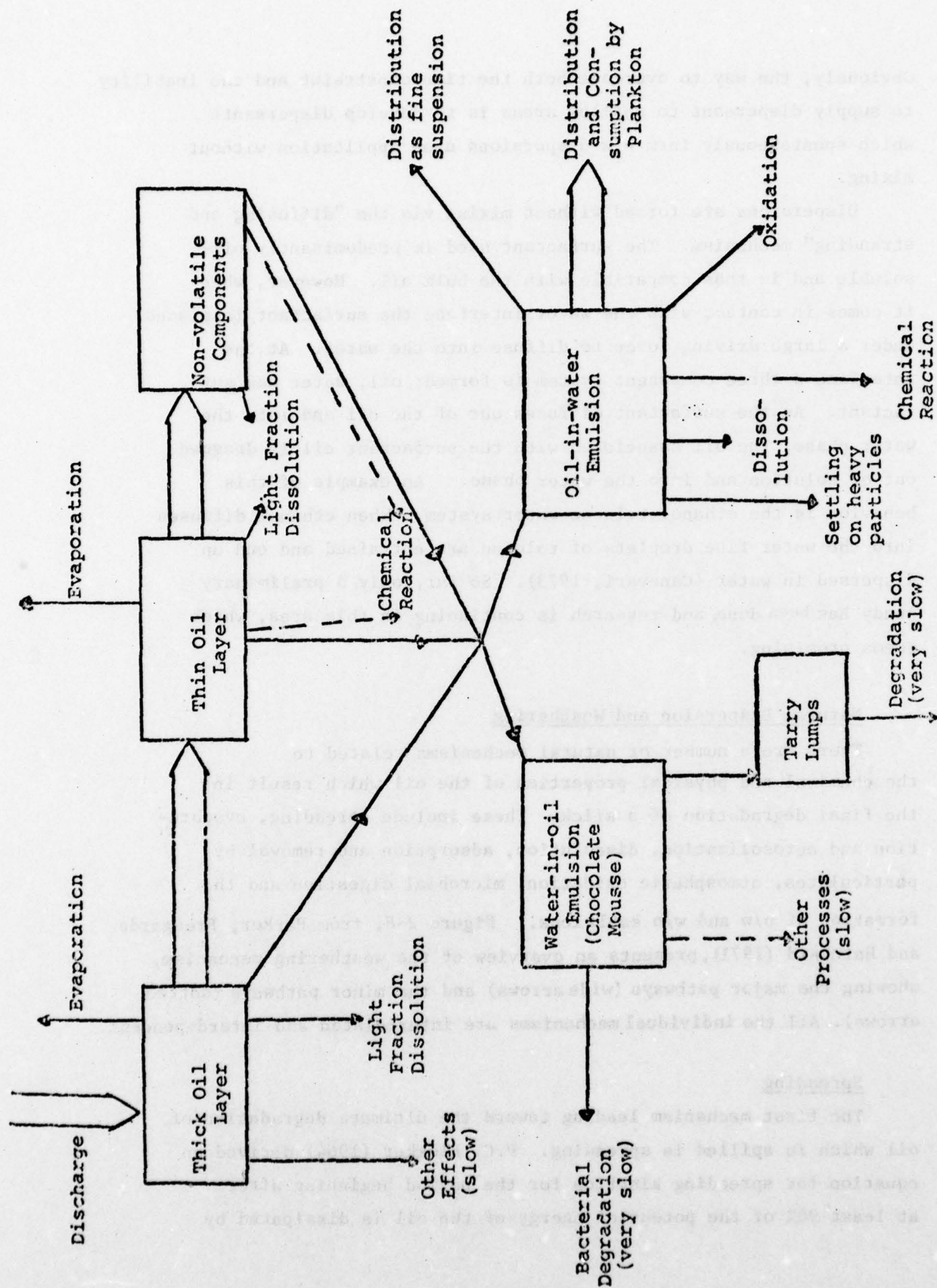
FIGURE 2-8 Processes Leading to the Degradation of Crude Oil at Sea. (After Parker, Freegard and Hatchard, 1971.)

friction. This requirement is met for slicks less than about
2 cm thick. He assumed the time necessary for oil to spread to
2 cm thick was negligible. After the 2 cm height was reached,
Blokker showed that the rate of spread at a specific moment was
independent of the history of spreading (i.e., the initial slick
thickness), but was approximately proportional to the mean layer
thickness of the oil at that moment. Neglecting small differences
in spreading layer thickness, he showed that for a one-dimensional
flow case (i.e., spreading in a trough):

$$\frac{d\ell}{dt} = K(\rho_w - \rho_o) \frac{\rho_o}{\rho_w} (h_t - h_\infty) \tag{2-48}$$

where ℓ is the length of the flow field, t is time, ρ is density,
K is the Blokker constant, the subscripts o and w are for oil and
water, respectively, h_t is the slick thickness at time t and h_∞ is
the final oil thickness. Assuming h_∞ is negligible (as for an
overflow at the end of the trough), and with $t_o = 0$, Eqn. (2-48) becomes

$$(\ell_t^2 - \ell_o^2) = 2K(\rho_w - \rho_o) \frac{\rho_o}{\rho_w} \frac{V_o}{b} t \tag{2-49}$$

where $V_o = b\ell h$, the volume of oil, and b is the trough width.
This equation was proven approximately correct, and K, the system
constant, could be determined for each system investigated. Jeffrey
(1971) tried using Blokker's empirical equation on an open sea
experiment. He obtained results with a wide scatter, due to changes
in environmental conditions, and reported K as 216±144.

An improved model of oil spread on the sea (Hoult, 1972) was based
upon the consideration that unrestrained oil has four forces acting upon
it as it flows: Gravity forces act as driving forces for spreading,
while the viscous drag and inertial forces act as retardants.
Surface tension forces initially may act as driving forces, but
at some point in time they may begin to inhibit spreading. Balancing

-49-

these forces leads to three flow regimes as modeled via an order
of magnitude analysis. At short times the gravitational forces
are balanced by inertial forces. The inertial force for the axisymmetric
case is

$$F_i \simeq \rho_w \ \frac{\ell}{t^2} \ h\ell^2 \qquad\qquad (2\text{-}50)$$

where ρ_w is the water density, ℓ is the slick length, t is time and
h is slick thickness. The gravitational driving force is

$$F_g \simeq (\rho_w g \Delta h) \ h\ell \qquad\qquad (2\text{-}51)$$

where g is the gravitational acceleration and $\Delta = (1-\rho_o/\rho_w)$, generally
on the order of 0.1. Gravity terms dominate the surface tension driving
force provided the oil is thick enough, i.e., if

$$h > (\frac{S}{\rho_o g \Delta})^{1/2} \qquad\qquad (2\text{-}52)$$

where S is the spreading coefficient. Equating the opposing forces
yields (Fay, 1971).

$$\ell = K_i (g \Delta V)^{1/4} \ t^{1/2} \qquad\qquad (2\text{-}53)$$

where K_i is the dimensionless inertial flow regime constant obtained
from the similarity solution of the spreading equations (Milgram and
Donnelly, 1975). V, the oil volume, has been substituted for $h\ell^2$,
giving a relation for the length of the slick in terms of the
amount of oil spilled and the time elapsed since spillage. For
one-dimensional flow, Equation (2-53) becomes (Hoult and Suchon, 1970):

$$\ell = K_i (\Delta g V t^2)^{1/3} \qquad\qquad (2\text{-}54)$$

For intermediate times, Equation (2-52) is still valid, but the constraint

$$h < \left[\frac{\mu_w t}{\rho_w}\right]^{1/2} \tag{2-55}$$

may also be met (here μ_w is the water viscosity). Under these conditions, the viscous regime is encountered. Gravitational acceleration is still the driving force, but the inertial force is replaced by the viscous retardation forces, F_v, where:

$$F_v \simeq \frac{(\mu_w \rho_w)^{1/2} \ell^3}{t^{3/2}} \tag{2-56}$$

The force balance now results in an equation of the form (Fay, 1971)

$$\ell = K_v \left[\frac{\mu_w}{\rho_w}\right]^{-1/12} (g\Delta)^{1/6} v^{1/3} t^{1/4} \tag{2-57}$$

where K_v is the viscous constant analagous to K_i. For the uni-directional case Equation (2-57) becomes (Hoult and Suchon, 1970):

$$\ell = K_v \left[\frac{(\Delta g v^2 t \rho_w^{1/2}}{\mu_w^{1/2}}\right]^{1/4} \tag{2-58}$$

The third flow process dominates for long times, as $h \to 0$. The surface tension force, F_s, balances the viscous retardation in this case, where

$$F_s \simeq S\ell \tag{2-59}$$

and

$$S = T_{wa} - T_{ow} - T_{oa} \tag{2-60}$$

-51-

as was shown graphically in Figure 2-5. A relation of the form

$$\ell = K_t \left(\frac{S^{1/2} t^{3/4}}{(\mu_w \rho_w)^{1/4}} \right) \qquad (2\text{-}61)$$

where K_t is the so-called "flow constant," is obtained for the surface tension regime by equating surface tension and viscous forces (Fay, 1971). The analogous one-dimensional form is

$$\ell = K_t \left(\frac{S^2 t^3}{\rho_w \mu_w} \right)^{1/4} \qquad (2\text{-}62)$$

The constants for each equation have been determined by various authors and the best values are given in Table 2-2.

Milgram and Donnelly (1975) contend that the viscous regime is theoretically invalid. The reasoning is twofold. First, in all previously published studies, the water boundary layer has been assumed to be laminar. In actuality the Reynolds number, as based on the mean interfacial velocity and slick radius, is on the order of several million. For the most important cases, then, the boundary layer is turbulent, not laminar. The lack of an exact form for the Reynolds stress in the water means the velocity profiles in the turbulent layer are not known. Therefore, he has developed a turbulent spreading theory using a typical velocity profile (specifically, the one-seventh law for the turbulent boundary layer velocity profile). For this case, the turbulent spreading law is

$$\ell = 3.27 (g\Delta)^{5/23} V^{10/23} (1-\Delta)^{5/23} (\mu_w \rho_w)^{-1/23} t^{9/23} \qquad (2\text{-}63)$$

The dimensionless coefficient is obtained from the similarity solution of the spreading equations, and will depend on the turbulent velocity profile used. Use of different velocity profiles will yield slightly different results, but the results of the final spreading equation should all be of the same order of magnitude. This order of magnitude

-52-

TABLE 2-2   Values for K, the Flow

Constant (Fay, 1971)

Flow Regime	K, 1-Dimensional	K, Axisymmetric
Inertial	1.5	1.14
Viscous	1.5	1.45
Surface Tension	1.33	2.30

TABLE 2-3   Volume of Oil Spilled for

Each Spill Discussed

Spill	Volume Spilled (m^3)
Santa Barbara	1.3×10^4
Torrey Canyon, total	1.2×10^5
Torrey, Cornish coast	3.0×10^4
Torrey, N. France	3.1×10^4
Torrey, Bay of Biscay	5.1×10^4
Platform Charlie	8.2×10^3
Argo Merchant, Massachusetts	2.7×10^4

predicts a spread of oil slower than that given by the published
laminar equations, for example Equation (2-57).

Secondly, Milgram cites the results of an order of magnitude
comparison of the gravitational and surface tension forces. For
the gravity-viscous regime to be favored over the surface tension-
viscous regime, the ratio F_s/F_g must be much less than one. From
the previous order of magnitude analysis F_s/F_g is

$$\frac{F_s}{F_g} = \frac{S\ell^4}{\rho_w g \Delta v^2} \tag{2-64}$$

where S is a defined in Equation (2-60).
A one million gallon spill typically covers one half of a square
nautical mile. Given the usual oil properties of $\Delta = 0.1$ and
$S = 20\text{-}25$ dyne/cm, the ratio in equation (2-64) is approximately 3.
The order of magnitude analysis demonstrates that the surface tension
forces are larger than the gravity forces, by a factor of four,
contrary to what has heretofore been published in the literature.
Addition of the surface tension forces to the viscous-gravity
regime should yield a faster spreading slick than is predicted
by the published theories.

The spreading process always ends in the surface tension controlled
regime. If the spreading pressure, S, changes from a positive to
a negative value, spreading ceases, the oil forms a lens and does
not thin further. Oil slick thinning has been observed to end before
a monomolecular layer of oil on the surface is attained. Ultimate
slick thickness based on observations is on the order of 2.5×10^{-3} cm.
Figure 2-9 depicts the length of the time in each flow regime as
a function of the volume of oil spilled, based on Hoult's analysis
(Hoult, 1972). For each of the spills previously mentioned, less
than five hours is required for the transition from the inertial
to viscous flow states. Table 2-3 presents the actual volumes
of oil spilled for the aforementioned spills in cubic meters.
Comparison of the volume spilled in the Platform Charlie spill
with the time correlation shows that less than three days are needed

-54-
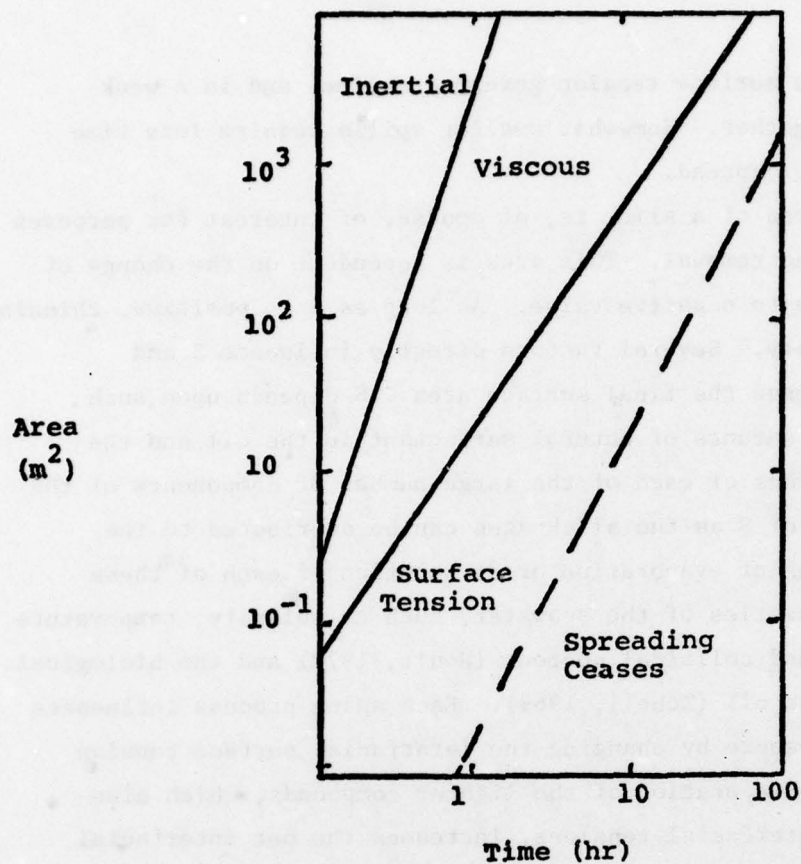
FIGURE 2-9   Flow Regime Length as a Function of the Volume of
Oil Spilled. (After Hoult, 1972.)
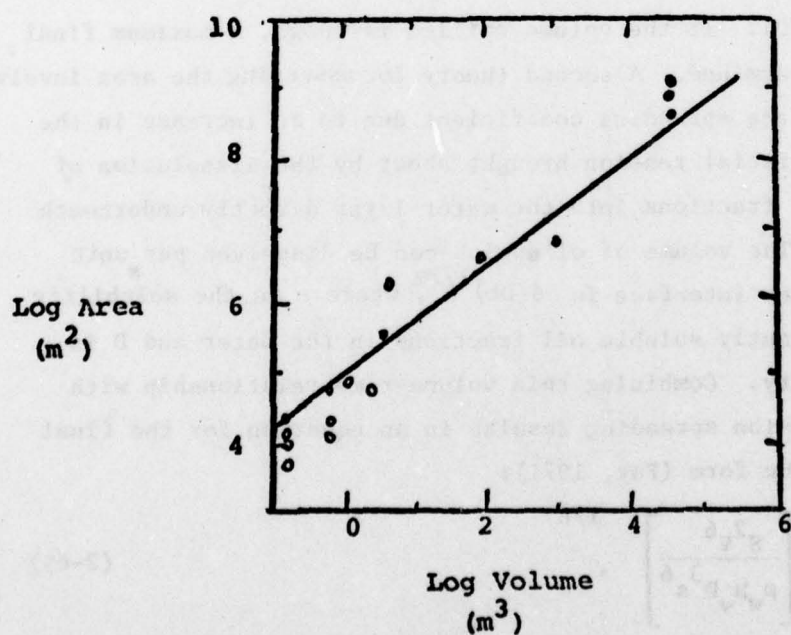
FIGURE 2-10   Maximum Slick Area as a Function of Volume. Field
Data and Theoretical Line Included. (After Fay, 1971.)

-55-

to enter into the surface tension governed regime, and in a week flow ceases altogether. Somewhat smaller spills require less time for termination of spread.

The final area of a slick is, of course, of interest for purposes of containment and removal. This area is dependent on the change of S from a positive to negative value. As long as S is positive, thinning occurs indefinitely. Several factors directly influence S and indirectly influence the final surface area. S depends upon such variables as the amounts of natural surfactant in the oil and the interfacial tensions of each of the large number of components of the oil. The change of S as the slick ages can be attributed to the differential rates of evaporation or dissolution of each of these species, the properties of the seawater, such as salinity, temperature and particulate and colloidal content (Hoult, 1972) and the biological degradation of the oil (Zobell, 1969). Each aging process influences the spreading pressure by changing the interfacial surface tension in some manner. Evaporation of the lighter compounds, which also have the lower interfacial tensions, increases the net interfacial surface tension.

In estimating the final area, it has been empirically noted that the thinnest a real slick ever becomes is 2.5×10^{-3} cm (Garrett and Barger, 1970). If the volume spilled is known, a maximum final area can be determined. A second theory for assessing the area involves a reduction of the spreading coefficient due to an increase in the water/oil interfacial tension brought about by the dissolution of some of the oil fractions into the water layer directly underneath the oil film. The volume of oil which can be dissolved per unit area of oil/water interface is $s(Dt)^{1/2}$, where s is the solubility of the significantly soluble oil fractions in the water and D is their diffusivity. Combining this volume-time relationship with the surface tension spreading results in an equation for the final slick area of the form (Fay, 1971):

$$A = K_a \left[\frac{s^2 V^6}{\rho_w \mu_w D^3 s^6} \right]^{1/8} \tag{2-65}$$

In this relation K_a is a constant of the order of unity. Figure 2-10 is a plot of this equation where one constant replaces s, D, and S, producing the dimensional equation

$$A \ (m^2) \ = \ 10^5 \ [V(m^3)]^{3/4} \qquad (2-66)$$

The typical values of $S = 10$ dyne/cm, $D = 10^{-5} \ cm^2/sec$, $K_a = 1$, and $s = 10^{-3}$ have been introduced. The plot will give a rough estimate of the final slick area for a typical crude.

Evaporation and Aerosolization

Mechanical transport takes place as the oil spreads. At the same time this is occurring another major mode of weathering, evaporation, is also proceeding. In the first two to three days on the water, the slick may lose as much as 30% of its bulk (Parker, et al 1971). Heavier crude oils, such as Tia Juana Pesado (with 78% residue>700°F) will evaporate to a much lesser extent, and much more slowly. Evaporation rates depend primarily on the vapor pressure of the oil at ambient temperature, but high winds will increase evaporation substantially. More oil can be lost to the atmosphere in the form of aerosols and sprays from the crests of waves if the weather becomes rough. Spreading enhances evaporation by providing more area from which evaporation can take place. However, the evaporation of the light fractions generally increases the surface tension and decreases the tendency to spread; this mechanism is self-inhibiting (Berridge, et. al., 1968a).

Blokker (1964) has derived equations for the concurrent spreading and evaporation of oil on water. For the evaporation equation he uses one of the forms of the theoretically-based Pasquill's equation:

for a channel:

$$\frac{dV}{dt} \ = \ -k \ U^{\alpha}_b \ell^{(1-\beta)}_{pM} \qquad (2-67)$$

or for a circular field:

$$\frac{dV}{dt} = -\frac{\pi}{4} k U^{\alpha} D^{2-\beta} pM \qquad (2\text{-}68)$$

where: V is the liquid volume (m^3); U is wind speed (m/s); D or ℓ is the diameter or length of the oil field (m); p is the vapor pressure (mm Hg); M is molecular weight; t is time (min); $k = 12 \times 10^{-8}$ for a neutral atmosphere and a temperature of 2°C. The two additional parameters are defined as

$$\alpha = \frac{2-n}{2+n} \qquad \text{and} \qquad \beta = \frac{n}{2+n} \qquad (2\text{-}69)$$

where n is a turbulence parameter. All oils have a range of boiling points and vapor pressures, and therefore an average vapor pressure must be calculated from the Clapeyron equation:

$$\log \frac{p_{BP}}{p} = \frac{\Delta H^{vap} M}{4.57} \left[\frac{1}{T} - \frac{1}{T_{BP}} \right] \qquad (2\text{-}70)$$

p_{BP} is the vapor pressure at the boiling point T_{BP} (760 mm), ΔH^{vap} is the latent heat of vaporization, and T and p are the absolute temperature and vapor pressure, respectively. Combining the spreading and evaporating equations gives

for a channel:

$$\frac{\partial^2 \ell}{\partial t^2} + \frac{1}{\ell} \left(\frac{d\ell}{dt} \right)^2 + \frac{kh_\infty}{\ell} \frac{d\ell}{dt} + KkU^{\alpha} \ell^{-\beta} pM = 0 \qquad (2\text{-}71)$$

for a circular field:

$$\frac{\partial^2 D}{\partial t^2} + \frac{2}{D} \left(\frac{dD}{dt} \right)^2 + \frac{2kh_\infty}{D} \frac{dD}{dt} + KkU^{\alpha} D^{-\beta} pM = 0 \qquad (2\text{-}72)$$

These equations can be solved either by graphical integration or numerically. Figure 2-11 shows the influence of volume on evaporation

-58-
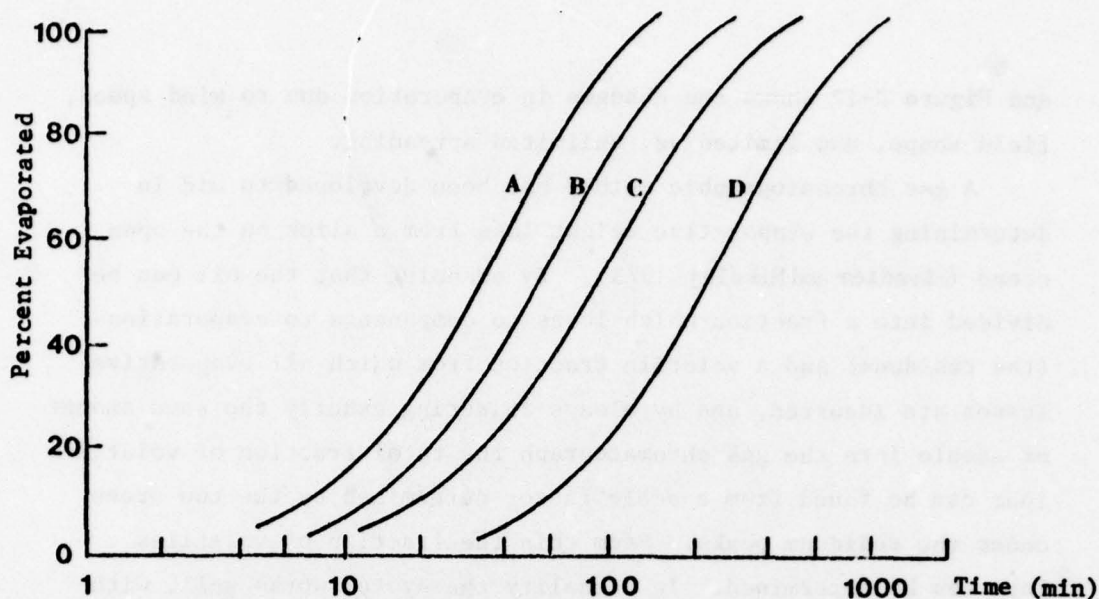
FIGURE 2-11 Influence of Volume on Evaporation and Rate of Spread of Gasoline at Wind Speed of 1 m/s and a Temperature of 2°C (Unlimited Spreading). For Circular Fields: A) 100m³, B) 1000m³; For Channels: C) 100m³, D) 1000m³ Spill Volumes. (After Blokker, 1964.)
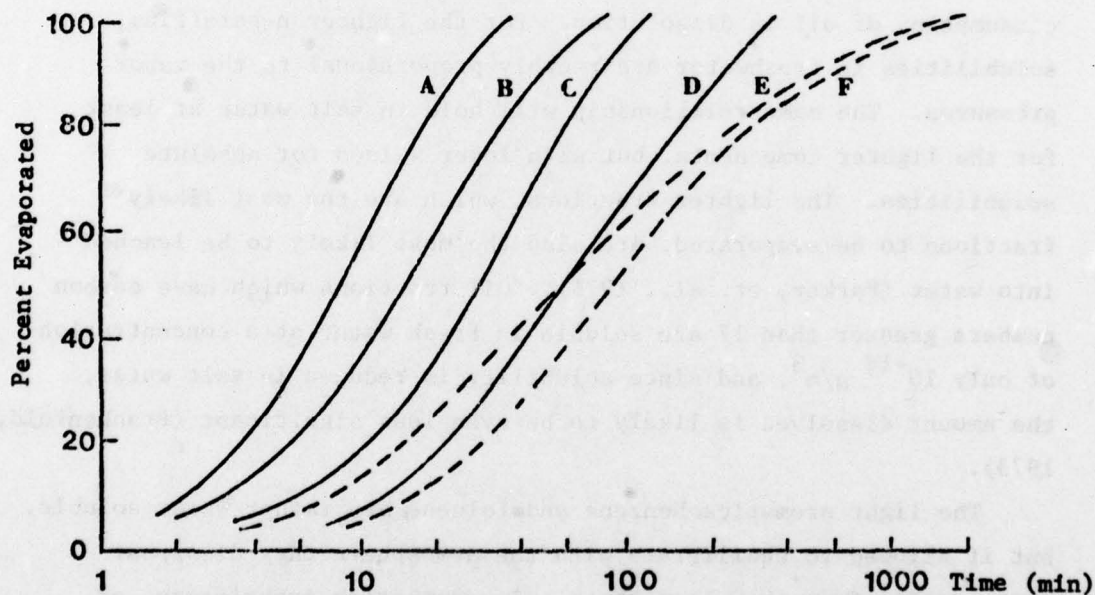
FIGURE 2-12 Influence of Wind Speed on Evaporation and Rate of Spread of Gasoline at 2°C, Spill Volume = 100m³. For Circular Fields: A) 15m/sec, C) 1m/sec, E) 1m/sec; for Channels, 50m Wide B) 15m/sec, D) 1m/sec, F) 1m/sec Wind Speeds. Solid Curve for Unlimited Spreading; Broken Curve for Spreading to h = 0.1cm. (After Blokker, 1964.)

and Figure 2-12 shows the changes in evaporation due to wind speed, field shape, and limited vs. unlimited spreading.

A gas chromatographic method has been developed to aid in determining the evaporative weight loss from a slick on the open ocean (Sivadier and Mikolaj 1973). By assuming that the oil can be divided into a fraction which loses no components to evaporation (the residuum) and a volatile fraction from which all evaporative losses are incurred, and by always injecting exactly the same amount of sample into the gas chromatograph the total fraction of volatiles lost can be found from a scale factor determined by the two areas under the residuum peaks. From this the fraction of volatiles lost can be determined. In actuality the system works well, with slick non-uniformity causing the only uncertainties in the data.

Dissolution

Referring back to Figure 2-8, another process leading to the consumption of oil is dissolution. For the lighter n-paraffins, solubilities in freshwater are roughly proportional to the vapor pressures. The same relationship will hold in salt water at least for the lighter components, but with lower values for absolute solubilities. The lighter fractions, which are the most likely fractions to be evaporated, are also the most likely to be leached into water (Parker, et. al., 1971). Oil fractions which have carbon numbers greater than 17 are soluble in fresh water at a concentration of only 10^{-14} g/m^3, and since solubility is reduced in salt water, the amount dissolved is likely to be even less significant (Frankenfeld, 1973).

The light aromatics, benzene and toluene, are rather water soluble, but if allowed to equilibrate with the atmosphere they disappear very rapidly from the water phase. In weathering experiments, or partitioning experiments, benzene and toluene are not found in the water phase, but some higher aromatics and olefins are indicated (Frankenfeld, 1973). Weathered crudes have much lower soluble fractions than unweathered crudes; just how much lower is dependent on the oil itself.

-60-

Adsorption by Particulates

Another mechanism of oil removal from a slick is by adsorption onto a solid particle with subsequent sinking or floating. Natural small particles suspended in the sea (e.g., fine sand, cell fragments, etc.) may act as sinking agents or adsorbents, but their action will be slow and will contribute little to the overall reduction of the slick size (Berridge, Dean and Fallows, 1968a).

Photochemical Oxidation

While the oil is sitting on the ocean it slowly undergoes chemical reactions, usually oxidation reactions because of the absorption of ultra violet light, which induces an auto-catalytic free radical reaction (Parker, et. al., 1971). The most easily oxidized molecules in crude oil are paraffins and aromatic hydrocarbons with suitable side chains. Tertiary hydrocarbons will be attacked most readily since tertiary C-H bonds are weaker than primary or secondary C-H bonds. Tetralin and cumene are also relatively susceptible to oxidation. Reaction products include acids, carbonyl compounds, alcohols, peroxides and sulphoxides. The majority of these are quite water-soluble and will be leached out of the oil phase (Berridge, et. al., 1968a). In the early stages of exposure, it is unlikely that photo-chemical oxidation contributes much to the overall removal of oil from the bulk (Parker, et. al., 1971).

Microbial Degradation

Still another slow process in the weathering of oil is the bio-logical degradation by aquatic organisms. Pseudomonas (Berridge, et. al., 1968a), dinoflagellates (Hoult and Suchon, 1970), and copepods (Parker, et. al., 1971) are among the organisms capable of utilizing oil as an organic nutrient. The rate of utilization is dependent on availability of other inorganic nutrients such as water, oxygen and nitrate, the temperature of the water (the higher the temperature, the higher the metabolism rate), and the

degree to which the oil is dispersed in the water. Microbial degradation is species-hydrocarbon selective; therefore, for complete degradation more than one species may be necessary (Berridge, et.al., 1968a).

Emulsion Formation

The final mode of aging to be considered is the formation of emulsions. In all crudes tested to date, one type of stable emulsion naturally formed was the W/O emulsion called chocolate mousse. This material is actually a complex dispersion of both water and air in oil, and thus has some properties of a highly viscous foam. Chocolate mousse floats and may contain up to 80% water. When weathered on the sea, it turns after a long time to tarry lumps which degrade no further, but eventually wash up on a coast (Berridge, et.al., 1968a). Major quantities of mousse were first encountered in the Torrey Canyon spill, and mousse has been noted to be associated with literally every spill of crude since then. A definitive study was done by Berridge, Thew and Loriston-Clark (1968b) at Southampton University, Wales on the nature and stability of W/O emulsions. A summary of their results will be presented here. Several different methods were used to produce mousse rapidly in the laboratory. They all were successful not only in forming mousses, but also in forming reproducible emulsions. In fact, it is hard to avoid producing W/O emulsions. All synthetic mousses were equivalent to natural mousses micro- and macroscopically. Rigidity tests revealed that cone penetration decreased with increasing water content - or rigidity increased with increasing water content. Distillate products (gasoline, kerosene) do not form mousses. Two predominantly light fraction oils produced unstable soft mousses which did not have the rigidity most of the emulsions had. Weathered crudes and Bunker C do form mousses. Salinity has no proven effect on mousse formation, but this area should be investigated more completely. Mousse stability was tested by exposure to weather on a tilted glass surface. Time to degradation was recorded. Addition of 0.1% of the surfactant Breaxit

broke the mousses after 2 minutes, at the most. The percentage
residue over 700°F, asphaltene content and vanadium content showed
definite correlations with mousse strength and stability. Porphyrin
compounds have been identified as promoting stable mousse formation
(Canevari, 1969b). High asphaltene mousses are especially stable
for long periods of time (Berridge, et.al., 1968b).

3. SCALING LAWS

The vertical dispersion of oil slicks by breaking waves is a
complex process which cannot be fully described analytically. It is
necessary, therefore, to conduct laboratory experiments in which
dispersion due to small breaking waves can be studied. In order to
draw useful information from these experiments, one must deduce from
theoretical considerations the proper way to scale the results to
at-sea conditions. Scaling laws are developed here for two
quantities:

    (a) the size of the droplets in the dispersion,

    (b) the depth to which these droplets are dispersed.

3.1 Droplet Size

There are two possible length scales which determine the droplet
size in the dispersion caused by a breaking wave. One is the length
scale at which the energy of the turbulence is just large enough
to overcome surface tension forces. This parameter depends on the
size of the breaking wave and the interfacial tension of the oil.
If representative oils are tested in a small wave tank, the size of
this turbulence-related length scale will differ from that at sea.
Therefore, it is important to know how it varies with wave frequency.
The other length scale is the original thickness of the oil slick.
Since laboratory experiments can be performed using full scale oil
thicknesses, this parameter need be considered theoretically only
insofar as it determines the scaling of the turbulence-related length
scale and the functional dependence of droplet size on that length
scale.

The largest length scale of the turbulence due to wave breaking
must be proportional to the height of the breaking wave. Regular
progressive waves break when they attain a height of approximately
1/7th the wavelength.   Since an active wind-generated sea can be
represented as a narrow band process, one can define the "significant"
wavelength to be proportional to g/ω^2 where ω is taken to be the
frequency of the peak of the frequency spectrum $F(\omega)$ or is given by

some integral operation on that spectrum, such as:

$$\overline{\omega}^2 = \frac{\int_0^\infty \omega^2 F(\omega)\, d\omega}{\int_0^\infty F(\omega)\, d\omega} \tag{3-1}$$

The large length scale L of the turbulence due to wave breaking must therefore be proportional to g/ω^2. The velocity, U, associated with these large eddies must be proportional to the wave velocities. Since the phase speed, and the fluid speed at the crest, is proportional to g/ω, one can deduce that the Reynolds number is proportional to the following expression:

$$R = \frac{UL}{\nu} \sim \frac{g^2}{\omega^3 \nu} \tag{3-2}$$

where ν is the kinematic viscosity of the water.

Experimental observations indicate that most droplet splitting occurs in the intensely turbulent bore on the face of the breaking wave. This is the region of the flow which was analyzed by Longuet-Higgins and Turner (1974). Within the bore, velocity differences are on the order of the phase speed, but the largest turbulent length scale L is significantly smaller than a wave height. Although the proportionality expressed in Equation (3-2) is accurate, the Reynolds number which is applicable to the turbulent bore is about an order of magnitude less than $g^2/\omega^3 \nu$. In the following development, the order of magnitude of any constant of proportionality, if known, will be given in parentheses following the sign of proportionality. Thus, Equation (3-2) becomes:

$$R \sim (10^{-1}) \frac{g^2}{\omega^3 \nu} \tag{3-2a}$$

Substituting typical full scale values of ω (2/sec), ν (10^{-2} Stokes), and g (10^3 cm/sec^2), one finds that a typical value of R is 1.2×10^6. The Reynolds number is very sensitive to wave frequency, however. In

small-scale experiments, ω will be about 6, so that the Reynolds number will be on the order of 5×10^4.

Since the Reynolds number is large, one can deduce the existence of an equilibrium range of length scales, as described by Batchelor (1953). In this equilibrium range, the turbulence is isotropic, quasi-steady, and uniquely determined statistically by two parameters: the kinematic viscosity ν, and the specific energy dissipation rate ε. The smallest length scale within this equilibrium range is the Kolmogorov microscale:

$$\eta \simeq (\frac{\nu^3}{\varepsilon})^{1/4} \tag{3-3}$$

The velocity scale is given by:

$$v_\eta \simeq (\nu\varepsilon)^{1/4} \tag{3-4}$$

Experimentally, it is found that:

$$\varepsilon \simeq \frac{U^3}{L} \tag{3-5}$$

Combining Equations (3-3) and (3-5), one gets:

$$\eta \simeq L/R^{3/4} \tag{3-6}$$

In the case of wave breaking turbulence,

$$\varepsilon \sim (10^1) \frac{g^2}{\omega} \tag{3-7}$$

$$\eta \sim (.6) \frac{\omega^{1/4}\nu^{3/4}}{g^{1/2}} \tag{3-8}$$

This last expression demonstrates the relatively weak dependence of the microscale on the macroscale. A factor of 10 in wavelength corresponds to a factor of 1/3 in frequency, and a factor of .76

-66-

in η.   Substituting typical values of ω, ν, and g, one finds that a typical value of η in a breaking wave at sea is 1/180 mm, or 6 microns.

Since there is only one velocity and length scale within the equilibrium range, the energy spectrum in this range can be put in the form:

$$E \simeq v_\eta^2 \; \eta \; E_e(\eta k) \tag{3-9}$$

where k is the wave number of the turbulence. The form of E_e was found experimentally by Grant, Stewart, and Moilliet (1962). Substituting for ϵ and η the expressions in Equations (3-6) and (3-7), one can write:

$$E \simeq \frac{g^{1/2}\nu^{5/4}}{\omega^{1/4}} - \; E_e(\frac{k\omega^{1/4}\nu^{3/4}}{g^{1/2}}) \tag{3-10}$$

Figure 3-1 shows a sketch of E_e. Note that since $E\omega^{1/4}/g^{1/2}\nu^{5/4}$ and $k\omega^{1/4}\nu^{3/4}/g^{1/2}$ are nondimensional, the form of E_e is independent of the size of the breaking wave.

If the Reynolds number of the turbulence is large enough, the equilibrium range of length scales will include an inertial subrange of length scales much larger than η. At these larger length scales, there is negligible dissipation, and the turbulence is therefore independent of the kinematic viscosity. In the inertial subrange, E_e must be of a form which makes E independent of ν. The only form of E_e which does this is $E_e \sim (\eta k)^{-5/3}$, so that

$$E = \alpha\epsilon^{2/3}k^{-5/3} \tag{3-11}$$

Grant, et.al. (1962) found the value of α to be 1.44. Using Equation (3-7),

$$E \sim (?) \; \frac{g^{4/3}}{\omega^{2/3}} \; k^{-5/3} \tag{3-12}$$

$$E \sim \frac{g^{4/3}}{\omega^{2/3}} k^{-5/3}$$

log E_e = log$\left(E\omega^{1/4}/\nu^{5/4} g^{1/2}\right)$

6

4

2

0

−2

Inertial Subrange

−4   −3   −2   0

log $\dfrac{k\omega^{1/4}\nu^{3/4}}{g^{1/2}}$
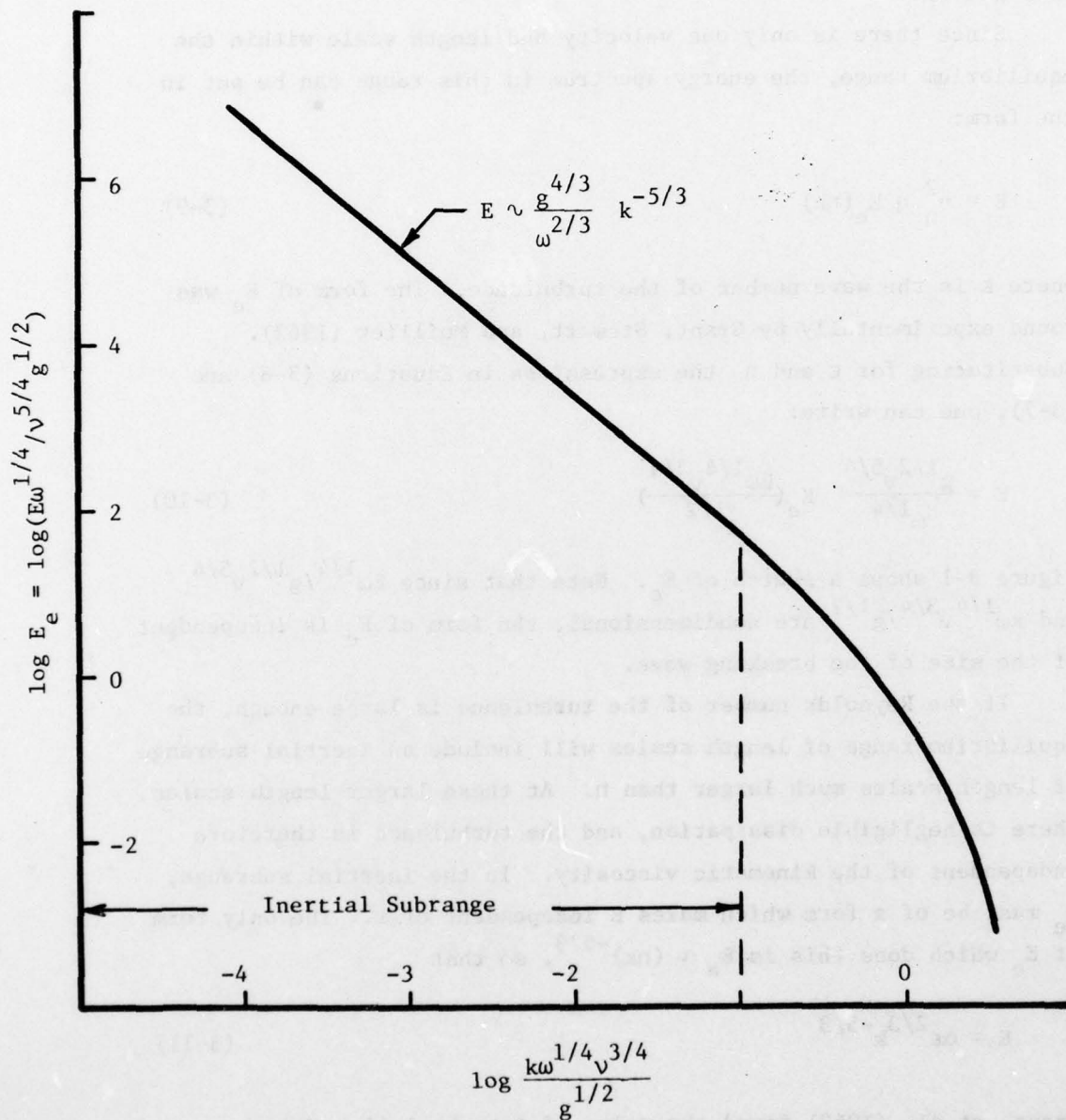
FIGURE 3-1 Equilibrium Range of Energy Spectrum of Turbulence Under
Breaking Ocean Waves

There has been no experimental confirmation of the existence of an inertial subrange within the turbulent bore of a breaking wave. Stewart and Grant (1962) found that an inertial subrange did exist beneath a field of breaking waves, but it is difficult to infer from their results the characteristics of the turbulent bore. It is possible to argue that since the Reynolds number of full scale breaking waves is quite large, the existence of an inertial subrange is quite likely. It is more difficult to make this argument in the case of small-scale experiments.

Under the influence of the turbulence created by wave breaking, an oil slick will be broken up, or split, into many oil droplets. These droplets, in turn, may be split further into smaller droplets. This process continues until the forces tending to split the oil droplets further are balanced by other forces tending to maintain their integrity. Hinze (1955) and Kolmogorov (1949) showed that when splitting occurs in the inertial subrange of the turbulence, the dominant splitting force is that due to dynamic pressures, whereas the dominant resisting force is that due to surface tension. The ratio of these quantities is the Weber number:

$$We = \frac{Td}{\rho v_d^2 d^2} = \frac{T}{\rho v_d^2 d} \tag{3-13}$$

where for the case of oil droplets in water, d is the diameter of the oil droplet, v_d is the RMS velocity difference over a distance d, ρ is the density of water, and T is the interfacial tension. If the Weber number is equal to 1 at a value of d which lies in the inertial subrange, the dominant splitting forces and the dominant resisting forces will be in balance, and the splitting process will cease. The smallest droplet size of the resulting dispersion will be the same order of magnitude as this value of d. If the oil is subjected to the turbulence for a long time, d will be the typical droplet size, since any droplet much larger than d must split eventually.

One does not know a priori that the splitting of oil in a

breaking wave takes place in the inertial subrange. However, one can compute the value of the Weber number at the turbulent microscale η to determine whether splitting takes place on such a small scale. From Equations (3-3) and (3-4), one has $v_\eta \eta \simeq \nu$, and the microscale Weber number is:

$$We_\eta \simeq \frac{T\eta}{\rho\nu^2} \qquad (3-14)$$

Substituting for η from Equation (3-8),

$$We_\eta \sim (.6) \frac{T\omega^{1/4}}{\rho g^{1/2}\nu^{5/4}} \qquad (3-15)$$

Thus, the microscale Weber number is only weakly dependent on wave frequency, whereas the Weber number at the macroscale varies as ω^4. If one substitutes typical values for T (30 dynes/cm), ω (2/sec), ρ (1 gm/cc), g (10^3 cm/sec^2), and ν (10^{-2} Stokes), one finds that the microscale Weber number is on the order of 200 or so. The probability of droplet splitting must become significant only for those size droplets for which the Weber number approaches unity. These droplets are significantly larger than the microscale, and probably lie in the inertial subrange.

Batchelor (1953) gives the following expression for v_d:

$$v_d^2 = 4 \int_0^\infty E(k)(1 - \frac{sinkd}{kd})dk \qquad (3-16)$$

When d is in the inertial subrange of length scales, the integral is dominated by the behavior of the integrand for values of k which correspond to the inertial subrange, so:

$$v_d^2 \simeq 4\alpha\varepsilon^{2/3} \int_0^\infty k^{-5/3}(1 - \frac{sinkd}{kd})dk$$

$$\simeq 4.82\alpha \ (\varepsilon d)^{2/3}$$

$$v_d^2 \sim (10^{3/2}) \frac{g^{4/3}}{\omega^{2/3}} d^{2/3} \qquad (3-17)$$

Substituting this relation into the expression for Weber number (Equation 3-13), one gets:

$$We \sim (10^{-3/2}) \frac{T\omega^{2/3}}{\rho g^{4/3} d^{5/3}} \qquad (3-18)$$

Since the Weber number of the droplets found in breaking waves of different lengths will be a constant of order 1, it follows that the diameter d_o of the smallest oil droplets formed will be:

$$d_o \sim (.12) \frac{T^{3/5}}{\rho^{3/5} g^{4/5} \omega^{2/5}} \qquad (3-19)$$

Therefore, the aforementioned factor of 10 in wave length results in a factor of 0.63 in droplet size.

Substituting the previously mentioned values for T, ω, ρ, and g in Equation (3-19), one finds that the typical value of d_o is about 1/20 mm - or 50 microns. Experimental observations indicate that this value of d_o is representative of the size of the smallest droplets, but not that of the typical droplets. It appears, therefore, that the oil escapes the bore region before the splitting process is complete. Since the time scale of the breaking process is inversely proportional to wave frequency, one might expect the dispersion caused by full scale ocean waves to be more uniform than those observed in the laboratory, so d_o may well represent the typical droplet sizes in these dispersions.

At this point, the dependence of droplet size on oil thickness can be estimated. If the oil thickness is small compared to the size of the turbulent bore, yet large compared with the droplet size as given by Equation (3-19), it will not influence the above results. However, when the oil thickness is small compared with d_o, the size of the smallest droplets will be reduced. The important parameter governing the splitting of the thin slick is still the Weber number, and Equation (3-19) still gives the length scale d_o at which the

inertial forces and surface tension are in balance. However, in this case d_o represents the diameter of the smallest portions of the slick which are broken off to form oil droplets. Since the volume of the droplet must equal that of the slick segment which forms it, one has the following expression for the diameter of the smallest droplets:

$$d_{o\ Thin} \sim 1.1\ d_o^{2/3} h^{1/3} \tag{3-20}$$

where h is the thickness of the slick. This gives:

$$d_{o\ Thin} \sim (.3)\ \frac{T^{2/5} \omega^{4/15} h^{1/3}}{\rho^{2/5} g^{8/15}} \tag{3-21}$$

Since $d_{o\ Thin} < d_o$, these smallest droplets do not split further. However, if the initial splitting of the slick results in droplets larger than d_o, they may split further, and may yield a large population of droplets of diameter d_o.

If the original oil thickness is quite large, and the oil viscosity is significantly larger than that of water, one might expect the turbulence to be damped out more readily than in the absence of the oil. In this case, a weighted average viscosity might be assumed, based on the relative thickness of the oil slick and the turbulent bore on the face of the breaking wave. The effect of this increased viscosity will be an increase in the microscale of the turbulence, and a decrease in the microscale Weber number. However, as long as the microscale Weber number remains significantly larger than 1, there will be no effect on the typical droplet size d_o, which depends only on the structure of the turbulence in the inertial subrange. If We_η is of order 1, or smaller, Equation (3-19) will no longer apply, but droplets will still be formed. In this case, viscous effects are important, and the Weber number is no longer the sole criterion for droplet splitting.

-72-

3.2   Depth of Dispersion

It is observed experimentally that when a wave breaks in an oil
slick, oil droplets are dispersed to depths significantly larger than
the depth of the turbulent bore on the face of the wave, and reach
their maximum depth well after the breaker has passed. It appears,
therefore, that the dispersion is not driven down so much by the
direct action of the breaker, but rather is entrained in the fluid
by the turbulent wake which lies behind the breaker.

Since external (wind) forces acting on a breaking wave are weak,
momentum must be conserved during the breaking process. As the wave
system loses momentum flux, there must be a corresponding increase
in non-wave momentum. This momentum is contained in the breaker's
wake. If $\dot{M}$ is the rate of loss of wave momentum flux per unit crest
length, one can write:

$$\dot{M} \simeq \rho C_p \int_{\text{wake}} u \, dz \tag{3-22}$$

where C_p is here defined to be the phase speed of the wave.

Like all wakes, the wake behind a breaking wave is turbulent,
and tends to become self-preserving. This means that at large dis-
tances behind the breaker there is one length scale and one velocity
scale which characterize the local flow. The best choice for these
are the thickness of the wake, b, and the maximum wake velocity, U_{max}.
One can now write:

$$\dot{M} \sim \rho C_p \, U_{max} \, b \tag{3-23}$$

Since $\partial b / \partial t$ is a local quantity which has the units of velocity, it
must be proportional to U_{max}.

$$\frac{\partial b}{\partial t} \sim U_{max} \tag{3-24}$$

Substituting for U_{max}, one gets:

-73-

$$b \frac{\partial b}{\partial t} \sim \frac{\dot{M}}{\rho C_p} \tag{3-25}$$

Integrating,

$$b^2 \sim \frac{\dot{M} t}{\rho C_p} \tag{3-26}$$

$$b = C \sqrt{\frac{\dot{M} t}{\rho C_p}} \tag{3-27}$$

where C is a constant. This is the classical form of a two-dimensional turbulent wake. The wake behind a breaker resembles one half of the wake behind a solid object which moves in an infinite fluid at the same speed and whose drag force per unit length is equal to $2\dot{M}$. From data presented by Schlichting (1968) for circular cylinders, one can estimate C to be approximately 1.14.

The maximum rate at which oil droplets will be driven down is the difference between the wake growth rate and the terminal velocity W of the oil droplets in calm water:

$$z_o(t) = 1.14 \sqrt{\frac{\dot{M} t}{\rho C_p}} - Wt \tag{3-28}$$

The maximum depth is attained at time t*, given by:

$$\dot{z}_o(t) = 0.57 \sqrt{\frac{\dot{M}}{\rho C_p}} \; t^{-1/2} - W = 0 \tag{3-29}$$

or

$$t^* = 0.32 \frac{\dot{M}}{W^2 \rho C_p} \tag{3-30}$$

The maximum depth $z_{o\;max}$ is obtained by substituting this expression in Equation (3-28):

$$z_{o\;max} = 0.32 \frac{\dot{M}}{\rho C_p W} \tag{3-31}$$

-74-

Thus, the average speed of an oil particle which is driven to $z_{o\ max}$ is W, its terminal velocity in calm water.

The smallest droplet size was previously estimated to be about 1/20 mm. When these droplets are freely rising through sea water, the flow is probably in the Stokes regime. If the viscosity or interfacial tension of the droplets is sufficiently high (Bond and Newton, 1928), their terminal velocity is given by:

$$W = \frac{1}{18} \frac{\Delta \rho g d_o^2}{\mu} \qquad (3-32)$$

where μ is the viscosity of sea water, and Δ is the density difference ratio $(\rho_w - \rho_o)/\rho_w$. Assuming that the flow is Stokesian, the Reynolds number of the flow is:

$$R = \frac{W d_o}{\nu} = \frac{1}{18} \frac{\Delta g d_o^3}{\nu^2} \qquad (3-33)$$

For $\Delta \sim .1$ and the above value of d_o, one finds that the Reynolds number is .007. Schlichting (1968) gives experimental evidence that the deviation of drag coefficient from that predicted from the assumption of Stokes flow is fairly small at Reynolds numbers less than 2, so Stokes flow can be assumed in the development of a scaling law for the depth of oil droplets whose diameters lie between d_o and $7d_o$. Combining Equations (3-19) and (3-21) with the above equation for terminal velocity, one gets the following expressions for the terminal velocity of the smallest droplets created from thin and thick slicks:

$$W_{thick} \sim (10^{-3}) \frac{\Delta T^{6/5} \omega^{4/5}}{\mu \rho^{1/5} g^{3/5}} \qquad (3-34)$$

$$W_{thin} \sim (10^{-2.3}) \frac{\Delta \rho^{1/5} T^{4/5} \omega^{8/15} h^{2/3}}{g^{1/15} \mu} \qquad (3-35)$$

Longuet-Higgins (1969) developed a relatively simple model for wave breaking which predicts that the average wave energy lost per

wave breaking occurrence is equal to the average wave energy. If one
assumes a Pierson-Moskowitz spectrum, this means that the average wave
which breaks loses 8% of its wave energy. Although this model is
crude, it is probably not unrealistic to assume that the energy
(or momentum flux) lost per wave breaking occurrence is a constant
percentage (say 10%) of the breaking wave's energy (or momentum flux).
Making this assumption, one gets:

$$\dot{M} \sim (10^{-2.3}) \rho \, \frac{g^3}{\omega^4} \tag{3-36}$$

Combining Equations (3-31), (3-34), (3-35), and (3-36), one can
form scaling laws for the maximum depths to which the smallest oil
droplets are driven, for thick and thin slicks, respectively:

$$z_{o \atop \text{max} \atop \text{thick}} \sim (1.6) \, \frac{\mu \rho^{1/5} g^{13/5}}{\Delta T^{6/5} \omega^{19/5}} \tag{3-37}$$

$$z_{o \atop \text{max} \atop \text{thin}} \sim (0.32) \, \frac{\mu g^{31/15}}{\rho^{1/5} \Delta T^{4/5} \omega^{53/15} h^{2/3}} \tag{3-38}$$

Non-dimensionalizing on wave height,

$$\frac{z_o}{H} \bigg|_{\text{max} \atop \text{thick}} \sim (1.8) \, \frac{\mu \rho^{1/5} g^{8/5}}{\Delta T^{6/5} \omega^{9/5}} \tag{3-39}$$

$$\frac{z_o}{H} \bigg|_{\text{max} \atop \text{thin}} \sim (0.36) \, \frac{\mu g^{16/15}}{\rho^{1/5} \Delta T^{4/5} \omega^{23/15} h^{2/3}} \tag{3-40}$$

Thus, given the assumptions made here, the relative depth of dispersion
is significantly greater at sea than in the laboratory.

For a 15 m long breaking wave, 2 m high, Equation (3-39) predicts
that the maximum depth of the smallest (50 μm) oil droplets created
from thick slicks is on the order of 50 wave heights - or 100 meters.

Larger droplets will not be driven so far. Droplets with a diameter equal to 5 times that of the smallest droplets (1/4 mm) will be dispersed to 2 wave heights – or about 5 meters.

It was previously pointed out that the average speed at which an oil droplet is dispersed to its maximum depth is its terminal velocity. Since the terminal velocity of a 50 μm droplet of specific gravity 0.9 is about 1/7 mm/sec, it can be seen that the dispersing effect of a wave is not shortlived. In fact, it will take almost 10 days for these droplets to attain their maximum depth. Droplets 1/4 mm in diameter move at 3 mm/sec, or 18 cm per minute. They reach their maximum depth in 20 minutes. Initially, the process is much faster. From Equation (3-28), one finds that some 50 μm oil droplets reach a depth of 1 m in 12 seconds.

It should be pointed out that an implicit assumption here is that the length of the wake (the distance over which the wave breaks) is much larger than z_o. If this is not the case, the theory has to be modified somewhat. The reason that waves break at sea is that they enter regions, or wave groups, where the energy density is too large for them to support. The excess in energy is generally not dissipated by a single wave, but rather by a series of waves. Since the wave group moves at half the wave velocity, each wave breaks one wavelength further downwind (Donelan, et.al., 1972). Therefore, when droplets are very deep, the wake region they see is due to a series of breaking waves, rather than a single breaker. This modification should not affect the basic relationships developed herein, although the constants of proportionality will of course be changed. If z_o is not small compared to the size of the region within which waves break, the classical wake model will no longer reliably predict the maximum depth of the dispersion.

The characteristics of the turbulence within a wake are relatively constant over the depth of the wake, and have the same integral length scales and velocity scales as the wake itself. Since the standard deviation of droplet position scales with the integral length of the turbulence, it appears that the above scaling laws for

-77-

initial dispersed depth also apply at later times, so long as one scales time in units of t* (Equation 3-30). The laws will break down, however, when the predominant source of turbulence is no longer the sequence of wave breaking events which originally created the oil dispersion under consideration.

4.0 THE RISE OF OIL DROPLETS IN THE PRESENCE OF TURBULENCE

When a wave breaks in the presence of an oil slick, the oil is broken up into small droplets which are carried down into the water column by the growing wake behind the breaker. Eventually, the velocity at which the droplets are carried down becomes less than the terminal rise velocity of the particles. At this point, the droplets begin a migration toward the surface. However, the existence of turbulence will cause some droplets to rise more slowly than others. Some may be carried to larger depths by the turbulence. The simplest probabilistic models for predicting the behavior of the oil droplets include the assumption that the instantaneous deviation of an oil drop's velocity from its terminal velocity in calm water is equal to the local water velocity. In other words, the relative velocity between the oil droplet and the water surrounding it is taken to be a constant, equal to the terminal velocity in calm water. This chapter consists of (1) the theoretical justification for this assumption, (2) a review of probabilistic models which are based on it, and (3) the presentation of experimental evidence confirming its validity.

4.1 Theoretical Justification

Friedlander (1957) calculated the mean square relative velocity in any one direction, $\overline{u_R^2}$, between an infinite fluid in a state of stationary turbulence and spherical particles which are much smaller than the Eulerian microscale of turbulence, and such that relative motion between particle and fluid be in the Stokes regime. In this regime, the viscous force on a particle increases linearly with relative velocity:

$$F = fu_R \qquad\qquad (4\text{-}1)$$

where $f = 3\pi\mu d$, μ is the fluid viscosity, and d is the diameter of the particle. His result was:

-79-

$$\overline{u_R^2} = (1 - \gamma)^2 \left[\overline{u_f^2} - \beta \int_0^\infty e^{-\beta\theta} R_p [\theta] d\theta \right] \tag{4-2}$$

where γ is the ratio of fluid density to that of the particle (ρ_f / ρ_p), $\beta = f/m$, m is the particle mass, u_f is the fluid velocity in the direction of interest, and R_p is the velocity correlation seen by the moving particle:

$$R_p(\theta) = \overline{u_f(t) u_f(t + \theta)} \tag{4-3}$$

For small droplets, β is large, and Watson's lemma can be utilized to approximate the value of the integral. The result is:

$$\overline{u_R^2} = 2(1 - \gamma)^2 \frac{\overline{u_f^2}}{\lambda_p^2 \beta^2} \tag{4-4}$$

where λ_p is the temporal Taylor microscale of the turbulence, as seen by the moving particle. This result is valid provided that $\lambda_p^2 \beta^2 \gg 1$. Thus, if $\lambda_p^2 \beta^2 \gg 1$, the mean square relative velocity will be small compared with the mean square turbulent velocities.

If one includes in Friedlander's analysis the effect of gravity, one finds that the above expression still holds if one takes u_R to be the difference between the actual relative velocity and the mean relative vertical velocity, W, which is the terminal velocity of the particle in the absence of turbulence. However, in analyzing vertical velocities, the requirement of Stokesian motion now becomes quite severe, since in mild turbulence the requirement of Stokesian flow reduces to

$$\rho \frac{Wd}{\mu} \leq 1 \tag{4-5}$$

or

$$\frac{1}{18} \frac{(1 - \gamma) g d^3}{\gamma \nu^2} \leq 1 \tag{4-6}$$

For oil of specific gravity 0.9 in water, this requires the diameter of
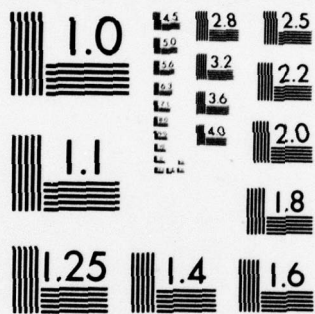
MICROCOPY RESOLUTION TEST CHART

NATIONAL BUREAU OF STANDARDS-1963-A

the oil droplets to be smaller than 0.25 millimeter. In order to ease
this restriction on particle size, one can approximate the $F(u_R)$
curve near the point $u_R = W$ by the first two terms of the Taylor
series about that point:

$$F(u_R) = F(W) - f(u_R - W) \qquad (4-7)$$

or

$$F(u_R) = m(\gamma - 1)g - f(u_R - W) \qquad (4-8)$$

where W and f can be calculated from an empirically derived drag
coefficient. When this is done, Friedlander's result still follows,
provided one substitutes for u_R the difference between u_R and W, and
providing that difference is small enough for the Taylor series
approximation to remain accurate. This will be the case if $|u_R - W|$
is small compared to W. Thus, Equation (4-4) becomes:

$$\overline{(u_R - W)^2} = 2(1 - \gamma)^2 \frac{\overline{u_f^2}}{\lambda_p^2 \beta^2} \qquad (4-9)$$

The velocity correlation $R_p(\theta)$ is the mean product of a fluid
velocity seen by the droplet at one time and that seen by the droplet
at a time θ seconds later. There is a difference in both spatial
coordinates and time between the two velocities correlated. This
correlation can be written:

$$R_p(\theta) = \overline{u_f(0,0)u_f(\int_0^\theta \overrightarrow{u_R} + \overrightarrow{u_f} \, d\tau, \theta)} \qquad (4-10)$$

where the first independent variable is the (vectoral) spatial
position of the particle and the second the time. When the RMS
turbulent velocity is much larger than the terminal rise velocity of
the particle $(\overline{u_f^2}^{1/2} \gg W)$, the particle follows closely the fluid
surrounding it, and the Lagrangian correlation, the reference frame of
which moves at $\overrightarrow{u_f}$, is a good approximation to the actual:

-81-

$$R_p(\theta) \simeq R_L(\theta) = \overline{u_f(0,0) \ u_f(\int_0^\theta \vec{u_f} d\tau, \theta)} \qquad (4\text{-}11)$$

On the other hand, when $W \gg \overline{u_f^2}^{1/2}$, a good approximation is that
correlation which is in a frame of reference moving with the mean
velocity W.

$$R_p(\theta) \simeq \overline{u_f(0,0) \ u_f(\vec{W\theta}, \theta)} \qquad (4\text{-}12)$$

This can be simplified using the assumption of "frozen turbulence",
which also follows from the above assumptions that $W \gg \overline{u_f^2}^{1/2}$:

$$R_p(\theta) \simeq R(\vec{W\theta}) = \overline{u_f(0,0) \ u_f(\vec{W\theta}, 0)} \qquad (4\text{-}13)$$

where $R(r)$ is the Eulerian spatial correlation.

The restriction that particle size be much smaller than the
microscale of the turbulence is not a necessary one. One can argue
that larger droplets will feel only those components of the turbulence
whose length scales are larger than or equal to the droplet diameter.
In the case where $W \gg \overline{u_f^2}^{1/2}$, u_R could therefore be modified by
truncating the integrals defining $\overline{u_f^2}$, $R_p(\theta)$, and λ_p:

$$\overline{u_f^2} = \int_0^{2\pi/d} S(k) dk \qquad (4\text{-}14)$$

$$R_p(\theta) = \frac{1}{2\pi} \int_0^{2\pi/d} e^{ik\theta W} S(k) dk \qquad (4\text{-}15)$$

$$\frac{\overline{u_f^2}}{W^2 \lambda_p^2} = \frac{1}{2\pi} \int_0^{2\pi/d} k^2 S(k) dk \qquad (4\text{-}16)$$

where $S(k)$ is the Fourier transform of the Eulerian spatial correlation
function:

$$S(k) = \int_{-\infty}^{+\infty} R(r) e^{-ikr} dr \qquad (4\text{-}17)$$

-82-

Without these corrections, Equation (4-9) will overestimate the ratio $\overline{(u_R - W)^2}/\overline{u_f^2}$, so the above criteria for this ratio's being small will be conservative.

As a result of the above considerations, it can be seen that two conditions are sufficient to make the assumption that the deviation of particle velocity from the mean is approximately equal to the instantaneous turbulent fluid velocity:

(1) $\lambda_p \beta \gg 1$
(2) Either (a) the relative motion is in the Stokes regime, or (b) $|u_R - W| \ll W$, or $u_f \gg W$.

4.2 Constructing a PDF for Oil Droplet Position

It is clear from the above considerations that under certain circumstances the variance in particle velocity can be approximated to be the mean squared turbulent velocity. Using this fact, Leibovich (1975) derived the PDF for the position at time t of an oil drop released at $z = z_o$ at t=0 in homogeneous, stationary turbulence. He found it to be Gaussian, the variance of position approaching $t S_p(0)$ for rise times large with respect to the integral time of the turbulence. This PDF can be written:

$$p(z,t) = \frac{1}{\sqrt{2\pi t\, S_p(0)}} \exp\left[-(z + Wt - z_o)^2/2t\, S_p(0)\right] \qquad (4\text{-}18)$$

where the "particle-based" spectral density $S_p(\omega)$ is given by:

$$S_p(\omega) = \int_{-\infty}^{+\infty} R_p(\theta) e^{-i\omega\theta} d\theta \qquad (4\text{-}19)$$

The effect of a free surface at z=0 on the PDF of particle position is a complicated one. The simplest treatment is merely to reduce the PDF to zero for z > 0, and to add an "impulse" at z=0 of strength equal to the reduction in area under the PDF.

$$p(z,t) = \begin{cases} \dfrac{1}{\sqrt{2\pi t\, S_p(0)}} \exp[-(z - Wt - z_o)^2 / 2t\, S_p(0)], & z < 0 \\[20pt] 0, & z > 0 \end{cases}$$

$$+\ \delta(z) \left\{ 1 - \frac{1}{2}\, \text{erfc}\left[\frac{Wt + z_o}{\sqrt{2t\, S_p(0)}} \right] \right\} \tag{4-20}$$

The conditional density for droplets, given that they are below the free surface, is:

$$p(z,t;\, z < 0) = p(z,t) \Big/ \frac{1}{2}\, \text{erfc}\left[\frac{Wt + z_o}{\sqrt{2t\, S_p(0)}} \right] \tag{4-21}$$

At times large compared to the average rise time of the droplet from depth z_o, this density approaches its limiting exponential form:

$$p(z,\, z < 0) = Ke^{+Kz} \qquad \text{where } K = \frac{W}{S_p(0)} \tag{4-22}$$

Leibovich made the mistake of assuming that this conditional density describes the position of all the oil, rather than just the oil which is still entrained. The actual large time limit of the complex PDF is:

$$p(z,t) = \begin{cases} Ke^{+Kz}\, \dfrac{1}{2\sqrt{\pi}}\, \dfrac{1}{\alpha}\, e^{-\alpha^2}, & z < 0 \\[20pt] 0, & z > 0 \end{cases}$$

$$+\ \delta(z) \left\{ 1 - \frac{1}{2\sqrt{\pi}}\, \frac{1}{\alpha}\, e^{-\alpha^2} \right\} \quad \text{where } \alpha = \sqrt{\frac{t}{2 S_p(0)}}\left(W + \frac{z_o}{t} \right) \tag{4-23}$$

A more careful treatment of the effect of the free surface would include the fact that it reduces somewhat the density of droplets below it, that is, for $z < 0$. In the absence of a free surface, some of the droplets at a point $z < 0$ are there only after crossing, and recrossing (perhaps more than once) the level $z = 0$. The presence of a free surface would eliminate these possible paths, and the resulting density of droplets below $z = 0$ will be less than the Gaussian distribution, with the difference in area under the PDF concentrated in the impulse at $z = 0$. Raj (1977) attempted to account for this effect, but in order to do so, he assumed a flat turbulence spectrum. This assumption leads to the fact that for each path which crosses the free surface more than once, there is another, equally likely, path which, upon reaching $z = 0$ the first time, follows the mirror image (about $z = 0$) of the first path. Therefore, the subtracted portion of the PDF for $z < 0$, in the case of neutrally buoyant drops, equals the mirror image of the Gaussian PDF for $z > 0$. In fact, however, due to the non-whiteness of the turbulence spectrum, the second path is less likely than the original, and is indeed only possible when the upward velocity of the particle at the first "zero touching" is in fact zero. Otherwise, the reversal of direction requires a step function in velocity which is only possible if there are all frequencies present in the turbulence spectrum.

It should be noted that Raj's result can also be derived from considering the PDF for droplet position in an infinite fluid to be the solution of the following initial value problem:

$$\frac{\partial p(z,t)}{\partial t} = D \frac{\partial^2 p(z,t)}{\partial z^2} - W \frac{\partial p(z,t)}{\partial z}$$

$$(4-24)$$

$$p(z,0) = \delta(z) \qquad\qquad p(\pm\infty,t) = 0$$

where D is the coefficient of eddy diffusivity $S(0)$ and p is the concentration of oil drops. The solution to this initial value problem is the Gaussian distribution of Equation (4-18). If one imposes the boundary condition $p(0,t) = 0$, and takes the case $W=0$, the solution

-85-

consists of the Gaussian Green's function and an image function of
equal but opposite strength, just as Raj found. Therefore, the
requirement for this solution to hold can take two forms: (1) the
turbulence spectrum must be flat, or (2) it must be possible to model
the turbulent mixing process in terms of eddy diffusivity.

It should also be noted that although Raj considers nonstationary
turbulence, he assumes that it is stationary over a time scale equal
to many average rise times of a droplet. Without this assumption,
and the assumption of homogeneity, the Gaussian distribution does
not follow and one must solve the general diffusion equation:

$$\frac{\partial p(z,t)}{\partial t} = D(z,t) \frac{\partial^2 p(z,t)}{\partial z^2} + \frac{\partial p(z,t)}{\partial z} \frac{\partial D(z,t)}{\partial z} - W \frac{\partial p(z,t)}{\partial z} \qquad (4-25)$$

Both spatial and temporal variations in D can be expected at sea.
Within the wake of a breaking wave, the length and velocity scales are
roughly constant with depth, but vary as the 1/2 and -1/2 power of
time, respectively. In the case where $W \gg \overline{u^z}^{1/2}$, $S_p(0) = S(0)/W$,
so $S_p(0)$ (or D) will vary as $t^{-1/2}$. If $W \ll \overline{u^2}^{1/2}$, $S_p(0) = S_L(0)$, so
$S_p(0)$ will be constant with time. Also, the existence of a free
surface is likely to dampen the turbulence in its vicinity, and result
in the existence of some kind of boundary layer there.

4.3 Experimental Verification

In order to confirm the accuracy of the theories discussed above,
a series of experiments was performed in the oil layer flume in the
Ocean Engineering Hydrodynamics Laboratory. In these experiments,
individual plastic spheres, made of low density polyethelene, were
released from a fixed point just behind a turbulence generating grid.
The time it took them to travel from a certain level to the free
surface was timed and the height of the free surface at the moment of
"impact" measured. This procedure was repeated fifty times for each
set of conditions, and the mean and standard deviation of average
rise velocity was computed. This average velocity over a fixed
height is easier to measure than the position in a fixed time, since

-86-

the spheres had to be near the center of the test section to avoid
boundary layer effects. The instantaneous water height had to be
measured to correct for small oscillations in the flume which would
otherwise contribute to deviations in average velocity. Plastic
spheres were used rather than oil droplets due to the difficulty in
generating oil droplets of a precise size. Manufacturing tolerances
of the spheres were checked by releasing a number of them in calm
water and ascertaining that they rose at the same terminal velocity.

Turbulence Grids

Two grids were used to generate turbulence. One was constructed
of 1.27 cm round dowels spaced on 5.08 cm centers horizontally
and vertically, giving a solidity of 0.56. Each dowel was cut away to
one-half of its depth at each intersection, so all dowels lay in a
single plane.

The second grid was made up of slats 0.95 cm thick by 1.90 cm
wide, placed on 3.81 cm   centers in each direction, giving a
solidity of 0.75. They were glued side to side, so that the horizontal
slats lay in a slightly different plane than that of the vertical
slats.

Experimental Variables

The following quantities were varied in the course of the
experiments:

Speed: 15.2, 30.5, 45.7 cm/sec (the 45.7 cm/sec speed
        was used only with the 0.318 cm spheres)

Sphere Size: 0.159 cm, 0.318 cm

Grid: dowel, slat, none

Thus, a total of fifteen sets of experiments were run, each
consisting of the timing of fifty spheres. For each set of conditions
the average distance traveled along the test section before crossing
the first timing mark was recorded as this determines the strength
of turbulence encountered over the timed portion of the rise.

-87-

Prediction of Variation in Rise Velocity

For each set of experimental conditions, the standard deviation of average rise velocity was predicted based on the assumption that (1) the mean square variation in particle velocity equals the mean square turbulent velocity, and (2) the effect of the free surface is negligible.

If h is the distance a sphere rises in time t, W is its terminal velocity in calm water, and u_z is the turbulent velocity in the vertical direction, the above assumption takes the form:

$$h = \int_0^t W + u_z(\tau)d\tau \qquad (4\text{-}26)$$

$$\frac{h}{t} = \frac{\int_0^t W + u_z(\tau)d\tau}{t} \qquad (4\text{-}27)$$

$$\overline{\left(\frac{h}{t}\right)^2} = \frac{\overline{\int_0^t W + u_z(\tau)d\tau \int_0^t W + u_z(\tau')d\tau'}}{t^2} \qquad (4\text{-}28)$$

$$= \frac{\int_0^t\int_0^t W^2 + \overline{u_z(\tau)u_z(\tau')}d\tau d\tau'}{t^2} \qquad (4\text{-}29)$$

For homogeneous, stationary turbulence,

$$\sigma^2 = \overline{\left(\frac{h}{t}\right)^2} - W^2 \approx \frac{\int_0^t\int_{\tau-t}^\tau R_p(\theta)d\theta d\tau}{t^2} \qquad (4\text{-}30)$$

where $R_p(\theta)$ is the temporal correlation of vertical velocities following the sphere. The integral scale of the turbulence as seen by the sphere is:

$$T_p = \int_\infty^\infty \frac{R_p(\theta)d\theta}{R_p(0)} \qquad (4\text{-}31)$$

When the time t during which the sphere rises is large compared with this integral scale, Equation (4-30) becomes:

$$\sigma^2 = \frac{\int_0^t S_p(0)d\tau}{t^2} = \frac{\overline{S_p(0)}}{t} \qquad (4-32)$$

Approximation of $S_p(0)$

$S_p(0)$ is the integral of the correlation function defined in a reference frame moving with the particle. The integral time T_p is defined as this integral divided by the mean square vertical velocity $\overline{u_z^2}$. T_p can be easily measured only in two limiting cases. If W is much greater than $\overline{u_z^2}^{1/2}$, the assumption of frozen turbulence allows one to approximate the integral time T_p as the vertical Eulerian integral length L_z divided by W. This integral length equals $S(0)/(\overline{u_z^2})$, where $S(k)$ is defined by Equation (4-17). If W is much smaller than $\overline{u_z^2}^{1/2}$, the appropriate integral time is the Lagrangian one, T_L, which one can approximate to be $L_z/(\overline{u_z^2})^{1/2}$.

Due to the limited length of the test section, the latter case could not be investigated, so efforts were made to satisfy the requirements of the former case. In order to avoid the requirement for multichannel anemometry, the vertical Eulerian integral length was approximated to be equal to the Eulerian integral time T_e multiplied by mean flow speed U. This approximation is based on rough isotropy between longitudinal and transverse turbulent velocities and the frozen turbulence approximation, which in this case is quite good. Therefore, for the case where W is much greater than u, the RMS velocity, one can write:

$$S_p(0) = \frac{U}{W} T_e u^2 = \frac{U}{W} S_e(0) \qquad (4-33)$$

where $S_e(\omega)$ is the Eulerian frequency spectrum.

Measurement of $S_e(0)$

$S_e(0)$ was obtained by filtering the output signal of a TSI 1050 Series anemometer. This anemometer consisted of a 1051-2D power supply and monitor, a 1054B anemometer, a 1056 decade resistance, and a 1212-20W cylindrical hot-film probe. The probe was oriented vertically, so that only longitudinal components of turbulent velocities contributed to the "effective velocity" to first order in u/U. The unit was calibrated against timed floats to obtain velocity as a function of the voltage. The slope of this curve was used to obtain turbulent velocities from fluctuations in voltage. In order to eliminate the D.C. component of the signal, it was high-pass filtered at about 0.1 Hz. The mean squared longitudinal turbulence velocity was obtained by then squaring the signal and averaging with a 40-second time constant. The value of $S_e(0)$ was obtained by first low-pass filtering the signal at about 1 Hz, and then squaring and averaging. The circuits used for this purpose are shown in Figure 4-1.

The output from the $S_e(0)$ circuit can be represented as

$$\overline{v^2} = \frac{1}{2\pi} \int_{-\infty}^{+\infty} S_{out}(\omega) d\omega \tag{4-34}$$

where

$$S_{out}(\omega) = \int_{-\infty}^{+\infty} R_{out}(\tau) e^{i\omega\tau} d\tau \tag{4-35}$$

and $R_{out}(\tau)$ is the voltage correlation function. Since

$$S_{out}(\omega) = |H(\omega)|^2 S_{in}(\omega) \tag{4-36}$$

where $H(\omega)$ is the transfer function of the filter, if $S_{in}(\omega)$ is defined similarly to $S_{out}(\omega)$, one has:

$$\overline{v^2} = \frac{1}{2\pi} \int_{-\infty}^{\infty} |H(\omega)|^2 S_{in}(\omega) d\omega \tag{4-37}$$

The pass band of the filter was selected to correspond to a frequency range over which S_{in} is nearly constant, so S_{in} can be taken outside the integral, and one gets:

-90-
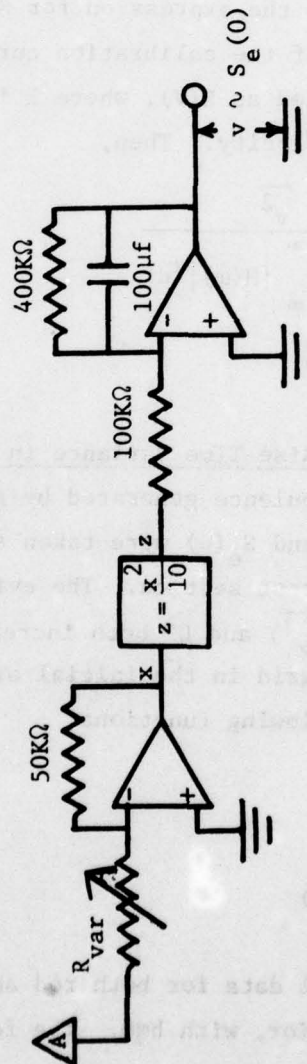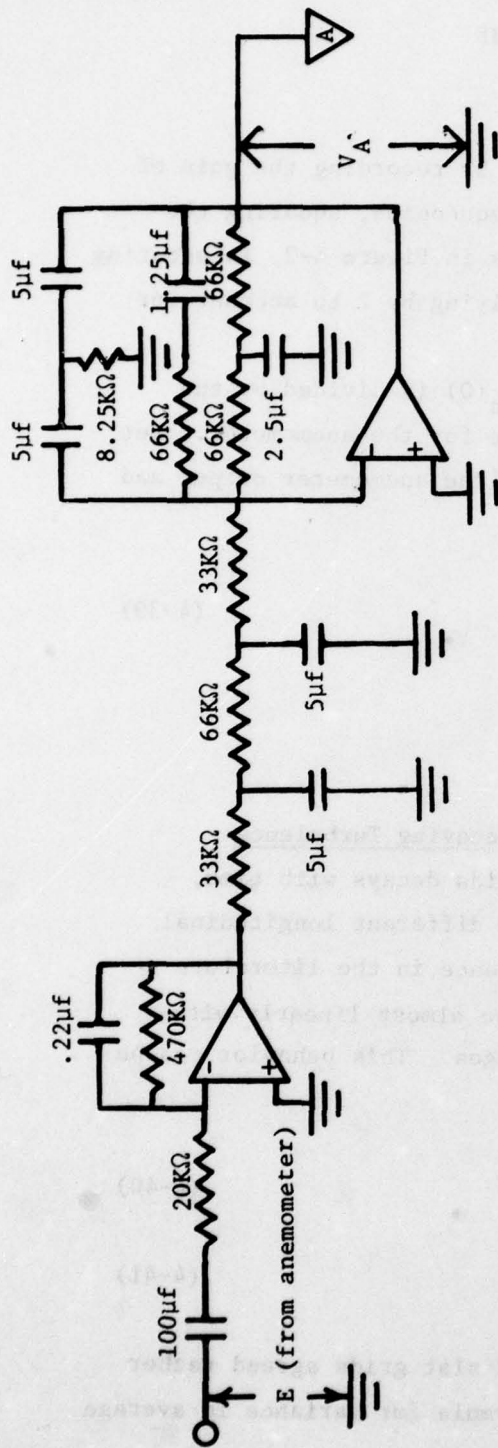
FIGURE 4-1

Circuits for Measurement of $S_e(0)$ and $\overline{u^2}$
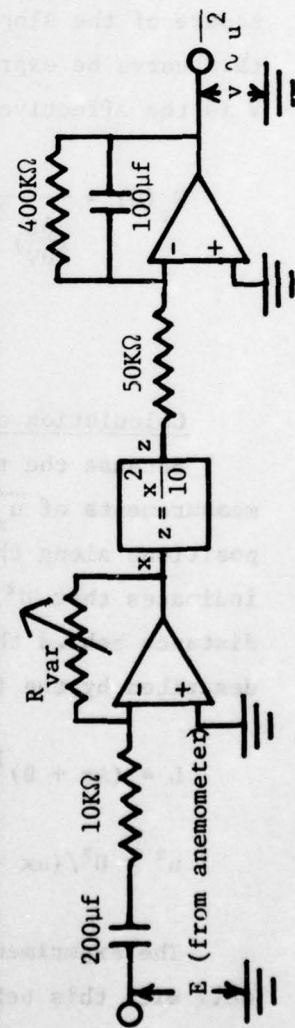
$$S_{in}(0) = \frac{2\pi \overline{v^2}}{\int_{-\infty}^{\infty} |H(\omega)|^2 d\omega} = \frac{\overline{v^2}}{\int_{-\infty}^{\infty} |H(\omega)|^2 df} \qquad (4\text{-}38)$$

The denominator can most easily be obtained by recording the gain of the high and low pass filters at various frequencies, squaring the results, plotting them against frequency, as in Figure 4-2, integrating the resulting curve numerically, and multiplying by 2 to account for the two-sidedness of $H(f)$.

To obtain $S_e(0)$, the expression for $S_{in}(0)$ is divided by the square of the slope of the calibration curve for the anemometer. Let this curve be expressed as $E(V)$, where E is the anemometer output and V is the effective velocity. Then,

$$S_e(0) = \frac{\overline{v^2}}{\left(\frac{\partial E}{\partial V}\right)^2 \int_{\infty}^{\infty} |H(\omega)|^2 df} \qquad (4\text{-}39)$$

Calculation of Rise Time Variance in Decaying Turbulence

Because the turbulence generated by grids decays with time, measurements of $\overline{u_x^2}$ and $S_e(0)$ were taken at different longitudinal positions along the test section. The evidence in the literature indicates that $U^2/(\overline{u_x^2})$ and L^2 both increase almost linearly with distance behind the grid in the initial stages. This behavior can be described by the following functions:

$$L = (Ax + B)^{1/2} \qquad (4\text{-}40)$$

$$u^2 = U^2/(ax - b) \qquad (4\text{-}41)$$

The experimental data for both rod and slat grids agreed rather well with this behavior, with b=0. The formula for variance in average rise velocity becomes:
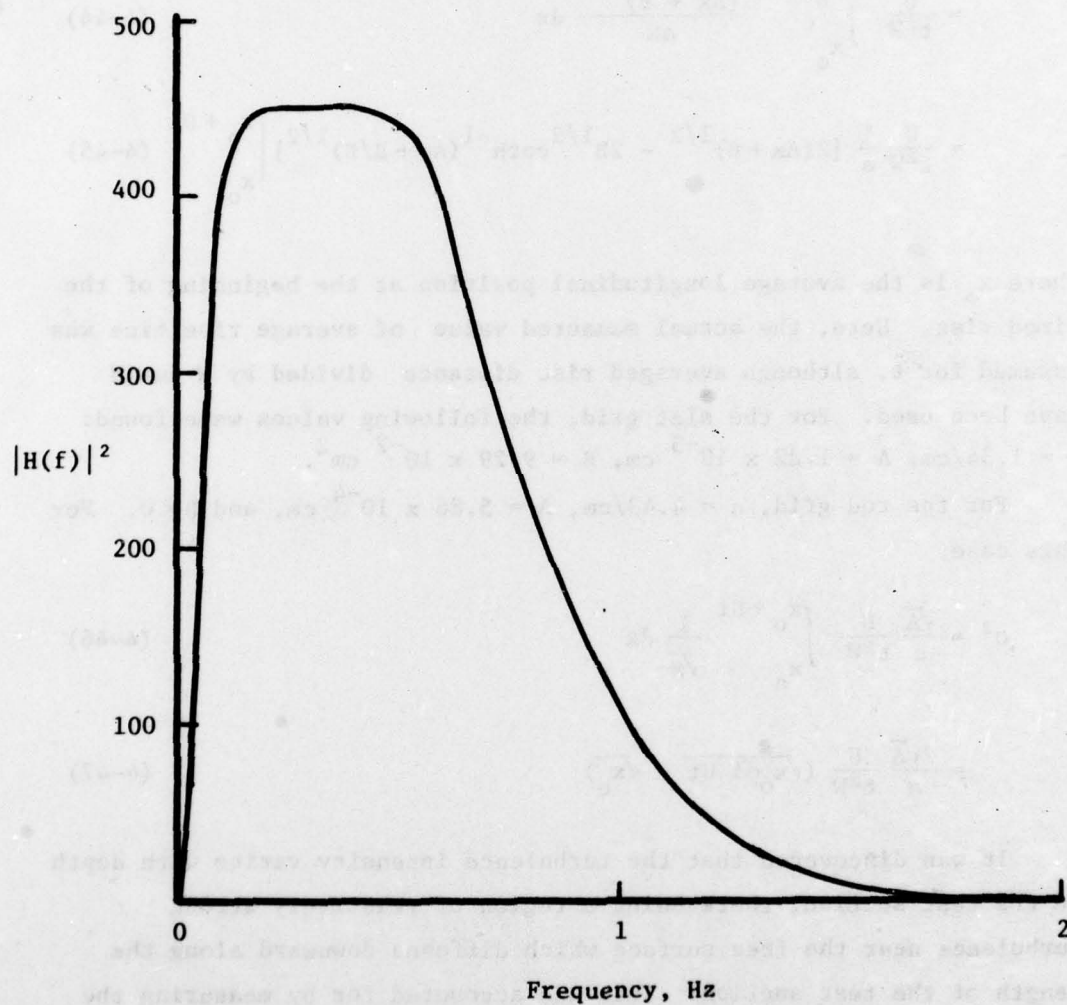
FIGURE 4-2 Square of Gain of Band-Pass Filter in $S_e(0)$ Circuit (V_A/E in Figure 4-1)

$$\sigma^2 = \frac{U}{t^2 W} \int_0^t S_e(0) d\tau \qquad (4\text{-}42)$$

$$= \frac{1}{t^2 W} \int_0^t L\, u^2 d\tau \qquad (4\text{-}43)$$

$$= \frac{U}{t^2 W} \int_{x_o}^{x_o + Ut} \frac{(Ax + B)^{1/2}}{ax} dx \qquad (4\text{-}44)$$

$$= \frac{U}{t^2 W} \frac{1}{a} \left[2(Ax + B)^{1/2} - 2B^{1/2} \coth^{-1}(Ax + B/B)^{1/2} \right] \Bigg|_{x_o}^{x_o + Ut} \qquad (4\text{-}45)$$

where x_o is the average longitudinal position at the beginning of the
timed rise. Here, the actual measured value of average rise time was
assumed for t, although averaged rise distance divided by W could
have been used. For the slat grid, the following values were found:
$a = 1.34/cm$, $A = 1.22 \times 10^{-3}$ cm, $B = 9.29 \times 10^{-2}$ cm^2.

For the rod grid, $a = 4.43/cm$, $A = 5.86 \times 10^{-4}$ cm, and $B = 0$. For
this case,

$$\sigma^2 = \frac{\sqrt{A}}{a} \frac{U}{t^2 W} \int_{x_o}^{x_o + Ut} \frac{1}{\sqrt{x}} dx \qquad (4\text{-}46)$$

$$= \frac{2\sqrt{A}}{a} \frac{U}{t^2 W} \left(\sqrt{x_o + Ut} - \sqrt{x_o} \right) \qquad (4\text{-}47)$$

It was discovered that the turbulence intensity varies with depth
in the test section, there being a region of relatively strong
turbulence near the free surface which diffuses downward along the
length of the test section. This was accounted for by measuring the
extent and strength of this region of increased turbulence at two
positions, estimating the fraction of the time the sphere was in each
region, and multiplying the predicted variance in average velocity
by a correction factor. For example, if it were estimated that for
one-half of the time the sphere was in turbulence whose mean square

-94-

value was twice as large as that predicted by the formulas of
Equations (4-40) and (4-41), the predicted variance would be multiplied
by 1.5.

Determination of λ_p

In order to estimate the inertial effects by use of Equation (4-9),
one must know the value of λ_p, the temporal Taylor microscale. For
isotropic turbulence, Batchelor (1953) gives the relation:

$$\varepsilon = \frac{-15\nu u^2}{\lambda_e^2} \qquad (4\text{-}48)$$

where ε is the specific energy dissipation rate, λ_e is the Eulerian
spatial Taylor microscale, and u is the RMS value of any velocity
component. With the assumption of frozen turbulence, one can
substitute the temporal microscale as observed by a particle moving at
velocity W:

$$\varepsilon = \frac{-15\nu u^2}{\lambda_p^2 W^2} \qquad (4\text{-}49)$$

or

$$\lambda_p^2 = \frac{-15\nu u^2}{\varepsilon W^2} \qquad (4\text{-}50)$$

$$= \frac{-10\nu u^2}{\frac{du^2}{dt} W^2} \qquad (4\text{-}51)$$

$$\simeq \frac{10\nu x}{UW^2} \qquad (4\text{-}52)$$

so that for a given particle, the smallest value of λ_p which will be
encountered during the timed portion of its rise is that at x_o:

$$\lambda_p = \sqrt{10\nu x_o / UW^2} \qquad (4\text{-}53)$$

Determination of η

In order to estimate the effect of particle size in filtering out the smallest scales of turbulence, one must know these scales. The Kolmogorov microscale η is given by:

$$\eta = (\frac{\nu^3}{\epsilon})^{1/4} \qquad (4\text{-}54)$$

or

$$\eta = (-\frac{2}{3}\frac{\nu^3}{\partial u^2/\partial t})^{1/4} \qquad (4\text{-}55)$$

$$\simeq (\frac{2}{3}\frac{\nu^3 x}{U u^2})^{1/4} \qquad (4\text{-}56)$$

For a given particle, the smallest value of η occurs at x_o.

Results

Table 4-1 summarizes the results of the experiments. For each test condition, there is listed the mean and standard deviation of the average rise velocity, along with the predicted standard deviation of average rise velocity. Also shown are those measured quantities which are used in the prediction, and those calculated quantities which support the validity of the theory. The actual and predicted standard deviations are plotted against each other in Figure 4-3. The agreement is judged to be quite good.

In arriving at the predicted standard deviations, the following parameters were assumed to be much greater than unity:

$$\frac{W}{u} , \frac{\beta^2 \lambda_p^2}{2} , (1-\gamma)^2 \beta^2 \lambda_p^2 , \frac{\eta}{d}$$

The first is necessary in order that the "frozen turbulence" approximation be made to convert from spatial to particle-based correlations and spectra. In these experiments, its lowest value was 1.12, which occurred at the beginning of the experiments with small spheres behind

-96-

d cm	GRID TYPE	U $\frac{cm}{sec}$	W $\frac{cm}{sec}$	x_o cm	MAX u $\frac{cm}{sec}$	MIN $\frac{W}{u}$	β sec⁻¹	MIN λ_p sec	MIN $\beta^2\lambda^2$	MIN η cm	MIN $\frac{\eta}{d}$	(h/t) $\frac{cm}{sec}$	$\bar{t}$ sec	σmeas $\frac{cm}{sec}$	σpred $\frac{cm}{sec}$
.318	ROD	15.2	6.38	52	1.01	6.34	24	.088	2.11	.037	.12	5.94	5.55	0.18	0.25
.318	ROD	30.5	6.38	85	1.56	4.10	24	.080	1.92	.028	.09	5.87	5.43	0.36	0.53
.318	ROD	45.7	6.38	116	2.01	3.17	24	.076	1.82	.024	.08	5.79	6.61	0.36	0.71
.318	SLAT	15.2	6.38	52	1.83	3.49	24	.088	2.11	.027	.09	6.33	5.68	0.79	0.66
.318	SLAT	30.5	6.38	85	2.41	3.17	24	.080	1.92	.023	.07	6.30	5.59	1.02	0.91
.318	SLAT	45.7	6.38	116	3.08	2.07	24	.076	1.82	.020	.06	6.33	5.48	1.32	1.25
.318	NONE	15.2	6.38	53	0.37	17.4	24					5.99	6.32	0.11	0.18
.318	NONE	30.5	6.38	116	0.61	10.4	24					5.79	6.40	0.19	0.20
.318	NONE	45.7	6.38	159	0.82	7.74	24					5.26	7.19	0.17	0.32
.159	ROD	15.2	2.25	122	0.67	3.35	40	.384	15.36	.055	.35	2.00	19.2	0.20	0.19
.159	ROD	30.5	2.25	134	1.25	1.80	40	.284	11.36	.034	.21	2.36	6.24	0.64	0.79
.159	SLAT	15.2	2.25	119	1.22	1.84	40	.379	15.16	.040	.25	2.04	18.4	0.33	0.53
.159	SLAT	30.5	2.25	122	2.01	1.12	40	.271	10.84	.027	.17	2.90	7.49	1.37	1.12
.159	NONE	15.2	2.25	153	0.37	6.15	40					1.83	21.1	0.08	0.18
.159	NONE	30.5	2.25	122	0.61	3.69	40					1.54	8.69	0.25	0.33

TABLE 4-¹. Results of Experiments
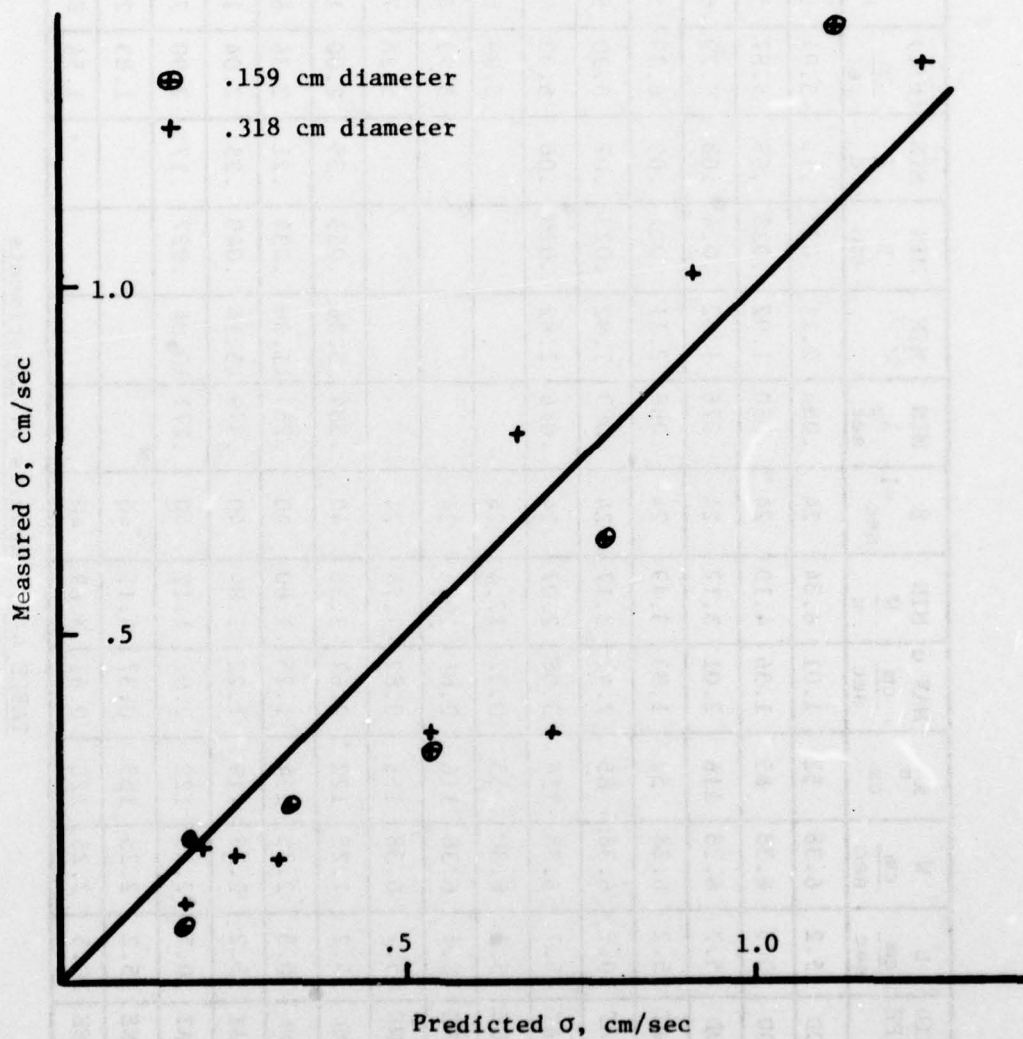
FIGURE 4-3 Comparison of Measured and Predicted Values of Standard Deviation of Average Rise Velocity

the slat grid at 30.5 cm/sec flow velocity. By the end of these particular experiments, it was about 2. The effect of making the assumption that $W \gg u$ when in fact $W \sim u$ is that the calculated values of σ will be too large, although this is not evident in the results.

The assumption that $\beta^2 \lambda_p^2 / 2$ is much greater than unity was assumed in deriving Equation (4-4), when the asymptotic series for the integral in Equation (4-2) was taken to be convergent through the second term. The experiments with the small spheres satisfied this requirement quite well, whereas those with large spheres corresponded to values of $\beta^2 \lambda_p^2 / 2$ of about 1. However, the questionable convergence of the asymptotic series should not cast too much doubt on the smallness of $\overline{(u_R - W)^2}/u_f^2$ which, according to Equation (4-9), includes an additional factor $(1 - \gamma)^2$, which is about 0.006.

The assumption that η/d is much greater than one is obviously not satisfied in these experiments. As discussed above, the primary effect of this would be to "filter out" the large wave number components of the turbulence. Since the predicted values for the standard deviation of average velocity depend on the spectrum at the lowest frequency $S(0)$, it is expected that the elimination of the highest frequencies will not have too much impact on the results. It will serve to increase λ_p, as shown by Equations (4-14) and (4-16), and this will improve the convergence of the series expansion leading to Equation (4-4), and reduce the ratio $|u_R - W|^2/u_f^2$.

In an infinite fluid, the presence of turbulence is not expected to alter the mean rise velocity of a buoyant sphere. The presence of a free surface, however, can, in theory, increase the average rise velocity due to the ability of the free surface to capture spheres at the first "crossing". In the experiments with large spheres, however, a trend was observed whereby for a given grid, the mean rise velocity decreased as flow speed, and therefore turbulence levels, increased. This is shown in Figure 4-4. One possible explanation is the existence of a secondary flow which causes a downward vertical velocity at the centerline of the flume. Presumably this secondary flow will increase

-99-
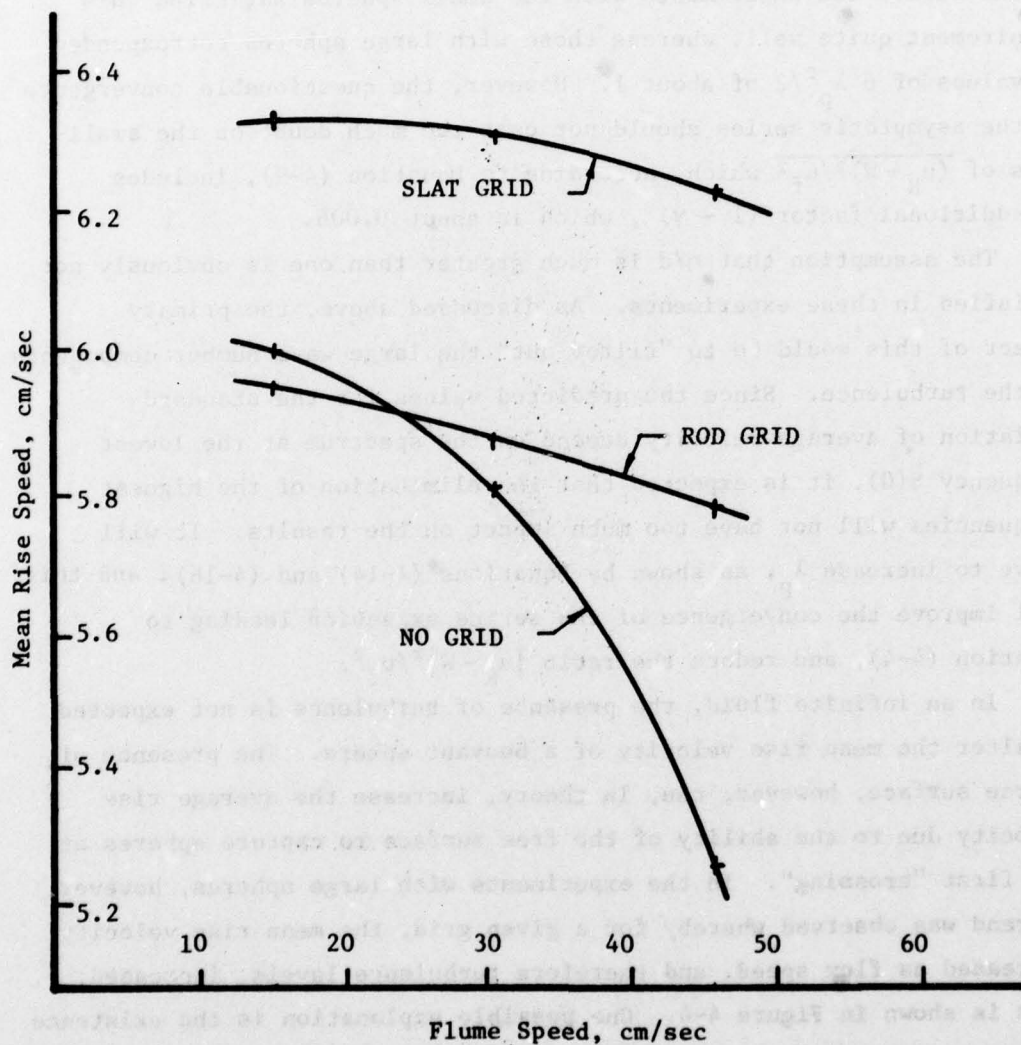
FIGURE 4-4   The Effect of Flume Speed on Mean Rise Speed of Large Spheres

as the flow speed increases, thereby yielding the observed results. The fact that for a given speed the mean rise velocity varies with grid selection could be due to the influence of the grid on the second flow pattern. As the grid becomes more solid, the dependence of mean velocity on flow speed decreases. For the slat grid, all values are within 2% of the calm water case. The smaller spheres evidenced the same behavior in the absence of a grid, but the opposite behavior when grids are present. Quite possibly, the influence of the secondary flow in these cases is overcome by the effect of the free surface in increasing average rise velocities. This latter effect is, of course, strongest in these cases.

Conclusions

It can be concluded from these results that Friedlander's treatment of small Stokesian particles can be extended to particles which are larger than the smallest eddies and well outside the Stokes regime. It is quite probable that all oil droplets at sea which are entrained for significant periods of time behave according to this theory, which is the basis for the work of Leibovich and Raj.

5. **EXPERIMENTS ON THE DISPERSION OF OIL BY BREAKING WAVES**

5.1 Introduction to the Experiments on the Dispersion of Oil by
    Breaking Waves

All accurate sources of information indicate that the major
influence on the dispersion of floating oil into the water column at
sea is breaking waves. These information sources include personal
observations of oil dispersion at sea, the studies of Raj (1977), and
the initial analysis and experiments we have carried out as part of
our studies. Therefore, a particularly important part of our experimental
program is comprised of experiments on the dispersion of oil by breaking
waves. Our experiments were carried out in a relatively small laboratory
facility and were oriented towards providing two important types of
information. The first is a direct determination of how oil slick
properties affect the dispersion of the oil by breaking waves. As
described in §3, it is impossible to achieve exact dimensional
similitude between actual conditions at sea and those in a small scale
laboratory apparatus. However, the laboratory experiments contain
the salient features of the actual mechanism at sea so that the small
scale experiments can be used for determining the relative influence of
the various slick properties such as slick thickness and the physical
and chemical properties of the oil. As described in §3, many aspects
of the smaller scales of the turbulent motion associated with breaking
waves in the laboratory experiments are very similar to actual full
scale conditions. Since many oil droplet diameters at these small
scales have been found to exist both in the laboratory and at sea, some
of our laboratory findings can be used directly for inferring what will
happen at sea. Effects related to the larger scales of the motion,
however, must be considered qualitative in the sense that conditions
leading to a specific quantitative effect on dispersion in the
laboratory may lead to a somewhat different quantitative effect at sea.
However, even in cases where the large scales of motion are important,
we believe that the relative qualitative observations between thick and
thin slicks and between different types of oil will apply to occurrences
at sea. The second type of information our experiments provide relates
to an understanding of the mechanisms that lead to the dispersion of
oil by breaking waves including the distribution of the dispersion both

horizontally and vertically. The overall subject of oil dispersion by breaking waves and associated turbulence is little understood from the standpoint of both overall mechanisms and quantitative details. Theoretical work on this subject is only beginning. Our experiments have suggested to us a means of using dimensional analysis to predict the order of magnitude of effects at sea as we have shown in §3. As additional theoretical analysis is carried out, the results of this analysis can be used for quantitative calculation of dispersion effects for the conditions of our experiments so that the experimental results can be directly compared with the results of the calculations. This will provide a means for evaluating the accuracy of that theoretical work.

The overall philosophy of the experimental program on the dispersion of oil by breaking waves was to subject each oil slick to the same type of breaking wave and then measure the dispersion following the passage of the breaker. Several types of oil slicks were used where the variables were the oil properties and the slick thickness. Since it was desirable to obtain quantitative measurements of dispersion at various times following passage of a breaker, a type of breaking had to be used which generated a single breaking wave in the observation region of our experimental wave channel.

A considerable amount of effort was used in developing the best type of breaking wave for our experiments. Most breaking waves in the open sea occur when a number of waves of differing frequencies have phases that are additive or nearly additive in one region of space with the resulting high and steep wave crest then breaking.

Initially, we planned to do the experimental study by generating a broad band wave group whose phases would be additive at the observation section of our test channel. The wave maker in our wave channel is a hinged paddle. For the broad band wave group, we drove this paddle by a servo-motor controlled with a signal which we recorded on magnetic tape. The signal on the tape was an oscillating signal with an increasing amount of time between adjacent zero crossings so as to produce short waves first and then longer waves which would overtake the short waves

to cause an addition of phases in the observation section. A detailed mathematical analysis was carried out to determine the optimum electric signal to use. Then tests were made using this signal and small variations of it to achieve the most satisfactory wave.

From the standpoint of observation, the broadband wave group produced a very satisfactory breaking wave at the observation section of the channel. However, we encountered one particular disadvantage with this wave; namely, we could not determine the amount of energy lost in breaking. A mathematical analysis was carried out to determine how to find the amount of wave energy passing a vertical section in the tank from measurements of the surface elevation at this section as a function of time. Accurate evaluation of the energy from the measured surface elevation could best be done with a laboratory digital computer. Since we do not have a digital computer in our laboratory at this time, an analog system was built to evaluate the wave energy from the measured surface elevation signal. The system was then used on the wave profiles observed both upstream of the breaking region and downstream of the breaking region with no wave breaking at the positions of measurement. Then, the energy lost in wave breaking should be able to be estimated by the difference in total energy observed at the two measurement stations. However, when we carried out this procedure, we did not find any difference in the energy at the two sections so that we could not evaluate the energy lost in breaking. Our procedure was simply not sufficiently sensitive and accurate to do the required job. As an alternative, we used a different method of generating breaking waves. This was done by installing a horizontal contraction in our wave channel as shown in Figure 5-1. If the wave generating paddle in this apparatus is driven sinusoidally in time, periodic waves propogate along the channel with an amplitude growing so as to maintain constant energy flux in spite of the narrowing of the channel with increasing downstream position. Under such conditions, if the wave height exceeds the critical height for breaking waves of the particular length used, the waves will then break and propagate with continuous breaking along the channel. Previous investigators (Van Dorn and Pazan, 1975)

found that under such conditions the breaking waves keep a constant height with the energy density associated with the contraction then going into breaking. Under such conditions, the rate at which wave energy goes into breaking can be accurately calculated.

For our experiments, the repetitive breaking wave caused by sinusoidal motion of the wave generating paddle in the contracting wave channel would be unsatisfactory. However, we were able to generate a narrow band wave group by running the paddle for only an accurately controlled short interval of time with only a single wave near the center of this group breaking within the observation section of our channel. During the time that the breaking wave is within the central region of the wave group (this being the time that it breaks within the observation section) the breaking wave acts in nearly the same way as a breaking wave in a sinusoidal train passing through a converging channel. Thus, the rate at which energy went into wave breaking could be calculated for our case which had only a single breaking wave within the observation station. Details of the calculation of the energy going into breaking are given in Appendix 1.

Considerable effort was also required in developing a method of measurement of the oil dispersion. Following the passage of a breaking wave through the observation station, the dispersed oil was in the form of droplets of widely varying sizes in the water column. Initially, we planned to measure the number and size distribution of droplets by photographic techniques. Two techniques were investigated. In one technique, light was passed horizontally through the dispersion into the camera. In the other technique, a special illumination source was constructed which generated a vertical column of light having a diameter of approximately 4 cm in the center of our observation section. Then photographs were made with a horizontally facing camera that "looked" through a glass wall in the wave channel. Thus, 90° scattered light was recorded on the photographic film. For both techniques, we found that it was difficult to determine droplet sizes since the diameters of the spots on the film did not correspond exactly to droplet diameters. Secondly, we found it essentially impossible to distinguish some oil droplets from dust particles in the water. Because of these problems,

the photographic techniques had to be abandoned.

The next technique investigated was that of centrifugal separation. This was investigated because of the success in industry of making a similar measurement of the amount of cream in skim milk by centrifugal separation. Since there is only a fraction of a percent of cream in skim milk and since the cream is lighter than the remainder of the milk, the measurement problem has many similarities with the measurement problem for the amount of oil in a dispersion. Of course, such a technique would not yield information on the distribution of droplet sizes, but might yield the total amount of oil in a measurement of a dispersion in a way which required only a modest amount of effort and only a modest expense. Special centrifuges and glassware known as Babcock skim milk bottles have been developed for this test. We obtained a centrifuge and the special bottles in order to test the method on our oil dispersions. Two major problems were found. The first was that in many cases the concentration of oil in our dispersions was substantially less than that which could be accurately resolved by the Babcock test. The second problem was that in some cases we observed that after centrifugation the dark region which might be taken to represent oil in the test bottle actually contained an oil-water emulsion so that it did not accurately represent the amount of oil.

Following the failure of physical measurements for determining the amount of oil in our dispersions, we concluded that the only suitable way of measuring the amount of oil would be by chemical analysis. An investigation of the available chemical techniques indicated that the most suitable one for measurements would be solvent extraction-infrared absorbtion. In this technique, an oil solvent is mixed with a sample of oil-water dispersion, with the solvent containing the oil separating to the bottom of a sample vessel when the solvent is heavier than water, as was the case with the technique we used. The solvent containing the oil is then separated from the water and the infrared absorbtion of a specific path length through the solvent-oil solution is measured. The infrared frequency used corresponds to the fundamental stretching frequency of the C-H bond and the absorption at the wavelength is

determined by the amount of oil that is present. This technique was
far more time consuming and expensive than the physical techniques we
first investigated, but it had to be used to obtain the necessary
information. Our quantitative measurements of the wave dispersions
were supplemented with the useful qualitative information provided by
both still and motion picture photographs of all experimental runs.

5.2 Apparatus

Wave Generation

All breaking wave experiments in this study were completed
in the wave tank shown in Figure 5-1. This tank is constructed of
0.25 inch (0.64 cm) aluminum plate which provides a rigid boundary to
prohibit loss of wave energy due to deformation of the walls, and
glass windows are fitted in the tank to permit observation of under-
water phenomena. A wave generating paddle is located near one end
which is hinged at the tank bottom and is activated by a cyclic mechanical
drive consisting of an electric motor and adjustable reduction gears.
This system is designed to produce waves by transmitting power to the
paddle through an electromagnetic clutch which is controlled by an
electronic timer, thus allowing accurate control of the number of
cycles or fraction of a cycle over which waves are generated. Wave
amplitude may be adjusted by varying the position of mechanical linkage
to the paddle and wave frequency may be changed by alteration of reduc-
tion gear ratios.

The convergence shown in Figure 5-1 was constructed of 0.5 inch
(1.27 cm) plywood sheet supported by 0.5 inch plywood frames. Convergence
dimensions which were used to provide an exponentially decaying channel
width are shown in Appendix 2. Avoidance of wave reflection losses
requires the leading edge of the convergence to be smooth, a criterion
which was satisfied by fairing the convergence to the permanent tank
wall with 0.25 inch (0.64 cm) plywood. Epoxy paint was used to finish
the entire structure surface. The convergence was also fitted with a
glass window adjacent to the wave tank test section window to provide
for variable back lighting to enhance dispersion observation and
photographing. This back lighting technique was used during experiments

-107-
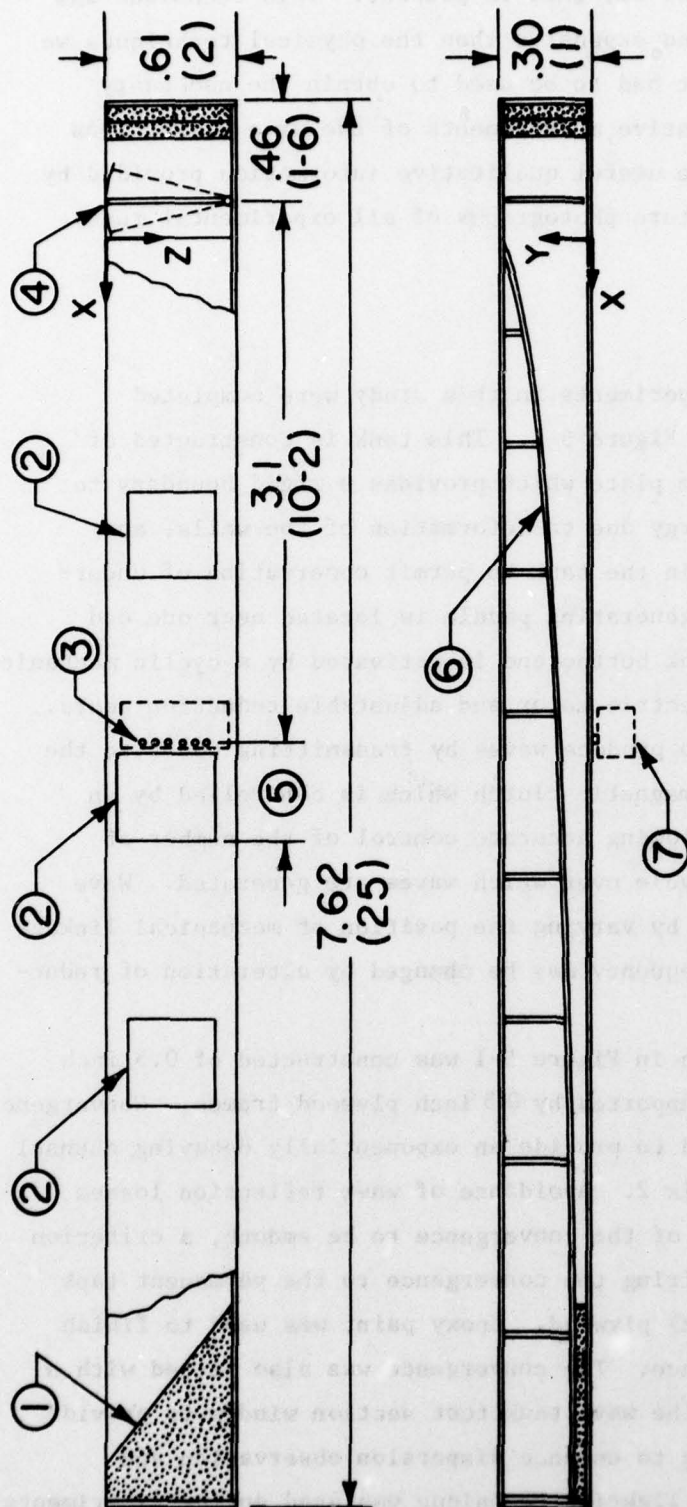
FIGURE 5-1 Wave Tank

1. ARTIFICIAL BEACH
2. OBSERVATION WINDOWS
3. TAPS FOR WATER SAMPLING
4. WAVE GENERATING PADDLE
5. TEST SECTION
6. WAVE CHANNEL CONVERGENCE (SEE APP. 2)
7. WATER SAMPLING SYSTEM (SEE FIG. 2)

DIMENSIONS: METERS
(FEET—INCHES)

.61
(2)

.30
(1)

.46
(1-6)

3.1
(10-2)

7.62
(25)

by directing stage lights at a white translucent plastic plate fitted behind the convergence window, thus producing nearly uniform diffuse lighting conditions.

Installation of the convergence in the tank was completed by placing viton rubber sealing strips at the two ends of the structure between it and the tank wall and securing the convergence in place with steel C clamps. Water filled the region behind the convergence, but was sealed against contamination from oil in the wave channel outside. This technique decreased the cleaning time required when changing to a new test oil.

Reflected waves from the wall at the end of the tank were damped by means of an artificial beach (Figure 5-1). The beach is composed of rubberized horsehair mat which is cut in a triangular shape and proved to be most effective in wave absorbance. This material was disposable and hence very useful in oil slick studies, since it could be discarded after a test with one oil and replaced with clean material for subsequent tests with a different oil. Horsehair was also placed behind the wave generating paddle to elimate splashing during wave production.

Tap water which was filtered to remove particles greater than 40 micrometers served as the wave medium.

Materials which were to be exposed to test water or oil in the wave channel were all tested for chemical leaching to the ambient fluid. This was done to avoid materials which might effect water-air, oil-air, or oil-water surface tensions, thus causing experimental bias of dispersion characteristics. Tests were conducted by exposing proposed material to a water or water-oil mixture in a beaker for several hours followed by surface tension measurements of the fluid to investigate deviation from normal values. None of the materials accepted for use in the wave tank affected surface tension values.

Dispersion Documentation

Recovery of water column samples containing oil dispersions was carried out by use of evacuated bottles which pulled in water through ports located in the tank wall to fill nearly their 250 ml volume.

Sampling by this system, shown in Figure 5-2, was controlled by a common valve handle which simultaneously actuated six ball valves comprising the intake manifold of the system. Water was carried through smooth walled clear plastic tubing into six bottles in a fill time of approximately 1.5 seconds. Bottle evacuation prior to sampling was accomplished through use of a manifold of independent toggle valves which control the connection to an electric vacuum pump. Clean water could be backflushed through the sampler following tests using a purge manifold which was incorporated in the system; hot filtered water was used for this purpose to remove oil deposits which may remain in the intake tubes after sampling a dispersion. Reference was made to the sample positions during tests as Numbers 1 through 6, beginning with the uppermost position.

Photographic techniques were used to supplement the quantitative information resulting from water samples with qualitative visualization of the corresponding dispersion. Sixteen-millimeter high speed motion pictures were taken at a rate of 200 frames per second with a Hycam K2004E camera in order to record the dynamic characteristics of the breaking wave and turbulence generated by the breaker. In addition, still pictures were taken with a Graflex Graphic View camera to document the instantaneous characteristics of the dispersion at the time of sampling.

Measurement Devices

Wave charactetistics were qualitatively recorded by use of a surface elevation gauge which consisted of a small float attached to a lightweight rotating arm connected to a continuous potentiometer. A voltage controlled by the potentiometer was then recorded by a Hewlett Packard 7702B Strip Chart Recorder. The response of the float guage was evaluated by comparing its measurement of waves in water without oil by those made of the same waves with a capacitance wave guage. It was found that the float gauge measurement had to be multiplied by 1.14 to account for float gauge response. Direct output from the float gauge-recorder system is a record of surface elevation vs time history. This record was supplemented in some cases by the addition of a double differentiator circuit which provides a record of vertical acceleration of the fluid surface. The measured peak acceleration had to be multiplied by 1.22 to obtain the actual peak acceleration because

-110-

(a) Sampling Configuration

(b) Purging Configuration
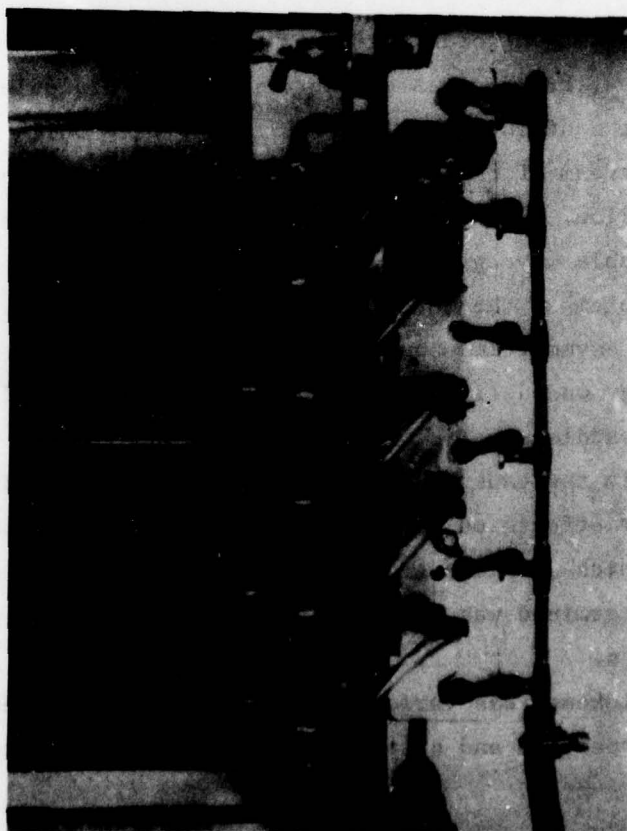
FIGURE 5-2 Dispersion Sampling System

-111-

of imperfect float gauge response.

Oil concentration of the water samples was determined using a Wilkes 5602 Infrared Analyzer. The technique used for this measurement was derived from water quality measurement procedures which use a solvent to remove hydrocarbons from the water for measurement by infrared spectroscopy. It should be noted here that any materials which come in contact with the solvent used to remove hydrocarbons from the water sample must not contain soluble hydrocarbons which might alter oil concentration measurements; for this reason teflon seals were used to replace standard rubber seals found in the sample bottle caps. Further details of the oil concentration measurement procedure are discussed later in the Water Sample Analysis section of this report.

5.3 Test Procedures and Oils

Before actual comparative tests were commenced, the standard conditions of wave characteristics and oil thicknesses (h) were developed.

Tests of a variety of breaking waves were made by using different wave paddle strokes, frequencies and duration of wave paddle motion. A group was sought containing only one breaking wave which commenced breaking well upstream of the test section and continued breaking past the test section. The wave generator settings which resulted in the most favorable wave group gave a paddle frequency of 1.33 Hz, and stroke of 12.6 cm at the waterline. It should be noted that the paddle stroke was asymmetric about its vertical position as shown in Appendix 2. Energy was delivered to the paddle for a period of 1.4 seconds with the paddle starting in its foremost position.

Water depth in the tank was made as large as possible in order to minimize bottom effects on waves and dispersions, and this was limited to the depth at which spillage over the tank walls became a problem. The depth thus determined was 47 cm (18.5 in) which was the standard used for all experiments.

Oil slick thickness was varied in a series of preliminary tests in which slick properties and dispersion characteristics were observed

-112-

during exposure to the standard wave group. A contraint on minimum slick thickness was immediately experienced when some oils did not spread sufficiently to cover the water surface. Hence, minimum slick thickness was dictated by physical properties to be that thickness required to provide a continuous oil slick over the water surface in the wave channel. Thickness was measured by relating the volume of oil placed in the tank to the surface area covered, and the minimum oil volume required was 0.5 liter corresponding to a thickness of 0.55 mm. Maximum slick thickness was arbitrarily set at 5.5 mm using 5.0 liters of oil. These two values of h, 0.55 mm and 5.5 mm, were used as standard slick thicknesses for all experiments and are referred to as "thin" and "thick" slicks, respectively.

Four crude oils, #2 diesel fuel, and heavy mineral oil were all tested using the standard conditions described above. The crude oils were a California crude oil called THUMS (for Tidewater, Humble, Union, Mobile and Shell), an Algerian crude oil called ARZ (for Arzew), an Arabian crude oil called ABL (for Arabian Light) and a Lybian crude oil called ZUE (for Zuetina). The oil properties are given in Table 5-1. Two special tests were also conducted under standard conditions using a particular crude oil at low temperature (cold ZUE), and a heavy mineral oil-surfactant mixture (Heavy Mineral + 0.1% Zonyl A) to investigate viscosity and surface tension effects, respectively.

The procedure outlined below was used to generate and document oil dispersions under standard conditions for each of the six test oils.

STANDARD TEST PROCEDURE

(1) Wave tank and convergence cleaned using a high pressure spray of hot water-soap (Alconox) solution, then rinsed with a high pressure spray of hot water.

(2) Convergence installed.

(3) Tank filled with filtered water near room temperature to 47 cm (18.5 in) depth, and water surface skimmed for one hour.

OIL	TEMP (°C)	SG	Δ*	ν (cSt)	μ (cP)**	T_oa (d/cm)	T_ow (d/cm)
ARZ	26.0	.804	.196	3.62	2.91	24.6	29.3
ABL	23.0	.860	.140	9.80	8.43	26.3	28.6
THUMS	26.5	.934	.066	145	136	29.9	24.0
ZUE	25.0	.822	.178	4.91	4.04	24.3	23.1
COLD ZUE	4.5	.833	.167	32.0	26.7	26.4	21.4
No. 2 DIESEL	25.0	.834	.166	3.34	2.79	26.9	22.6
HEAVY MINERAL	31.2	.878	.122	99.2	87.1	29.9	40.5
HEAVY MINERAL + ZONYL A (0.1%)	20.5	.879	.121	207	182	29.6	1.20

$* \quad \delta = 1.0 - SG$

$** \quad \mu = \rho\nu$

TABLE 5-1

-114-

(4) Ceased skimming and waited thirty minutes before recovering a sample from the tank to conduct water-air surface tension measurement. A minimum surface tension of 64.0 dynes/cm was required and skimming was resumed if this criterion was not met. (This additional skimming was rarely necessary.) When water-air surface tension was satisfactory, it was recorded and the procedural sequence resumed.

(5) Placed 500 ml of the oil to be tested into the tank to create a thin slick (h=.55 mm).

(6) Surface samples of oil and water were recovered in order to make T_{oa}, T_{ow}, SG, and ν measurements. Water/oil temperature also measured and all these values were recorded as pre-test data.

(7) Wave generator settings were checked and one or two preliminary waves generated to ensure the presence of standard conditions. Four consecutive breaking waves were then generated for purposes of sampling and filming the dispersions. Samples were taken at 2, 5, 10, and 20 seconds after passage of the breaker, using a separate wave for each case. Each case required removal of sample bottles from the sampler and acidification of samples to a pH of 2.0 using 5N sulfuric acid to prevent subsequent biological action. The sampler was purged after each case to remove contaminants. Sufficient time was allowed between these cases to permit the oil to return to a continuous slick and for visible dispersed oil to return to the surface. High speed motion pictures were taken of passage of each breaker, and a still photo was taken at the time of sampling for each test case.

(7a) After testing several oils, the effect of oil

-115-

properties on wave characteristics became of
interest. Measurement of wave height in the
presence of the oil slick using the float
guage before and after the test series for a
given oil thickness was incorporated in
standard test procedures.

(8) Surface samples were recovered and T_{oa}, T_{ow},
SG, ν, water temperature, and T_{wa} were
measured and recorded as post test data.

(9) The test oil was skimmed from the tank and
collected for disposal. The tank was drained
and rinsed with a high pressure hot water
spray using no soap.

(10) Steps (5) through (9) were then repeated using
5.0 liters (rather than 0.5 liter) to create
a thick slick (h=5.5 mm).

Situations were encountered during attempts to carry out the
standard test procedure which required modification of those procedures
in order to complete testing in a manner as close to the standard
procedure as possible. These situations involved ABL, Cold Zue, and
Mineral oil tests.

Due to the resistance to spreading exhibited by ABL and Mineral
oil described in the previous section, the thin slick test for ABL
was modified by increasing the amount of oil used, and thin tests for
mineral oil had to be aborted. Additional ABL crude was added to the
tank after the standard 500 ml until the increased oil volume forced
the lenses to join, forming a continuous slick. A total of one liter
was placed in the tank so that the slick thickness for thin ABL tests
was 1.1 mm, double the standard value. The same technique was attempted
with Mineral and Mineral + Zonyl A oils, but the oil volume necessary
to form a continuous slick approached 5 liters, the volume to be used
in thick slick tests, so that thin tests would vary little from the
standard thick slick tests. Thin slick tests for mineral oils were
therefore abandoned.

The Cold Zue experiment was designed to isolate the effects of oil viscosity on dispersion characteristics by reducing oil/water temperature, thereby changing ν while holding all other oil characteristics constant. All test oils were analyzed as possible candidates for this test, but Zue proved to have the most temperature dependent viscosity. The standard test procedure was executed on this oil a second time with the exception that 800 lbs of ice were placed behind the convergence to lower water/oil temperature during test runs. Since so much ice was not readily available in the laboratory, optimum use of this ice was desired. It was felt that the same tank water could be used for both thin and thick slick tests if proper precautions were taken to ensure no experimental bias in thick slick tests which were to be conducted following thin slick studies. Following thin test, all oil was skimmed from the tank and wiped from the wave channel walls. A two-hour delay then enabled all dispersed oil to surface and in the final thirty minutes of this delay skimming was again carried out to remove surfacing oil. The water-air surface tension was then measured and found to be comparable to the initial value before tests were conducted, thus indicating a very low concentration of oil on the surface and implying low oil concentrations everywhere within the tank. Thick slick tests were then carried out according to the standard test procedure.

Interfacial tension effects were investigated in the Mineral + Zonyl A experiment where a second test was run on heavy mineral oil to which 0.1% (by volume) of the surfactant Zonyl A was added to produce a mixture with reduced oil-water tension. The standard test procedure was used to evaluate dispersion characteristics for this oil-surfactant mixture. It was suspected that inhomogeneous migration of the Zonyl A might bias the test, so an additional experiment was conducted to study this possibility. The approach and results of the additional experiment are presented in Appendix 3.

A supplementary experiment was conducted to investigate the nature of the oil slick after exposure to breaking waves. The Mineral + Zonyl A slick in particular showed obvious entrainment of air or water bubbles into the oil, and it was suspected that other oils might also contain less visible entrainment. The experiment which was conducted to study entrainment is described in Appendix 4.

Water and Dispersion Sample Analysis

Determination of oil concentration found in water samples from
oil dispersions was completed using a technique developed for use
in water quality measurements. The procedure used in this study
was closely modeled after the techniques prescribed by the Mirian
Application Report #1 (Wilkes Scientific Corp., 1972) and by a
procedure proposed for ASTM 19.06 (Cleary, 1977).

Calibration samples were made by placing 0.001, 0.01, 0.1, and 1.0
ml of a given test oil in 200 ml of filtered tap water, thus providing
mixtures of known concentrations of 5, 50, 500, and 5000 ppm (parts
per million) respectively. The samples were then acidified to a pH
of 2.0 according to the requirements of the referenced procedures,
using 5N sulfuric acid. Additional samples with concentrations of
20 and 200 ppm were sometimes tested to provide additional data
points.

Actual dispersion samples and calibration samples were analyzed
using an identical procedure. The oil-water mixture was poured from
the sample bottle into a separatory funnel, and 8 ml of Freon or
carbon tetrachloride solvent was poured into the empty sample bottle.
The bottle was then capped with its original sealing cap and shaken
to remove oil deposits from the bottle sides and teflon cap liner.
The solvent was subsequently poured into the separatory funnel with
the water sample. The funnel was then capped and shaken for two
minutes with intermittent loosening of the cap to permit off-gasing.
Because the solvent is heavier than water, it settles, carrying with
it oil removed from the water during shaking. After sufficient
settling time, usually about twenty minutes, the oil laden solvent
was drained from the separatory funnel into a 25 ml volumetric
flask. This procedure including sample bottle wash with solvent,
water-solvent mixing, solvent settling, and solvent drainage was
repeated twice more and the volumetric flask finally filled to 25 ml
with additional solvent. If any water was present in the solvent,
it was allowed to rise to the surface and removed with a syringe.

The extract contained in the flask was mixed well by shaking the

capped flask, and approximately 2.5 ml was then immediately poured into a 1 cm optical path-length quartz cell (cuvette) for infrared analysis. All extracts were tested by placing the cuvette in the infrared analyzer and were evaluated at a wavelength of 3.41 microns, which is the fundamental stretching frequency of the C-H bond, and an optical slit opening of 1.0 millimeters. The absorbance reading given by the analyzer is an indication of the hydrocarbon concentration of the sample and when calibrated by samples of known oil concentration, yields absolute oil concentration values. If the absorbance reading for a particular extract was too high and off scale, that extract was diluted using additional solvent and the product of the dilution factor and absorbance of the diluted extract was used as an extrapolated absorbance value.

Calibration curves were generated for each test oil by plotting absorbance vs. oil concentration on log-log paper for each corresponding set of calibration samples. These calibration curves are given in Appendix 5. All the water samples taken of oil dispersions generated in this study were analyzed for absorbance by the above technique and corresponding oil concentrations were subsequently determined by entering the calibration curves.

In addition to chemical analysis, the photographs proved useful in understanding dispersion effects. Figure 5-3 shows two of the photographs as an example.

5.4 Data

Oil Dispersion Data

Figures 5-4 through 5-19 are based on data obtained using the standard test procedure described previously. The discrete data points are actual oil concentrations measured from individual sample bottles. The curves connecting these points are hand-drawn and serve as an aid to visualization only, although it is likely that the curves follow actual oil concentration, since the observed dispersions were generally continuous over depth.

Tables stating oil properties represent those values measured immediately before and after the tests represented on the same graph. Explanations for substitute or auxiliary tests, which are identified by a suffix letter, are listed below.

TEST	DESCRIPTION
2A	Reproduceability check, three hours had elapsed and about ten waves run between this test and Test 2.
5A	Test 5 failed due to only partial filling of a sample bottle; Test 5A was run immediately thereafter.
5C,6A,7A,8A	These tests were run as reproduceability checks with Tests 5A, 6, 7, and 8 respectively; about one hour had elapsed and four waves run between any test and its mate.
10A	This test was conducted as a check on oil aging; about one hour elapsed and four waves were run between Tests 10 and 10A.
10B	This test was conducted as a check on static oil aging; about two hours elapsed in the absence of breaking waves between Tests 10A and 10B.
10C	Test 10C was a static oil aging test; seventeen hours in the absence of breaking waves elapsed between Tests 10B and 10C.
24A	Test 24 was a failure due to only partial filling of a sample bottle; Test 24A was run immediately thereafter.
45-52	The high viscosity of cold Zue crude made interfacial tension measurements by the standard method of pulling the Tensiomat ring up through the interface difficult because no clean break was noted as the ring passed into the oil. Interfacial measurements (T_{ow}) were therefore made by lowering the ring through the interface and monitoring the break into water.

The units of measure listed for fluid characteristics are centi-poise and dynes per centimeter for absolute viscosity (μ) and surface tensions (T_{wa}, T_{ow}, T_{oa}), respectively.
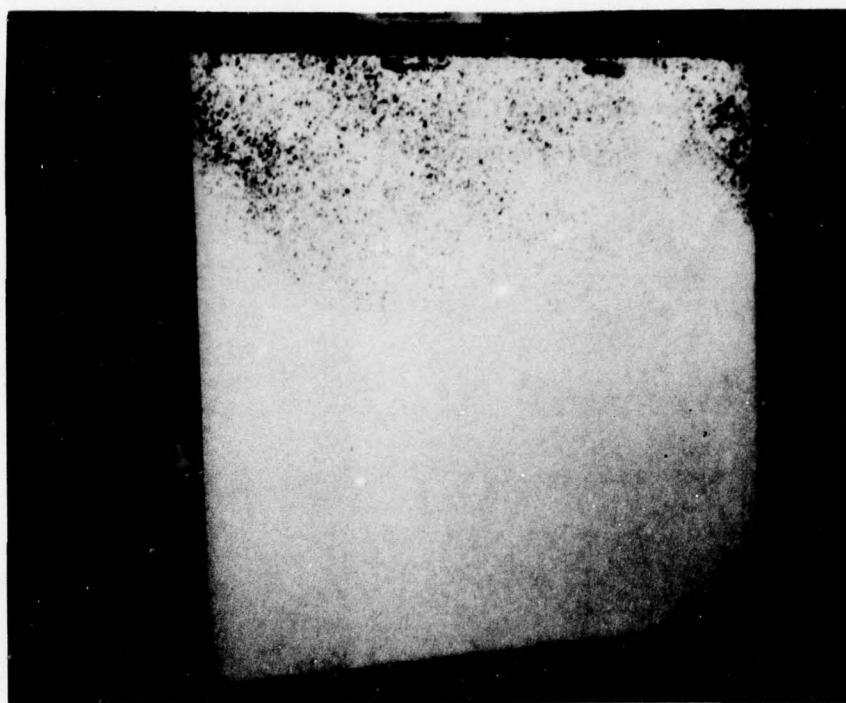
(a) 2 sec After Breaker Passage
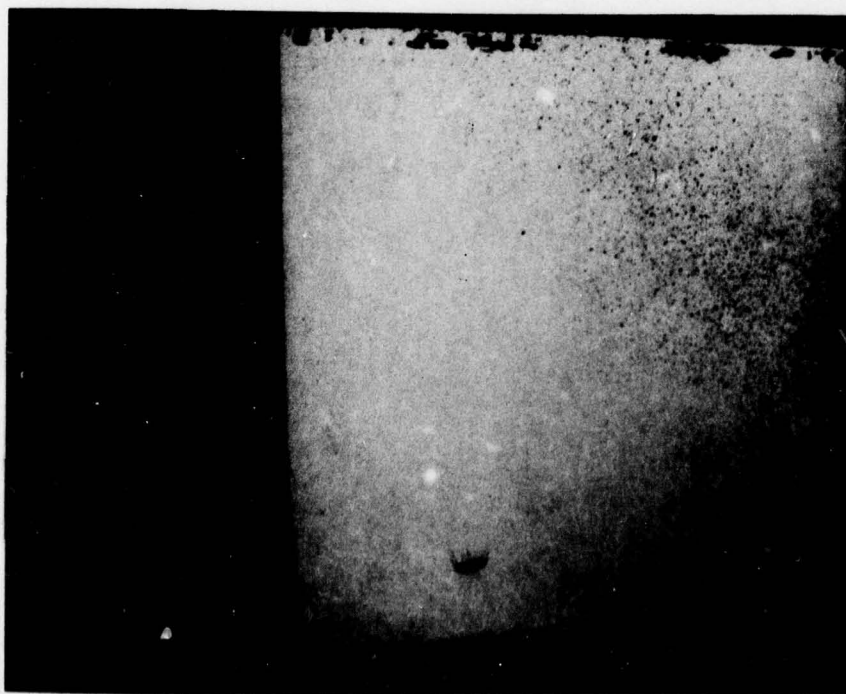
(b) 10 sec After Breaker Passage

FIGURE 5-3 ZUE Crude Dispersions

-122-
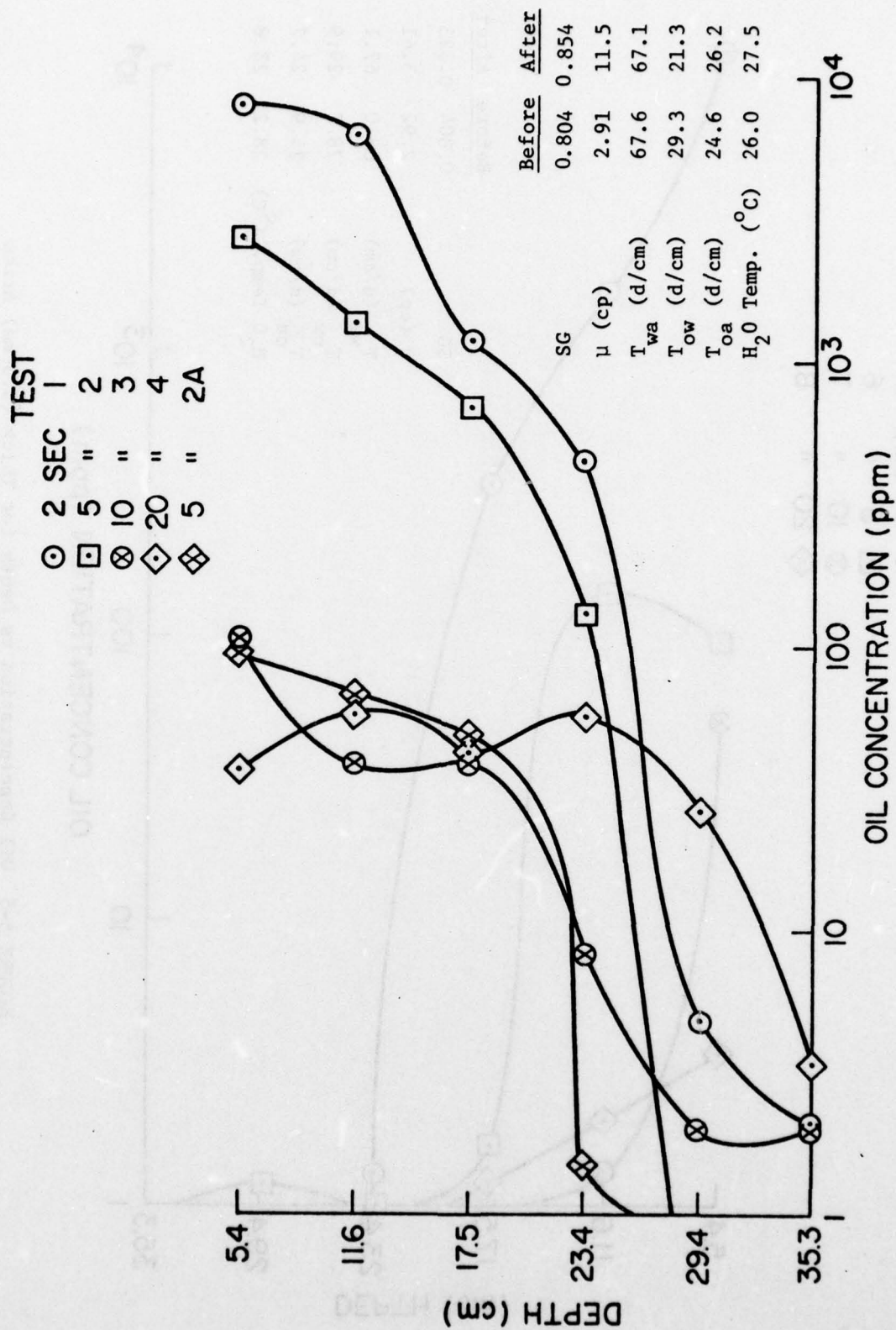
FIGURE 5-4 Oil Concentration vs Depth for Thin (0.55 mm) Arzew

TEST

⊙ 2 SEC 5A
▣ 5 " 6
⊗ 10 " 7
◇ 20 " 8

	Before	After
SG	0.804	0.823
μ (cp)	2.92	3.61
T_{wa} (d/cm)	68.0	67.1
$T_{ow.}$ (d/cm)	28.7	29.9
T_{oa} (d/cm)	24.9	24.7
H_2O Temp. (°C)	28.2	28.8

OIL CONCENTRATION (ppm)

DEPTH (cm)

10^4 10^3 100   10   1

5.4 11.6 17.5 23.4 29.4 35.3
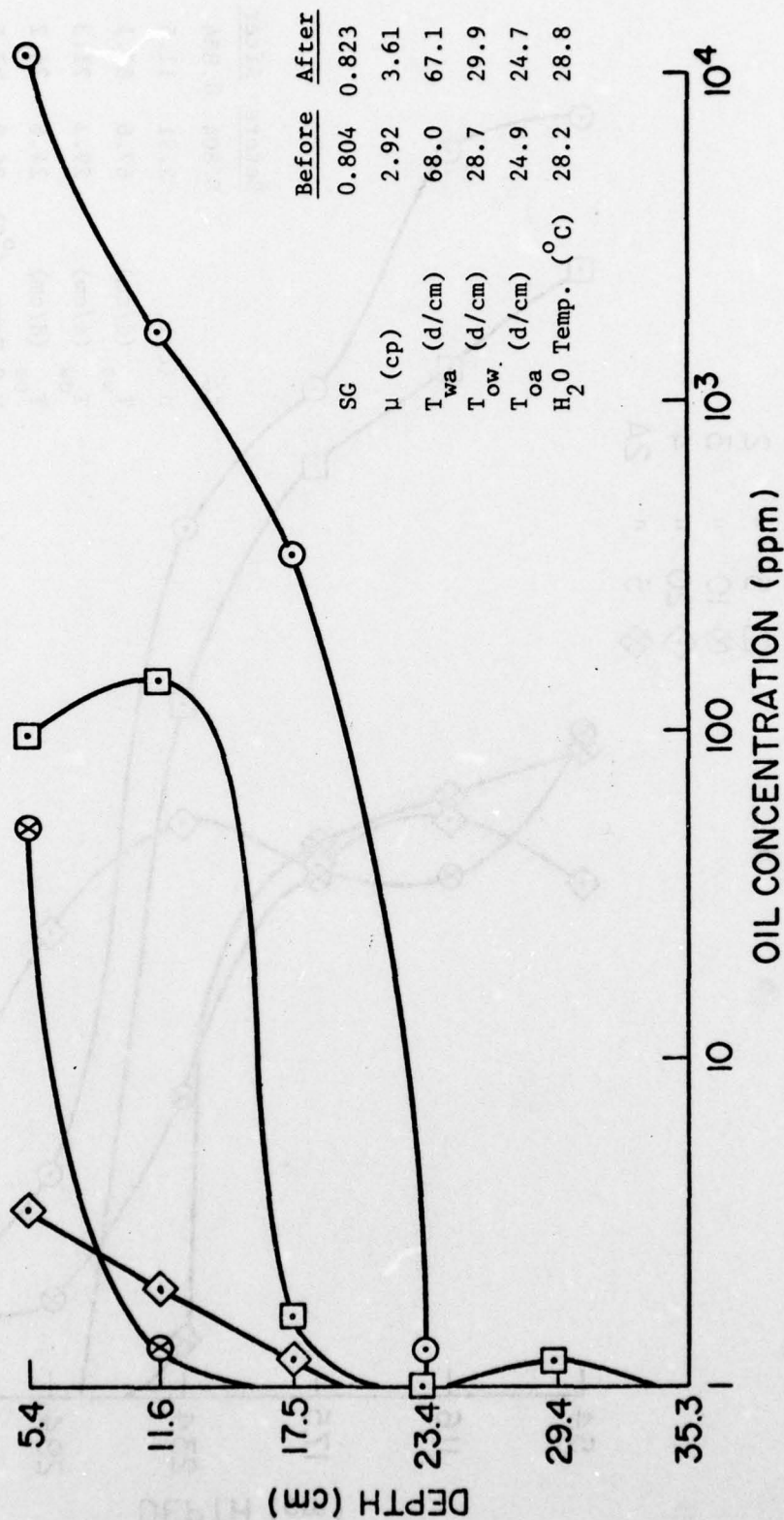
FIGURE 5-5 Oil Concentration vs Depth for Thick (5.5 mm) Arzew

TEST

⊙ 2 SEC	5C		
☐ 5 "	6A		
⊗ 10 "	7A		
◇ 20 "	8A		
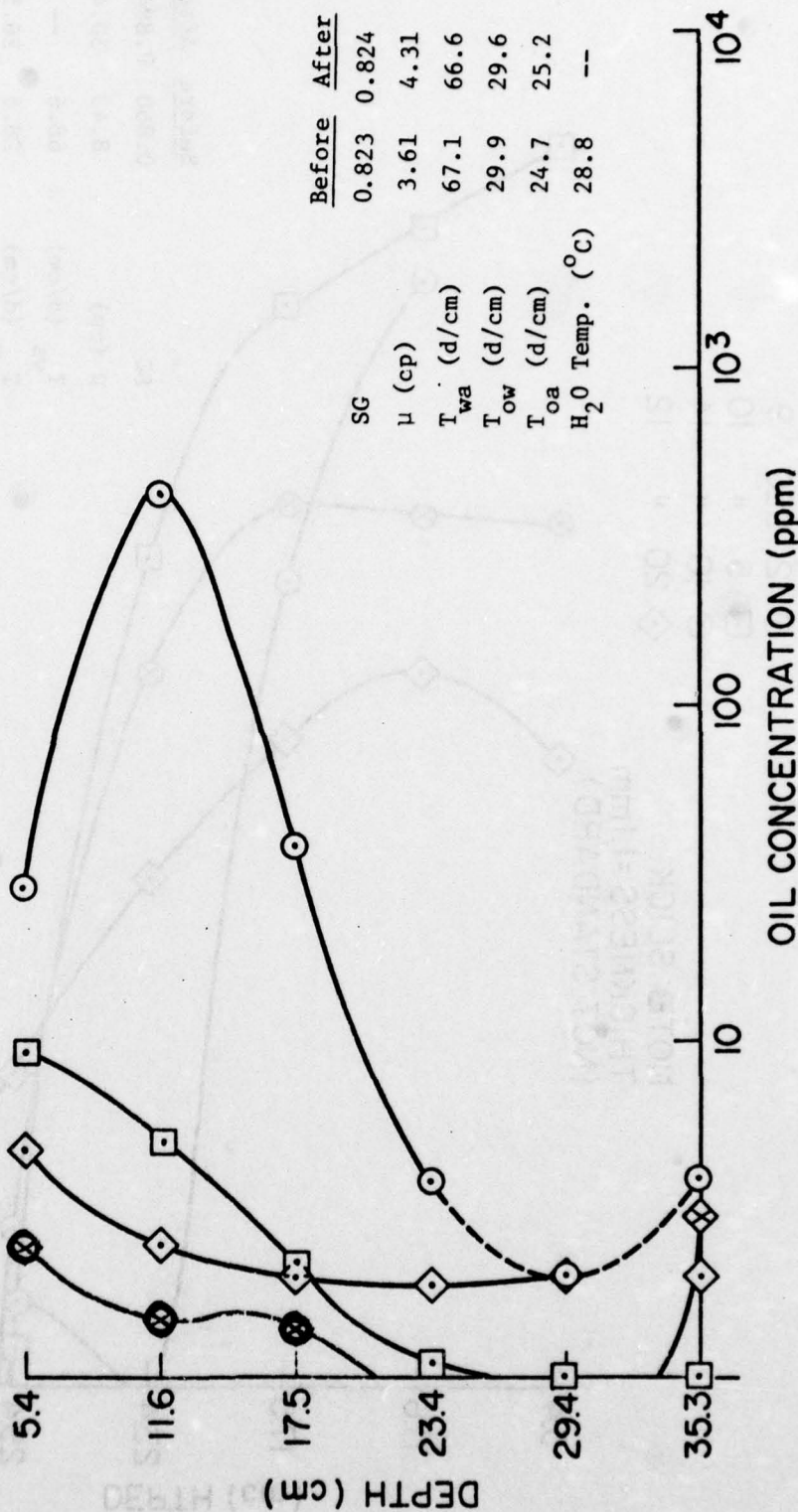
	Before	After
SG	0.823	0.824
μ (cp)	3.61	4.31
T_{wa} (d/cm)	67.1	66.6
T_{ow} (d/cm)	29.9	29.6
T_{oa} (d/cm)	24.7	25.2
H_2O Temp. (°C)	28.8	—

OIL CONCENTRATION (ppm)

10^4 10^3 100 10

DEPTH (cm)

5.4 11.6 17.5 23.4 29.4 35.3

FIGURE 5-6 Oil Concentration vs Depth for Thick (5.5 mm) Arzew .
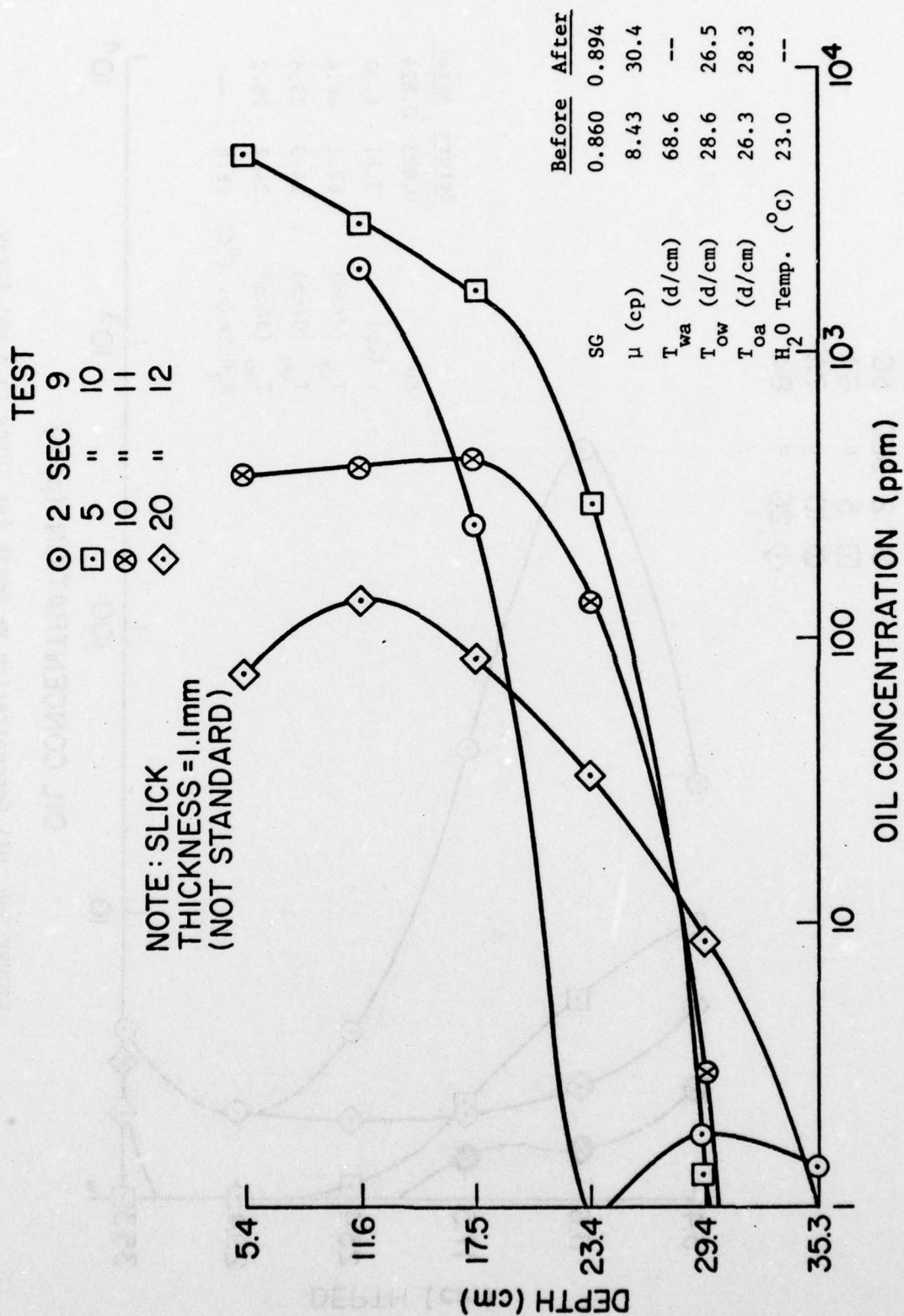
FIGURE 5-7 Oil Concentration vs Depth for Thin (1.1 mm) ABL

FIGURE 5-8 Oil Concentration vs Depth for Thin (0.98 mm) ABL

TEST
◇ 5 SEC 10A
▣ " " 10B
◉ " " 10C

NOTE: SLICK
THICKNESS = 0.98 mm
(NOT STANDARD)

	Before 10A	After 10A,10B	After 10C
SG	0.894	0.901	0.923
μ (cp)	30.4	41.6	--
T_{ow} (d/cm)	26.5	22.7	--
T_{oa} (d/cm)	28.3	27.7	33.2
H_2O Temp. (°C)	--	--	22.2

OIL CONCENTRATION (ppm)

DEPTH (cm)

5.4
11.6
17.5
23.4
29.4
35.3

FIGURE 5-9 Oil Concentration vs Depth for Thick (5.5 mm) ABL

TEST

⊙ 2 SEC 13
▫ 5 " 14
⊗ 10 " 15
◇ 20 " 16

	Before	After
SG	0.859	0.862
μ (cp)	7.32	10.7
T_{wa} (d/cm)	68.8	64.0
T_{ow} (d/cm)	28.1	22.0
T_{oa} (d/cm)	25.7	26.0
H_2O Temp. (°C)	23.4	24.0
Air Temp. (°C)	24.0	25.0

OIL CONCENTRATION (ppm)

DEPTH (cm)
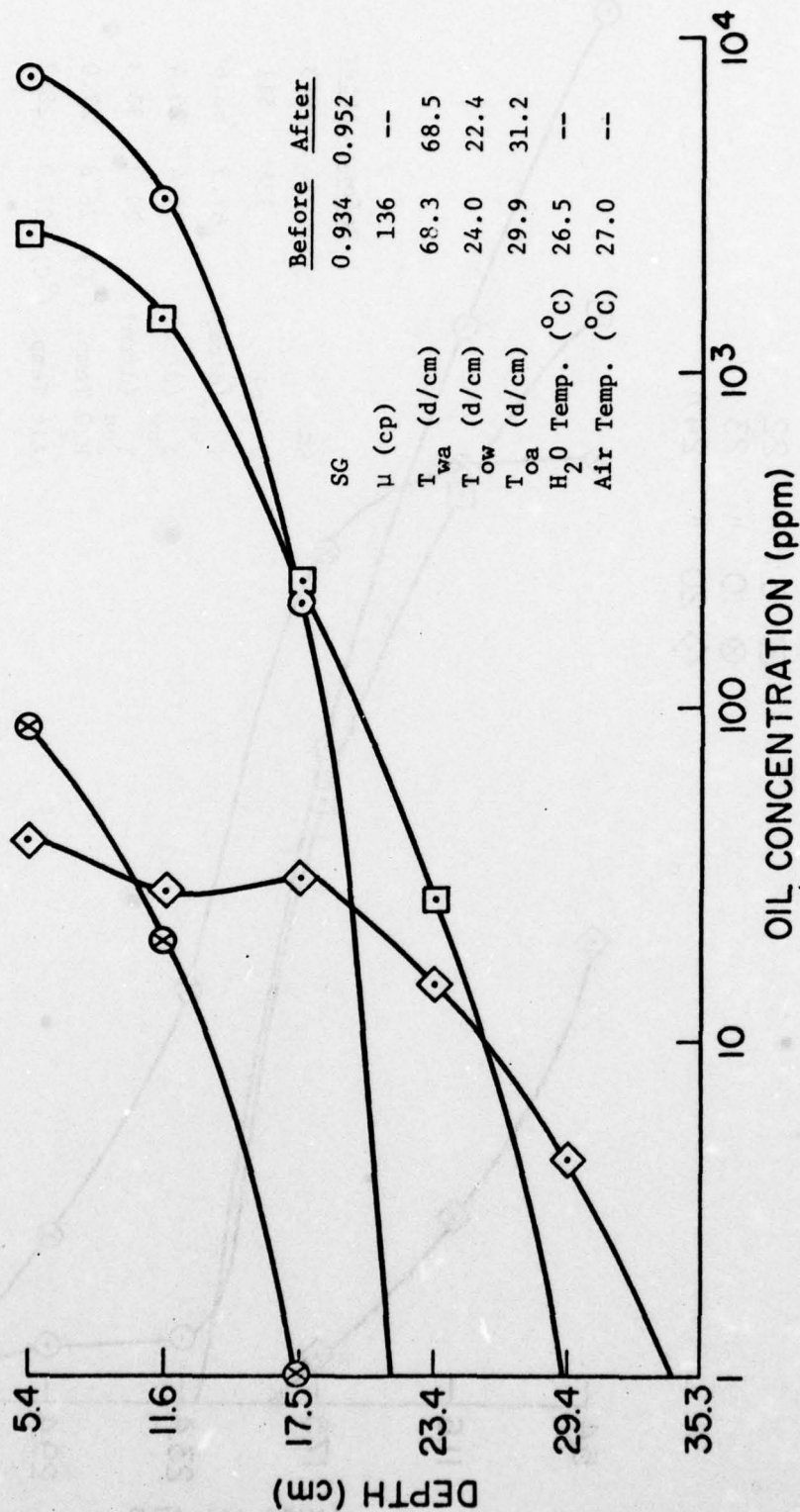
FIGURE 5-10 Oil Concentration vs Depth for Thin (0.55 mm) THUMS
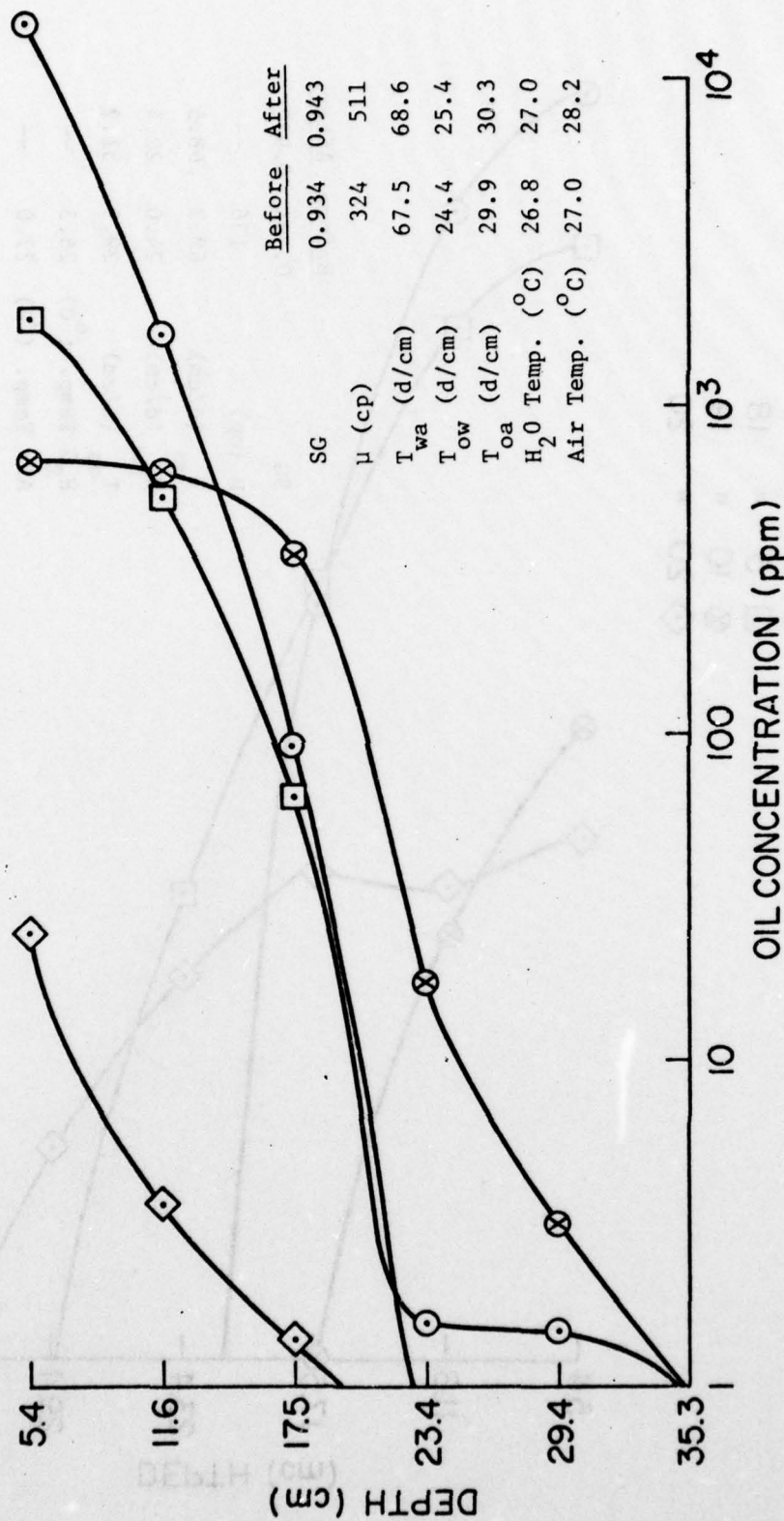
FIGURE 5-11 Oil Concentration vs Depth for Thick (5.5 mm) THUMS

FIGURE 5-12 Oil Concentration vs Depth for Thin (0.55 mm) ZUE at Room Temperature

TEST

⊙ 2 SEC 25
☐ 5   "   26
⊗ 10   "   27
◇ 20   "   28

	Before	After
SG	0.824	0.860
μ (cp)	4.29	25.2
T_{wa} (d/cm)	68.2	67.6
T_{ow} (d/cm)	23.1	12.8
T_{oa} (d/cm)	24.3	27.9
H_2O Temp. (°C)	22.5	23.0
Air Temp. (°C)	24.5	26.0

OIL CONCENTRATION (ppm)

DEPTH (cm)

5.4   11.6   17.5   23.4   23.4   35.3

10^4 10^3 100   10

-131-

FIGURE 5-13 Oil Concentration vs Depth for Thick (5.5 mm) ZUE at Room Temperature

	Before	After
SG	0.822	0.829
μ (cp)	4.04	5.12
T_{wa} (d/cm)	67.5	68.7
T_{ow} (d/cm)	23.2	25.4
T_{oa} (d/cm)	24.6	25.6
H_2O Temp. (°C)	25.0	25.0
Air Temp. (°C)	24.6	25.4

TEST

⊙ 2 SEC 29
☐ 5 " 30
⊗ 10 " 31
◇ 20 " 32

OIL CONCENTRATION (ppm)

DEPTH (cm)

-132-

FIGURE 5-14 Oil Concentration vs Depth for Thin (0.55 mm) #2 Diesel

TEST

⊙ 2 SEC 37
⊡ 5 " 38
⊗ 10 " 39
◇ 20 " 40

	Before	After
SG	0.834	0.831
μ (cp)	2.79	2.76
T_{wa} (d/cm)	66.3	69.4
T_{ow} (d/cm)	24.2	24.8
T_{oa} (d/cm)	26.7	27.1
H_2O Temp. (°C)	25.0	26.0
Air Temp. (°C)	27.0	28.5

OIL CONCENTRATION (ppm)

10^4 10^3 100 10 1

DEPTH (cm)

5.4 11.6 17.5 23.4 29.4 35.3
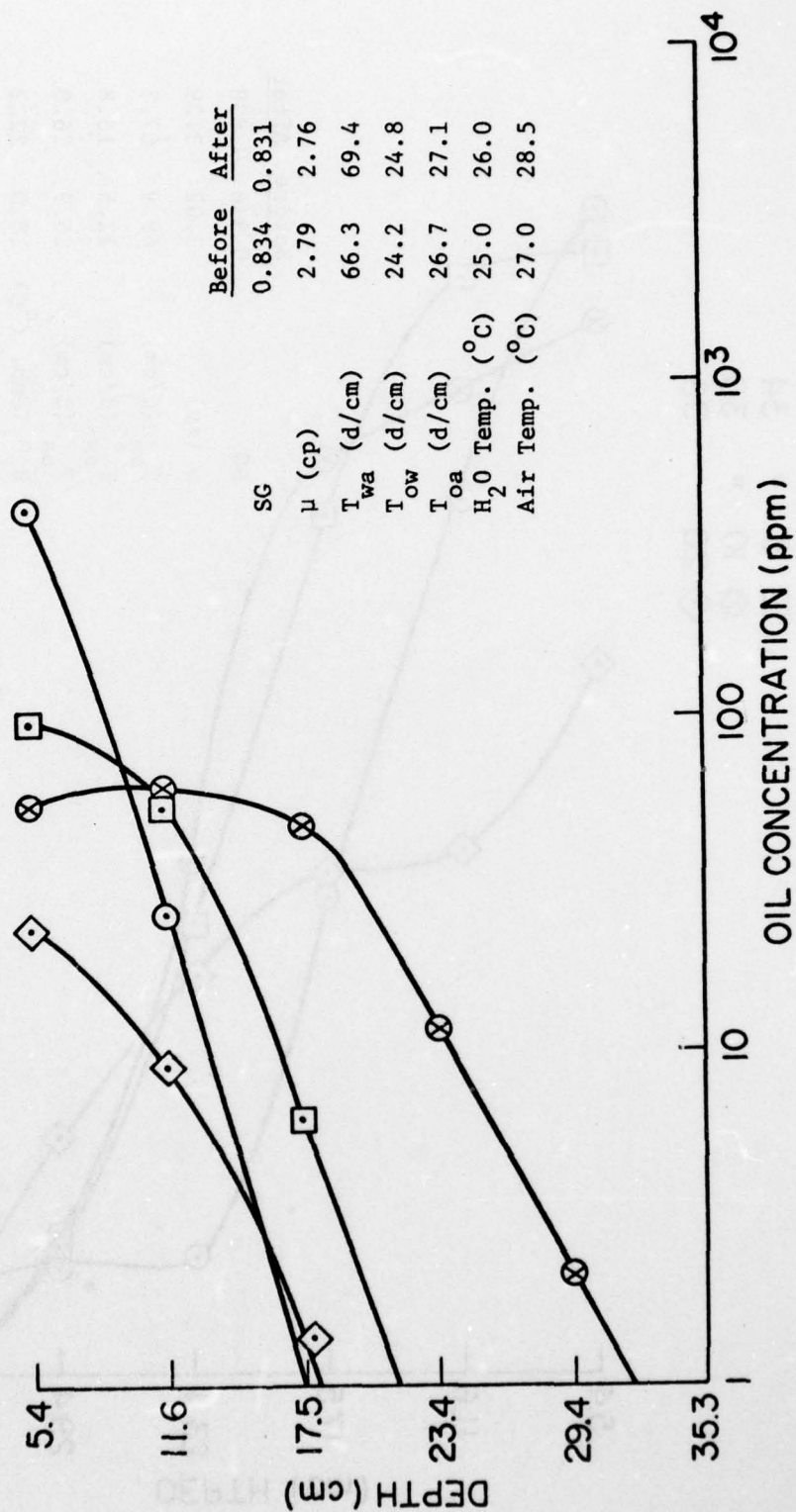
FIGURE 5-15 Oil Concentration vs Depth for Thick (5.5 mm) #2 Diesel.

-134-
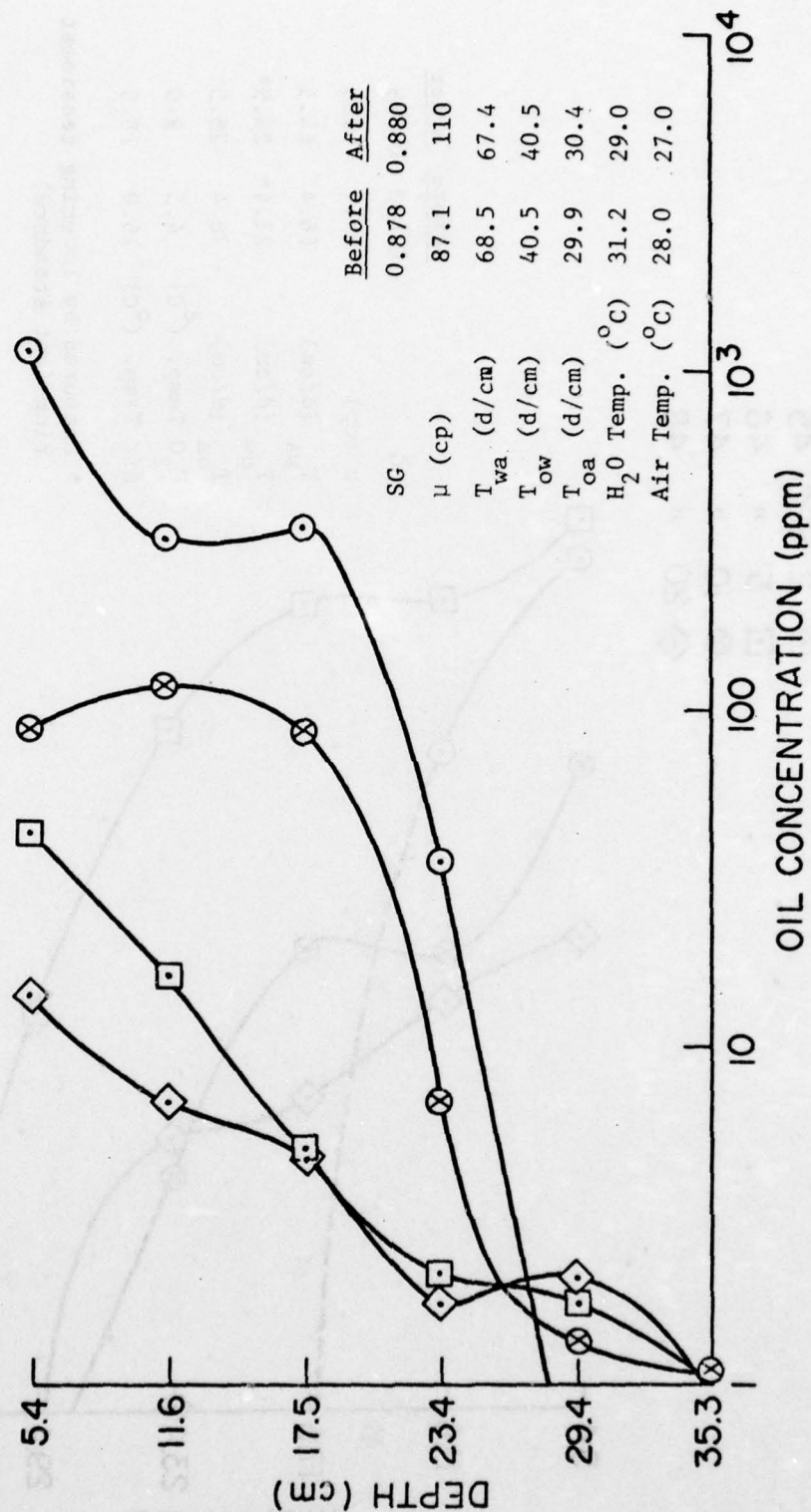
FIGURE 5-16 Oil Concentration vs Depth for Thick (5.5 mm) Mineral Oil
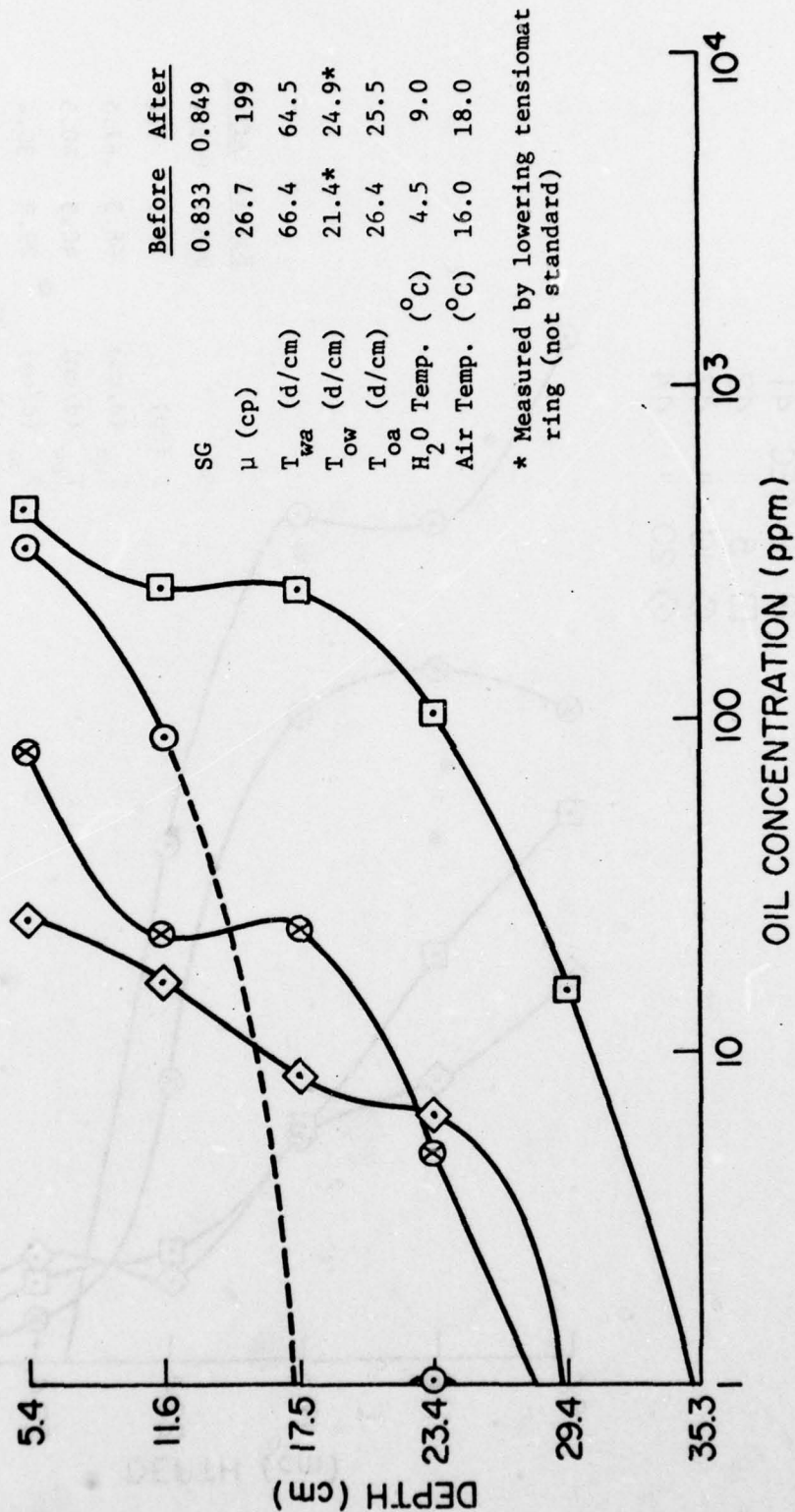
FIGURE 5-17 Oil Concentration vs Depth for Thin (0.55 mm) Cold Zue

-136-
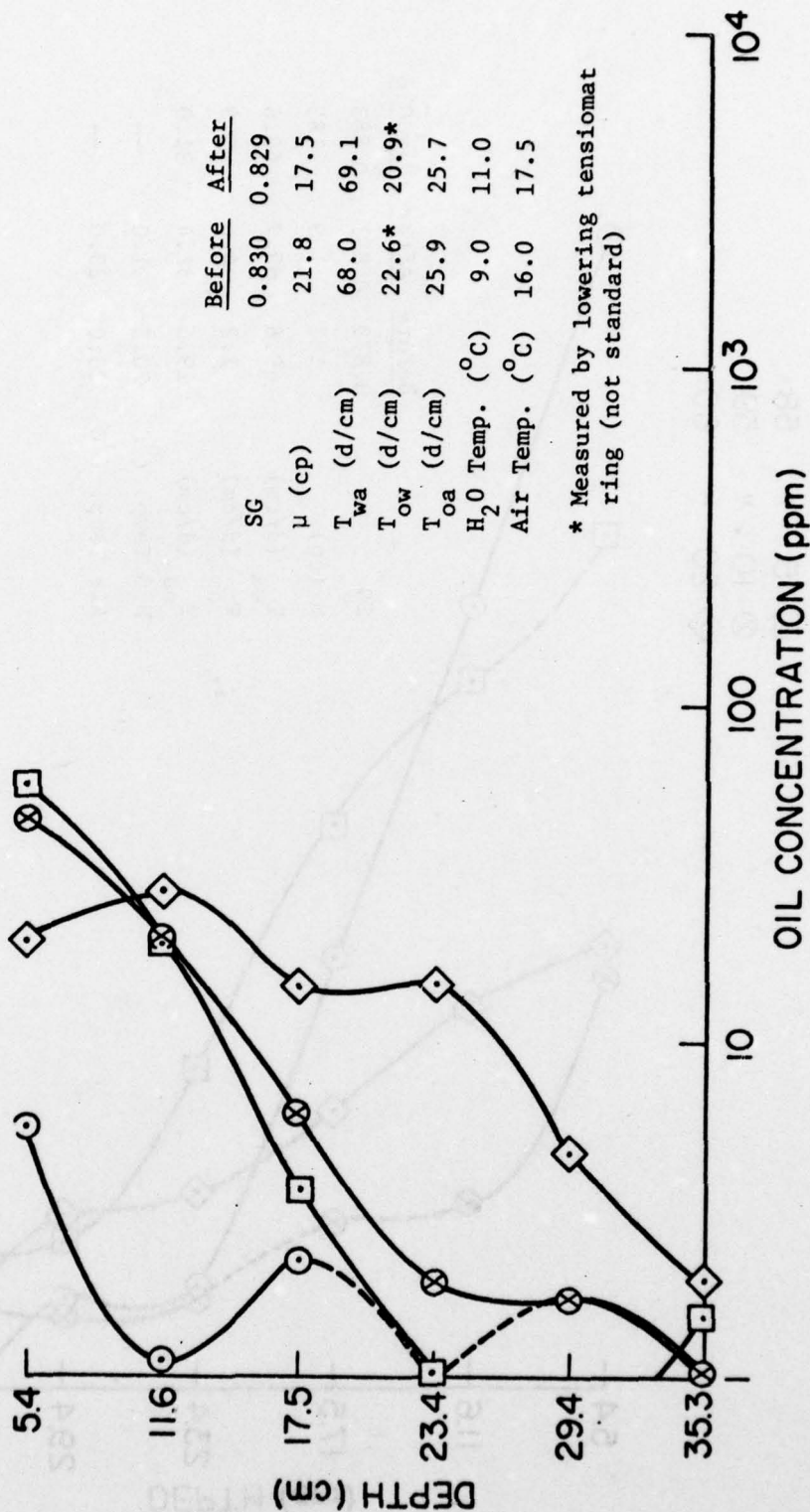
FIGURE 5-18 Oil Concentration vs Depth for Thick (5.5 mm) Cold Zue.

-137-
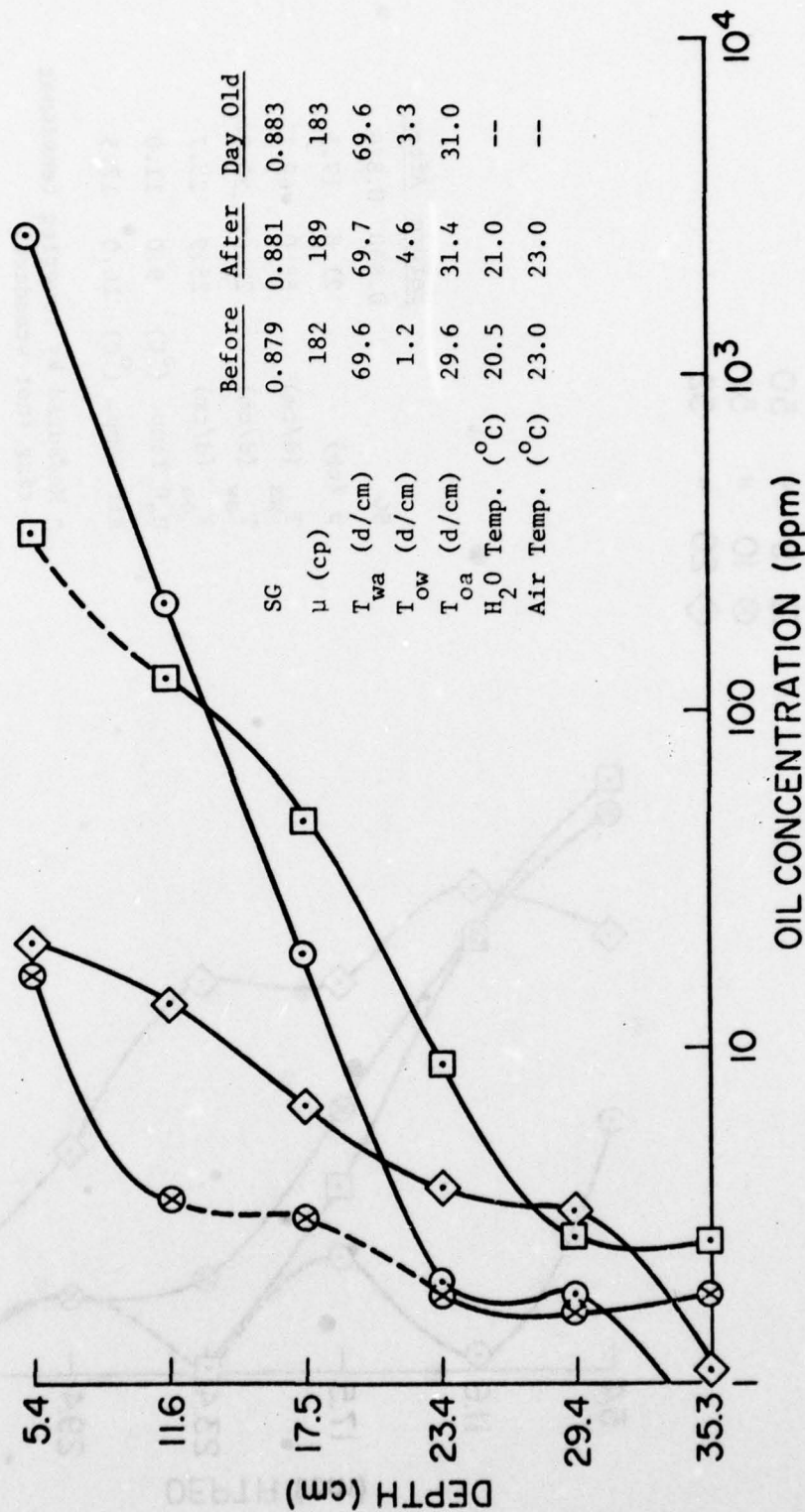
FIGURE 5-19 Oil Concentration vs Depth for Thick (5.5 mm) Mineral Oil + Zonyl A

Wave Data

Surface elevation and vertical acceleration were recorded as a
function of time for the standard experimental wave group in clean
water using both a float guage and a capacitance wave probe. Because
the capacitance probe is not operable in the presence of an oil slick,
it was used only to establish a correction factor for the float gauge,
which has poorer dynamic response. The float gauge was used to record
the standard wave group surface elevation for several oil slicks. Not
all tests had wave data taken, as the wave measurements were added to
the program after some of the dispersion tests were already done.
Vertical acceleration of the surface for the standard wave group was
recorded for clean water and in the presence of a Mineral + Zonyl A
oil slick by using a double differentiator circuit which followed the
surface elevation output.

It was found that in clean water the float gauge measurements
were 14% and 22% lower than the capacitance probe measurements for
surface elevation and acceleration, respectively, when static
calibrations are used. The float gauge data presented here are the
direct data based on static calibration. To obtain actual wave heights,
direct float gauge data must be multiplied by 1.14. To obtain actual
accelerations from float gauge acceleration data, they must be multiplied
by 1.22.

For all cases shown in the following wave records, time zero is
at the breaking crest and the leading face of the breaking wave is to
the left of zero. The vertical acceleration at the breaking crest
is the greatest negative peak found in the acceleration profile.
Surface elevations recorded before and after actual experimental tests
are presented in numerical order by test number. All profiles were
measured using the float gauge except for the one case noted as
capacitance probe data.

Figures 5-20 through 5-22 show elevation and acceleration data
for clean water and for the tests of mineral oil with 0.1% Zonyl A
surfactant. More acceleration data does not exist as the acceleration
measurements were added to the test plan at the very end of the testing

-139-

program. Figures 5-23 through 5-35 show surface elevation measurements
with several different oil slicks.
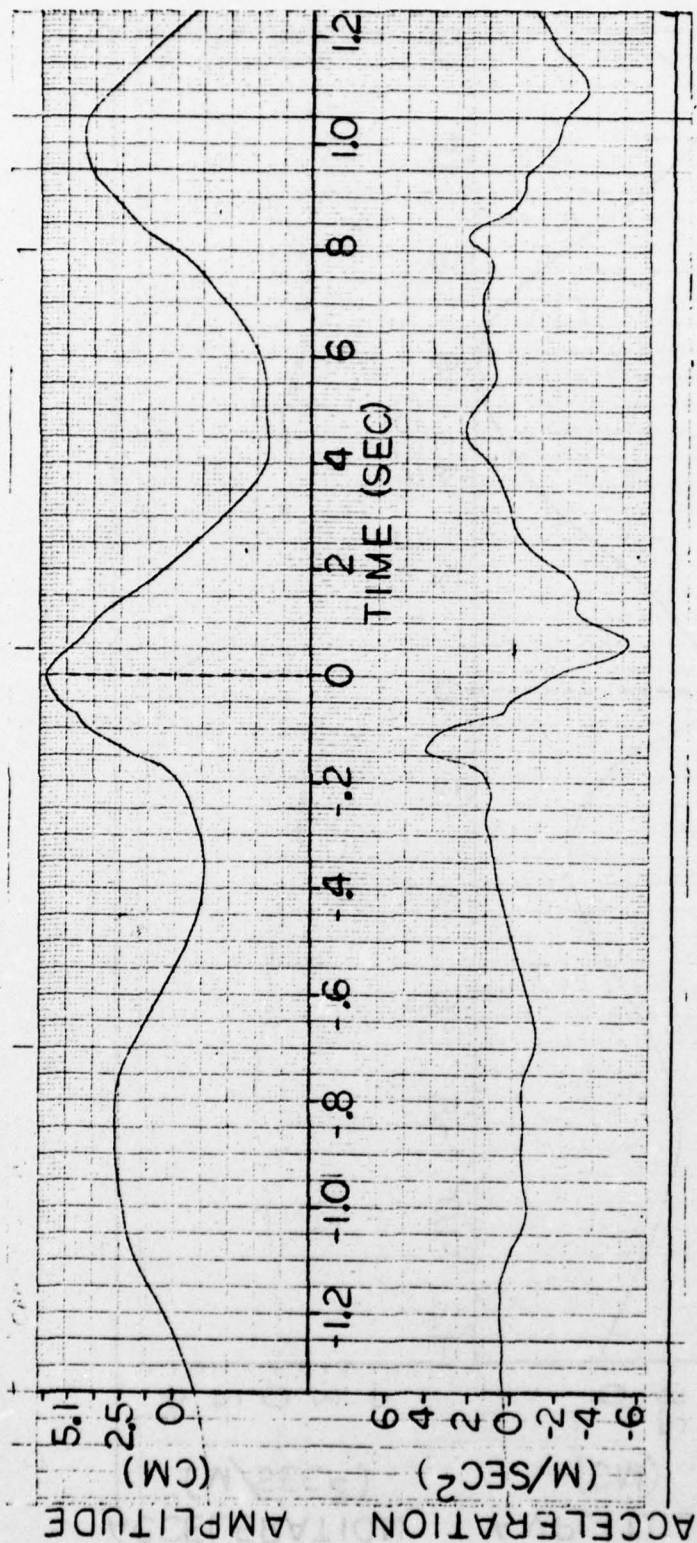
FIGURE 5-20 Water Surface Elevation and Acceleration Record with a Capacitance Probe
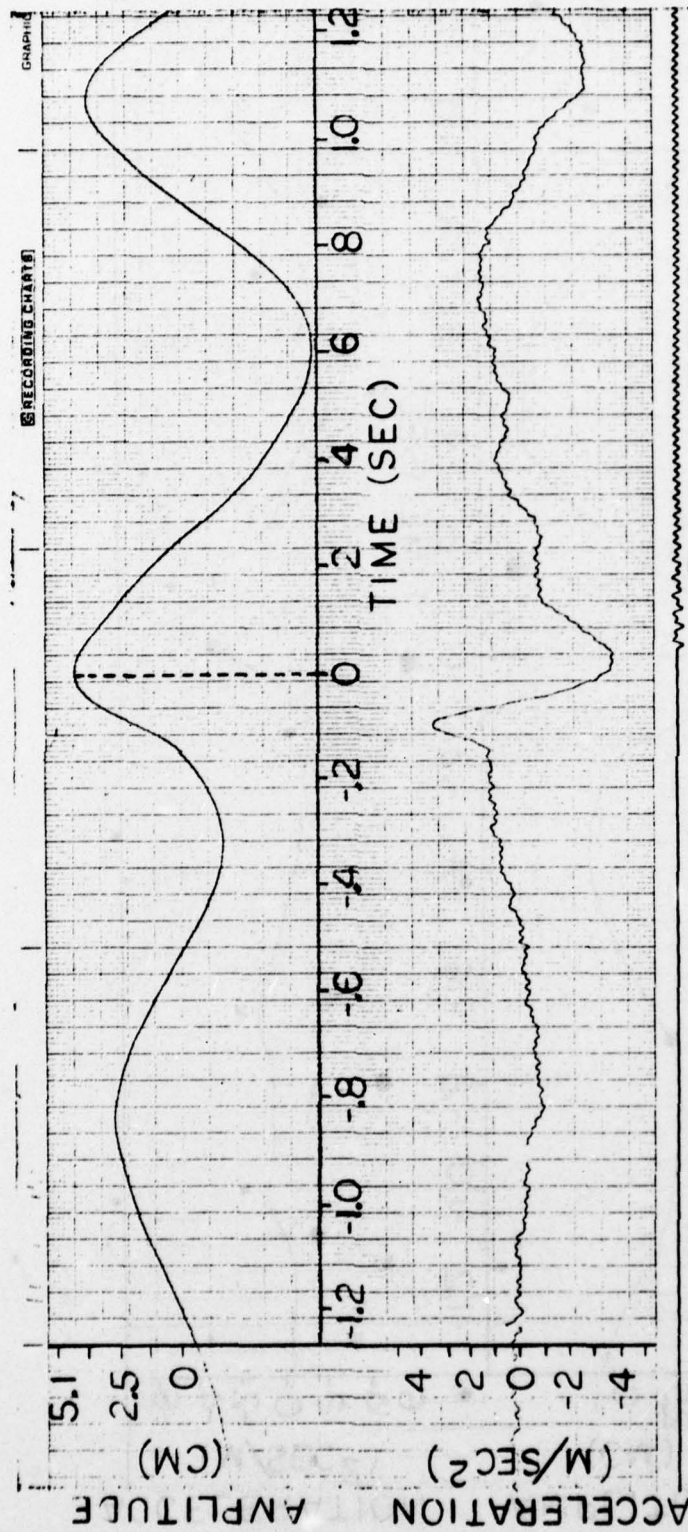
FIGURE 5-21 Water Surface Elevation and Acceleration Recorded with a Float Gauge

-142-
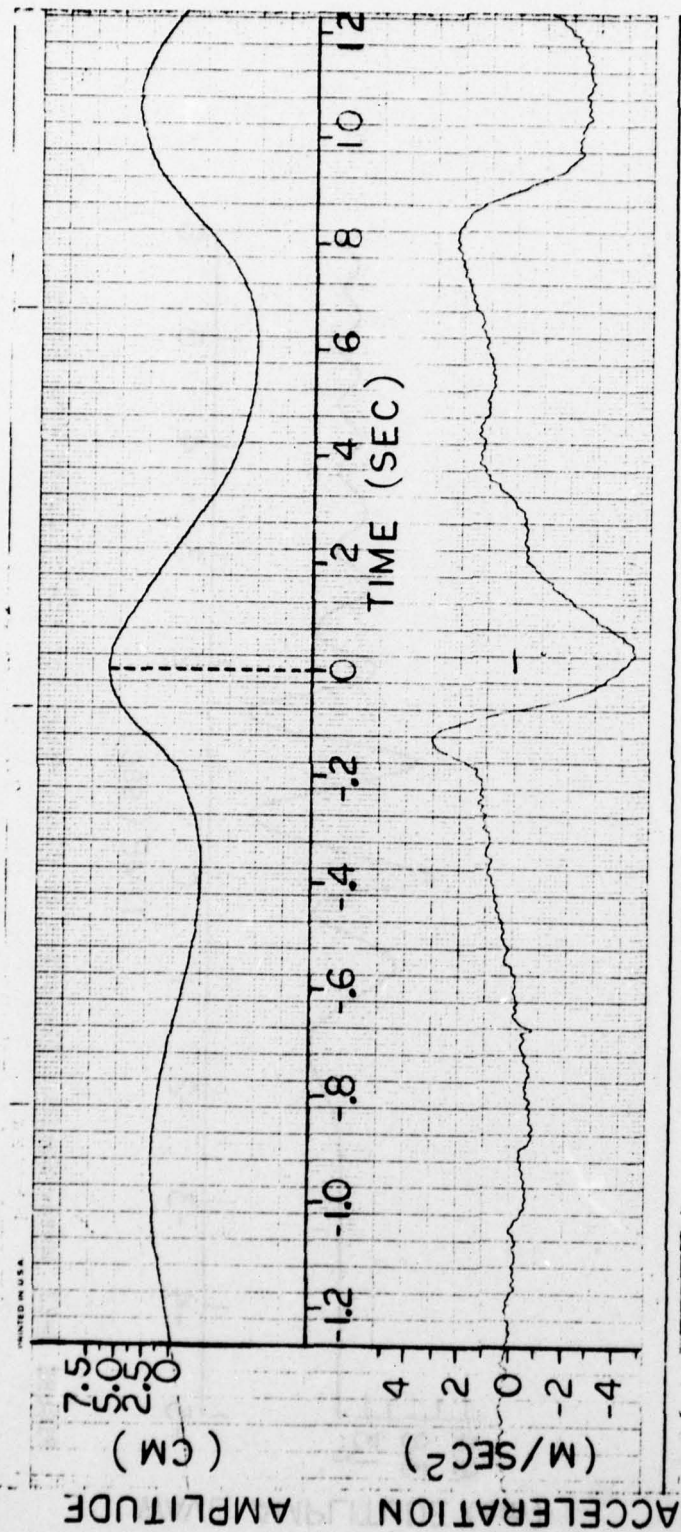
FIGURE 5-22 Water Surface Elevation and Acceleration Recorded with a Float Gauge in the Presence of a Thick (5.5 mm) Mineral + Zonyl A Oil Slick
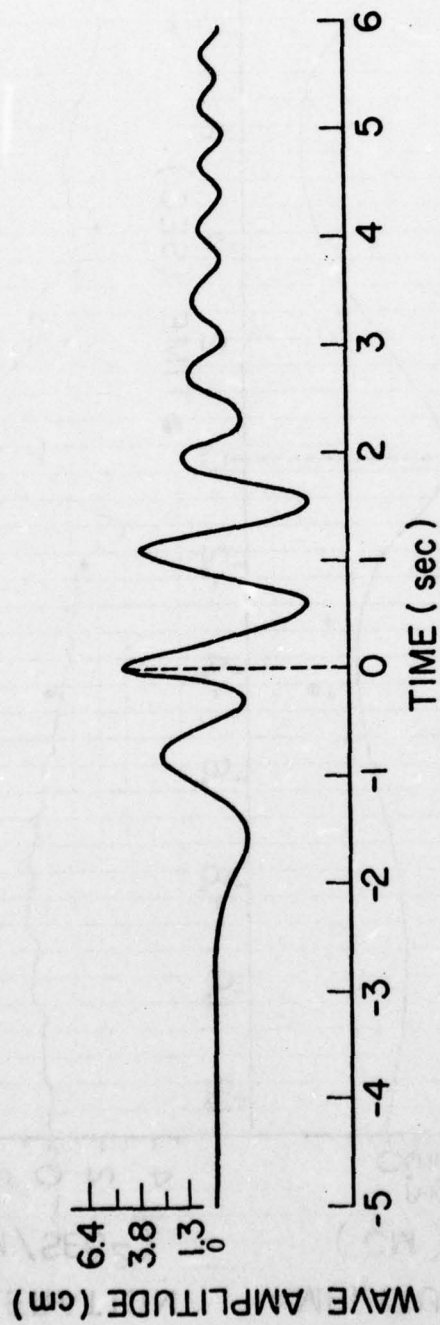
FIGURE 5-23 Water Surface Elevation in Clean Water for the Standard Wave Group

-144-
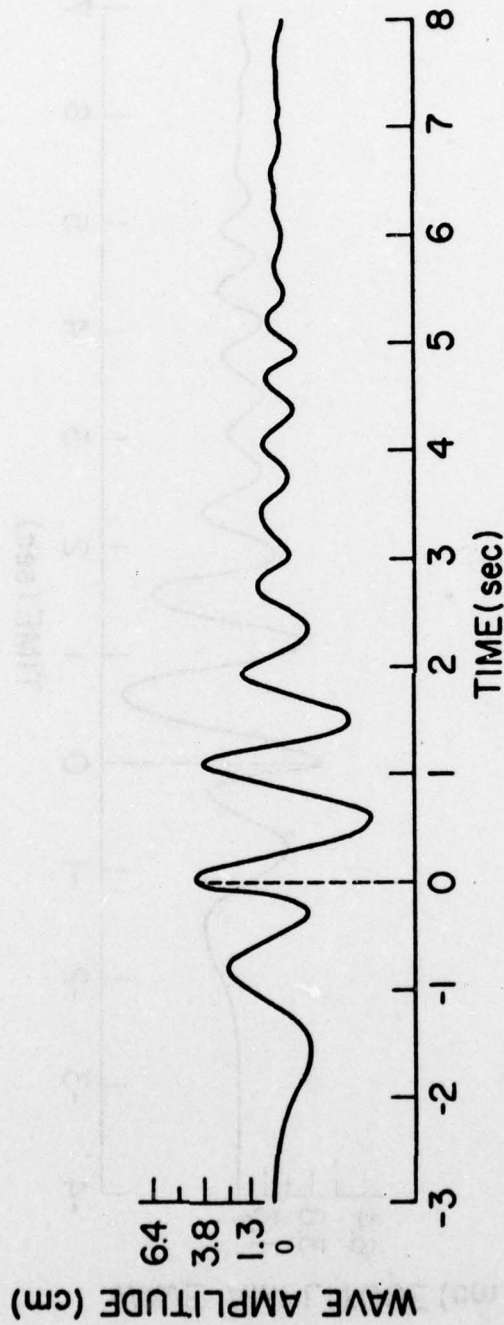
FIGURE 5-24 Water Surface Elevation in Thin (0.55 mm) Zue Recorded Before Test 25
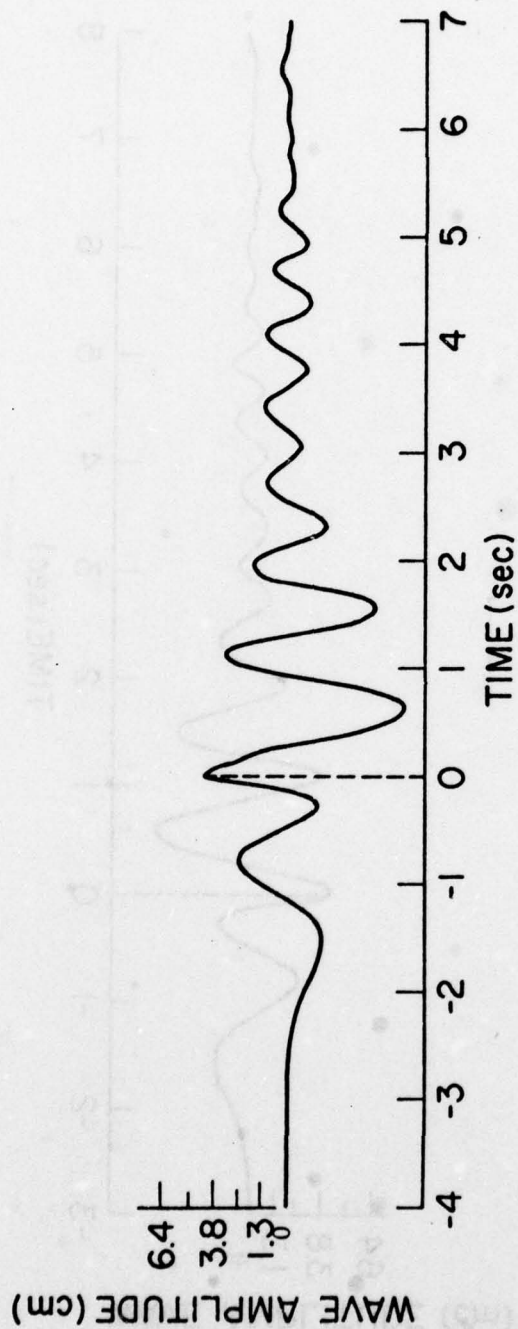
FIGURE 5-25 Water Surface Elevation in Thin (0.55 mm) Zue After Test 28
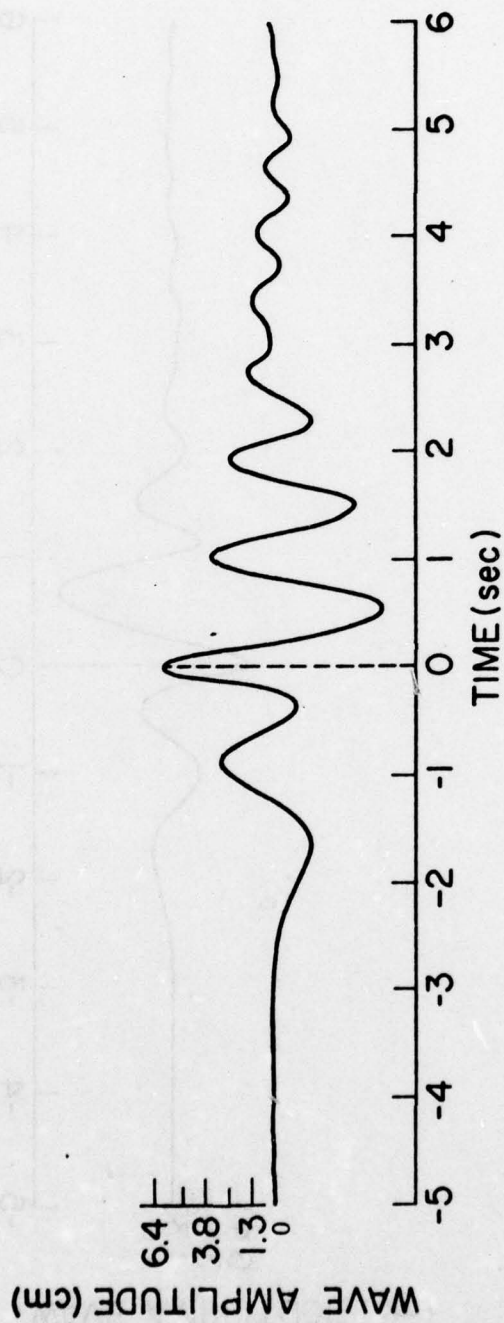
FIGURE 5-26 Water Surface Elevation in Thick (5.5 mm) Zue Before Test 29

-147-
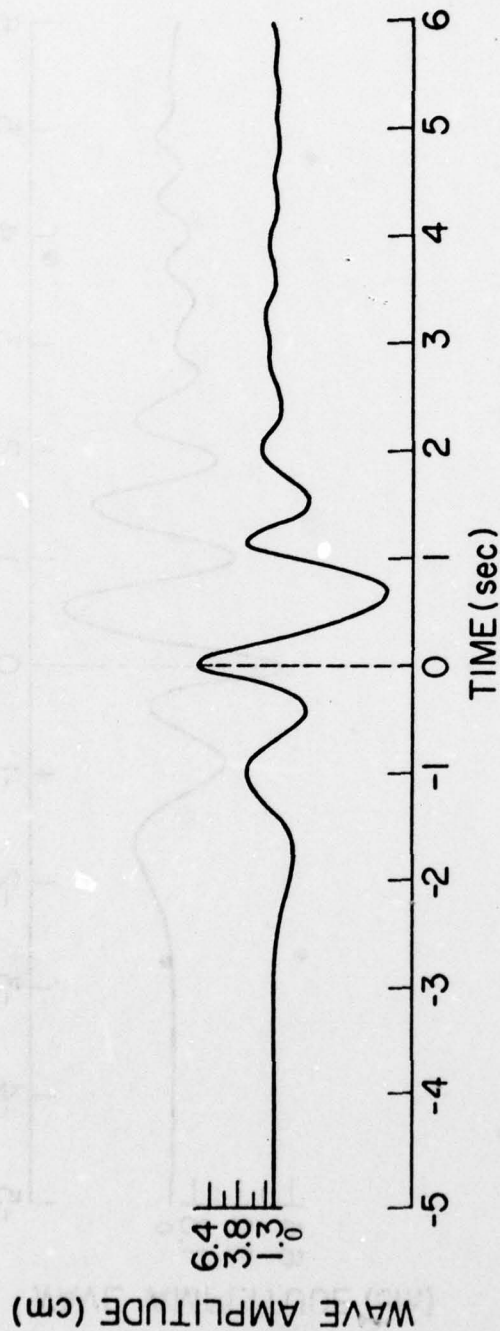
FIGURE 5-27 Water Surface Elevation in Thick (5.5 mm) Zue After Test 32
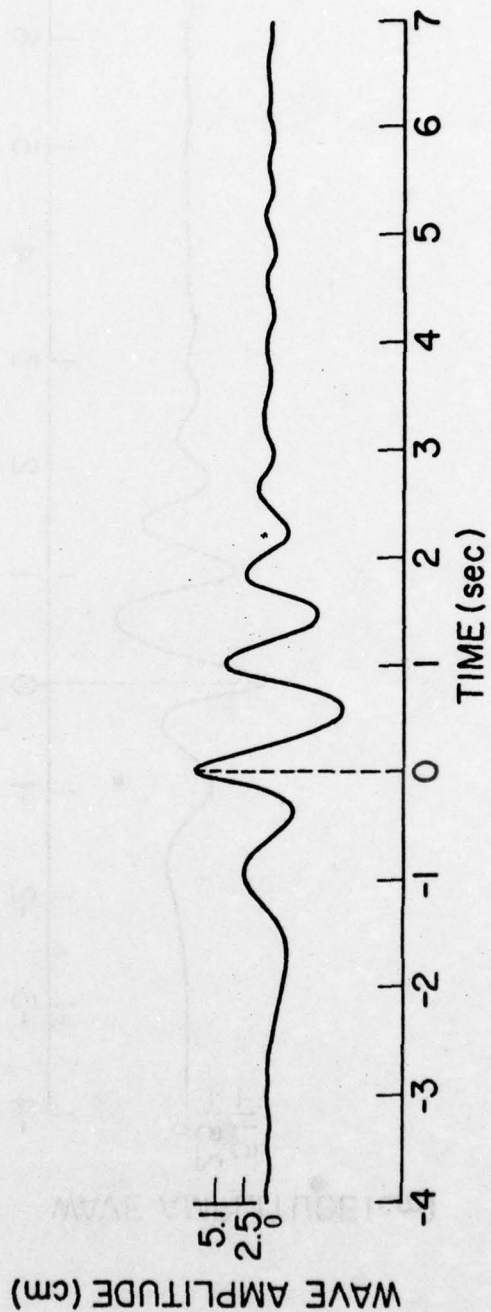
FIGURE 5-28 Water Surface Elevation in Thick (5.5 mm) Mineral Oil Before Test 41
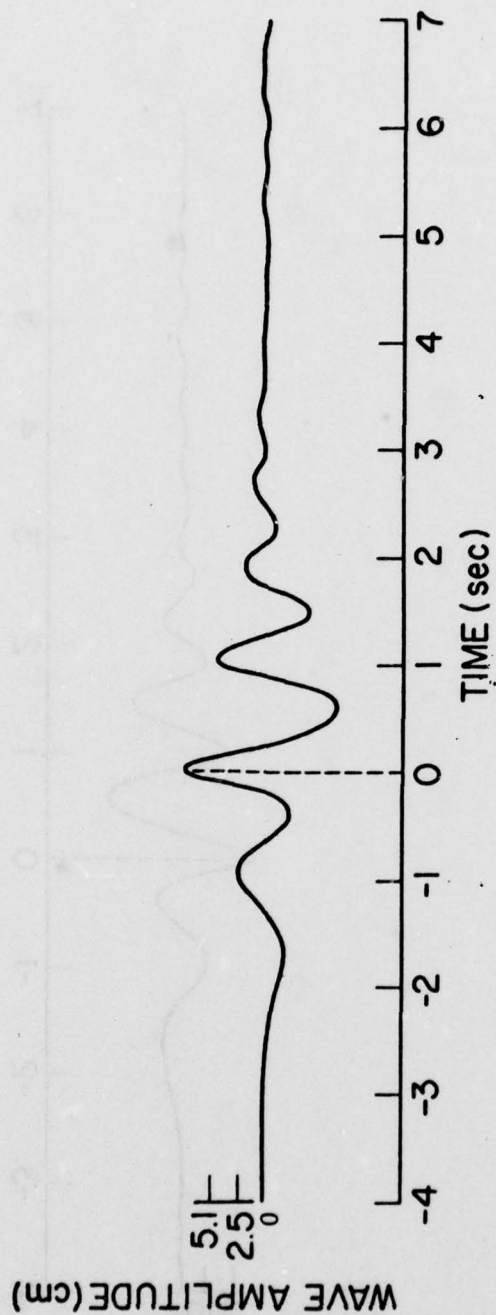
FIGURE 5-29 Water Surface Elevation in Thick (5.5 mm) Mineral Oil After Test 44

-150-
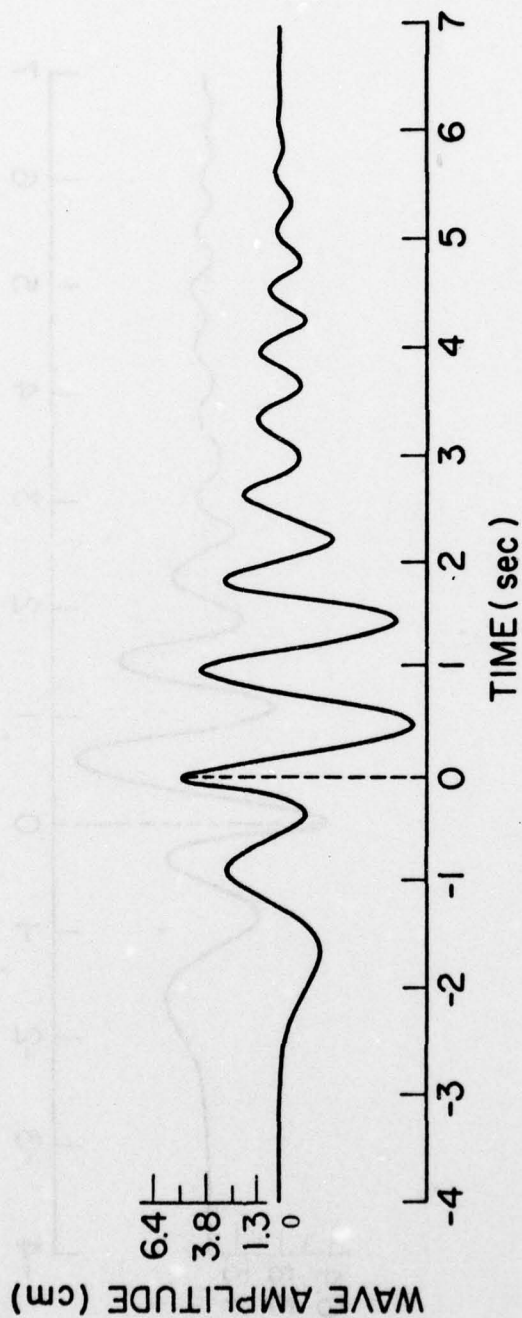
FIGURE 5-30 Water Surface Elevation in Thin (0.55 mm) Cold Zue Before Test 45
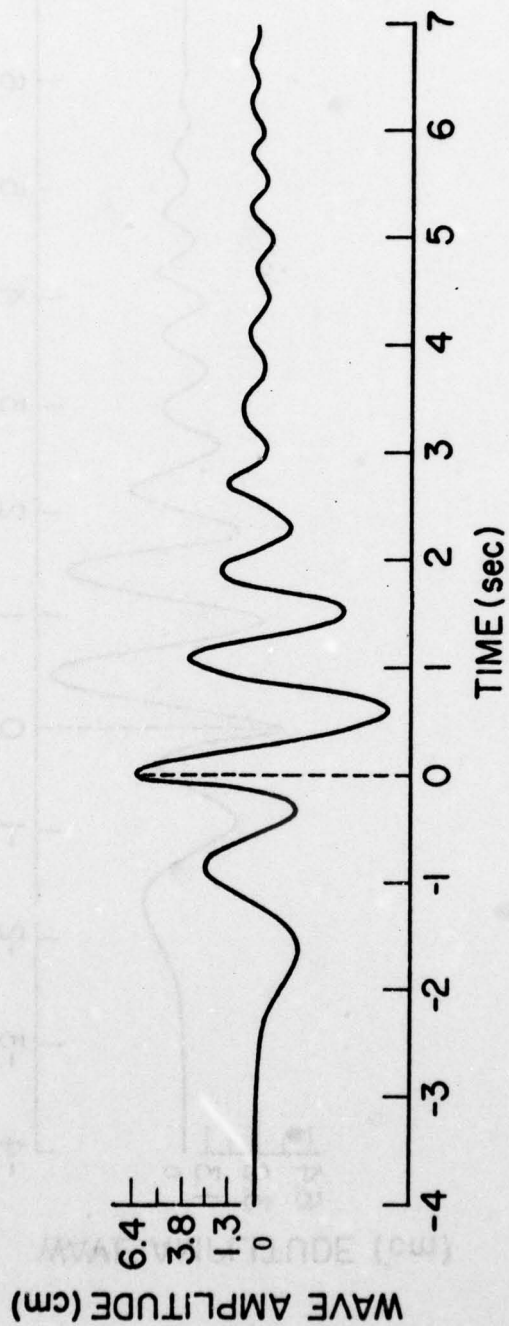
FIGURE 5-31 Water Surface Elevation in Thin (0.55 mm) Cold Zue After Test 48
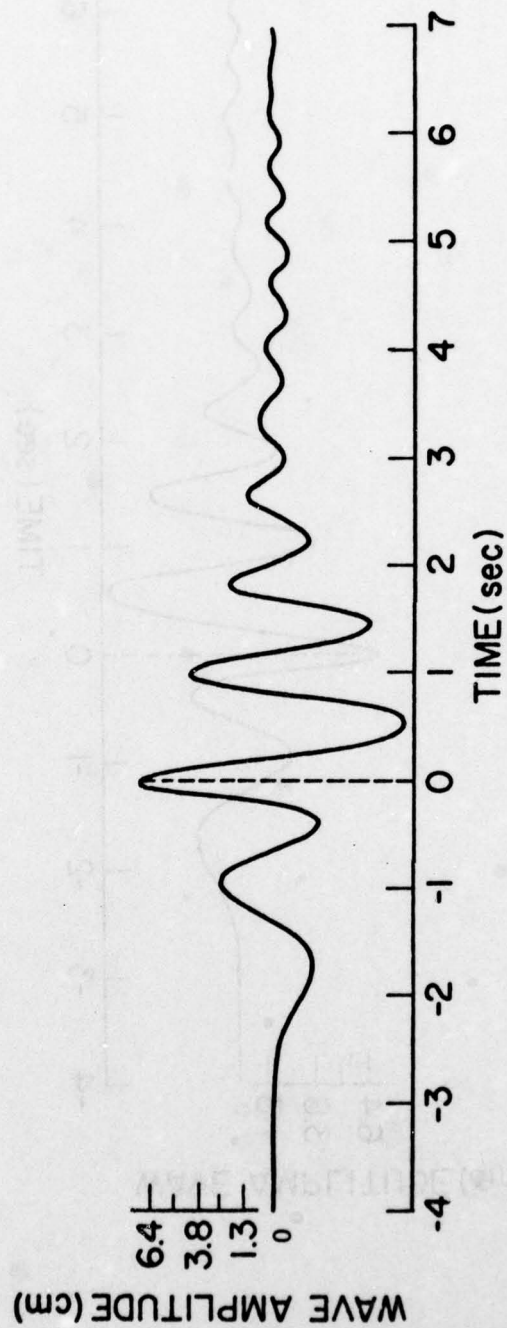
FIGURE 5-32 Water Surface Elevation in Thick (5.5 mm) Cold Zue Before Test 49
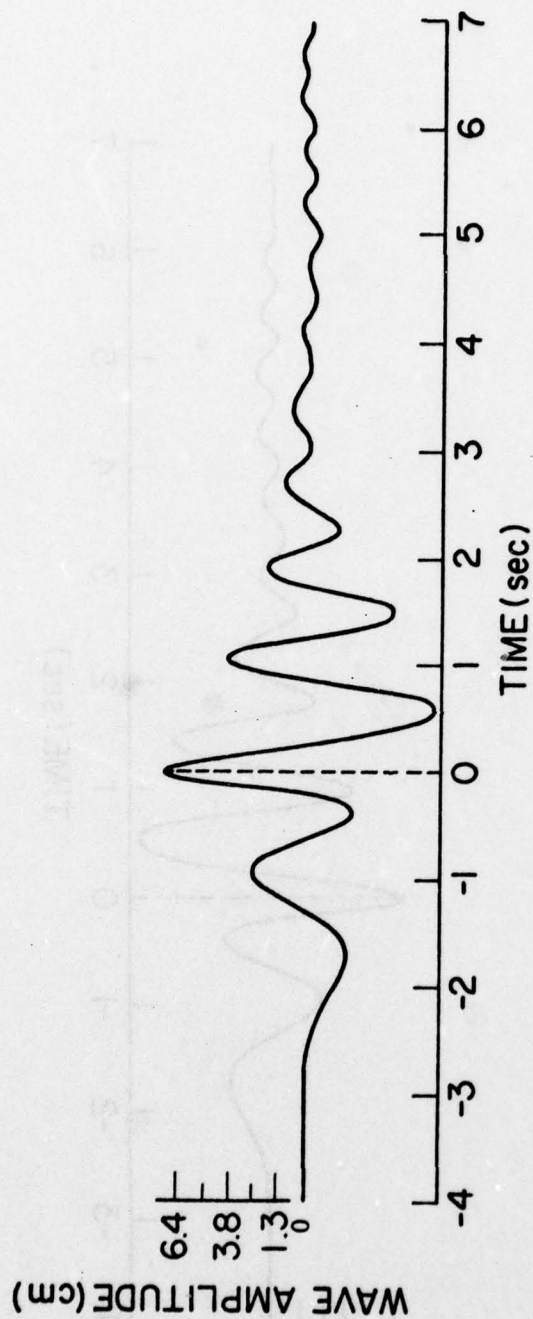
FIGURE 5-33 Water Surface Elevation in Thick (5.5 mm) Cold Zue After Test 52

-154-
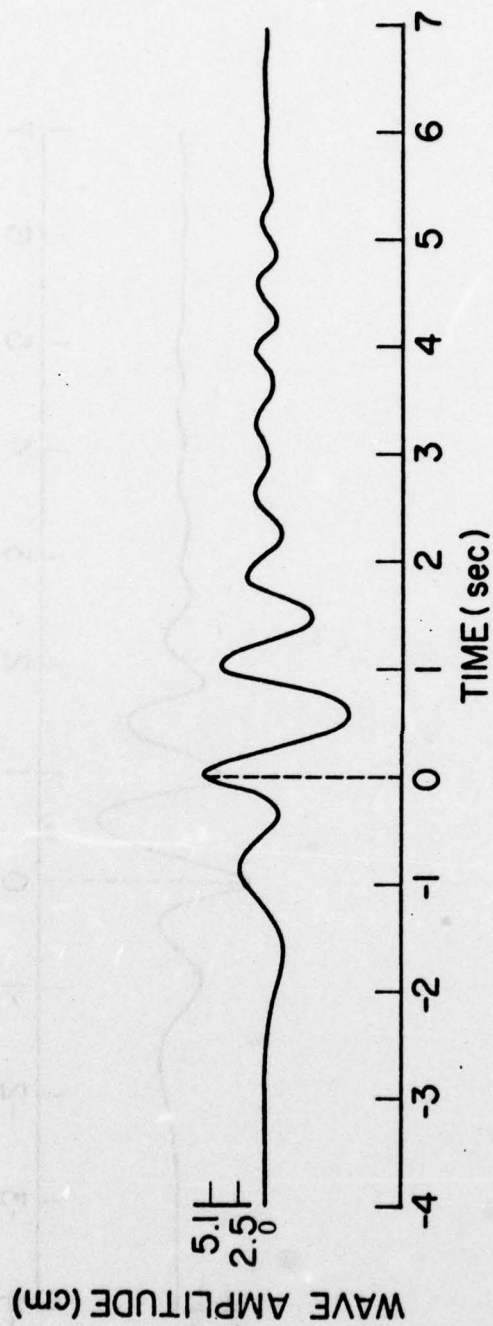
FIGURE 5-34 Water Surface Elevation in Thick (5.5 mm) Mineral Oil + Zonyl A Before Test 57
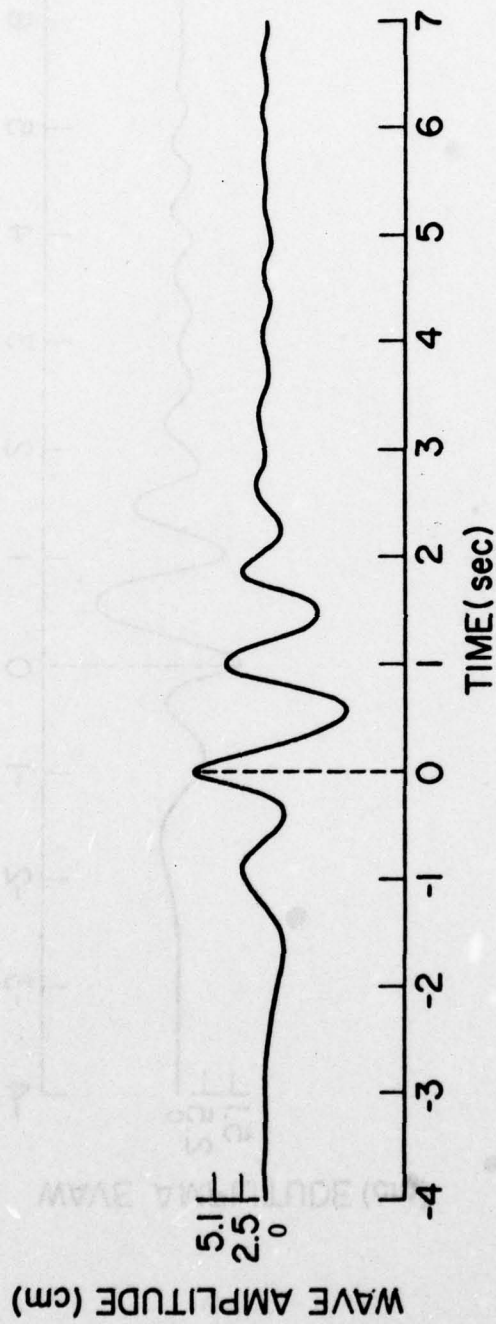
FIGURE 5-35 Water Surface Elevation in Thick (5.5 mm) Mineral + Zonyl A After Test 60

5.5 Data Analysis

Dispersion Characterization

To improve the usefulness of the experimental data for comparative studies, it is appropriate to obtain simplified information from the oil concentration vs depth curves. Total oil volume per unit area of the free surface (Ψ), average dispersion depth (AVGZ), and maximum dispersion depth (MAXZ) are three characteristics which were chosen to represent a dispersion. These parameters are used because they are useful in studying the phenomenon of oil slick dispersion at sea, and they are readily obtained from the data of this study.

Total oil volume per unit horizontal area is obtained by integrating the dispersion concentration over depth:

$$\Psi = \int_o^D \sigma \, dz \tag{5.1}$$

where σ is oil concentration and D is any depth greater than the maximum dispersion depth. The problem which now arises is the formulation of a suitable curve for σ which converts the discrete data points of this study to an integrable function. Because this is a comparative study and, too, because the dispersion process is far from precise, a trapezoidal approximation which assumes straight lines between discrete data points was used. The shape of the dispersion curve above the shallowest sampling position is unknown and must be assumed. Constant oil concentration from the shallowest sampler to the surface is assumed in order to ease calculation; yet this choice is as valid or more valid than any others because observed dispersions showed no marked discontinuity in oil concentration except at the water-oil interface, and observation of the curves shows that many oil concentration curves tend to level off in shallow depths.

Average dispersion depth was defined as the vertical distance from the free surface to the centroid of the area under the σ curve. This distance is given by the following equation:

$$AVGZ = \frac{\int_o^D z\sigma dz}{\int_o^D \sigma dz} \tag{5.2}$$

A computer program was prepared to calculate Ψ and AVGZ based on Equations (5.1) and (5.2) and using the trapezoidal rule for each of the test cases shown in the graphs. In addition, the percentage of the oil slick dispersed (%DISP) was also calculated using the following relation,

$$\%DISP = \frac{\Psi}{h} \times 100 \tag{5.3}$$

This parameter provides a measure which indicates the dispersion size relative to slick thickness (h) and therefore is useful for comparing dispersions generated by slicks of varied thicknesses.

Maximum depth of dispersion (MAXZ) is by nature a subjective parameter; ideally MAXZ is that point where σ becomes zero and remains so as depth is increased. However, background levels of oil concentration will always be present, and σ will not reach zero in the tests. MAXZ was arbitrarily defined for this study as that depth at which σ was 1.0 ppm with no increase in σ with increasing depth.

In Table 5-2 which follows, Ψ (cm) or VOL/SA (cm), AVGZ (cm), and %DISP were calculated by the computer program described above. The first digit under RUN# corresponds to test number, and a second digit of 1, 2, or 3 corresponds to the test number suffix A, B, C respectively. MAXZ was estimated from the curves; here the notation >35.3 signifies that MAXZ was at an undetermined depth greater than the deepest sample position.

It is interesting to note that the %DISP values occasionally exceed 100%, seeming to indicate that more oil was dispersed than was present in the slick. These values are not erroneous, they simply indicate that oil from a large surface area of the slick may be momentarily concentrated at a small volume in the water column, a phenomenon actually observed during some experiments.

In addition to the numerical reduced data presented in this subsection, statistical data for oil slick effects on dispersion are

-158-

presented in Appendix 6. Those data can only indicate gross effects on the dispersion process because of the large number of variables.

TABLE 5-2 DISPERSION ANALYSIS RESULTS

RUN #	VOL/SA (CM)	%DISP	AVGZ (CM)	MAXZ (cm)	
1 0	0.112E 00	204.114	8.04	>35.3	THIN ARZ
2 0	0.353E-01	65.024	8.00	27.6	
3 0	0.143E-02	2.592	8.70	>35.3	
4 0	0.138E-02	2.515	16.02	>35.3	
2 1	0.126E-02	2.289	7.32	27.6	
5 1	0.110E 00	20.079	5.31	23.4	
6 0	0.171E-02	0.311	8.30	34.1	
7 0	0.444E-03	0.081	4.89	15.7	
8 0	0.596E-04	0.011	11.37	20.5	THICK ARZ
5 3	0.309E-02	0.563	11.61	>35.3	
6 1	0.139E-03	0.025	9.79	29.4	
7 1	0.445E-04	0.008	12.14	>35.3	
8 1	0.966E-04	0.018	14.19	>35.3	
9 0	0.304E-01	27.682	7.88	>35.3	
10 0	0.709E-01	64.499	8.44	29.4	
11 0	0.886E-02	8.057	11.74	30.0	
12 0	0.217E-02	1.970	12.31	35.3	THIN ABL
10 1	0.721E-02	6.552	7.00	>35.3	
10 2	0.136E-01	12.335	6.75	27.0	
10 3	0.343E-02	3.118	7.09	>35.3	
13 0	0.203E-01	3.788	4.48	22.2	
14 0	0.433E-02	0.788	5.99	29.4	
15 0	0.228E-03	0.041	8.73	27.6	THICK ABL
16 0	0.708E-04	0.013	7.06	19.3	

RUN #	VOL/SA (CM)	TDISP	AVGZ (CM)	MAXZ (cm)	
17 0	0.853E-01	155.133	6.29	21.6	THIN THUMS
18 0	0.322E-01	58.531	7.03	29.4	THIN THUMS
19 0	0.887E-03	1.612	5.49	17.5	THIN THUMS
20 0	0.805E-03	1.466	11.80	34.1	THIN THUMS
21 0	0.175E 00	31.733	4.88	34.7	THICK THUMS
22 0	0.191E-01	3.473	5.87	22.8	THICK THUMS
23 0	0.117E-01	2.110	9.24	34.7	THICK THUMS
24 1	0.236E-03	0.643	5.56	19.9	THICK THUMS
25 0	0.853E-01	155.131	7.31	>35.3	THIN ZUE
26 0	0.336E-01	61.059	4.77	30.0	THIN ZUE
27 0	0.307E-02	5.573	8.38	>35.3	THIN ZUE
28 0	0.260E-02	4.737	12.07	>35.3	THIN ZUE
29 0	0.244E-02	0.443	8.37	20.5	THICK ZUE
30 0	0.152E-02	0.276	5.77	19.3	THICK ZUE
31 0	0.244E-03	0.044	5.60	12.8	THICK ZUE
32 0	0.384E-04	0.007	6.49	11.6	THICK ZUE
33 0	0.240E-01	50.986	5.15	>35.3	THIN #2 DIESEL
34 0	0.322E-01	58.531	7.86	35.3	THIN #2 DIESEL
35 0	0.202E-01	36.805	8.51	35.3	THIN #2 DIESEL
36 0	0.164E-02	2.974	5.41	35.3	THIN #2 DIESEL
37 0	0.365E-02	0.664	4.73	17.5	THICK #2 DIESEL
38 0	0.118E-02	0.215	5.80	21.6	THICK #2 DIESEL
39 0	0.119E-02	0.217	11.09	32.4	THICK #2 DIESEL
40 0	0.261E-03	0.047	6.35	18.1	THICK #2 DIESEL

RUN #	VOL/SA (CM)	%DISP	AVGZ (CM)	MAXZ (cm)	
41 0	0.143E-01	2.605	7.55	27.9	THICK MINERAL
42 0	0.528E-13	0.066	7.67	35.3	
43 0	0.204E-02	0.372	10.73	>35.3	
44 0	0.217E-03	0.039	2.88	34.7	
45 0	0.340E-02	6.176	5.60	17.5	THIN COLD ZUE
46 0	0.735E-02	13.369	10.38	34.7	
47 0	0.962E-03	1.739	7.83	27.6	
48 0	0.401E-03	0.728	9.63	29.4	
49 0	0.768E-04	0.014	10.63	35.3	THICK COLD ZUE
50 0	0.630E-03	0.115	6.59	>35.3	
51 0	0.573E-03	0.104	7.73	35.3	
52 0	0.549E-03	0.100	13.32	>35.3	
57 0	0.237E-01	4.307	4.91	32.9	THICK MINERAL + ZONYL A
58 0	0.406E-02	0.738	7.13	>35.3	
59 0	0.208E-03	0.031	9.25	>35.3	
60 0	0.342E-03	0.062	10.66	>35.3	

Analysis of ZUE and Cold ZUE Data to Determine Effects of Oil
Viscosity on Dispersion.

The data from the Zue-Cold Zue experiment may be evaluated to
determine the effects of absolute oil viscosity (μ) on dispersion
characteristics. A perfectly controlled experiment requires all oil
parameters except μ to be held constant. This was not exactly the case;
T_{ow} and SG both vary slightly. However, μ is changed much more than
these other parameters; thus viscosity alterations are primarily
responsible for dispersion parameter changes.

The viscosity measurements actually made before and after
experiments are the appropriate values for use in 2 sec and 20 sec
tests, respectively, and are entered as such in the following tables.
Viscosity values for 5 sec and 10 sec runs are unknown and were
interpolated from the 2 sec and 20 sec measurements. The % variation
values are calculated by the function:

$$\% \text{ Variation} = \frac{\beta_c - \beta_{rt}}{\beta_{rt}} \times 100 \tag{5.4}$$

where β is μ, Ψ, or AVGZ; and c, rt signify cold and room temperature
conditions, respectively.

Table 5-3 shows values of test conditions and Ψ, AVGZ and MAXZ
for the ZUE tests under standard (room temperature) conditions and for
the cold ZUE tests.

-163-

Table 5-3 Summary of Analyzed Data for ZUE and Cold ZUE Tests

ZUE	Thin				Thick			
Temp (°c)	22.5			23.0	25.0			25.0
TEST #	25	26	27	28	29	30	31	32
Time (sec)	2	5	10	20	2	5	10	20
μ (c p)	4.28	11.3	18.2	25.2	4.04	4.40	4.76	5.11
∀ x 10³ (cm)	85.3	33.6	3.07	2.60	2.44	1.52	.244	.038
AVG ƶ (cm)	7.31	9.77	8.38	12.1	8.27	5.77	5.00	6.49
MAX ƶ (cm)	>35.5	30.0	>35.3	>35.3	20.5	19.3	12.8	11.6

COLD ZUE	Thin				Thick			
Temp (°c)	4.5			9.0	9.0			11.0
Test #	45	46	47	48	49	50	51	52
Time (sec)	2	5	10	20	2	5	10	20
μ (c p)	26.7	84.1	142	199	21.8	20.4	18.9	17.5
∀ x 10³ (cm)	3.40	7.35	.989	.401	.077	.630	.513	.549
AVG ƶ (cm)	5.60	10.4	7.80	9.63	10.6	6.57	7.73	13.3
MAX ƶ (cm)	17.5	34.7	27.6	29.4	35.3	>35.3	35.3	>35.3

% Variation	Thin				Thick			
Time (sec)	2	5	10	20	2	5	10	20
μ	524	644	680	690	440	364	297	242
∀ x 10³	-96.0	-78.1	-67.8	-84.6	-96.8	-58.6	134	1344
AVG ƶ	-23.4	-6.45	-6.92	-20.4	28.2	14.2	54.6	105
MAX ƶ	–	15.6	–	–	72.2	+	175	+

These results may be analyzed further by averaging the variation for the four time samples. It is noted that the sample for Test 32 is atypical because it has such a low value for Ψ relative to the 10 sec sample. Examination of all test data shows only a few cases with such a large change. The Ψ value for Test 52 is also a bit unusual since most 20 sec samples have less concentration than do 10 sec samples. The combination of these two effects leads to a large positive value for variation as shown in the table. Based on the arguments above, it is felt that the 20 sec data for the thick slick is not representative of the usual phenomenon, hence it was not included in variation averages. The averaged data are given in Table 5-4.

Table 5-4   Averaged Variation Results for Dispersion Changes in ZUE Oil Tests Due to Viscosity Increase

THIN SLICK: μ increased by a factor of 7

               Ψ decreased by 80%

               AVGZ decreased by 10%

               MAXZ decreased *

THICK SLICK: μ increased by a factor of 4

               Ψ decreased by 10%

               AVGZ increased by 30%

               MAXZ increased *

* Undefined maximum values prohibit determination of percentage values.

It is noteworthy that increased viscosity caused an increase in the height of the breaking wave (see Figures 5-24 through 5-27 and 5-30 through 5-33). One would expect this phenomenon to cause increased breaking intensity which must increase dispersion. Since the increased viscosity case shows less dispersion, the reduction in dispersion due to the viscosity increase is shown to be stronger than the increased dispersion due to the more energetic wave.

-165-

Analysis of Mineral and Mineral + Zonyl Data to determine Effects
of Oil-Water Interfacial Tension on Dispersion.

The data from the Mineral and Mineral + Zonyl A tests may be
compared for direct observation of the effects of interfacial tension
(T_{ow}) on dispersion characteristics. A true test for T_{ow} effects
requires all other variables to remain constant and this was not
exactly the case. In particular, the value of μ for the Mineral +
Zonyl A tests is roughly twice the value of its Mineral test counter-
part because the Mineral + Zonyl A test was conducted at a lower
temperature. However, the change in μ works in opposition to the
results of this experiment according to the ZUE-Cold ZUE results;
i.e., increased μ should decrease Ψ. This consideration supports
the argument that T_{ow} is responsible for dispersion changes in the
Mineral, Mineral + Zonyl A experiment, yet also indicates that dis-
persion changes due to T_{ow} are offset by μ effects. Thus, the results
of data evaluation for this experiment give only qualitative indi-
cation of the direction of T_{ow} effects.

In the tables which follow, the T_{ow} values for 2 sec and 20 sec
tests were taken from measurements made before and after those tests
respectively, and values for the 5 sec and 10 sec tests were inter-
polated. The variation percentages were calculated by the equation:

$$\% \text{ Variation} = \frac{\beta_z - \beta}{\beta} \times 100 \tag{5.5}$$

where β is T_{ow}, Ψ, AVGZ, or MAXZ; no subscript indicates a value for a
Mineral test, and z indicates a Mineral + Zonyl A value.

Test conditions and reduced data are shown in Table 5-5.
Averaging the associated groups of four experiments gives the results
of Table 5-6.

TABLE 5-5 <u>Summary of Analyzed Data for Mineral and</u>
<u>Mineral + 0.1% Zonyl Tests</u>

MINERAL (thick)

Test #	41	42	43	44
Time (sec)	2	5	10	20
T_{OW} (dyne/cm)	40.5	40.5	40.5	40.5
$\Psi \times 10^3$ (cm)	14.3	.528	2.04	.217
AVG Z (cm)	7.55	7.67	10.7	9.88
MAX Z (cm)	27.9	35.3	>35.3	34.7

MINERAL + ZONYL A (thick)

Test #	57	58	59	60
Time (sec)	2	5	10	20
T_{OW} (dyne/cm)	1.2	2.3	3.5	4.6
$\Psi \times 10^3$ (cm)	23.7	4.06	.209	.342
AVG Z (cm)	4.91	7.13	9.25	10.7
MAX Z (cm)	32.9	>35.3	>35.3	>35.3

% VARIATION

Time (sec)	2	5	10	20
T_{OW}	-97	-94	-91	-89
Ψ	65.7	669	89.8	57.6
AVG Z	-34.9	-7.04	-13.6	8.30
MAX Z	17.9	+	0	+

TABLE 5-6   Averaged Variation Results for Dispersion Changes
for Mineral Oil Tests

T_{ow} decreased by a factor of 10

V increased by 180%

AVGZ decreased by 10%

MAXZ increased *

* Undefined maximum values prohibit determination of percentage
  values.

Analysis of Effect of Slick Thickness on Dispersion

The standard experimental procedure provides an excellent test for slick thickness effects as it tests each oil for two different thicknesses, hence varying thickness (h) while holding all other parameters essentially constant. A total of twenty-four case studies are available from the data by comparing dispersion characteristics of thin (h=0.55 mm) and thick (h=5.5 mm) slick tests for the six oils which were tested with both thicknesses.

The variation in dispersion characteristics due to the change in slick thickness may be expressed as a percentage by the equation:

$$\% \text{ Variation}^* = \frac{\beta_{tn} - \beta_{tk}}{\beta_{tn}} \times 100 \qquad (5.6)$$

where β may be %DISP, or AVGZ, and tn, tk indicate a value for the thin slick and thick slick, respectively. This expression for the change in dispersion characteristics with slick thickness was used to calculate variation values for each of the twenty-four test cases. Average variation values were then calculated for each oil. An example of the procedure is shown in Table 5-7 for ARZ, and the results from using the same technique for other oil data are listed in Table 5-8. These results are then averaged over all oils to yield the general effect of increased oil thickness as shown in Table 5-9. THUMS data cannot be included in this overall average because it is based on the thin h value of 1.1 mm.

MAXZ was often too large to be measured experimentally so it was subjectively evaluated.

---

* NOTE: This definition of % Variation is not consistent with those for other slick properties since the difference is divided by the first, not second, quantity in the numerator, i.e., $\beta_a - \beta_b / \beta_a$ rather than $\beta_a - \beta_b / \beta_b$. This inconsistency was necessary to avoid excessively large and confusing % Variation values. The change has little effect on data interpretation since % Variation is independently evaluated for different oil slick properties.

TABLE 5-7 ARZ Crude Thickness Effect Evaluation

Time (sec)		2	5	10	20
THIN	% DISP	204	65.0	2.59	2.52
	AVG Z	8.04	8.00	8.70	16.0
THICK	% DISP	20.1	.311	.081	.011
	AVG Z	5.31	8.30	4.89	11.4
% Variation	% DISP	90.1	99.5	96.9	99.6
	AVG Z	34.0	-3.8	43.8	28.8

Average % Variation

%DISP	96.5
AVGZ	25.8

By observation of the data (Appendix 8), MAXZ decreases with increased thickness for the ARZ tests.

TABLE 5-8   Effects of Increasing Oil Slick Thickness

| OIL | Average % Variation * | | MAX Z̶ |
	% DISP	AVG Z̶	
AR̶Z̶	96.5	25.8	DECREASE
ABL	96.8	35.0	DECREASE
THUMS	59.8	1.83	INCREASE
Z̶UE	99.6	28.6	DECREASE
COLD Z̶UE	63.5	-22.4	INCREASE
#2 DIESEL	99.1	3.94	DECREASE

* Positive values indicate a decrease in %DISP or AVGZ as oil thickness
   was increased.

TABLE 5-9   Variations Averaged Over All Oils (Except THUMS)

h increased by a factor of 10

%DISP decreased by 80%

AVGZ decreased by 10%

MAXZ decreased

5.6 Error Analysis

This section describes possible errors due to experimental techniques; for a discussion of instrument tolerances, refer to Appendix 2.

The standard breaking wave for water with no oil slick was found to be reproduceable within ±5% in wave height and ±2% in wave period. Therefore, the oil test cases where variations exceed these values must be indicative of wave characteristic changes due to the presence of the oil slick. In fact, as shown § 5.4, when a thick (5 mm) layer of viscous oil is present, the breaking waves are larger. This must be due to inhibition of breaking by the oil, thus allowing the waves to grow larger as they pass through the contraction.

Some variation in wave and oil dispersion characteristics may be partially due to lack of uniformity of slick thickness. After each test, the slick was allowed to return to uniform thickness by delaying the subsequent test. This return to uniformity was often accelerated by blowing surface oil back to the breaking region while being careful not to disperse additional oil. The slick was assumed to be of uniform thickness when it was continuous and covered the entire free surface of the wave channel. This criterion is far from precise, and variations in thickness may have been as much as 50%. This error could not be avoided since the excessive length of time necessary to assure uniform thickness after each test conflicts with the problem of oil aging, a phenomenon which requires that tests be conducted rapidly before oil properties change due to evaporation.

The possibility of experimental bias due to hydrodynamic wall effects at the water sampler ports was investigated by using 2.54 cm (1.0 in) extender tubes which were press fit into the sampler ports located in the tank wall. The concentrations of samples taken for ARZ crude oil dispersions three seconds after passage of the breaking wave with and without extension tubes showed significant variation in only one sample. Hence, wall effects were not significant and the use of extension tubes was discontinued.

-172-

It is quite possible that the hydrodynamic effects of the test

tank bottom caused experimental bias in the maximum depth to which oil

was dispersed (MAXZ); yet this problem does not appreciably affect the

oil volume dispersed (VOL/SA) or average dispersion depth (AVGZ). The

data in Table 5-2 shows that MAXZ often approached the 47 cm tank

bottom with values in excess of the sampler limit of 35.3 cm. However,

AVGZ is generally less than 10 cm, and has a maximum value of 16.02 cm.

Because the bulk of the dispersed oil remained near the surface and

because the time frame observed was short (avoiding circulation

problems), it is felt that tank bottom effects may be neglected for

all data evaluation, with the exception of MAXZ.

Dispersion nonuniformities in the horizontal plane were observed
to exist and, in fact, breaking nonuniformity probably cannot be
avoided. (See Longuet-Higgins and Turner, 1974.) This is probably the
largest stochastic variable in these experiments and could easily affect
individual results markedly. (See Figure 5-3.) It can only be reduced
by repeating the experiments many times and averaging results which
would reduce the variance of the effect by the inverse of the number
of tests used to generate the average. Funds and time for repeated
tests were not available.

Water sample contamination due to residual oil in the sampling
system was minimized by using smooth bore valves and keeping intake
tubing as short and straight as possible. In addition, the purge
system was used to flush the intake lines with clean hot water after
sampling. Purging duration was restricted to a few seconds in order
to avoid significant effects on tank water temperature. The effective-
ness of this system in excluding oil contamination was tested by
drawing a sample of clean water through one port of the sampler
following a standard test with Thums crude. The oil concentration of
the sample which preceded purging was 24.2 ppm, and the concentration
found for clean water was 3.3 ppm. It is therefore reasonable to
assume that 1 to 5 ppm may be attributed to sample contamination for
any instance where the previous sample collected had a concentration
of at least 10 ppm. This bias may cause excessively large average and maximum
dispersion depth values since here small concentrations are important,
but contamination has very little effect on total dispersion volume
considerations where large oil concentration values (10^2 to 10^4 ppm)

are encountered.

Calibration samples used in infrared analysis should generate
straight lines on an absorbtion vs. oil concentration plot, but the
curves generated in this study varied from straight lines by a
maximum of about 10% on the average and as much as 100% for the 5 ppm
sample (Appendix 5). This apparent large error for small oil concen-
trations may be attributed to the sample preparation technique or to
the extraction technique. However, this departure from straight lines

-174-

may be due to water contaminants which are representative background levels, in which case an accurate calibration is provided. If an error is in fact present, since it occurs only at low concentrations, it affects the accuracy of dispersion depth representations but is negligible relative to dispersion volume. Calibration curves used were linear approximations to calibration sample data and if background levels were present, they were ignored, causing dispersion depth values which would be slightly larger than true values.

The emulsions observed in the oil following the Zue and Mineral + Zonyl A tests may have a marked effect on viscosity and surface tension measurements. Because the viscometer tubes are not designed for mixtures, it is possible that water or air bubbles in suspension within the oil cause erroneous viscosity measurements. If, however, these bubbles are small relative to the viscometer tube diameter, a value will be measured which is representative of the effective viscosity of the mixture. Similar arguments may be made for surface tension measurements, but here the critical bubble size is not obvious. Surface tension measurements are placed in question for only the oils cited above because the emulsion problem may be readily observed at the fluid interface if it is extensive enough to alter measurements seriously. However, any post-test viscosity measurements which are exceptionally high must be held in question because the opacity of crude oil and the smaller critical bubble size make detection of critical bubbles suspended within the oil quite unlikely.

The surfactant migration experiment performed with Mineral Oil + 0.1% Zonyl A mixtures indicates a tendency for dispersed oil to have lower surface tension (Appendix 3), thus indicating a tendency for surfactant to migrate to the oil-water interface of the oil slick. However, this tendency does not discount the general results of the special experiment using Mineral + Zonyl A to evaluate interfacial tension effects on dispersion characteristics since migration of surfactant to the interface would only further decrease the value of T_{ow}. Hence, Mineral + Zonyl A tests would still represent a reduction in T_{ow} from its value for mineral oil alone. It is possible that

-175-

surfactant migration effects are important as a short lived phenomenon occurring during formation of oil droplets, a mechanism not detectable by this surfactant migration experiment since the oil collected from dispersions had recoalesced before surface tensions were measured. If this phenomenon does exist, then the results of the Mineral – Mineral + Zonyl A experiment would need more careful interpretation. No further evidence in this study supports the short lived phenomenon hypotheses, yet it should be kept in mind when evaluating the Mineral – Mineral + Zonyl A experiment results.
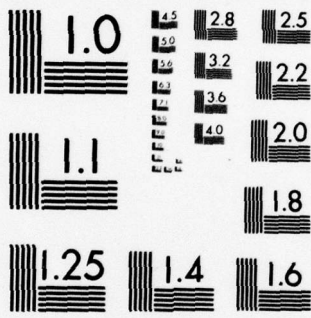
MICROCOPY RESOLUTION TEST CHART
NATIONAL BUREAU OF STANDARDS-1963-A

5.7   Results

Effect of Oil Properties on Total Oil Volume Dispersed (∀)

The dependence of dispersed oil volume on the oil absolute
viscosity is isolated by comparison of Zue (Tests 45-52) and Cold Zue
(Tests 45-32) data. For these data, a sevenfold increase in the
viscosity of Zue Crude results in an 80% reduction in the oil dispersed
from a thin slick, and a fourfold increase in viscosity results in
7.0% reduction in the oil dispersed from a thick slick. Strong
viscosity effects are not observed when comparing the dispersions
of various oils as is demonstrated by the statistical approach of
Appendix 6. This study therefore indicates that increased oil
viscosity does decrease the total oil volume dispersed but that
this mechanism apparently does not outweigh as yet unexplained
offsetting effects due to other oil properties when oils of differ-
ing chemical composition are compared.

A focus on the effects of oil-water interfacial tension is made by
comparison of Mineral (Tests 41-44) and Mineral + Zonyl A (Tests 57-60)
data. In this experiment, a decrease in interfacial tension by a
factor of ten increased the dispersed oil volume by 180%. The statis-
tical approach to data evaluation (Appendix 6) proves to be unsatis-
factory for evaluation of interfacial tension effects on oil disper-
sion. Results from this approach are unreliable primarily due to the
small variation of interfacial tension for the oils tested and also
due to unknown masking interactions caused by other oil properties.
The conclusion which must be drawn is that decreased interfacial
tension does tend to cause greater volumes of oil to be dispersed
but the relative strength of this mechanism in the dispersion process
is unknown.

A controlled experiment in which oil density is varied while
holding other oil properties constant was not possible because addition
or removal of any oil components to alter density also changes other
oil characteristics. It is possible, however, to look for changes in
dispersion characteristics due to variance in oil specific gravity or
in Δ (Δ=1.0-SG) by comparing the data from different oils. Statistical

analysis which completes these comparisons for all possible cases
available from test data (Appendix 6) shows that Δ has no apparent
effect on the total oil volume dispersed. It is quite possible,
however, that Δ has an effect on ∀ which is balanced by the interaction
of other oil characteristics and hence is undetected by the statistical
analysis.

Effect of Oil Properties on Short-Term Average Dispersion Depth (AVGZ)

The results of this study indicate that absolute oil viscosity
has no obvious effects on average dispersion depth. Results appear to
be contradictory for the Zue, Cold Zue experiment where a 10% decrease
in AVGZ was caused by sevenfold increase in viscosity in the thin slick
and a 30% increase in AVGZ was found for a fourfold increase in viscosity
for the thick slick. This apparent contradiction may, however, be the
result of an unknown interaction between slick thickness and oil
viscosity effects in the dispersion process. Evaluation of data from
different oil tests shows no correlation between viscosity and average
dispersion depth (Appendix 6).

When interfacial tension was decreased by a factor of ten in the
Mineral – Mineral + Zonyl A tests, AVGZ was decreased by 10%. Statis-
tical evaluation of all test data shows a slight correlation between
interfacial tension and average depth which supports this finding
(Appendix 6). It is possible that these, and other, results may be
related to small variations in breaking wave height and intensity in
our experiment due to variations in oil slick properties.

Oil specific gravity effects on average dispersion depth can only
be investigated by the statistical comparison of different oils shown
in Appendix 6. This analysis shows no correlation between Δ and
AVGZ; hence it is concluded that other oil properties must affect
average dispersion depth to at least the same degree that it is affected
by Δ so that density effects are masked.

-178-

Effects of Slick Thickness on Percentage of Oil Dispersed (%DISP)

A very strong dependence of dispersion concentration on slick thickness was exhibited by all test oils. Of the twenty-four comparative cases between slicks of different thickness but composed of the same oil, twenty-two cases showed a definite decrease in %DISP, and twenty of these cases actually showed a decrease in the total oil volume dispersed when slick thickness was increased. This decrease in total oil dispersed might be surprising to some readers since one would expect a thick slick to provide more oil for dispersion than a thin slick of similar oil. However, the reliability of the experimental result is quite good since all oil slick parameters were held constant while thickness was varied to provide a well controlled experiment and many tests are available for evaluation. Averaged results for the controlled experiment cases show a decrease of 80% in %DISP for a tenfold increase in slick thickness. Comparison of various oils by the less controlled statistical methods (Appendix 6) yields a strong correlation between %DISP and slick thickness which supports the results cited above, thus indicating that slick thickness is a parameter which is extremely important in the dispersion process.

Effect of Slick Thickness on Dispersion Depth

When the data are compared for a given oil with varying slick thickness, it is found that on the average a tenfold increase in slick thickness decreased AVGZ by about 10%.

Statistical comparison of various oils also indicates that AVGZ decreases with increasing slick thickness, therefore indicating that slick thickness has a greater effect on average dispersion depth than do oil properties.

Observation of dispersion data for different slick thicknesses of the same oil indicates that maximum dispersion depth is less for thick slicks on the average, although data for two of the six oils so evaluated exhibit the opposite trend. Comparison of different oils as shown in Appendix 6 yields a weak correlation between slick thickness and MAXZ, which also indicates a tendency for maximum dispersion depth to decrease with increased slick thickness.

Effect of Slick Thickness on Oil Droplet Size Distribution

Observation of still photographs taken of oil dispersions during sampling reveals that average and maximum droplet size increase with increased slick thickness. The photographs also show that thickness effects on droplet size are less apparent at longer periods after breaker passage. This phenomenon is due to the greater terminal rise velocity of large buoyant droplets which reach the water surface much sooner than do small droplets. Hence, the large oil droplets which distinguish thick slick dispersions are not present long after the breaker has passed.

Evaluation of effects of slick thickness on minimum droplet size is not possible using dispersion documentation from this study, since the smallest oil droplets are too small for detection by the unaided eye and are definitely too small to be observed in the photographs taken.

Effects of Oil Slick Aging on Dispersion

Aging is the change in oil slick properties due to exposure to air and water and may be modeled as two distinct phenomena. Static aging is defined here as the process where oil slick properties are changed due to exposure with no breaking waves. This form of exposure provides conditions for evaporation of lighter factions to the atmosphere and migration of other fractions into the water column due to gravity or chemical diffusion. Dynamic aging may be defined as oil slick property changes due to the turbulent mixing of breaking waves.

The results of this study show that for the oil properties measured (ν, T_{ow}, and SG) the more predominant form of aging appears to be dynamic aging. This conclusion is reached by reviewing oil property measurements made before and after oil slick exposure in the test tank while considering phenomena which were observed during tests. For example, ABL crude was noted to have an extremely pungent odor signifying a high evaporation rate of some oil components, thus indicating rapid static aging. This oil, however, exhibited less change in its properties due to general aging than did other oils

-180-

which produced very little odor. Another argument supporting the
concept that dynamic aging dominates is found upon examination of
Cold Zue crude data. Lowering oil temperature for this
experiment should decrease evaporation and migration of oil components
yet no significant difference is observed in aging effects between
room temperature Zue and Cold Zue crude. Hence, it is observed that
the effects of static aging on oil properties are weak relative to
dynamic aging effects.

Reviewing the changes in oil properties for all test oils shows
that aging has the general effect of increasing absolute viscosity,
decreasing oil-water interfacial tension, and increasing oil density
(decreasing Δ). Of these properties, oil viscosity exhibits the
greatest change due to aging with the most pronounced changes occurring
in thin slicks. Increased oil density indicates that evaporation or
water entrainment has occurred, yet it is not clear from the data
which of these mechanisms is most influential. The results of special
tests (2A, 5C, 6A, 7A, 8A, 10A, 10B, and 10C) which were conducted
to evaluate aging effects on dispersion show that less oil is dispersed
from an aged slick than from a young slick.

In summary, it is obvious that the amount of oil dispersed
decreases with increasing oil slick age, but the mechanisms which
cause this effect are complex and as yet unknown. The influence of
water entrainment, for example, may not be ascertained from data
produced by this study, but it has been shown that extensive entrainment
occurs in some oils (Appendix 4).

Effects of the Oil Slick on Wave Characteristics

The changes in wave amplitude, period, surface slope, and surface
vertical acceleration of waves in the standard wave group due to oil
slick properties may be observed by comparing strip charts for various
test con :ions. This analysis indicates that the amplitude of the
breaking wave generally increases with increasing slick thickness,
oil viscosity, oil-water surface tension, and aging as shown in
Appendix 6. Slick thickness is found to be the most critical parameter;

the average breaking wave amplitude increase for thin slicks is about
10% and is approximately 40% for thick slicks. Oil viscosity seems to
be important in determining breaker amplitude where increased viscos-
ity increases wave amplitude. Evidently, increased viscosity and ten-
sions inhibit breaking and allow the contraction to generate larger
waves before breaking begins.

The time interval between the first wave node of the standard
wave group and the node preceding the breaking crest was found to
increase by generally about 5% due to the presence of an oil slick,
with a maximum change of 10% for aged Zue crude in a thick slick. It
was also found that time intervals between wave nodes following the
breaker sometimes changed when oil was placed in the tank. The relative
phase shifts indicated by such changes are believed to be caused when
the oil slick alters wave phase speed (Milgram, MIT Ocean Engineer-
ing Department, 1978, unpublished). Here, the rate at which frequency
components of the wave group separate changes due to oil so that the
relative position of waves within the group at any given instant is
also changed.

The average free surface vertical acceleration of the breaking
crest in clean water was found to be 4.4 m/sec^2 (14.4 ft/sec^2) when
measured with the capacitance probe, a value in fair agreement with
the 1/2g predicted by Longuet-Higgins (1969). This was found by aver-
aging the peak acceleration (actually a deceleration) of three separate
breaking waves. This same acceleration measured and averaged in the
same way with the float wave gauge was 3.6 m/sec^2 (11.8 ft/sec^2). The
discrepancy between the two instruments is due to the mechanical lag
of the less accurate float gauge. Correcting the float gauge reading
to match the capacitance probe requires a 22% increase in the float
gauge acceleration measurement.

It was observed that free surface vertical acceleration for the
standard breaker was increased by the presence of an oil slick. The
float gauge measurement for this acceleration in the presence of a
thick (5.5 mm) Mineral + Zonyl A oil slick was 4.6 m/sec^2 (15.2 ft/sec^2),
showing a definite increase above the 3.6 m/sec^2 value found for clean

-182-

water. The corrected acceleration value for water with an oil slick based on the 22% factor previously discussed is 5.6 m/sec^2 (18.5 ft/sec^2), which is well above the theoretical prediction of 1/2g for clean water. Although acceleration measurements were made only for Mineral + Zonyl A, the increased wave amplitude measured for other oils is evidence that they too exhibit increased acceleration due to the oil slick.

These observations indicate that an oil slick increases the wave steepness required to support breaking. Therefore, for a given sea state with wave breaking in the absence of oil, introduction of an oil slick will reduce or may completely eliminate the number of waves which break.

Energy loss rate due to breaking waves in the wave channel used for experiments is proportional to the square of wave amplitude according to Equation (A1.9) of Appendix 1. Applying this relationship to the average values found for wave amplitude increase due to thin oil slicks (10%) and for thick oil slicks (40%) reveals that the energy loss rates must increase by about 20% and 90% respectively. In the wave channel convergence energy loss rate for a given wave was held constant in the observation region after initial breaking began (Appendix 1). It is interesting to learn that increased slick thickness reduced dispersion even though the energy lost in breaking was increased.

Observations of Dispersion Characteristics

It is difficult to present a discussion or photograph of a "typical" dispersion because the detailed appearance and time behavior of each dispersion was indeed unique. The dispersions shown in Figure 5-3 therefore serve as example cases and should not be interpreted as being descriptive of all oils. Although direct observation of oil slick dispersions does not provide the detailed information necessary to quantify their characteristics, it does provide some insight to trends common in all dispersions. This insight is useful in interpreting the quantitative results from water and dispersion sample analysis.

Close observation of breaking wave passage through the oil slick revealed that oil was dispersed by both the breaking face of the wave, and by the turbulent wake which followed the breaking crest. It appeared that the leading edge of the breaker destroyed the continuity of the slick and forced a number of irregularly shaped oil masses and a very large number of spherical oil droplets of varying diameters beneath the water surface. The turbulent wake which subsequently acted on the infant dispersion tended to increase the depth of the smaller oil droplets while the large oil masses simultaneously rose toward the surface. Areas of horizontal nonuniformity in the dispersion which are probably due to either wake instabilities of the type discussed by Townsend (1976) or breaking instabilities described by Longuet-Higgins and Turner (1974) were often observed and are illustrated in Figure 5-3. These photographs show oil dispersions viewed through the 43.2 cm (17 in) wide observation window in the tank test section after wave passage from right to left. The dark edge framing the top of the white background is the oil slick.

Dispersions generally appeared to be continuous over vertical distance but varied in oil concentration and droplet size. This differs from horizontal nonuniformities in that the dispersion appeared to have intermittent regions of high oil concentration over horizontal distance, while oil concentration generally decreased monotonically with vertical distance.

The depth to which oil was carried was often observed to increase with time, a phenomenon which is exemplified by comparison of Figures 5-3a and 5-3b. Droplet size for the oil masses which were small enough to stabilize into spherical shapes ranged from diameters of less than one millimeter to approximately three millimeters. It is suspected that droplets as small as 0.1 millimeter or less which escaped detection by eye were also present in the dispersions. The presence of oil droplets smaller than visible size is also evidenced by water samples which contained no visible oil but had oil concentration levels exceeding possible background levels for clean tank water.

-184-

Water filled oil droplets were also occasionally found in the dispersion with diameters of approximately 0.5 to 1.5 centimeters. These droplets are recognized as water filled because they are lighter in color than oil droplets and exhibit a slower rise velocity than do oil droplets of similar size, thus indicating reduced buoyancy due to a water filled center.

The horizontal spreading properties of most crude oils did not vary significantly with the exception of ABL crude, which exhibited a strong tendency to form many thick lenses on the water surface rather than the thin continuous slick which resulted for most oils. This phenomenon is unusual and unexplained by data taken in this study, since T_{oa}, T_{wa}, and Δ values were quite similar to those values for ARZ crude, which spread rapidly, and both oils were placed on water of the same surface tension. Mineral and Mineral + Zonyl A both exhibited the same resistance to formation of a continuous slick, giving unconditional evidence that this characteristic is not solely dependent on statically measured interfacial surface tension.

It was observed that for the same oil and slick thickness the position in the wave channel convergence where wave breaking began sometimes varied as much as .3 meters from the standard position of approximately one meter upstream of the sampler. The position of initial wave breaking was quite reproduceable for clean water; therefore this variable condition must be attributable to oil slick thickness or oil property nonuniformities.

Emulsion formation in the oil slick was observed for the thin ZUE crude and Mineral + Zonyl A tests. The entrainment of bubbles or water droplets within the oil recovered from the oil slicks formed an emulsion which was readily obvious by visual inspection of the oil. The nature of this emulsion was not investigated during standard test procedures, but it is apparent that the bubbles must be composed of either air or water.

5.8 Conclusions from the Breaking Wave Experiment

These experiments have investigated the effects of various oil slick properties on the characteristics of oil dispersions generated

by a "nearly" standard breaking wave. The standard breaking wave was approximately 6 cm (2.4 in) in amplitude from the still water level to the crest and caused oil slick dispersions whose oil volume per unit surface area varied by a factor of about 200. The average depth of dispersed oil was found to be between one and two times the wave amplitude and the maximum depth at which oil was found was five times the wave amplitude or greater. These values all varied for different oils and different oil thicknesses and with time after passage of the breaking wave. The roles of oil thickness, absolute viscosity, and oil-water interfacial tension were each investigated by comparative analysis under controlled conditions with the results shown below in Table 5-10.

TABLE 5-10   Oil Slick Dispersion Parameters

OIL SLICK PROPERTY VARIATION	OIL VOLUME DISPERSED	AVERAGE DISPERSION DEPTH	MAXIMUM DISPERSION DEPTH
Increase slick thickness	DECREASE	DECREASE	DECREASE
Increase oil viscosity	DECREASE	NO APPARENT EFFECT	DECREASE
Increase oil-water interfacial tension	DECREASE	INCREASE	DECREASE

In addition to controlled conditions which isolated the effects of specific oil slick properties, comparative analysis between different oils has shown that complex interactions generally mask the effects of all oil slick properties except slick thickness.

Based on observations of high speed motion pictures of the dispersion process and on the effects of oil-water interfacial tension, it appears that dispersion occurs in two phases. The first phase consists of destruction of oil slick continuity by the face of the breaking wave which causes an initial downward thrust of oil into the water column. After passage of the breaker the turbulent wake dominates the second phase of the dispersion process where small stable oil droplets are carried to greater depths as the wake grows and large buoyant droplets rise towards the water surface. Throughout the initial phase and in the early stages of the second phase large unstable oil masses rise and rejoin the slick or split up due to turbulence to form stable smaller droplets.

Aging of the oil slick due to evaporation and turbulent mixing was found to have a marked effect on oil properties and dispersion characteristics. In general, increased exposure time brought about increased absolute oil viscosity, decreased oil-water interfacial tension, and increased oil density. It was also noted that exposure to breaking waves caused water entrainment in some oils, and it is suspected that other oils exhibit this phenomenon to a lesser degree. These changes in oil properties due to aging generally caused a decrease in the amount of oil dispersed due to the standard breaking wave.

The procedures used to recover and evaluate dispersion data in this study were adequate for an initial investigation of the oil dispersion process. However, many improvements are necessary if further studies are to provide additional information. Oil droplet size and distribution should be accurately measured, and maximum sampling depth should be increased. Also, a deeper wave tank would dispell any doubts that data is biased by bottom effects. Perhaps the most productive improvement would be the development of a procedure

similar to the one used in this study but which is more time efficient. The man-hours required for the oil measurements limited the amount of data that could be taken. This study has shown that the process of oil dispersion due to breaking waves is indeed complex, involving many interactions which can effectively mask the involvement of any given oil property. These interactions coupled with the basic random nature of breaking waves make up a process which requires a very large number of test cases to evaluate phenomena of the process with more detail than was done here.

6. THE TURBULENCE GENERATED BY A BREAKING WAVE

Breaking waves are the most important natural influence on the dispersion of oil slicks into droplets. The strong turbulence within the breaking crest accounts for the initial mixing of oil droplets into the water. The splitting of these droplets into smaller droplets is related to the intensity and the length scale of the turbulence. In addition, as shown elsewhere in this report, the rise time of oil droplets depends on the droplet size and the statistics of the turbulent velocity field.

There is extremely little information about the near surface turbulence in the vicinity of breaking waves. In fact, we have found no references containing measurements of the near surface turbulence beneath ordinary spilling breakers. Since this is the type of breaking wave most commonly found at sea, we undertook a program for the measurement of this kind of turbulence.

Instrumentation

The wavemaking system used for these experiments was the same one used in our experiments on the dispersion of oil by breaking waves, and the wave channel and wavemaking apparatus are described in the report section describing those experiments. For the experiments involving turbulence measurements, however, no oil was used and the wave channel was filled with clean water.

The problem of how to measure the fluid velocities beneath a breaking wave is a difficult one. At a fixed point in space the velocity direction reverses because of the orbital motion of the fluid particles. As a result, velocity measurement by hot film anemometry would have the following two major disadvantages:

(1) Hot film anemometry provides the flow speed, but not direction, so the direction would be unknown in reversing flows, and

(2) The relationship between hot film anemometer output voltage and flow speed is extremely nonlinear for the low fluid velocities that would be encountered near the times that the flow direction reversed.

Because of the above two difficulties with hot film anemometry, we measured the fluid velocities by laser anemometry. A schematic diagram of the laser anemometer system is shown in Figure 6-1. A very brief description of the laser anemometer system is given here to familiarize the reader with its fundamentals. The system we used is called forward scattering laser anemometry because the detection system is opposite the laser with the fluid whose velocity is to be measured lying between the laser and the detection system. The laser beam is initially passed through a beam splitter in order to obtain two laser beams. An optical system separates these two beams and then directs them so they cross at the point in the fluid where the velocity is to be measured. At the crossing point, the two beams generate an interference pattern of alternate dark and light lines spaced about one micrometer apart.

The detection system consists of an optical subsystem which focuses the laser beam crossing region in the fluid on a photomultiplier tube. When a suspended particle in the fluid having a velocity component v in the direction of alternating dark and light regions passes through the crossing point, it scatters light so that a photomultiplier tube output signal is generated at frequency $f = v/\lambda$, where λ is the distance from one light region to the next in the interference pattern. Thus, the output signal has a frequency which is proportional to speed.

The system described above could not discriminate between particles moving in one direction through the interference pattern from those moving in the opposite direction. This discrimination is provided by a system modification. As shown in Figure 6-1, after the laser beam is split into two beams by the beam splitter, one of the beams is passed through a Bragg cell. This is a block of glass which is mechanically driven at an ultrasonic frequency, thereby setting up acoustic waves within the glass. The laser beam interacts with the acoustic waves, and this generates an output light beam having a frequency equal to the sum of the incident laser light frequency and the ultrasonic frequency. A result of the two interfering beams

Laser System

Transmitting Optics and Freq. Shifter Assembly

Receiving Optics Assembly

Photomultiplier Assembly

Power Supply

PM.

Freq. Shifter

Bragg Cell

DC Exciter

Oscilloscope

Oscilloscope

Oscillograph

Tracker

Signal Conditioner

Signal Processor

Monitor & Power Supply
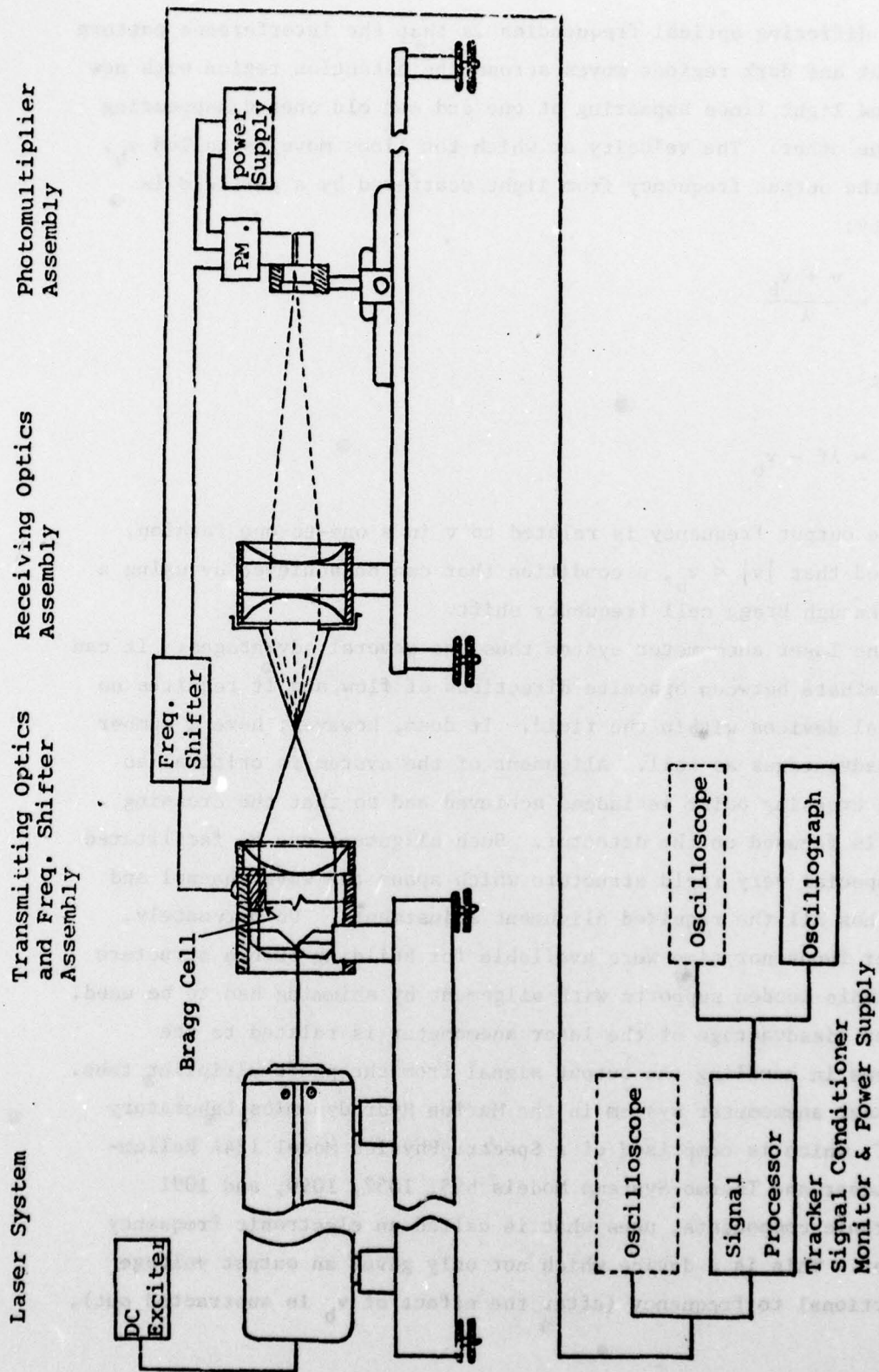
FIGURE 6-1 Forward-Scattering Laser Anemometer System

having differing optical frequencies is that the interference pattern
of light and dark regions moves across the detection region with new
dark and light lines appearing at one end and old ones disappearing
from the other. The velocity at which the lines move is called v_b.
Thus, the output frequency from light scattered by a particle is
given by:

$$f = \frac{v + v_b}{\lambda}$$

so that

$$v = \lambda f - v_b$$

and the output frequency is related to v in a one-to-one fashion,
provided that $|v| < v_b$, a condition that can be achieved by using a
large enough Bragg cell frequency shift.

The laser anemometer system thus has several advantages. It can
discriminate between opposite directions of flow, and it requires no
physical devices within the fluid. It does, however, have a number
of disadvantages as well. Alignment of the system is critical so
that a crossing point is indeed achieved and so that the crossing
point is focused on the detector. Such alignment can be facilitated
by a special very rigid structure which spans the wave channel and
which has all the required alignment adjustments. Unfortunately,
neither funds nor time were available for building such a structure
and simple wooden supports with alignment by shimming had to be used.
Another disadvantage of the laser anemometer is related to the
problems in handling the output signal from the photomultiplier tube.
The laser anemometer system in the Marine Hydrodynamics Laboratory
at MIT, which is comprised of a Spectra-Physics Model 124A Helium-
Neon Laser and Thermo-Systems Models 895, 1057, 1090, and 1091
electronic components, uses what is called an electronic frequency
tracker. This is a device which not only gives an output voltage
proportional to frequency (after the effect of v_b is subtracted out),

but also continues to give the last value of output voltage at times
when there is no small particle scattering light within the measure-
ment volume. In using this system, we found that the tracker,
Thermo-Systems Model 1090, gave output noise equivalent to an rms flow
speed of about 3 cm/sec, which is about an order of magnitude
larger than the manufacturer's specifications for the device. This
noise was relatively broadband with much of its frequency content
falling within the anticipated frequencies of hydrodynamic turbulence,
and therefore it could not be completely eliminated by filtering.
We undertook the experiments in spite of this problem because of the
importance of obtaining initial data about the turbulence beneath
breaking waves. We do point out, however, that improved experimental
results can be obtained in the future by use of a specially designed
and built adjustable metal structure and a different data handling
device (for which funds were not available within the present work).

Experimental Procedure

Our laser anemometer system can measure either horizontal or
vertical velocity components, but one at a time and not both
simultaneously (more sophisticated systems can measure both components
simultaneously). Therefore, we measured the horizontal and vertical
velocity components separately with a different breaking wave being
used for each measurement. Measurements were made at a variety of
depths beneath the free surface.

The wave profile used for these experiments was the same as was
used for the oil dispersion by breaking wave experiments and the
wave elevation as a function of time above the measurement point is
shown in Figure 5-20. Figure 6-2 shows our measurements of the
velocities as functions of time.

Following completion of the measurements shown in Figure 6-2,
we found that a substantial noise reduction within the laser system
would be possible by using a shorter focal length lens to focus the
laser beams at the crossing point. This increased the crossing angle
of the beams and therefore decreased the spacing between the light

-193-

**FIGURE 6-2   Measurements of Velocities in Water
at Fixed Locations Beneath Breaking Waves**

- - - - -

In each case, measurements were made for two
breaking waves, each generated by the same wave-
maker paddle motion.

Arrows on the time scales show direction of
increasing time.

Arrows on vertical velocity scales show direction
of upward velocity.

Arrows on horizontal velocity scales show
direction of wave propagation.

Heavy vertical bar on each figure indicates the
time of passage of the breaking crest.
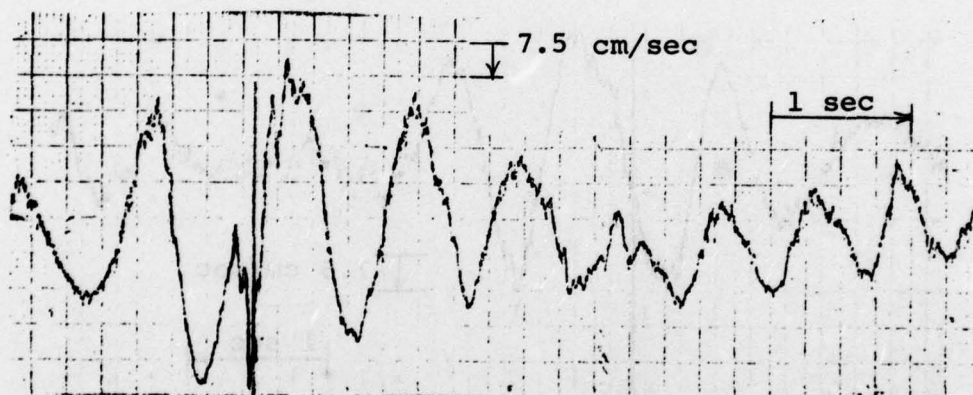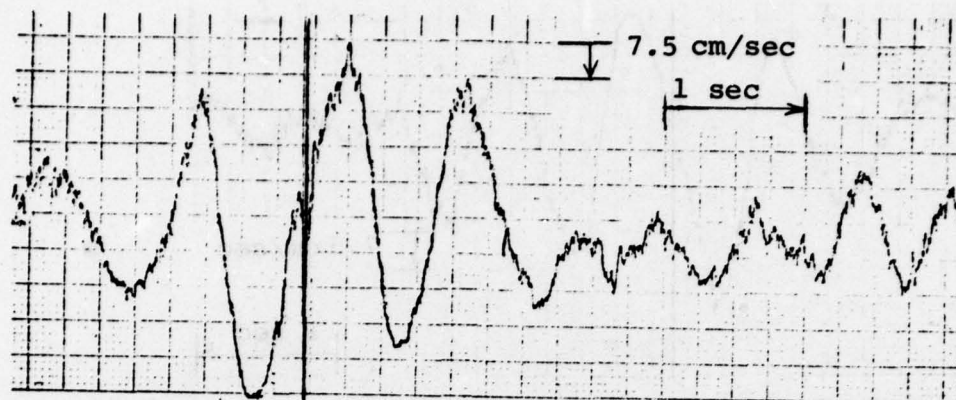
FIGURE 6-2(a)   Vertical Velocities 6.6 cm Below Rest Free Surface
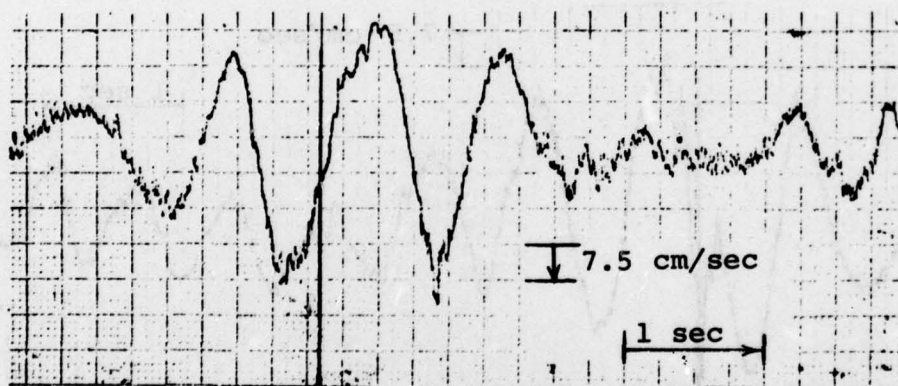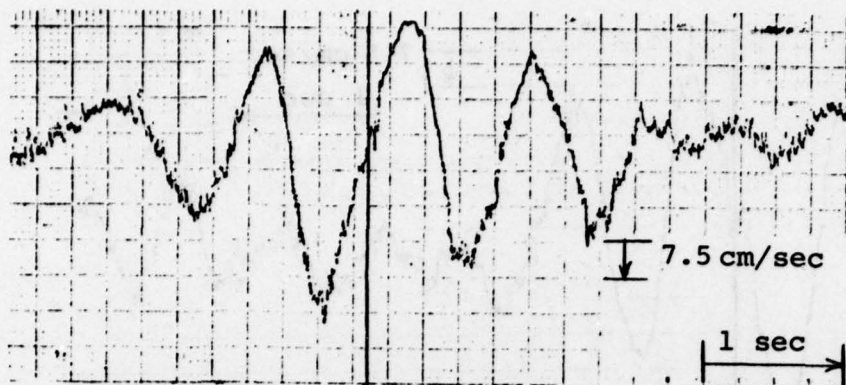
FIGURE 6-2(b)   Vertical Velocities 8.7 cm Below Resting Free Surface
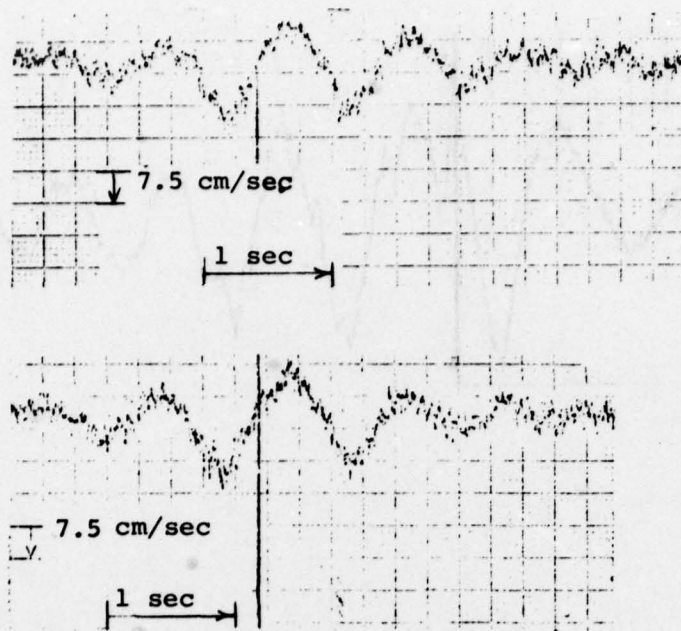
FIGURE 6-2(c)   Vertical Velocities 12.6 cm Below Rest Free Surface
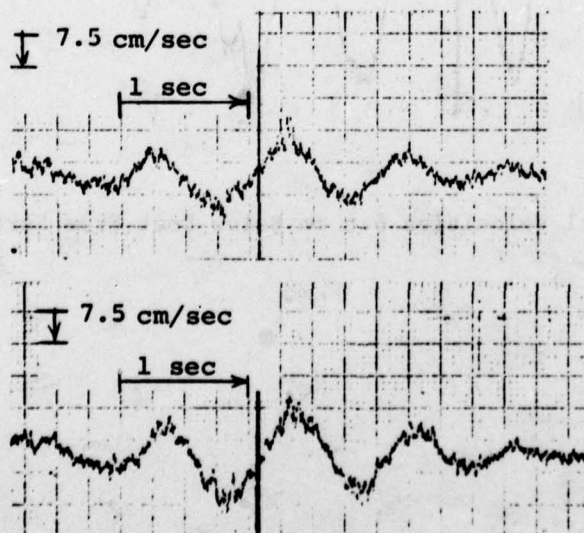
FIGURE 6-2(d)   Vertical Velocities 16.4 cm Below Rest Free Surface
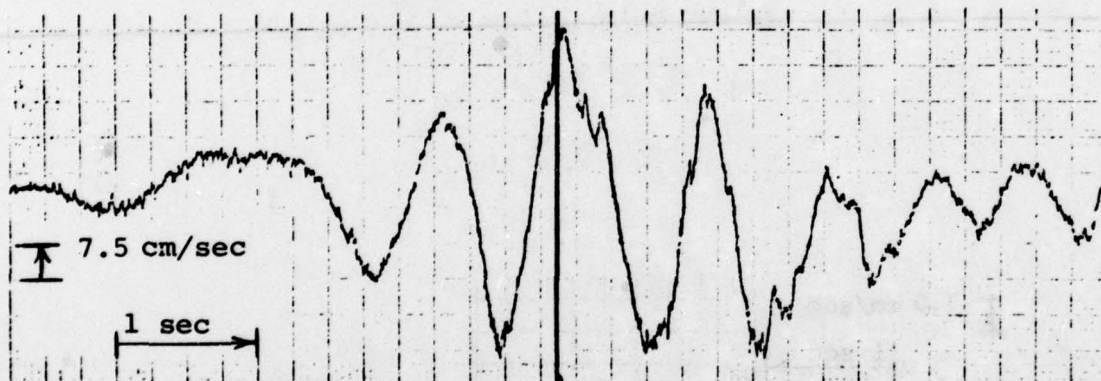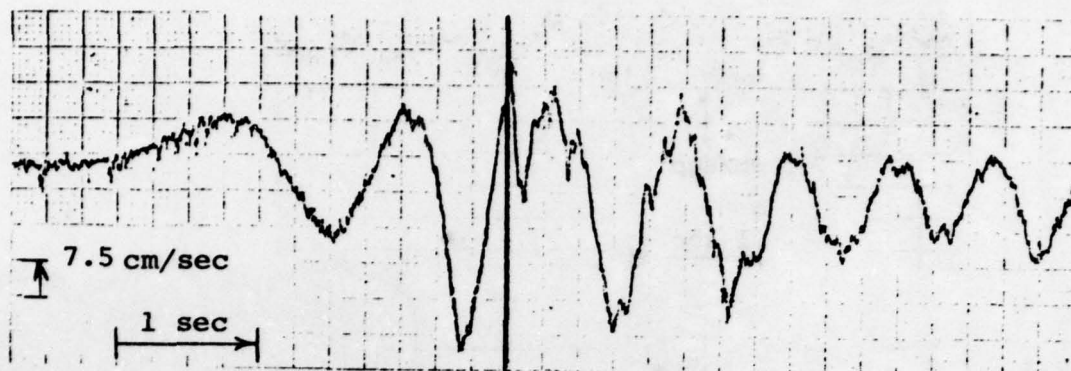
FIGURE 6-2(e) Horizontal Velocities 6.6 cm Below Rest Free Surface

-198-
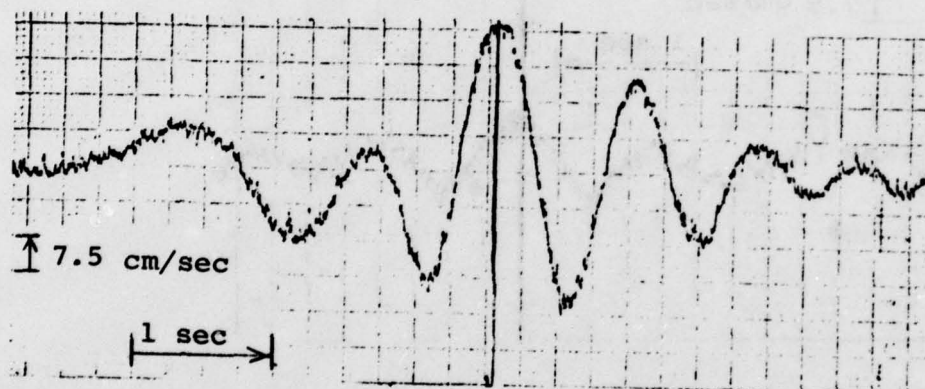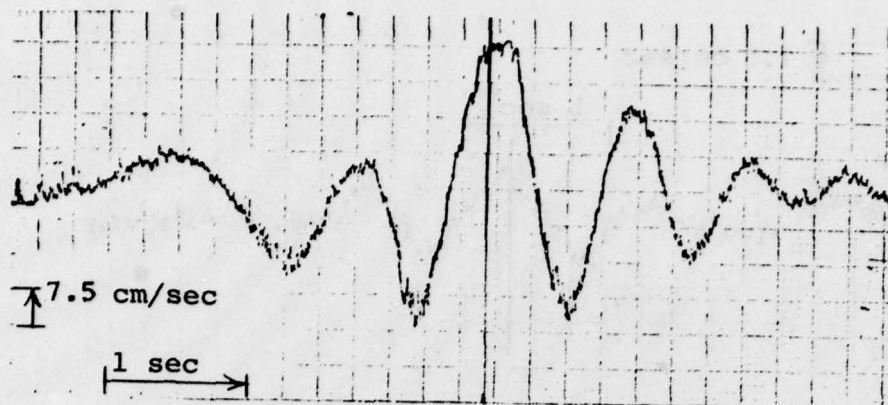
FIGURE 6-2(f) Horizontal Velocities 8.7 cm Below Rest Free Surface
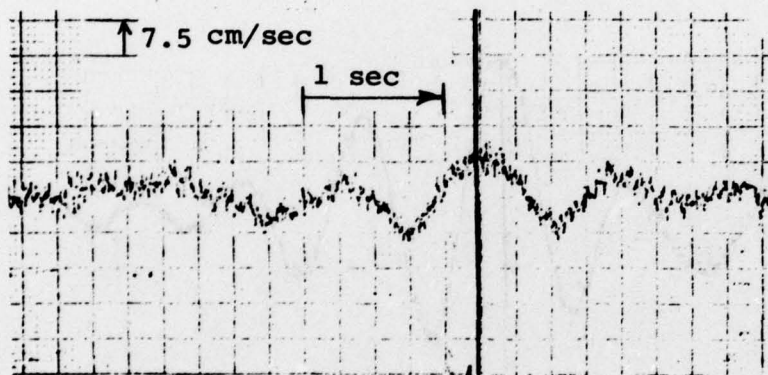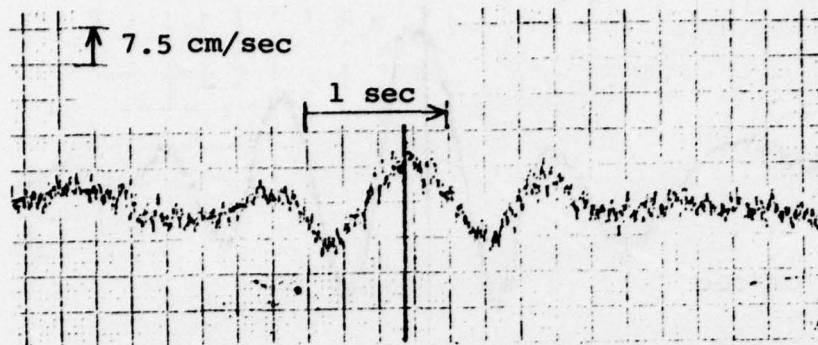
FIGURE 6-2(g)   Horizontal Velocities 16.4 cm Below Rest Free Surface
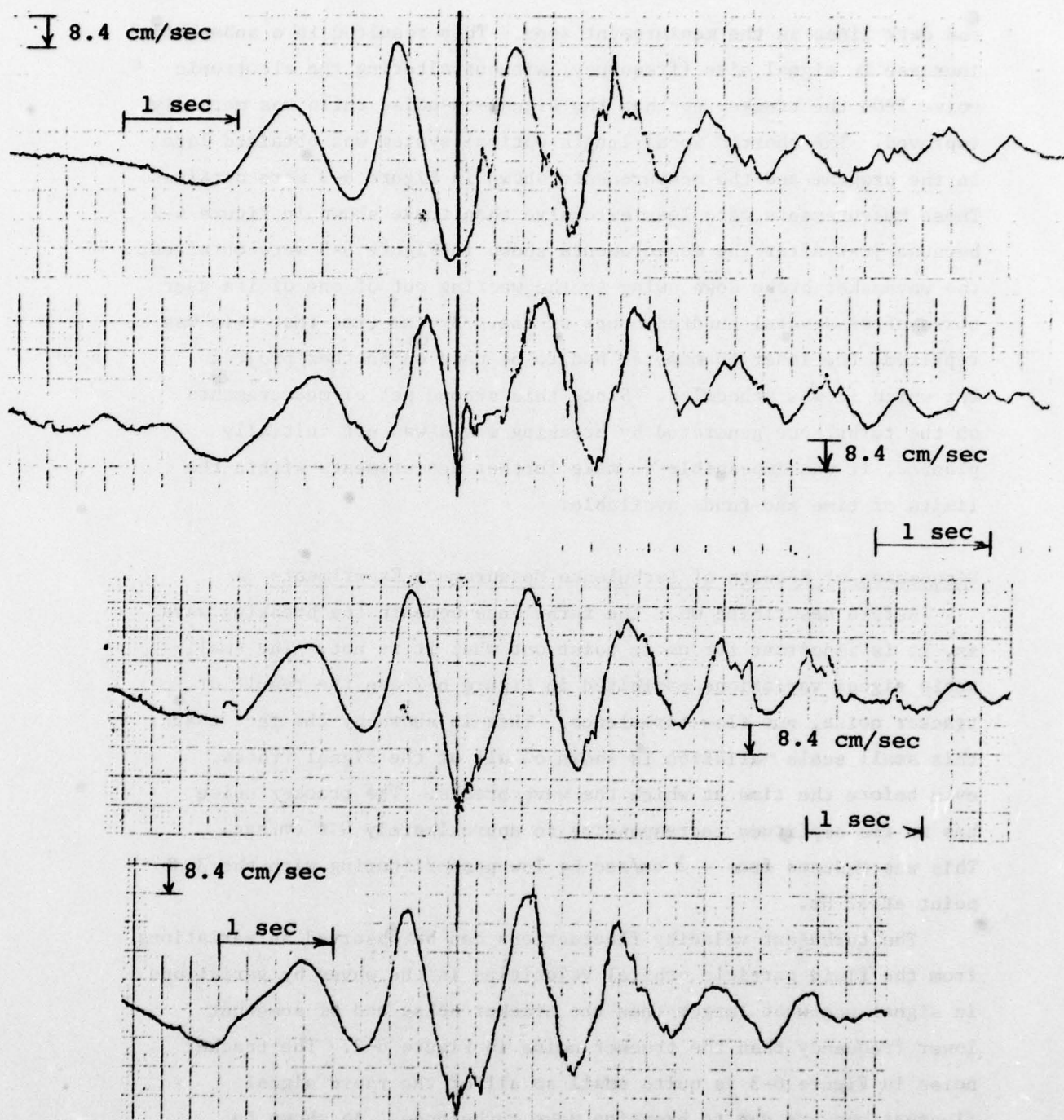
FIGURE 6-3 Measurements of Four Horizontal Velocity Time Histories
Beneath Breaking Waves, 7.4 cm Below the Mean Free Surface

Conditions and conventions are the same as in Figure 6-2, except that
these measurements were made with the improved optical subsystem in
the laser anemometer.

and dark lines in the measurement zone. This resulted in a substantial increase in signal size (frequency) without altering the electronic noise from the tracker so that the signal-to-noise ratio was markedly improved. The shorter focal length optical system was obtained late in the program and the measurements shown in Figure 6-3 were obtained. These measurements were less extensive than those shown in Figure 6-2 because just after the measurements shown in Figure 6-3 were obtained, the wavemaker broke down owing to the wearing out of one of its gear boxes after several hundred hours of use. By the time that this was repaired, the laser anemometer had to be used on another project for which it was scheduled. Since this second set of measurements on the turbulence generated by breaking waves was not initially planned, it was impossible to make further measurements within the limits of time and funds available.

Discussion of Results of Turbulence Measurement Experiments

Before describing what the turbulence beneath the breaking wave is, it is important for us to point out what it is not. The small-scale signal variations exhibited in Figure 6-2 are the result of tracker noise, not flow turbulence. This is shown by the fact that this small scale variation is shown on all of the signal traces, even before the time at which the wave breaks. The tracker noise has an rms amplitude corresponding to approximately 0.6 cm/sec. This was reduced from 3 cm/sec by low pass filtering with the 3 db point at 32 Hz.

The turbulent velocity fluctuations can be observed as variations from the fluid particle orbital velocities in the waves by variations in signal somewhat larger than the tracker noise and of somewhat lower frequency than the tracker noise in Figure 6-2. The tracker noise in Figure 6-3 is quite small so all of the rapid signal fluctuations are due to breaking wave turbulence. As shown in Figure 5-20, the wave profile extends from about 5 cm above the mean free surface to 5.5 cm below the mean free surface. Therefore, measurements could not be taken closer to the free surface than 5.5 cm

-202-

and still keep the measurement region continuously in the water. Hence, measurements were taken no closer to the mean free surface than 6.6 cm beneath it. Figure 6-2(a) shows two sample measurements of the vertical velocity at a position 6.6 cm below the free surface. Typical turbulent fluctuations are about 25% of the maximum orbital velocity, but the lower of the two examples shown in the figure shows a sharp turbulent velocity peak in the upward direction as large as the orbital velocity itself. The figure also shows that for this laboratory experiment, the observable turbulent velocity decays to very small values in about 4 seconds. It is important to remember that the very low speed components of the turbulence cannot be observed in these "Eulerian measurements" and that the large length scale parts of the low speed components do not decay so quickly (see §3). Figure 6-2(b) shows turbulent fluctuations of about 20% of the orbital velocity at a distance of 8.7 cm below the free surface. In Figure 6-2(c), for measurements 12.6 cm below the free surface, it is difficult to determine if any of the velocity fluctuations are due to turbulence or if they are all resulting from tracker noise. The same applies to Figure 6-2(d), which are samples of the vertical velocities 16.4 cm below the free surface.

Figure 6-2(e) shows the horizontal velocities at a distance of 6.6 cm below the mean free surface. Again, on one of the samples there are turbulent velocity fluctuations of the same order of magnitude as the orbital velocities. Thus, we can conclude that the turbulence in the near surface zone has velocities of the same order of magnitude as the orbital velocities. As was the case with the vertical velocities described above, the observable horizontal turbulent fluctuations decay rapidly so that 4 seconds after the breaker has passed there is no observable turbulent velocity in the measurement record. Small horizontal turbulent velocities are shown in Figure 6-2(f) for a location 8.7 cm below the free surface. At a distance of 16.4 cm below the mean free surface, there is no observable velocity fluctuation resulting from the turbulence.

Figure 6-3 shows four sample measurements of the horizontal

velocity at a distance of 7.4 cm below the free surface made with the shorter focal length optical system. This gave us a large increase in signal-to-noise ratio, and as a result the features of the turbulence are more clearly defined. The results are similar to those described for Figure 6-2, so that Figure 6-3 serves to confirm our former statements.

It is important to note that the measurements at a given height are not identical for repeated experiments, showing that there is a random variation between one breaker and another. This may account, in part, for some of the variations observed in our experiments on the dispersion of oil by breaking waves.

There is one important paper in the literature which bears on this subject. This is the work of Longuet-Higgins (1974) in which he reported measurements of the turbulence beneath the breaking bow wave of a ship model in a towing tank. By measuring fluctuations with respect to the moving towing carriage, measurements of the turbulence a fixed distance beneath the instantaneous free surface were made directly without there being a measured effect owing to the wave changing in time since the bow wave is a steady flow with respect to the moving ship. In addition, the steady velocity equal to the towing speed is superimposed upon the motion so there are no flow reversals and unidirectional anemometry could be used. Longuet-Higgins used an electromagnetic flow meter which was capable of measuring two components of the flow. Figure 6-4 is a reproduction of Longuet-Higgins' results. They represent far more extensive measurements beneath a breaker than we have made, albeit they are for a different kind of breaker. The largest rms turbulence levels shown in the results of Longuet-Higgins are about 10% of the velocity in the basic underlying wave motion. These levels are somewhat smaller than the results we observed directly beneath the breaking crest, but generally the overall features can be observed to be similar. In particular, the effects of the breaking turbulence extend beneath the mean free surface only a distance of about two wave heights. This effect was observed in our data as well. It has an important implication on the

dispersion of oil slicks into the sea by breaking waves. This is that
the rapid dispersion of oil beneath a breaker results in most of the
oil being within two wave heights of the surface. That is not to say
that some of the oil does not go deeper. It does. However, oil
which goes deeper does so as a result of the slow diffusion of
turbulence by molecular and eddy viscosities with the latter possibly
strengthened by the occurrence of multiple breakers in the same
region over a short time interval. As shown in §3, this slow diffusion
of the turbulence disperses deeply only the very small oil droplets,
so unless most of the oil is split into these very small droplets,
most of the oil will not be deeply dispersed. For the oil types
used in our dispersion by breaking wave experiments, concentrations
at depths lower than two wave heights were small since most of the
droplets were large enough to rise relatively rapidly. However, when
dispersants are used on oil slicks, droplets having sizes between
1 and 10 microns can be formed and some of these droplets can be
expected to be found at large depths.

The experiments we have presented on measurements of turbulence
below breaking waves must be considered to be of a preliminary nature.
More work on determining the turbulence beneath breaking waves at sea
is recommended. We have demonstrated the feasibility of making these
measurements by laser anemometry and we have established the gross
features of the turbulence. We recommend that a comparative study
be carried out between ordinary spilling breakers and a "stationary"
breaker like that studied by Longuet-Higgins. It may be possible
to make the stationary breaker really fixed in space by doing the
experiment with a surface piercing obstruction in a flume. This will
result in a "bow wave" which will break if it is large enough. The
velocity and length scales of this wave can be measured. Then, a
spilling breaker having the same velocity and length scales can be
generated in a wave channel and the details of the turbulence of the
two types of breakers can be compared. If these details are nearly
the same, then further studies can be done on the stationary breaker
for which the experiments can be much more straightforward and for

which hot film anemometry is entirely practical.

Once all of the details of the turbulence beneath a breaker are characterized and the droplet size distribution is better known, many of the effects of the turbulence on dispersion can be studied theoretically. For example, we have already seen that when a breaker sweeps through a region it deposits a zone of turbulence in the upper surface layers. From measurements of this turbulence, the eddy diffusivity as a function of space can be estimated with the result that the diffusion of the turbulence into the water beneath the zone originally containing turbulence can be calculated. Furthermore, analysis of the form of the turbulence including the nature of the eddy types would allow calculation of conditions leading to droplet splitting so that the droplet size distribution for any specific oil type might then be estimable by combining the theoretical results with an experimental program that measures droplet sizes.
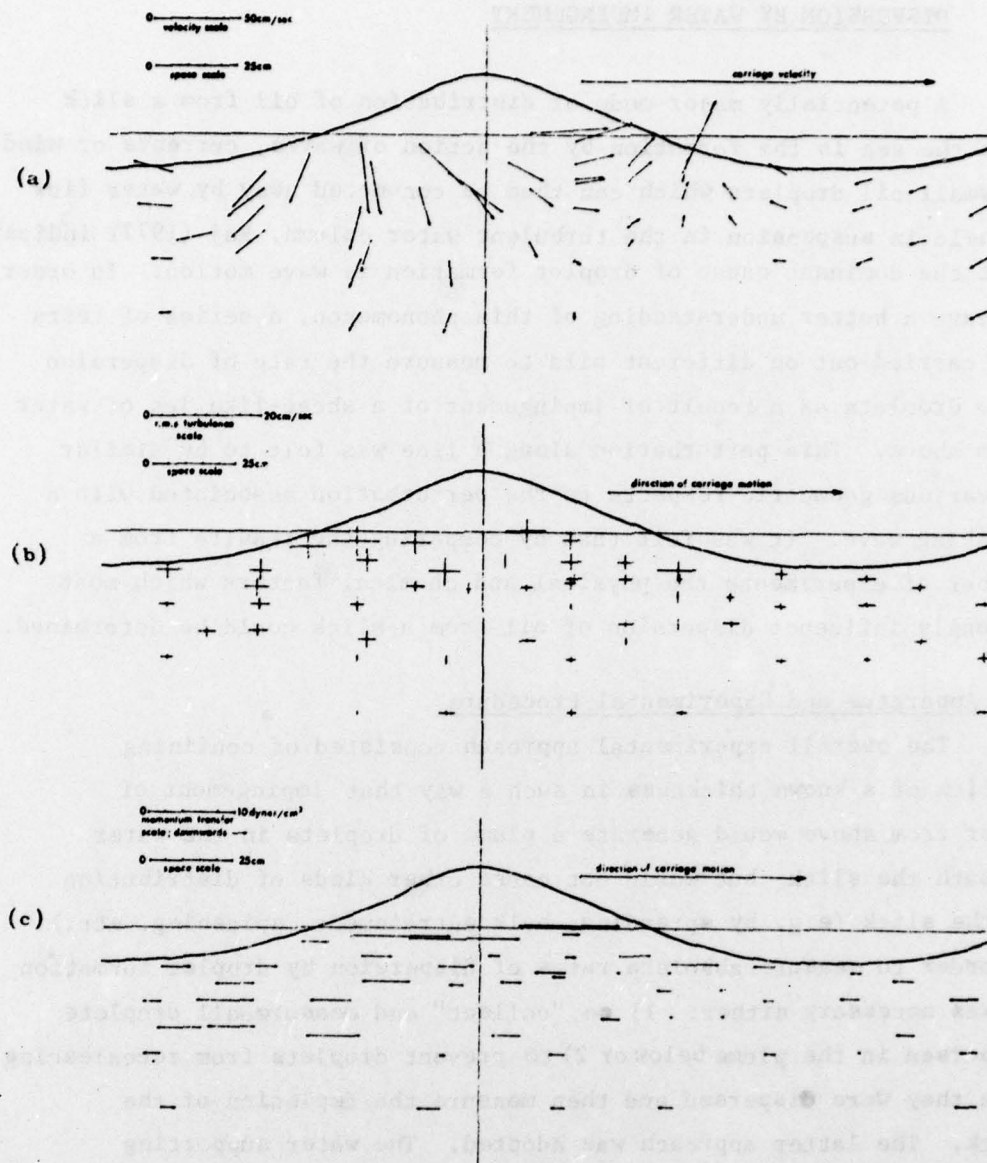
FIGURE 6-4   Longuet-Higgins' Results for the Characteristics of the
Turbulence Beneath the Breaking Bow Wave of a Ship Model in a Towing Tank.
(a)   Mean velocity field after subtraction of the carriage velocity.
(b)   rms levels of turbulence; the horizontal and vertical arms of the
      crosses represent $(u_x^2)^{1/2}$ and $(u_z^2)^{1/2}$ respectively.
(c)   The "shear" component of the turbulence: $\overline{(u_x u_z)}$. A vector pointing
      to the right indicates a downward component of x-momentum.

Source: "Breaking Waves in Deep or Shallow Water", by M.S. Longuet-Higgins,
          Tenth Symposium on Naval Hydrodynamics, 1974.

7. DISPERSION BY WATER IMPINGEMENT

A potentially major mode of distribution of oil from a slick into the sea is the formation by the action of waves, currents or wind of small oil droplets which can them be convected away by water flow or held in suspension in the turbulent water column. Raj (1977) indicates that the dominant cause of droplet formation is wave motion. In order to have a better understanding of this phenomenon, a series of tests was carried out on different oils to measure the rate of dispersion into droplets as a result of impingement of a sheet-like jet of water from above. This perturbation along a line was felt to be similar in various geometric respects to the perturbation associated with a breaking wave. It was felt that by comparing the results from a number of experiments the physical and chemical factors which most strongly influence dispersion of oil from a slick could be determined.

7.1 Apparatus and Experimental Procedure

The overall experimental approach consisted of confining a slick of a known thickness in such a way that impingement of water from above would generate a plume of droplets in the water beneath the slick but would not cause other kinds of distribution of the slick (e.g. by spreading, bulk entrainment, splashing, etc.). In order to measure absolute rates of dispersion by droplet formation it was necessary either: 1) to "collect" and measure all droplets dispersed in the plume below or 2) to prevent droplets from recoalescing once they were dispersed and then measure the depletion of the slick. The latter approach was adopted. The water supporting the slick was flowed at a steady rate under the slick to carry away droplets smaller than a certain approximate critical size. Experimental variables then consisted of the oil type, slick thickness, water jet velocity, and angle of impingement of the water jet.

A schematic diagram of the experimental apparatus is shown in Figure 7-1. The dispersion experiments were conducted in a 45x45x92cm glass tank. Oil slicks floating on the surface of the water (24cm above the bottom of the tank) were confined in a square area of 36x43cm by Teflon barriers. Water level was controlled
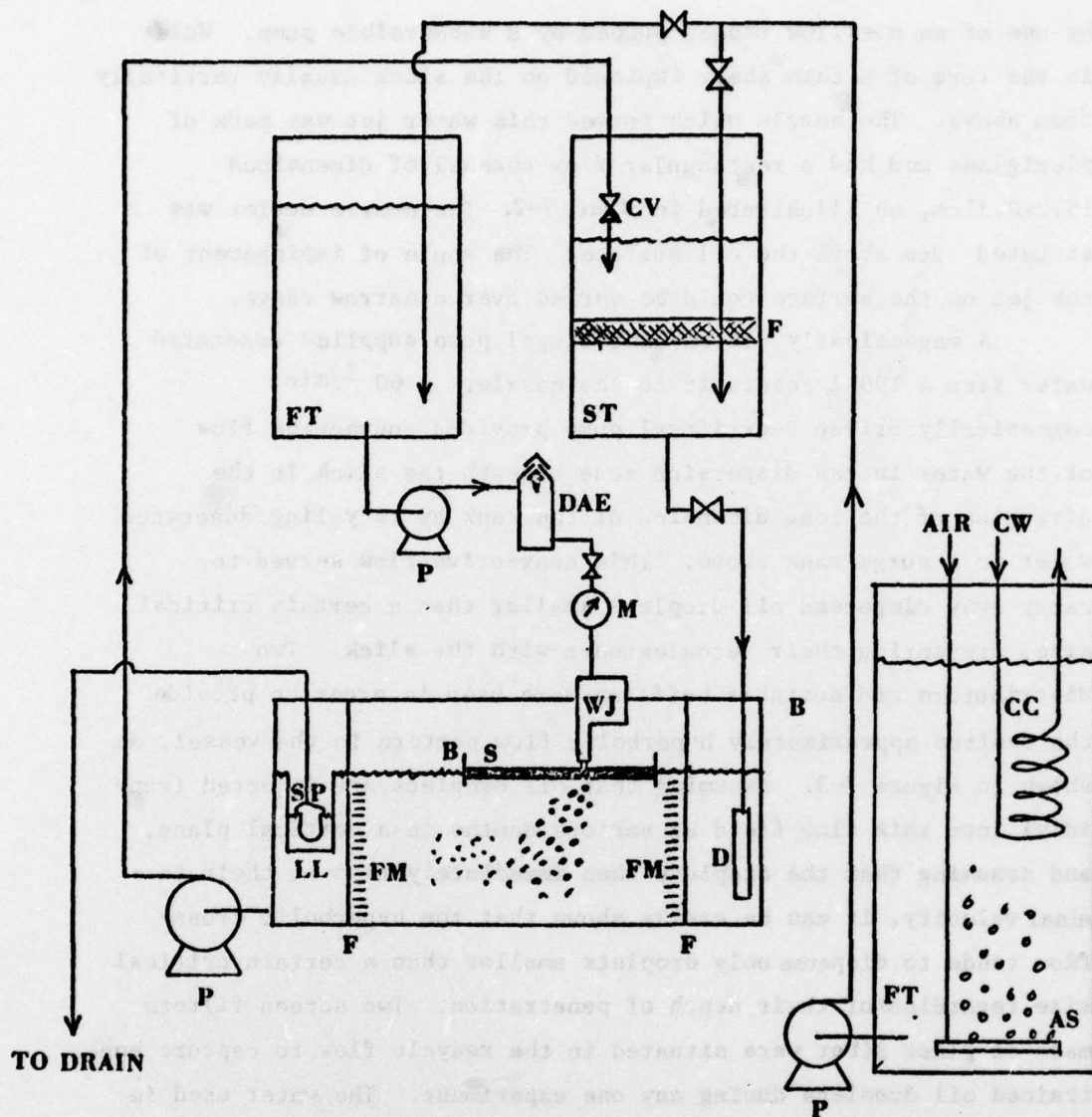
FIGURE 7-1 Flow Schematic of Water Impingement Apparatus.
Key: AS, air sparger;
B, barrier
CC, cooling coil;
CV, check valve;
CW, cold water '
D, distributor;
DAE, dissolved air eliminator;
F, filter
FM, flow modifier;
FT, feed tank;
LL, liquid level control;
M, meter;
P, pump;
S, slick
SP, submersible pump
ST, surge tank;
WJ, water jet.

-209-

by use of an overflow vessel pumped by a submersible pump. Water in the form of a thin sheet impinged on the slick usually vertically from above. The nozzle which formed this water jet was made of plexiglass and had a rectangular flow channel of dimensions 15.2x0.11cm, as illustrated in Figure 7-2. The nozzle outlet was situated 2cm above the oil surface. The angle of impingement of the jet on the surface could be varied over a narrow range.

A magnetically driven centrifugal pump supplied deaerated water from a 190 l reservoir to the nozzle. A 60 l/min magnetically driven centrifugal pump provided convective flow of the water in the dispersion zone beneath the slick in the direction of the long dimension of the tank by recycling deaerated water to a surge tank above. This convective flow served to carry away dispersed oil droplets smaller than a certain critical size, preventing their recoalescence with the slick. Two distributors and suitable baffling were used in order to provide the desired approximately hyperbolic flow pattern in the vessel, as shown in Figure 7-3. Assuming that oil droplets are injected (rapidly) into this flow field at various depths in a vertical plane, and assuming that the droplets then immediately rise at their terminal velocity, it can be easily shown that the hyperbolic cross-flow tends to disperse only droplets smaller than a certain critical size regardless of their depth of penetration. Two screen filters made of glass fiber were situated in the recycle flow to capture entrained oil droplets during any one experiment. The water used in the experiments was deaerated, cooled hot tap water. A 570 l polyethylene pretreatment tank was filled with hot tap water and simultaneously deaerated and cooled by air sparging and by heat exchange to a coil. The air sparging served to speed deaeration of supersaturated tap water and to assure that water used in the experiments was always saturated at the ambient temperature. A third magnetically driven pump was used to pump the water to the recyle tank and to the water jet reservoir.

The thickness of the oil slick was measured using a depth micrometer graduated in 0.0025cm increments. A Polaroid SX-70
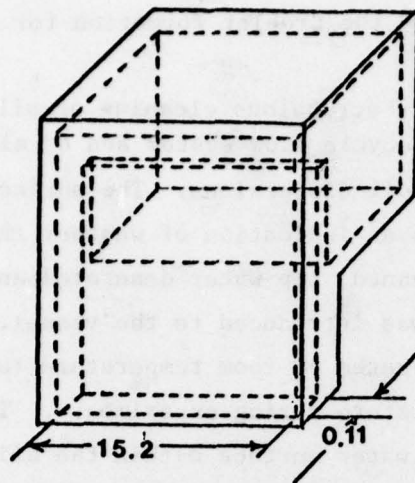
FIGURE 7-2 Nozzle for Water Impingement Study,
Showing Orifice Dimensions in cm.
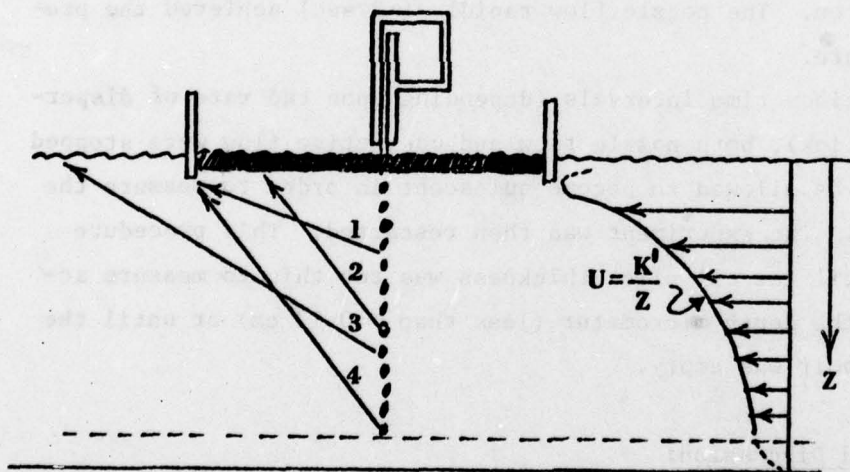
FIGURE 7-3 Approximate Flow Profile Under the Slick is
Hyperbolic. Trajectories 1 and 4 are for Drop-
lets of Critical Size, Trajectory 3 for a Smaller
Droplet, Trajectory 4 for a Larger Droplet. (see text.)

Model 2 camera was used to record the droplet formation for each experiment.

The experiments started by scrupulous cleaning of all tanks, lines and other devices in the recycle flow system and of all other surfaces in contact with oil or oil dispersions. The surface tension of the recycle water was used as an indication of whether the tank was clean. After the tanks were cleaned, tap water deaerated and cooled in the 570 l pretreatment tank was introduced to the vessel. The temperature of the water was adjusted to room temperature (usually 18°C) to avoid changes of temperature during experiments. The oils were carefully layered onto the water surface within the slick area confined by the Teflon barriers. After the few large droplets which formed during the layering of oil had recoalesced with the slick and the slick had reached a uniform thickness, the thickness of the slick was measured. At that point the convective (recycle) flow beneath the slick was started and after a steady flow developed, the water jet pump was turned on. The nozzle flow rapidly ($\sim$2 sec) achieved the pre-adjusted flow rate.

After various time intervals (depending upon the rate of dispersion from the slick), both nozzle flow and convective flow were stopped and the system was allowed to become quiescent in order to measure the slick thickness. The experiment was then restarted. This procedure was repeated until the oil slick thickness was too thin to measure accurately using the depth micrometer (less than $\sim$ 0.12 cm) or until the water jet reservoir was empty.

7.2 Results and Discussion:

The oils studied in the water impingement experiments included the following: 1) several crude oils: Arzew, South Louisiana Crude (SLC), Zuetina, Kuwait, THUMS and Arabian light; 2) two fuel oils: No. 6 fuel oil, No. 2 diesel oil; 3) pure and modified mineral oils: Drakeol 5, Drakeol 5 with 0.5 vol% of Span 85 or Atmos 300. In order to compare the relative dispersion rates of the various oils under fixed conditions a slick thickness h = $\sim$ 0.64 cm and a nozzle flow rate of Q = 5.4 l/min were used. In addition, several experiments were conducted using a slick thickness h = $\sim$ 0.32 cm and Q = 5.4 l/min to

study the effect of slick thickness. A second nozzle flow rate of $Q = 3.9$ l/min was utilized in some cases to ascertain the effect of water jet rate. In addition, for all oils investigated photographic evidence of dispersion rate was obtained as a function of nozzle flow rates ranging from $Q = 3.1$ l/min to 5.4 l/min in increments of 0.8 l/min. Table 7-1 summarizes the conditions under which the various experiments were conducted.

On the basis of the observed results of the experiments the oils can be categorized as being one of two types. The first type consists of those oils which showed no significant mousse formation during the water impingement experiments. The second type consists of oils which did show indication of mousse formation during the water impingement experiments. These include No. 6 fuel oil, South Louisiana crude, and Kuwait crude.

For oils of the second type the mousse always formed first at the bottom of the oil slick, giving the appearance and mechanical behavior of a gel-like foam. The thickness of this layer differed from one oil to another. For No. 6 fuel oil the layer was so thick that the thickness of the slick was difficult to measure using the depth micrometer. South Louisiana crude and Kuwait crude formed mousse layers substantially thinner than No. 6 fuel oil. It was found that the formation of mousse was related in a complex manner to oil type and water impingement rates. Higher water rates in some cases led to rapid dispersion of a slick of an oil which at lower water rates would show substantial mousse formation. It is unclear whether the higher water rates prevented the formation of mousse on some hydrodynamic grounds or whether the slick was simply dispersed so rapidly that sufficient time for mousse formation was not available.

The raw data from all of the experiments are plotted in Figures 7-4 to 7-12 as instantaneous slick thickness versus time under water impingement. A few comments are in order. The figures are ordered in the order of the listing in Table 7-1. Two plots, Figures 7-4 and 7-5, are given for Arzew crude, the latter illustrating the effect of a wide variation in water impingement rate at a slick thickness of $h = 0.32$ cm. Arzew was chosen for this more extensive study because it was "well behaved," showing no tendency to mousse formation and easy filterability in the recycle system. An indication of the reproducibility of this experiment from run to run is given in Figure, 7-10 for No. 2 diesel oil. Finally, the effect of a variation in interfacial tension is shown for the mineral oil Drakeol 5

TABLE 7-1
Summary of Experiments

Slick Thickness

Oil \ Flow Rate ($\frac{1}{min}$)	h = 0.64cm			h = 0.32cm			Other Expts[b]
	Q=3.9	Q=5.4	Q_c[a]	Q=3.9	Q=5.4	Q_c[a]	
Arzew Crude	✓	✓	✓	✓	✓		I, II
South Louisiana Crude				✓	✓		
Arabian Light Crude				✓			
Kuwait Crude				✓			
Zuetina Crude				✓			
THUMS Crude				✓			
Diesel No. 2	✓	✓		✓			
Fuel Oil No. 6		✓	✓		✓	✓	
Drakeol 5		✓	✓		✓		III
Drakeol 5 w. Span 85		✓		✓	✓		

a) $Q_c \equiv$ critical flow rate for "significant" dispersion, based upon photographic evidence (see text)

b) Additional experiments
   I h = 0.32cm, Q = 3.1 1/min (Arzew crude)
   II h = 0.32cm, Q = 4.6 1/min (Arzew crude)
   III angle of impingement varied from 60 to 90°
       at h = 0.64cm, Q = 5.4 1/min (Drakeol 5)
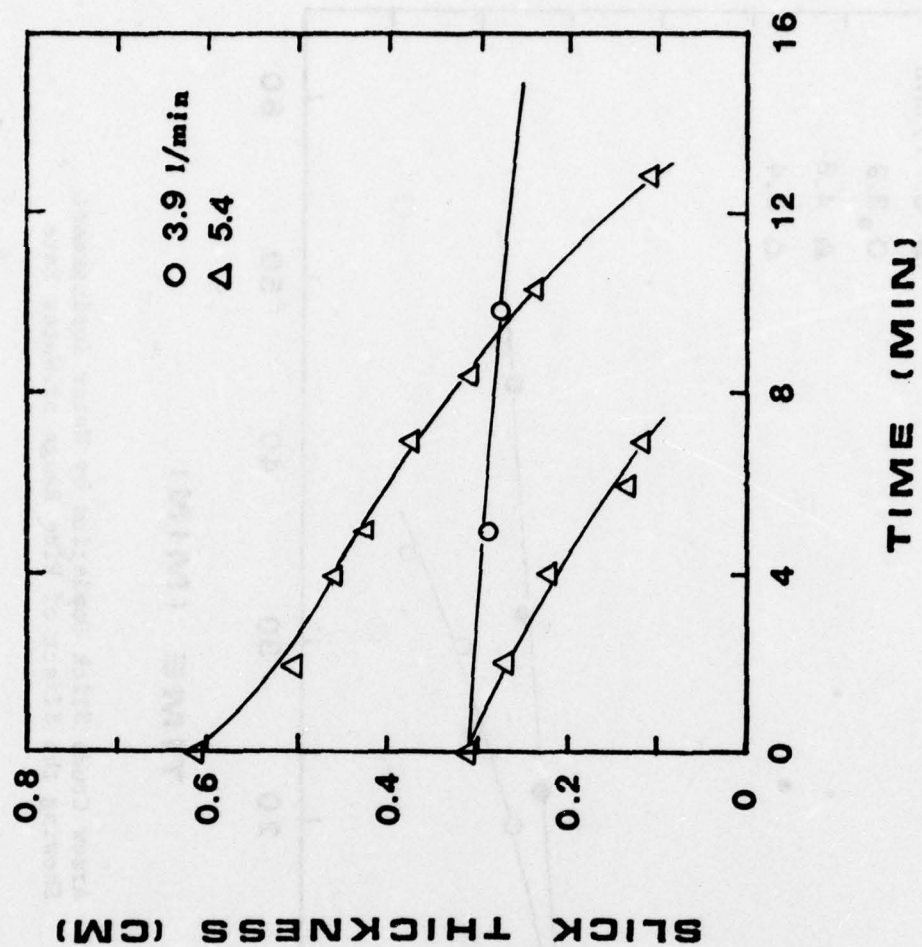
FIGURE 7-4 Arzew Crude Slick Depletion by Water Impingement
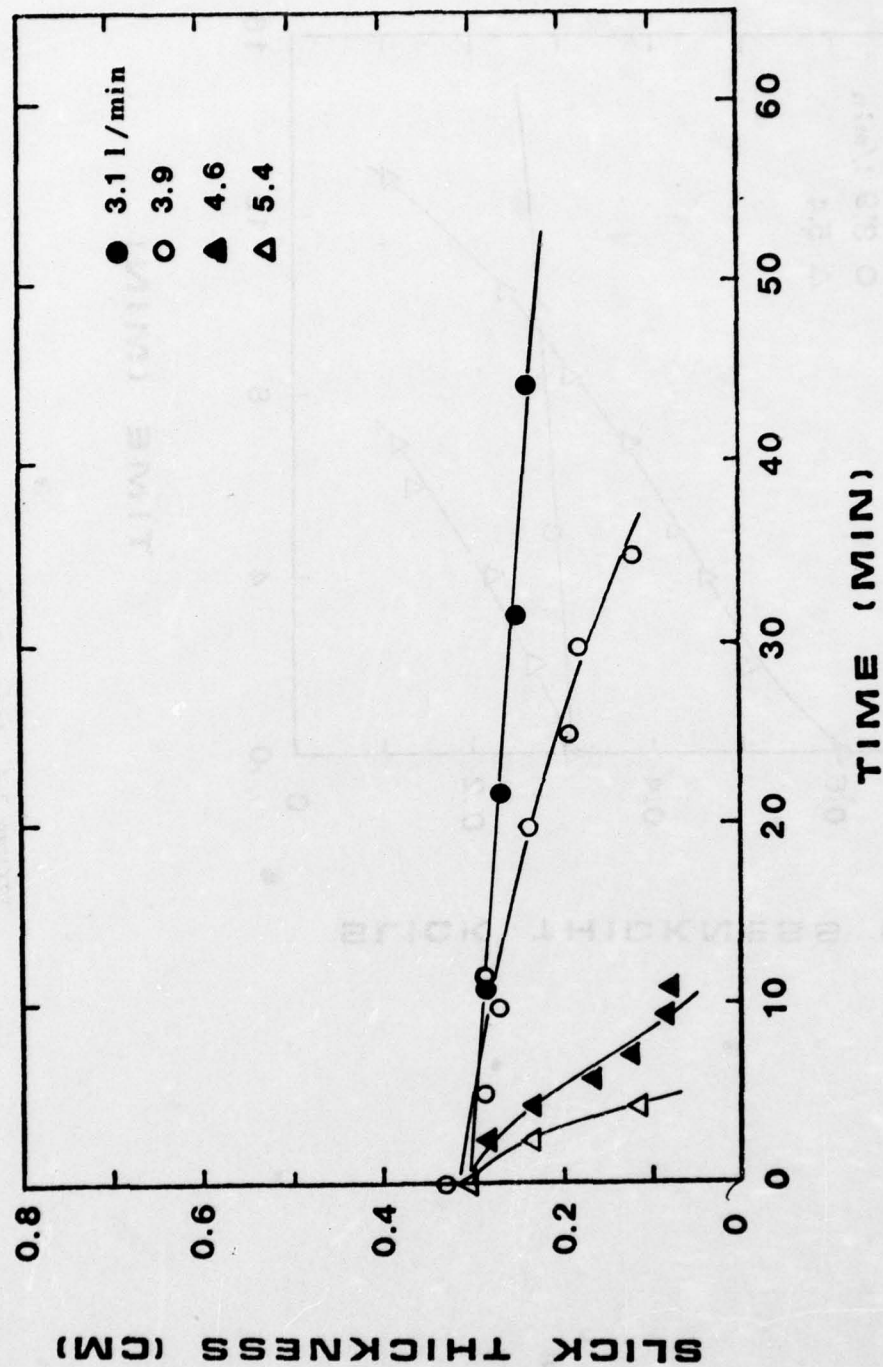
FIGURE 7-5 Arzew Crude Slick Depletion by Water Impingement
Showing the Effect of Wide Range of Water Rate
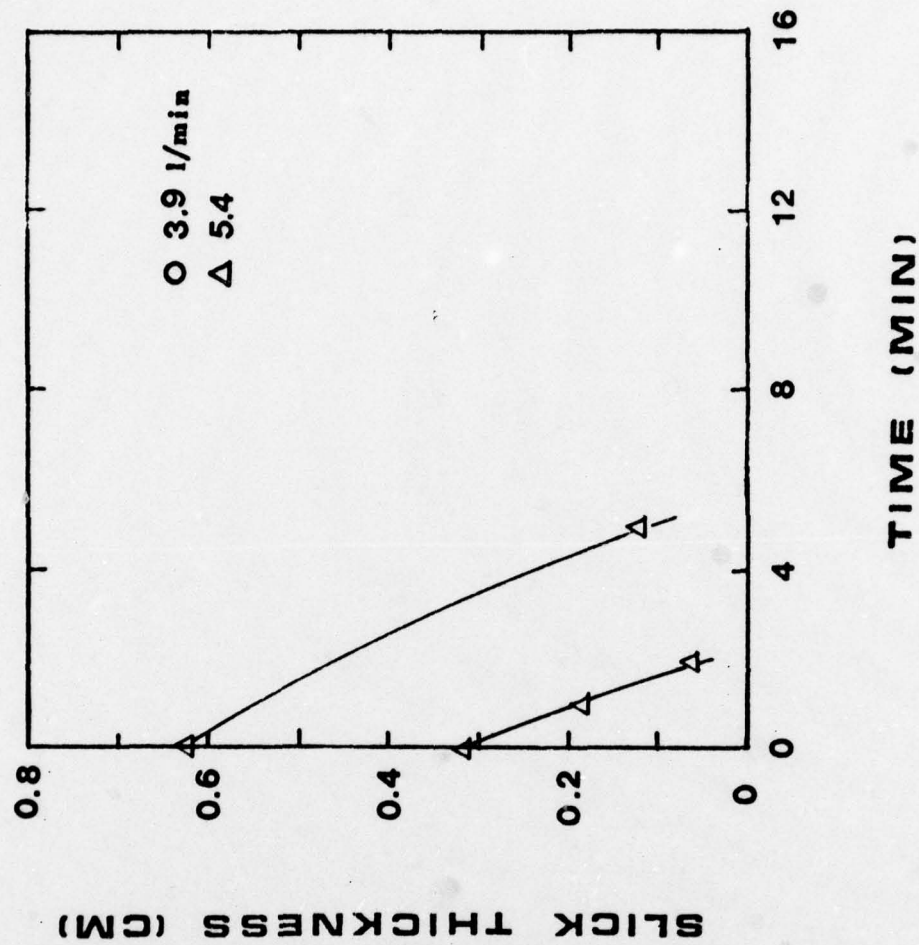
FIGURE 7-6 South Louisiana Crude Slick Depletion by Water Impingement
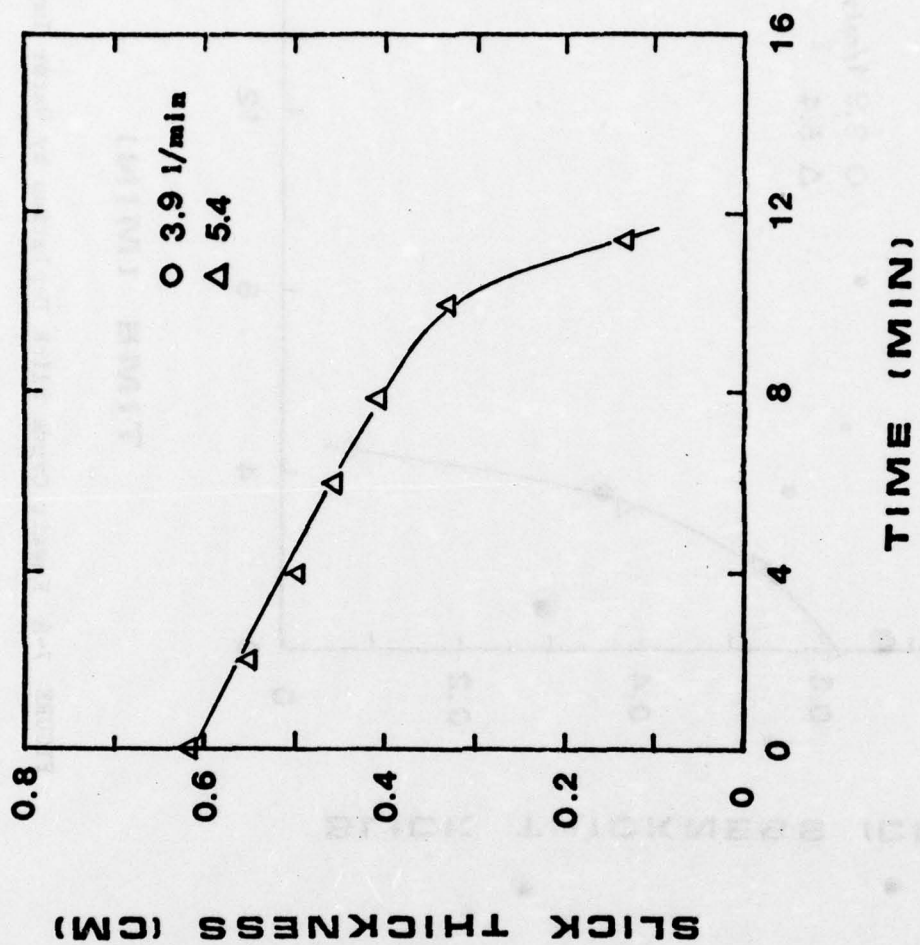
FIGURE 7-7 Arabian Light Crude (II) Slick Depletion by Water Impingement
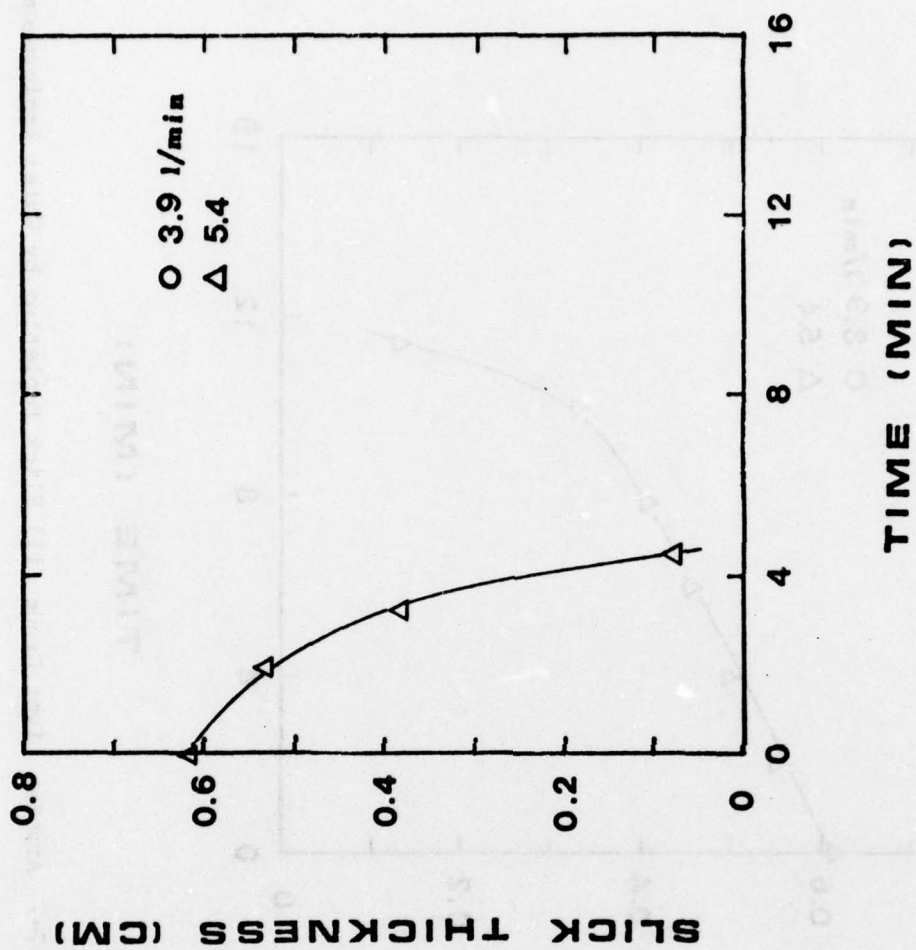
FIGURE 7-8 Kuwait Crude Slick Depletion by Water Impingement
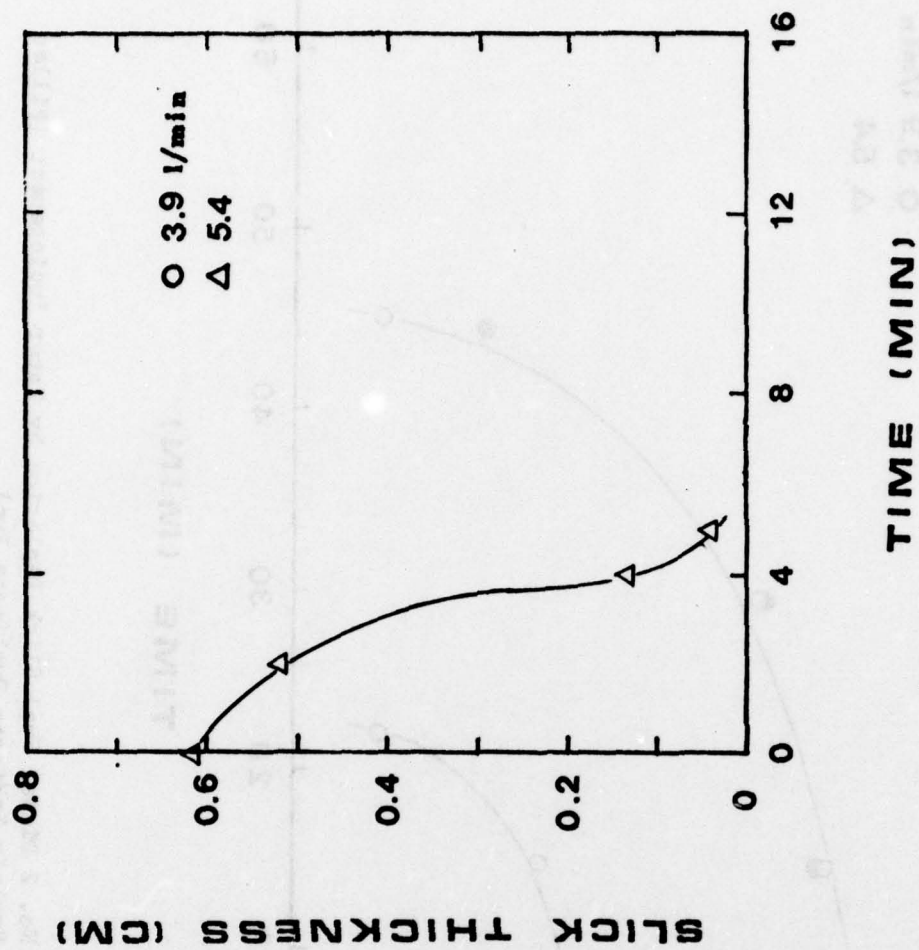
FIGURE 7-9 Zuetina Crude Slick Depletion by Water Impingement
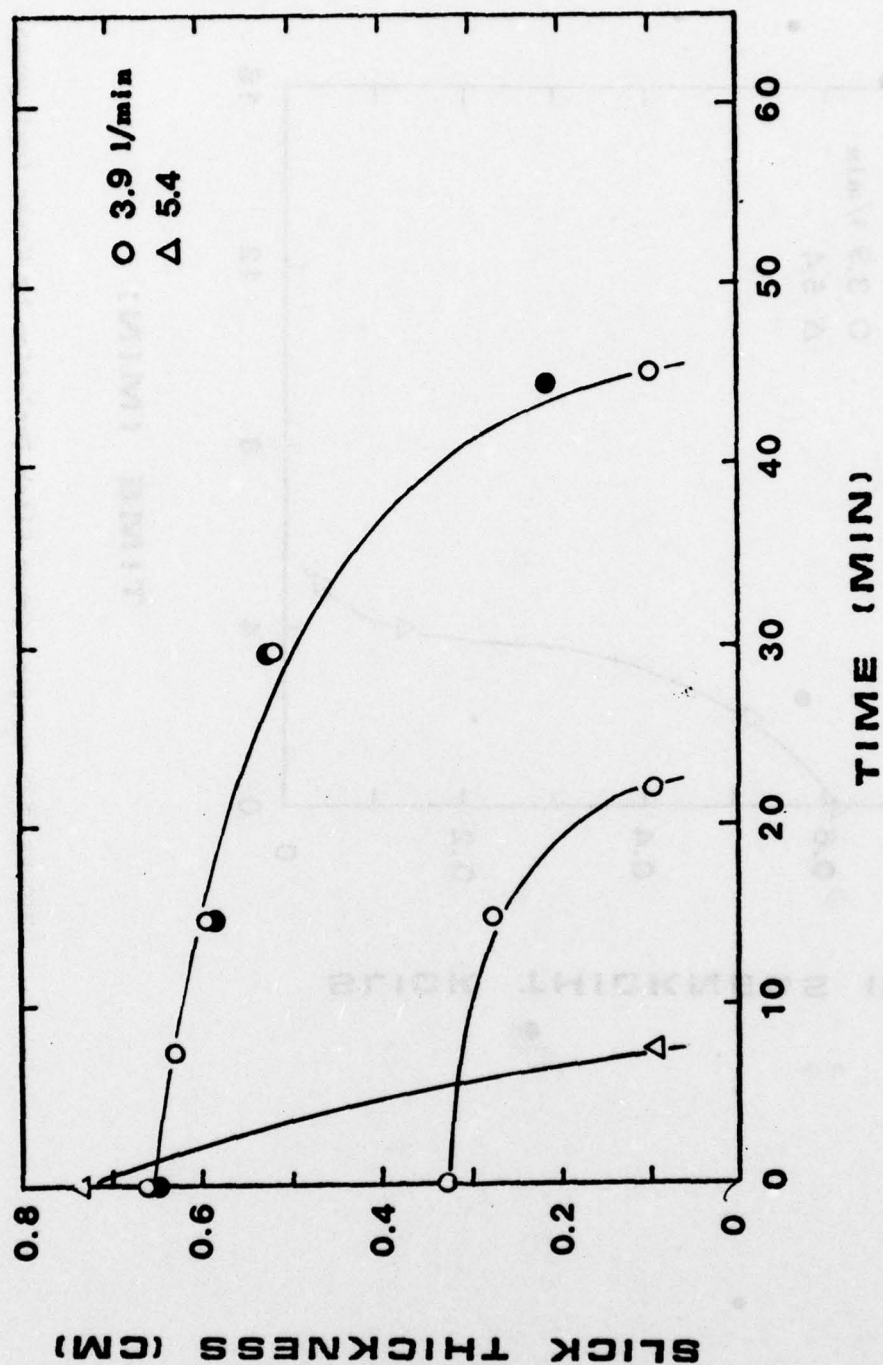
FIGURE 7-10 No. 2 Diesel Fuel Slick Depletion by Water Impingement (Filled Symbols Indicate Duplicate Run)
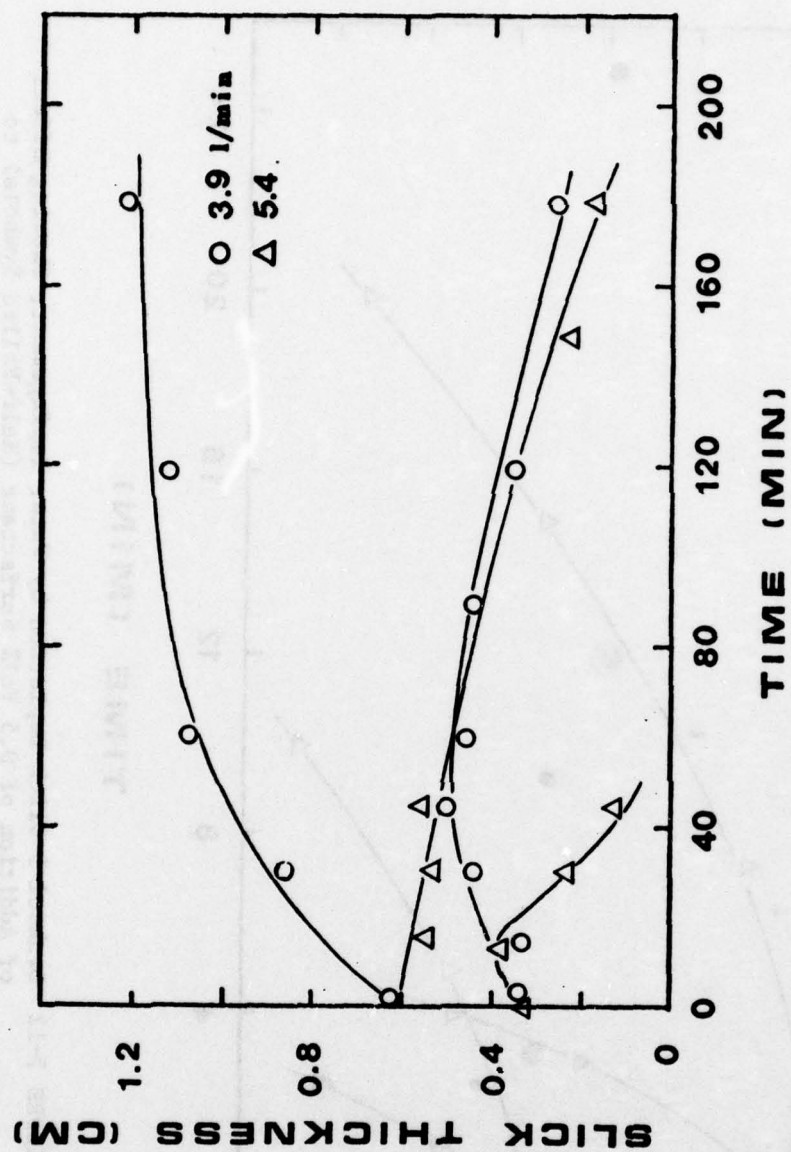
FIGURE 7-11 No. 6 Fuel Oil Slick Depletion by Water Impingement

-221-
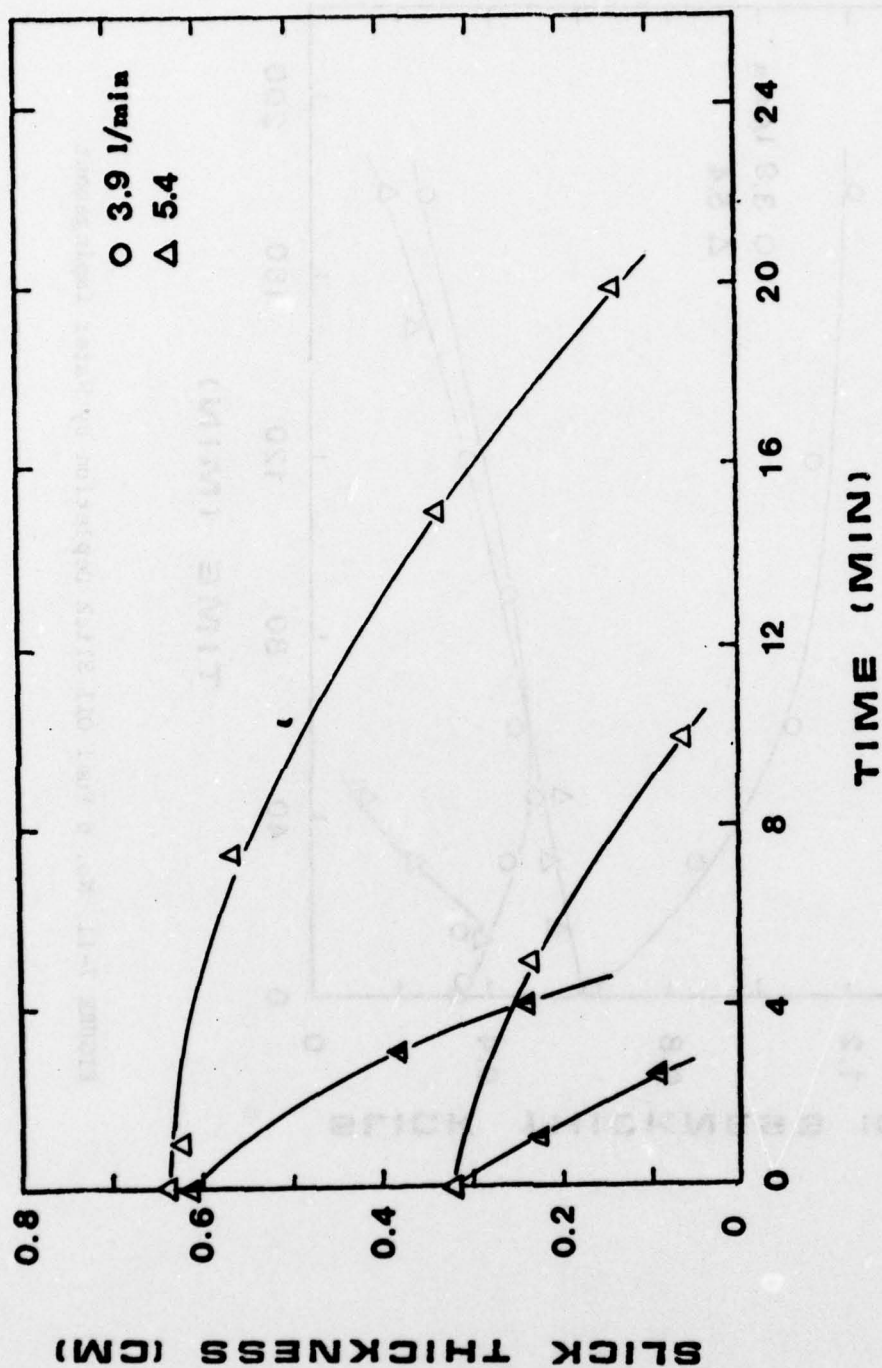
FIGURE 7-12 Drakeol 5 Slick Depletion by Water Impingement, Showing Effect of Addition of 0.5 Vol% Surfactant (Half-Filled Symbols) to Give $T_{o/w}$ = 3 dyne/cm.

in Figure 7-12.

The data show that the dispersion rate differs considerably from oil to oil. The time required to reduce the thickness from 0.64 cm to 0.25 cm, for example, varies from two minutes to two hours at a water impingement rate of 5.4 l/min. The technique used to measure the dispersion rate was the observed change of slick thickness, as discussed above. For the oils of the first type, which do not show mousse formation, slick thickness results are directly interpretable as dispersion rates. Slicks of oils of the second type, which incorporated water and/or air under the action of the water jet, had thicknesses which did not directly represent the volume of the oil remaining after a certain dispersion had occurred, but rather included also the volume of water and air in the slick. Nonetheless, there are interesting and revealing features of these results which can be interpreted to give quantitative dispersion rate information, as we discuss below.

South Louisiana crude, Kuwait crude and No. 6 fuel oil were all observed to form a gel-like slick underlayer during dispersion by water impingement. However, as shown in Figure 7-6 and 7-8 the presence of this layer did not appear to interfere substantially with dispersion at a water rate of 5.4 l/min. The slick thickness decreased monotonically with time. No. 6 fuel oil (Figure 7-11) is a more complex case in which slick thickness is seen first to increase, apparently as the result of incorporation of water and/or air and then subsequently decrease. The exception is the behavior at the lower water rate 3.9 l/min for a slick which was initially thick ($h_{initial}$ = 0.62cm). In this case the slick continued to grow in thickness for the full 3 hour duration of the test. Observation indicated that only minute dispersion occurred under these conditions. Apparently, the major role of the impingement water jet was to provide sufficient mixing energy to continue mousse growth.

In order to assess a relative dispersion rate for the various oils the rate at fixed flow rate of 5.4 l/min and slick thickness of h = 0.25cm was determined by differentiating the appropriate slick thickness curves of Figures 7-4 to 7-12 at this point. The

relative dispersion rates under these conditions are given in
Table 7-2. For some oils two runs at the two different initial
slick thicknesses were made, and for these oils two values of dispersion
rate are given--one for the relatively "old" slick of initial
thickness 0.64cm and one for the "younger" slick of initial thickness
0.32cm. Agreement between these paired values is seen to be quite
good, with no strong indication that the slicks of the different
ages behave very differently.

The effect of water impingement rate upon dispersion rate
indicates that a complex phenomenon is involved. The droplet
formation rate is far from linearly dependent on nozzle flow rate,
as the photographs taken during the water impingement experiments
with Arzew crude typically illustrate. (See Figure 7-13.) An
extensive study of the effect of water rate upon dispersion was
conducted for Arzew crude oil of slick thickness 0.32cm. (The
results were presented in Figure 7-5.) By examining the intial
dispersion rate determined in these experiments (no mousse formation
for Arzew), it is possible to eliminate any variations caused by
aging of the oil undergoing dispersion. Figure 7-14 gives a plot
of the initial dispersion rate versus water impingement rate, showing
the very strong dependence. This illustrates something akin to a
"critical" water impingement rate for dispersion. Such a phenomenon
appears to be involved in dispersion of each of the oils studied
on the basis of observations made during the experiments. From
photographic recording of plume size and character as a function
of water impingement rate for each of the oils a rather coarse
estimate of the critical water rate can be made for each oil studied.
These estimates are given in Table 7-3. Note that the No. 6 fuel
oil data (Figure 7-11) graphically illustrate such a critical effect,
with one slick failing to disperse at all at a water rate of 3.9 1/min
while dispersion occurs readily, if slowly, at a water rate of
5.4 1/min. From these data it can also be seen that there is an
expected effect of slick thickness on the critical water rate, since
at 3.9 1/min a slick of initial thickness 0.32cm is readily dispersed,
while a slick of initial thickness 0.64cm is not. Consistent behavior
is shown by the accelerating disperison rate as a slick thins during
water impingement. This can be seen in many of the Figures 7-4 to 7-12.

TABLE 7-2
Relative Dispersion Rates

Oil	Dispersion Rate [a] $h_{initial} = 0.64\,cm$	$h_{initial} = 0.32\,cm$
Zuetina Crude	0.23	
Kuwait Crude	0.23	
South Louisiana Crude	0.15	0.14
No. 2 Diesel Oil	0.12	
Drakeol 5 w. Span 85 [b]	0.12	0.14
Arabian Light Crude	0.10	
Arzew Crude	0.04	
Drakeol 5	0.04	0.04
No. 6 Fuel Oil	<0.01	0.04

a) instantaneous rate at $h = 0.25\,cm$ for water rate of 5.4 l/min, in units of cm/min

b) with 0.5 vol% Span 85 added, giving $T_{o/w} = 3$ dyne/cm

-225-
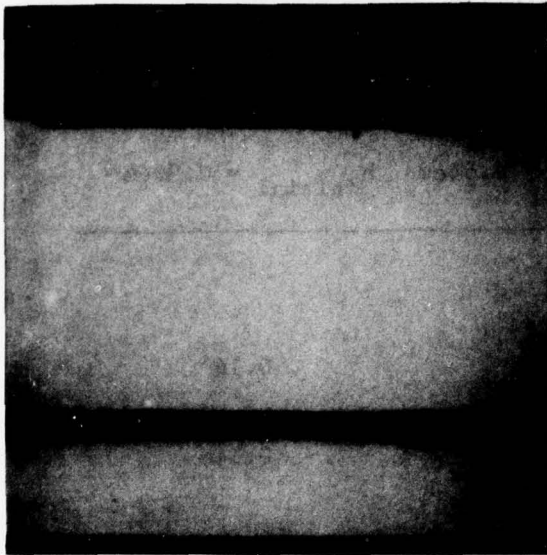
a) 3.1 l/min
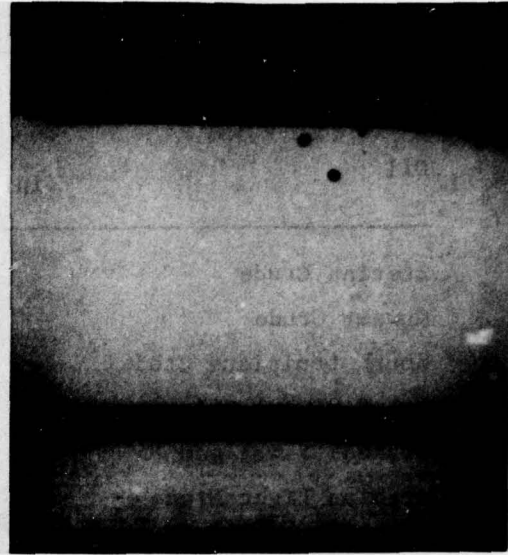
b) 3.9 l/min
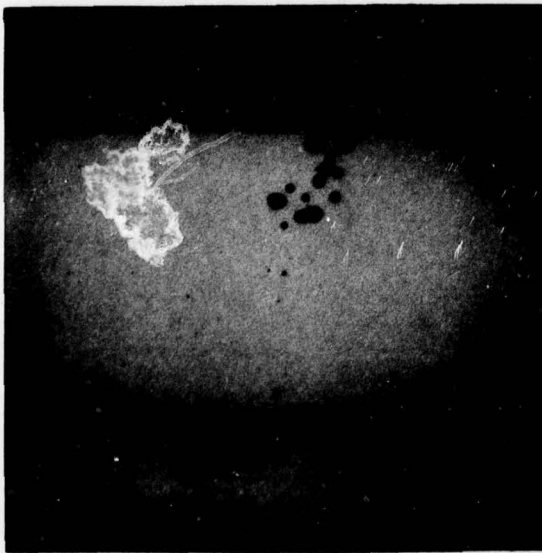
c) 4.6 l/min
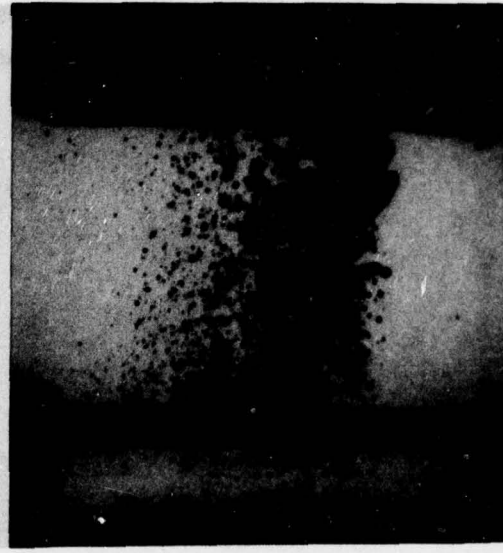
d) 5.4 l/min

Fig. 7-13: No. 6 fuel oil plume character
as a function of water impingement
rate

-226-
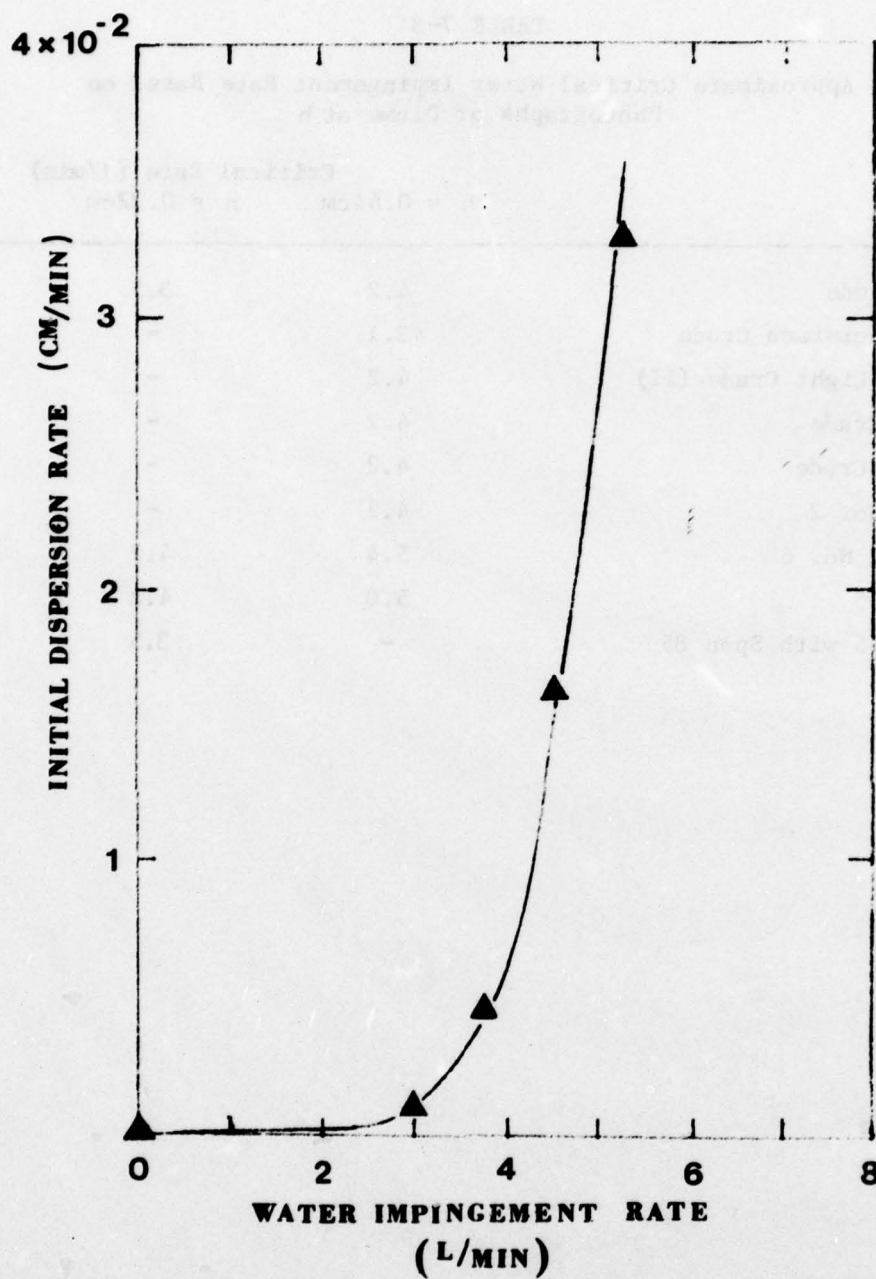
FIGURE 7-14   Arzew Crude Initial Dispersion Rate for δ = 0.32cm

-227-

TABLE 7-3

Approximate Critical Water Impingement Rate Based on Photographs of Plume at h

Oil	Critical Rate (1/min)	
	h = 0.64cm	h = 0.32cm
Arzew Crude	4.2	3.5
South Louisiana Crude	<3.1	-
Arabian Light Crude (II)	4.2	-
Kuwait Crude	4.2	-
Zuetina Crude	4.2	-
Diesel No. 2	4.2	-
Fuel Oil No. 6	5.4	4.2
Drakeol 5	5.0	4.2
Drakeol 5 with Span 85	-	3.5

Attempts at simple correlation of the dispersion rate data of Table 7-2 were unsuccessful, as can be seen by comparing the dispersion rate data with the physical property data given in Table 9-1. No general trends as a function of either absolute or kinematic viscosity, of interfacial tension or of density are exhibited. This is perhaps not surprising given the complexity of the dispersion process under study. The water jet loses momentum in penetrating the slick, the momentum loss depending on oil density and viscosity as well as slick thickness (e.g., the tendency for the slick to thin or part along the line of impingement). The jet energy consumed by accelerating oil droplets and generating a larger oil/water interface probably would not scale directly with dispersion rate either. A large droplet caused to plunge deeply into the tank would constitute a substantial energy sink for the jet, but would probably not contribute to net dispersion, since it would rise to the slick before being convected away. Very low interfacial tension would result in a smaller droplet size distribution and contribute more to net dispersion in our experiment, but it is apparent that this is not an overriding factor. We call attention again, then, to the critical nature of the slick thickness—water impingement rate relation, emphasized above. From the standpoint of the application of the phenomena investigated here, controlling dispersion from a slick requires keeping the slick thick. Further, the higher the seas, the thicker the slick should be.

-229-

8.   DROPLET-SLICK RECOALESCENCE

Let us consider the situation of a slick on the ocean. Wave
action tends to break up the leading edge of the slick, while ocean
currents and turbulence may tend to carry the resulting droplets
underneath the slick. These oil droplets rise to the oil-water
interface where they remain for a finite time. From the standpoint
of understanding the fate of these droplets the kinetics of their
coalescence with the slick is of interest. Laboratory study of
droplet/slick recoalescence cannot, of course, accurately simulate
all aspects of the processes occurring at sea. For example, in the
laboratory the droplet rises vertically through a quiescent medium
to a quiescent interface. In contrast, both turbulence and bulk
convection are present at sea. Nevertheless, it is believed that
the relative rates of coalescence determined in the laboratory should
have applicability in the field case.

A priori estimation of the slick coalescence behavior of
crudes and other multicomponent fuel oils of the types which might
be involved in a spill has not proved possible, primarily as a
result of the complex nature of the oils involved. The crude oil,
for example, is typically a poorly characterized mixture of various
alkyl, cyclic, unsaturated, and aromatic hydrocarbons, oxygen
derivatives thereof, trace metals, heterocyclic compounds, etc.

Some theoretical work has been performed concerning the
coalescence of single droplets at a liquid/liquid interface and some
data have been published for systems in which two pure phases are
present. Unfortunately, the effects on the coalescence process of
the physical and chemical properties of the oil phase have not often
been considered, however. Notably lacking are basic data on the
effects of these properties on the stability against coalescence
of the droplets. The sparse data recorded in the literature include
those for pure oils by Davis and Smith (1976). These data indicate
that an increase in molecular weight decreases the droplet half life
for alkyl and cyclic compounds and increases the droplet half life
for aromatic compounds. These authors also found that aliphatic
alcohols had essentially infinite half lives.

8-1   Apparatus and Experimental Procedure

In order to provide basic data on droplet slick recoalescence kinetics for the crudes and distillates of interest in this work, the apparatus in Figure 8-1 has been constructed. An oil droplet is formed at the tip of the syringe and is released once it has attained the requisite size. [See Appendix 7]. The droplet rises to the interface as a result of its natural buoyancy and usually remains distinct beneath the interface. The length of time required for the droplet to coalesce with the surface layer, the rest time τ, is then determined. Since this quantity is statistical, many events are observed---typically 50 to 100. The most probable coalescence time, τ^*, is then taken as a measure of droplet stability for a given system. On a plot of the total fraction of droplets coalescing by time τ vs. τ, the point of inflection yields the most probable coalescence time.

8.2   Results and Discussion

Variables which might conceivably influence τ are listed in Table 8-1. Of the variables investigated it was found that the following most strongly influenced τ: the droplet diameter, the oil slick thickness, the equilibration of the vapor space over the oil slick with vapors from an excess of oil, and the oil type. Table 8-2 lists the various combinations of variables investigated along with the values obtained for τ^*. A summary of the major findings follows:

A)   For most crude oils, decreasing the diameter of the oil droplet decreases τ^* for the range of droplet diameters 1.4 to 2.5 mm. An example is shown graphically in Figure 8-2 for South Louisiana Crude (SLC). When the droplet diameter is decreased from 2.54 mm to 1.80 mm and then to 1.40 mm, resulting τ^*'s are 7.1 sec, 2.3 sec and 1.5 sec, respectively, approximately following the droplet volume. It can also be seen that as τ^* increases, the half-width of each curve increases; in general the half-width is approximately equal to 0.9 τ^*. This conclusion is felt to be general since the trend is followed for Arabian light crude, Arzew crude and Zuetina crude, as well.

-231-
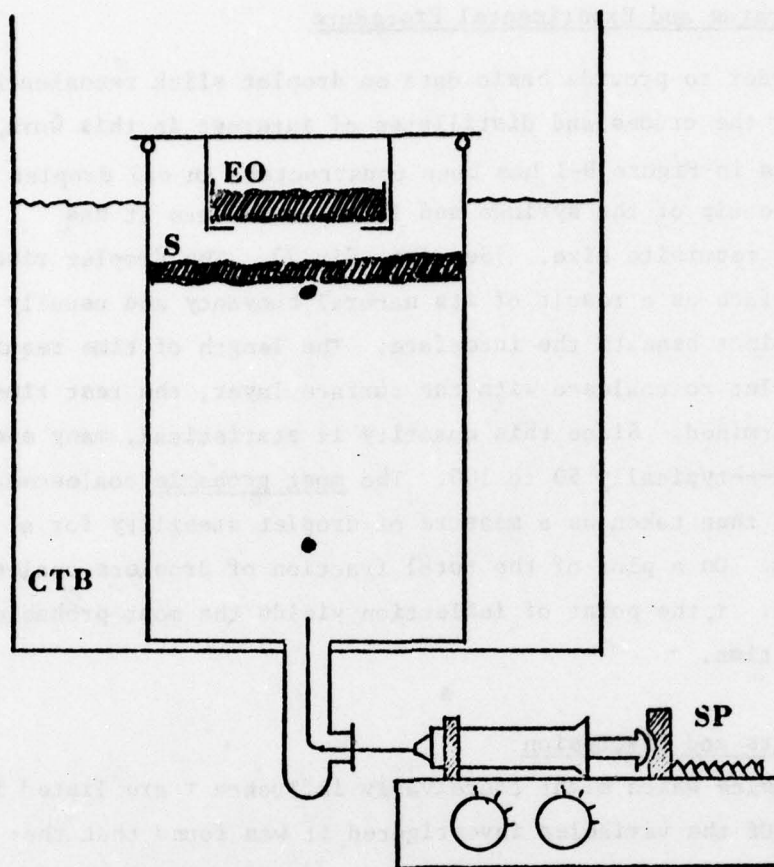
FIGURE 8-1 Apparatus Schematic. CTB: Constant Temperature
Bath; EO: Excess Oil; S: Slick; SP: Syringe
Pump.

TABLE 8-1

Possible Influential Variables

	Investigated ?	
size of oil droplet	Y	
slick thickness	Y	
type of oil	Y	
open or closed to atmosphere	Y	
aging of oil	Y	
salinity of water	Y	N = No
vibration of surface	Y	Y = Yes
temperature	N	
aging of droplet on needle	N	
distance from needle to surface	N	
effect of relative boundary velocity	N	
effect of rotation of droplet	N	
particle content of water	N	

-233-

TABLE 8-2

Most Probable Coalescence Times τ^*

Summary

S L I C K   T H I C K N E S S

OIL	h = 2.0 mm	h = 0.4 mm	h = 0$^+$ mm[a]
Droplet Diameter d = 1.80 mm:			
South Louisiana Crude (SLC) closed[b]	3.2 sec	2.3 sec	~0.5 sec
open[c]	0.8	5.5	~17
aged[d]	~11.	~11.	
Arabian Light Crude (ALC) closed	-	90	
open	26.	38.	
aged	~11	~11	
Kuwait Crude closed	25.	18.	
Zuetina Crude closed	I	31	~18 min
Arzew Crude closed	12.	12.	
THUMS Crude closed	> 60 min	10 min	
No. 6 fuel oil closed	I	~13	
aged		~37	
No. 2 diesel closed	~43	I	
aged	-	> 20 min	
Droplet Diameter d = 1.44 mm:			
SLC closed	~1.5	~1.5	-
open	~0.5	I	
ALC closed	~19	~22	-
Droplet Diameter d = 1.14 mm:			
SLC closed	~1	~1	-
open	~1	~1	-
ALC closed	~50	~45	-
Droplet Diameter d = 2.6 mm:			
SLC closed	7.1	7.1	~2
open	~1.5	~1.	~0.5
Droplet Diameter d = 3.4 mm:			
ALC closed	~13	~43	~13
aged	~15	~35	~13

a) droplet coalesces beginning at oil free air - water interface; each droplet adds to slick thickness (see Figs. 8-3 and 8-4).

b) vapor space closed; pool of excess oil present to equilibrate vapor space.

c) vapor space above slick open to lab atmosphere

d) oil subjected to jet of air prior to droplet release and vapor space above slick open to lab atmosphere

I) Inconclusive; data not sufficiently numerous to define most probable time.
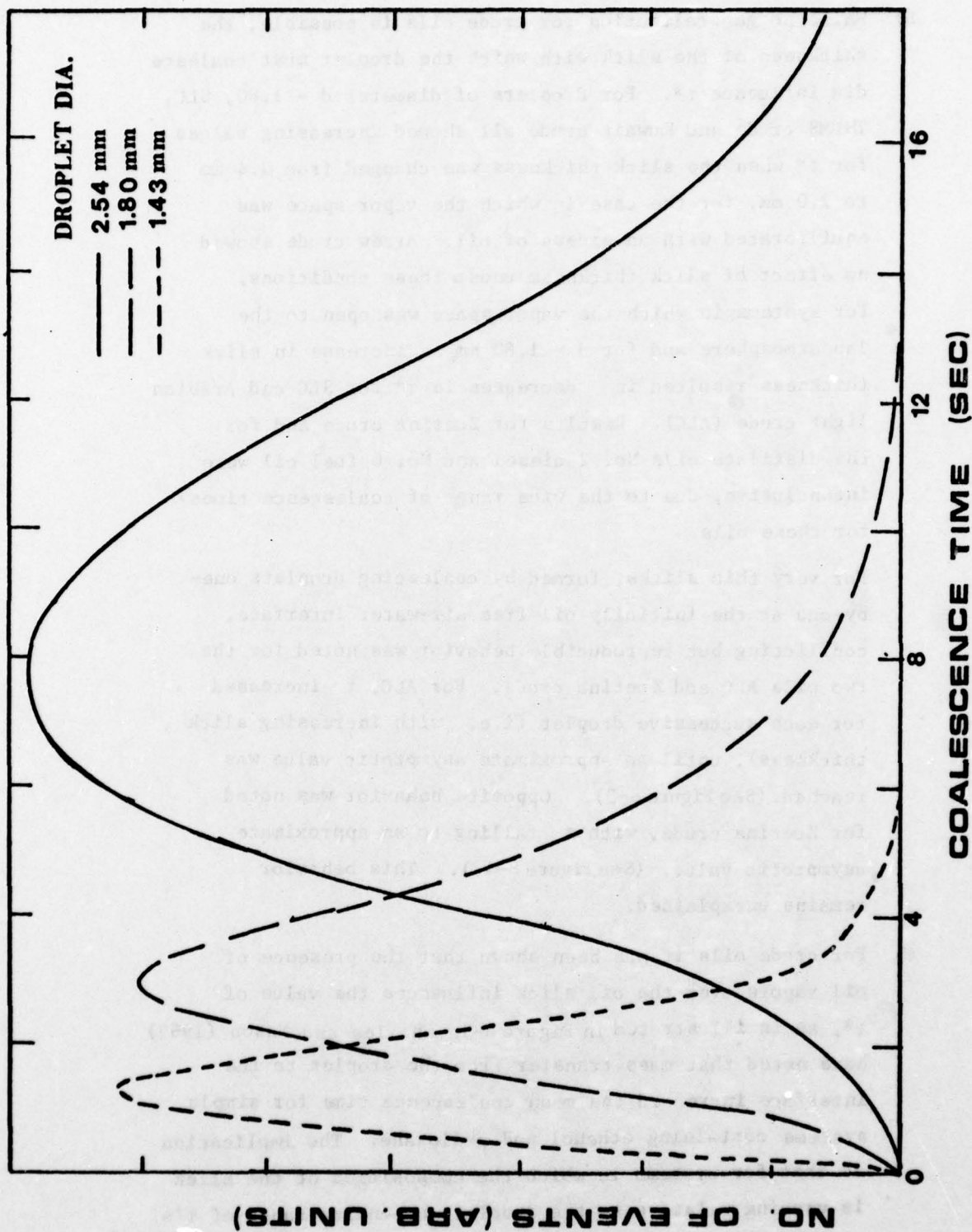
FIGURE 8-2 Effect of Droplet Diameter on Coalescence Time for
South Louisiana Crude, h = 0.4mm, Vapor Space Closed

B) While no generalization for crude oils is possible, the
thickness of the slick with which the droplet must coalesce
did influence τ^*. For droplets of diameter d = 1.80, SLC,
THUMS crude and Kuwait crude all showed increasing values
for τ^* when the slick thickness was changed from 0.4 mm
to 2.0 mm, for the case in which the vapor space was
equilibrated with an excess of oil. Arzew crude showed
no effect of slick thickness under these conditions.
For systems in which the vapor space was open to the
lab atmosphere and for d = 1.80 mm, an increase in slick
thickness resulted in decreases in τ^* for SLC and Arabian
light crude (ALC). Results for Zuetina crude and for
the distilate oils No. 2 diesel and No. 6 fuel oil were
inconclusive, due to the wide range of coalescence times
for these oils.

For very thin slicks, formed by coalescing droplets one-
by-one at the initially oil-free air-water interface,
conflicting but reproducible behavior was noted for the
two oils ALC and Zuetina crude. For ALC, τ increased
for each successive droplet (i.e. with increasing slick
thickness), until an approximate asymptotic value was
reached. (See Figure 8-3). Opposite behavior was noted
for Zuetina crude, with τ falling to an approximate
asymptotic value. (See Figure 8-4.). This behavior
remains unexplained.

C) For crude oils it has been shown that the presence of
oil vapors over the oil slick influences the value of
τ^*, as is illustrated in Figure 8-5. Charles and Mason (1962)
have noted that mass transfer from the droplet to the
interface increased the mean coalescence time for simple
systems containing ethanol and p-dioxane. The implication
is that for systems in which the composition of the slick
is varying relative to the droplet, an entire range of τ's
is possible, depending on the history of the slick, the
history of the droplet, etc.

-236-
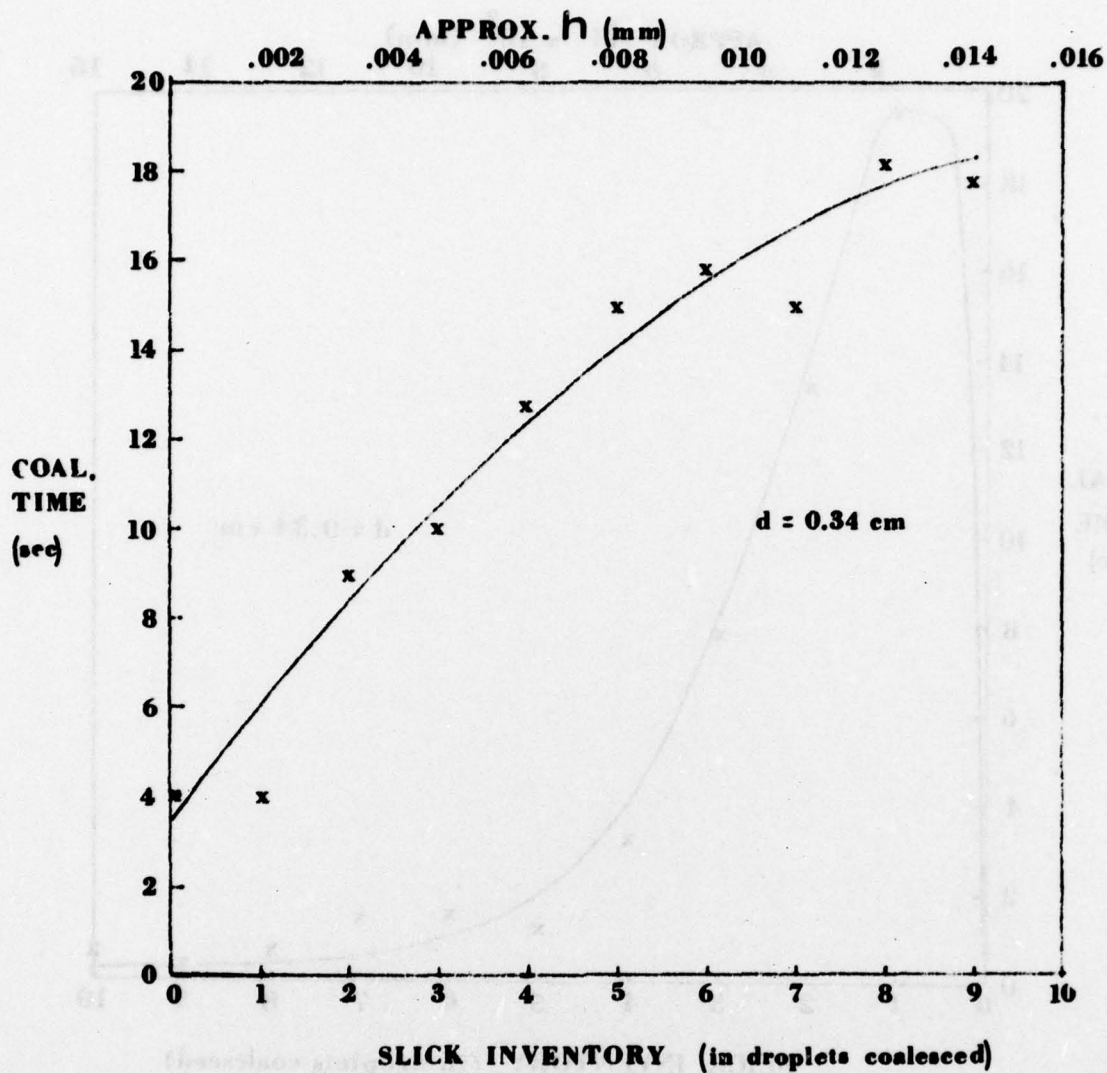
FIGURE 8-3 Most Probable Coalescence Times for Arabian Light Crude Coalescing
at an Initially Oil-Free Interface.
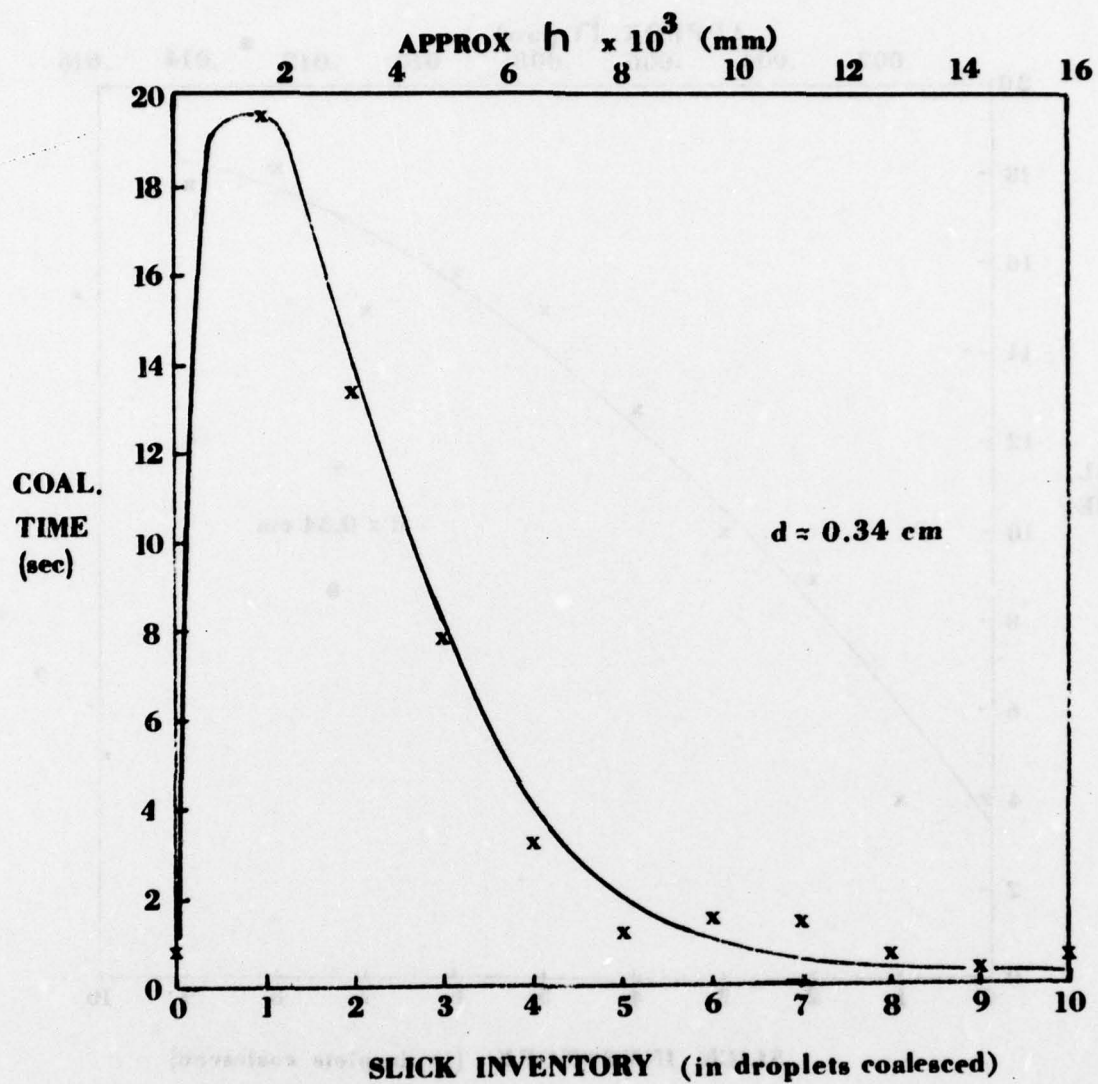
FIGURE 8-4   Most Probable Coalescence Times for Zuetina Crude
Coalescing at an Initially Oil-Free Interface.
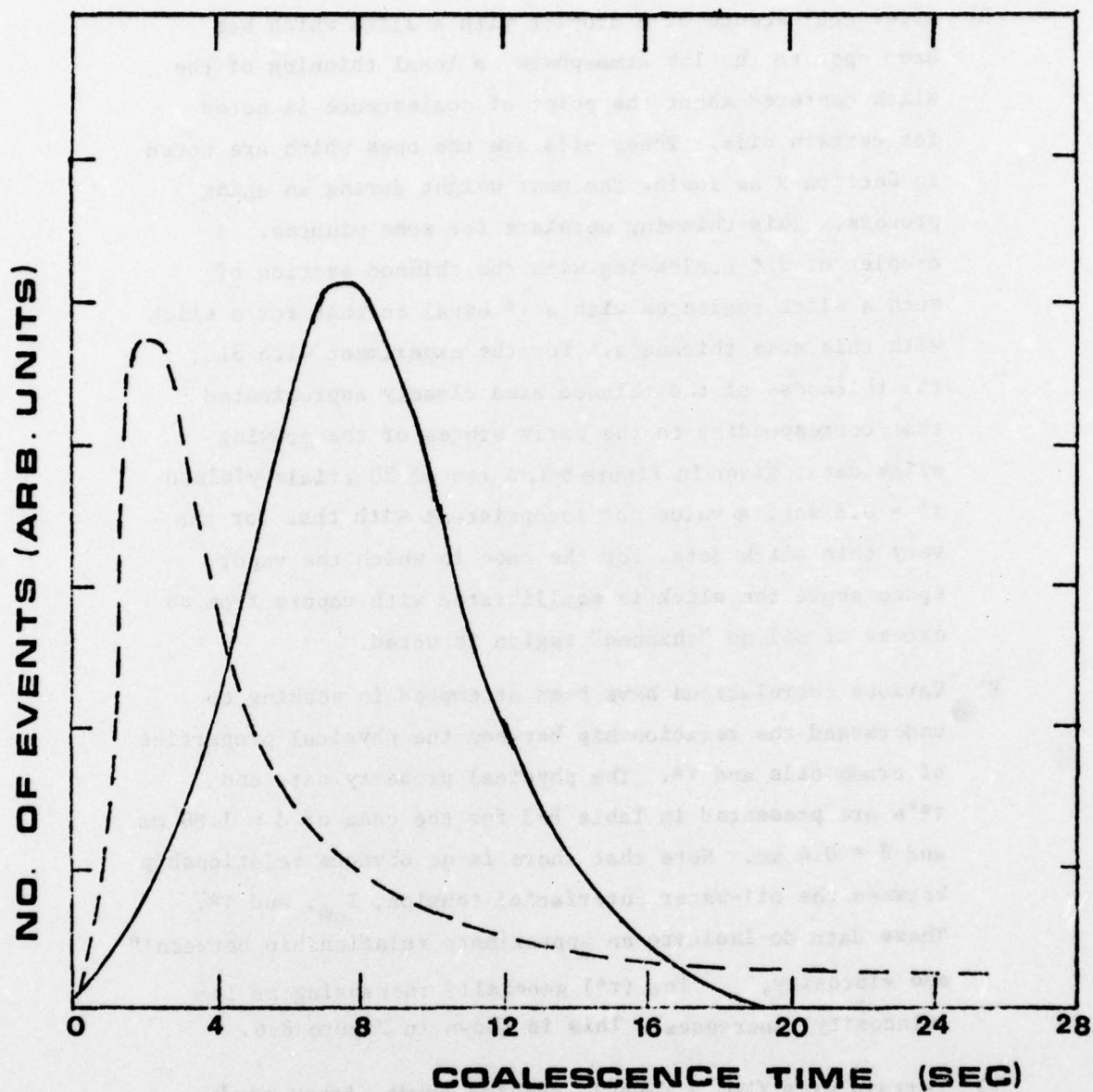
FIGURE 8-5 Effect of Evaporation on Coalescence Times for South Louisiana Crude, h = 0.4mm, d = 2.6mm. Solid Curve: Air Space Above Slick Closed and Equilibrated with Excess Oil. Broken Curve: Airspace Above Slick Open; Air Exchanged Continuously Over Slick for 10 Min. Between Coalescence Events.

D) After coalescence of a droplet with a slick which has
been open to the lab atmosphere, a local thinning of the
slick centered about the point of coalescence is noted
for certain oils. These oils are the ones which are noted
in Section 9 as losing the most weight during an aging
process. This thinning persists for some minutes. A
droplet of SLC coalescing with the thinned section of
such a slick coalesces with a $\tau*$ equal to that for a slick
with this same thickness. For the experiment with SLC,
the thickness of the thinned area closely approximated
that corresponding to the early stages of the growing
slick data, given in Figure 8-3. A run of 20 trials yielded
$\tau* = 0.8$ sec, a value not inconsistent with that for the
very thin slick data. For the case in which the vapor
space above the slick is equilibrated with vapors from an
excess of oil no "thinned" region is noted.

E) Various correlations have been attempted in seeking to
understand the relationship between the physical properties
of crude oils and $\tau*$. The physical property data and
$\tau*$'s are presented in Table 8-3 for the case of $d = 1.80$ mm
and $\delta = 0.4$ mm. Note that there is no obvious relationship
between the oil-water interfacial tension, T_{ow}, and $\tau*$.
These data do indicate an approximate relationship between $\tau*$
and viscosity, $\log (\tau*)$ generally increasing as log
(viscosity) increases. This is shown in Figure 8-6.

F) Certain oils (No. 2 diesel, Zuetina crude, Arzew crude,
Kuwait Crude) undergo stepwise coalescence, leaving
smaller "satellite" droplets behind after a coalescence
event. In all cases observed the diameter between
successive droplets decreased by a factor of approximately
two. No more than three stages were noted (Zuetina)
and in most cases a single secondary droplet was produced.
In general, secondary droplets coalesced more slowly than
primaries, and tertiaries coalesced more slowly than secon-
daries.

-240-

TABLE 8-3

Summarized Results for Comparable
Cases for Crude Oils

Crude Oil	τ^{*a} (sec)	density[b] (g/cm^3)	viscosity[b] (cP)	interfacial tension[b] (dyne/cm)
South Louisiana	5.5	0.86[c]	3.8	19.2[c]
Arzew	13.	0.80	2.9	29.3
Kuwait	18.	0.87[c]	8.7	17.9[c]
Zuetina	31.	0.82	4.1	23.2
Arabian light	90.	0.86	8.4	28.6
THUMS	∿600.	0.93	136.	24.0

a) for the case of d = 1.80 mm, h = 0.4 mm, T = 25±1°C

b) at 25±1°C

c) at 20±1°C
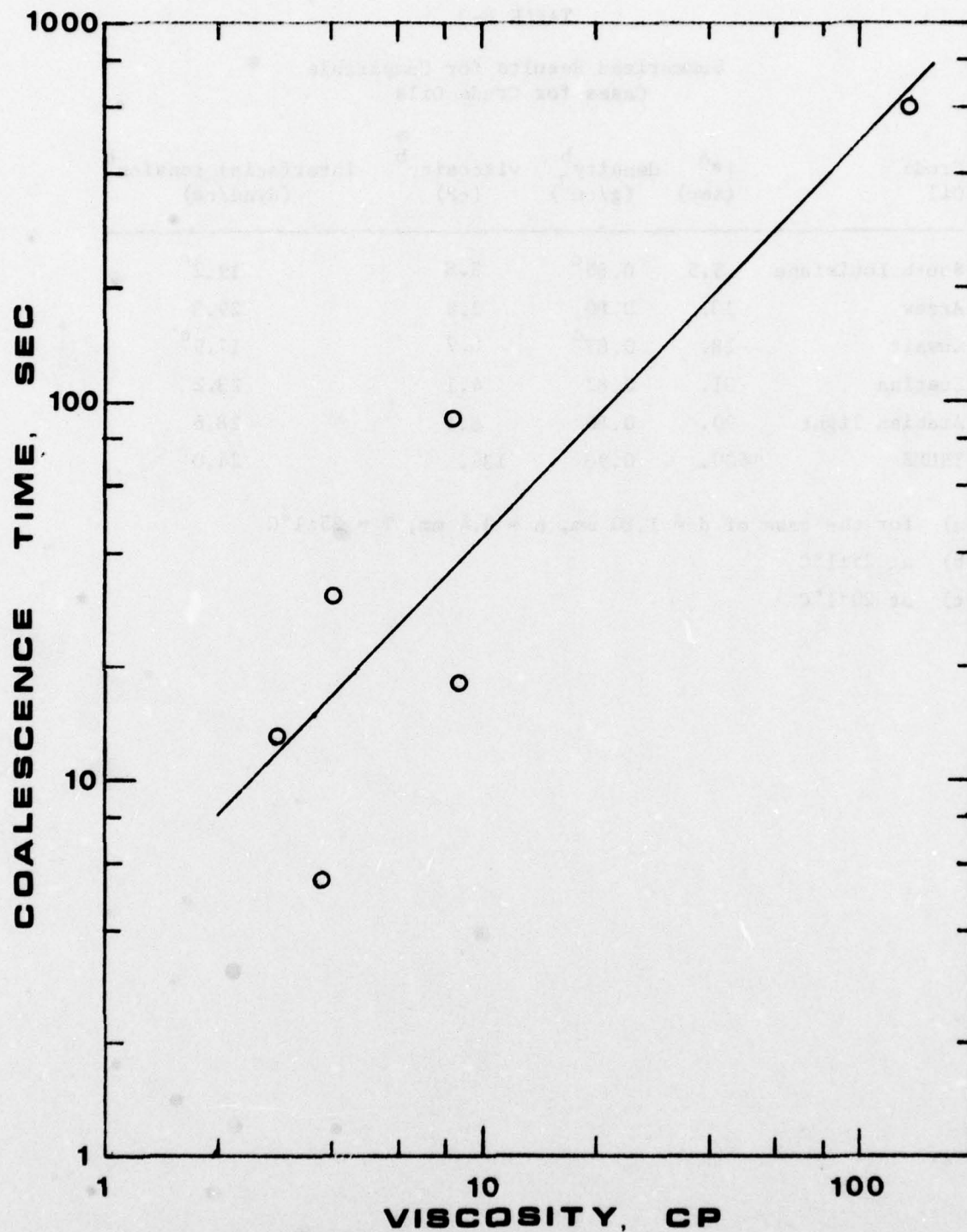
FIGURE 9-6 Approximate Relationship Between Most Probable Coalescence Time and Viscosity for Crude Oils. (See Table 8-3.)

G) In the cases in which the bulk water phase consisted of a synthetic seawater, and therefore contained enough electrolyte to minimize electrostatic stabilization effects, no significant change in τ^* was noted as compared to τ^* for the pure water equivalent. The two oils investigated, Arabian light crude and No. 2 diesel fuel, showed changes in τ^* of less than ten percent. In the synthetic seawater τ^* for Arabian light crude droplets of $d = 1.44$ mm increased from 38 to 40 sec. For No. 2 diesel fuel droplets of this diameter, τ^* decreased from 28 to 26 sec.

H) When the apparatus was subjected to substantial vibration, τ^* was decreased by approximately 25% for SLC droplets of $d = 1.80$ mm. Since no adequate method for quantifying vibration was available, the system was kept as vibration-free as possible

Results are summarized in Table 8-4, in which the lack of generality of some phenomena is noted.

TABLE 8-4

Summarized Results

Phenomenon	Generalization
1) diameter of oil droplet affects coalescence time	as d↑ τ*↑
2) oil slick thickness affects coalescence time	none possible
3) crude oil viscosity affects τ*	as η↑ τ*↑
4) mass transfer (diffusion of some species) between droplet and slick affects τ*	for all cases, closing the system to the lab atmosphere and equilibrating with vapor over excess oil increases τ*
5) for cases of open vapor space, presence of thinned region	not generally found; where present, effect can be removed by equilibrating vapor space with excess oil

9.   OIL PROPERTIES AND THE EFFECTS OF AGING

In a series of weathering experiments samples of both crude
oils and distillate (fuel) oils were aged through a process of
continuous exposure to air by gentle sparging. Weight-loss was
monitored as a function of time. Several physical properties of
the oils, including density, viscosity, surface tension and inter-
facial tension were also measured after different time intervals of
the weathering process.

The information gathered from these experiments gives an
indication of what may happen to a slick after it has been sitting
on water for some period of time. This information is of interest
when coupled with the results of experiments on rates of dispersion
and droplet-slick recoalescence. In some cases these processes
have been found to vary significantly as the slick ages. By examining
the variation in the four parameters mentioned, one ultimately seeks
a capability to predict changes in such things as coalescence times
and dispersion rates as functions of the physical properties, which
are in turn functions of weathering.

A second series of experiments consisted of work with mineral
oils, treated in some cases with reagent grade surfactant. Incorporation
of these surfactants into the oils, even at very low concentrations,
has a marked effect on interfacial tension. At the same time, surface
tension changes very little, and there is virtually no effect on
density or viscosity. Therefore, it is possible to hold three of
the four basic properties nearly constant while changing the inter-
facial tension. Theoretically, both the dispersion and coalescence
process can be dependent on interfacial tension; these experiments
allow us to determine the nature of this relationship.

A tabulation of the physical properties density, viscosity,
surface and interfacial tension determined according to the procedures
detailed below for each of the oils studied is given in Table 9-1.

-245-

TABLE 9-1

Physical Properties of Oils

Oil	density[a] (g/cm^3)	viscosity[b] (cP)	surface tension[b] (dyne/cm)	interfacial tension[b] (dyne/cm)
Arzew crude	0.799	2.70[(20.4)]	27.0[(21.6)]	34.4[(20.2)]
South Louisiana crude	0.855	5.73[(20.0)]	30.4[(18.2)]	19.2[(18.2)]
Arabian light crude (II)	0.802	2.78[(19.9)]	25.9[(20.0)]	33.0[(20.4)]
Kuwait crude	0.866	12.60[(20.4)]	27.2[(21.6)]	17.9[(21.6)]
Zuetina crude	0.821	3.00[(20.4)]	25.8[(17.0)]	21.8[(21.6)]
THUMS crude	0.943	420.[(20.4)]	26.4[(21.4)]	29.3[(21.4)]
Diesel No. 2	0.840	2.95[(20.4)]	29.2[(20.8)]	26.8[(20.8)]
Fuel Oil No. 6	0.910	108.9[(20.4)]	39.4[(21.6)]	25.5[(21.6)]
Drakeol 5	0.835	9.68[(20.4)]	29.8[(19.7)]	51.5[(19.7)]

a) recorded at 20±1°C

b) exponent refers to temperature (°C) at which property is determined

9.1 The Effects of Aging --- Procedures

Aging (or weathering) experiments were performed using four different oils, starting with 200 ml samples of each. The oils studied were:

Zue crude oil

South Louisiana crude oil

No. 6 fuel oil

No. 2 diesel oil

The aging of the samples was accomplished by gentle sparging with laboratory compressed air supplied through long-stemmed Pasteur pipettes (~ 2 cm^3), which were immersed directly into each sample. The sparging was vigorous, but not so vigorous as to cause splashing.

Weight loss was followed for all of these oils. Extensive data on changes in density, viscosity, surface tension and interfacial tension were recorded for both South Louisiana crude and for No. 2 diesel oil. Weighings were taken at the following approximate intervals: 0.5, 1, 6, 17, 20, 45, 86, and 92 hrs. (Times include only total time of aeration, not time stopped.) Small aliquots were removed from each oil sample at 20 hrs and more frequently for some samples in order to measure density and viscosity.

The results were recorded in the following units to the indicated precision:

% wt loss (-)	to 0.01%
density (g/cm^3)	to 0.001 g/ml
viscosity (cP)	to 0.01 cP
surface tension (dynes/cm)	to 0.1 dyne/cm
interfacial tension (dynes/cm)	to 0.1 dyne/cm

Density was determined using specific gravity bottles (pycnometers) in which the weight of an exact volume of oil is determined. Viscosity was determined using standard capillary viscometers, measuring with a stopwatch the time required for a liquid to flow a certain length through a capillary. This measurement is performed in a constant temperature bath, a 95 L tank with two immersible heaters/circulators, which is kept as 20.2 (±0.2) °C. The tubes are calibrated with water and the known values of its viscosity at

various temperatures, according to the relation:

$$\frac{\nu_1}{t_1} = \frac{\nu_2}{t_2} = \text{constant}$$

where ν = kinematic viscosity (centistokes) and t = time (sec).
The constant for each tube is found through these calibrations.

Surface and interfacial tensions are determined using a CENCO tensiometer, model 70545. This procedure involves lowering a circular platinum ring into a surface (or interface), then measuring the amount of force necessary to remove the ring from the surface. The vernier scale allows measurements to a precision of 0.1 dyne/cm.

The glassware used is cleaned in chromic acid and distilled water. To insure that each dish (usually 70x50 mm) is sufficiently clean, the surface tension of distilled water is tested first, checking for close agreement with known values.

For surface tension, the ring is submerged in a 1 cm thick layer of the liquid of interest. The sample holder is lowered until the ring is in the surface, with the scale zeroed. Force is applied until the ring breaks free of the surface. The ring must be scrupulously clean in these experiments. This is usually accomplished by heating the ring in a gas flame. For interfacial tension, the ring is first submerged in distilled water, at least 2 cm deep. A layer of oil about 1 cm thick is then added by pipette. The table holding the sample is carefully lowered until the ring is in the interface, with the scale at 'zero' setting. Force is then gradually applied until the ring breaks from the interface. The values resulting from the above procedures are apparent surface or interfacial tensions. To get the true tension, straight-forward correction factors are applied (Zuidema and Waters, 1941).

9.2 The Effects of Aging---Results and Discussion

It was found that all of the oils lost weight most rapidly in the first six hours, leveling off after approximately the one day point. (See Figure 9-1.) As expected, the crudes had a much higher volatile composition than the fuel oils. The percent losses were

-248-
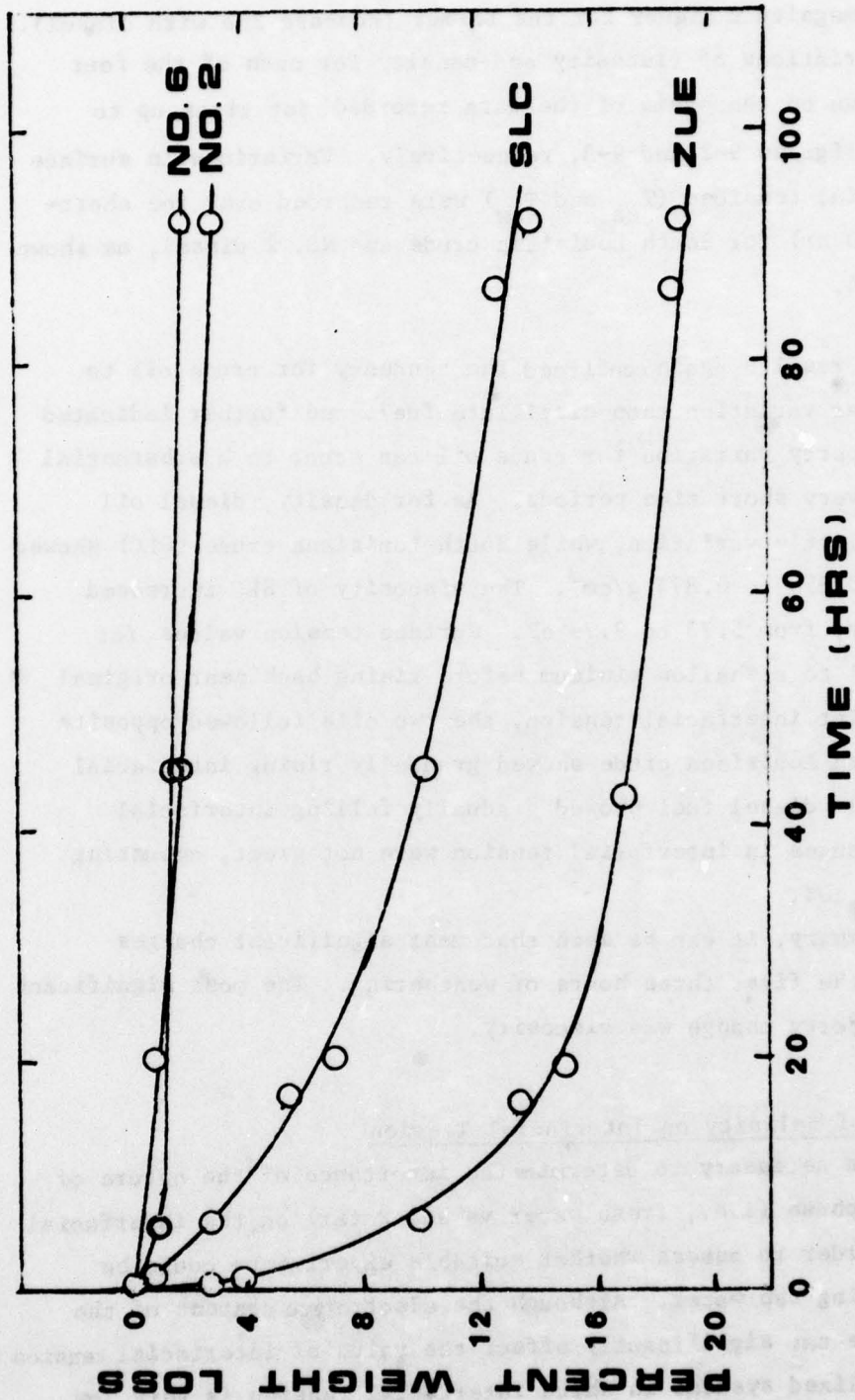
FIGURE 9-1 Oil Weight Loss During Aging

PERCENT WEIGHT LOSS

0 4 8 12 16 20

TIME (HRS)

0 20 40 60 80 100

NO. 6
NO. 2
SLC
ZUE

-249-

an order of magnitude higher for the former (compare Zue with diesel).

Variations of viscosity and density for each of the four oils are shown on the basis of the data recorded for times up to 92 hours in Figures 9-2 and 9-3, respectively. Variations in surface and interfacial tensions (T_{oa} and T_{ow}) were recorded over the short-term (0 to 20 hr) for South Louisiana crude and No. 2 diesel, as shown in Figure 9-4.

These results again confirmed the tendency for crude oil to undergo larger variation than distillate fuel, and further indicated that the property variation for crude oil can occur to a substantial extent over very short time periods. As for density, diesel oil showed very little variation, while South Louisiana crude (SLC) showed a rise from 0.856 to 0.874 g/cm^3. The viscosity of SLC increased significantly, from 5.73 to 9.79 cP. Surface tension values for each oil fell to a shallow minimum before rising back near original values. As for interfacial tension, the two oils followed opposite trends. South Louisiana crude showed gradually rising interfacial tension, while diesel fuel showed gradually falling interfacial tension. Changes in interfacial tension were not great, amounting to only 5 to 10%.

In summary, it can be seen that most significant changes occurred in the first three hours of weathering. The most significant physical property change was viscosity.

9.3 Effects of Salinity on Interfacial Tension

It was necessary to determine the importance of the nature of the aqueous phase (i.e., fresh water vs sea water) on the interfacial tension in order to assess whether suitable experiments could be performed using tap water. Although the electrolyte content of the aqueous phase can significantly affect the value of interfacial tension for those specialized systems in which interfacial tension is very low (< 1 dyne/cm), for typical crude oils for which interfacial tension is typically 20-35 dyne/cm this effect has been found to be small. Data determined in this laboratory and listed in Table 9-2 indicate that variations of 2-4 dyne/cm between distilled water and seawater interfacial tensions are typical.

-250-
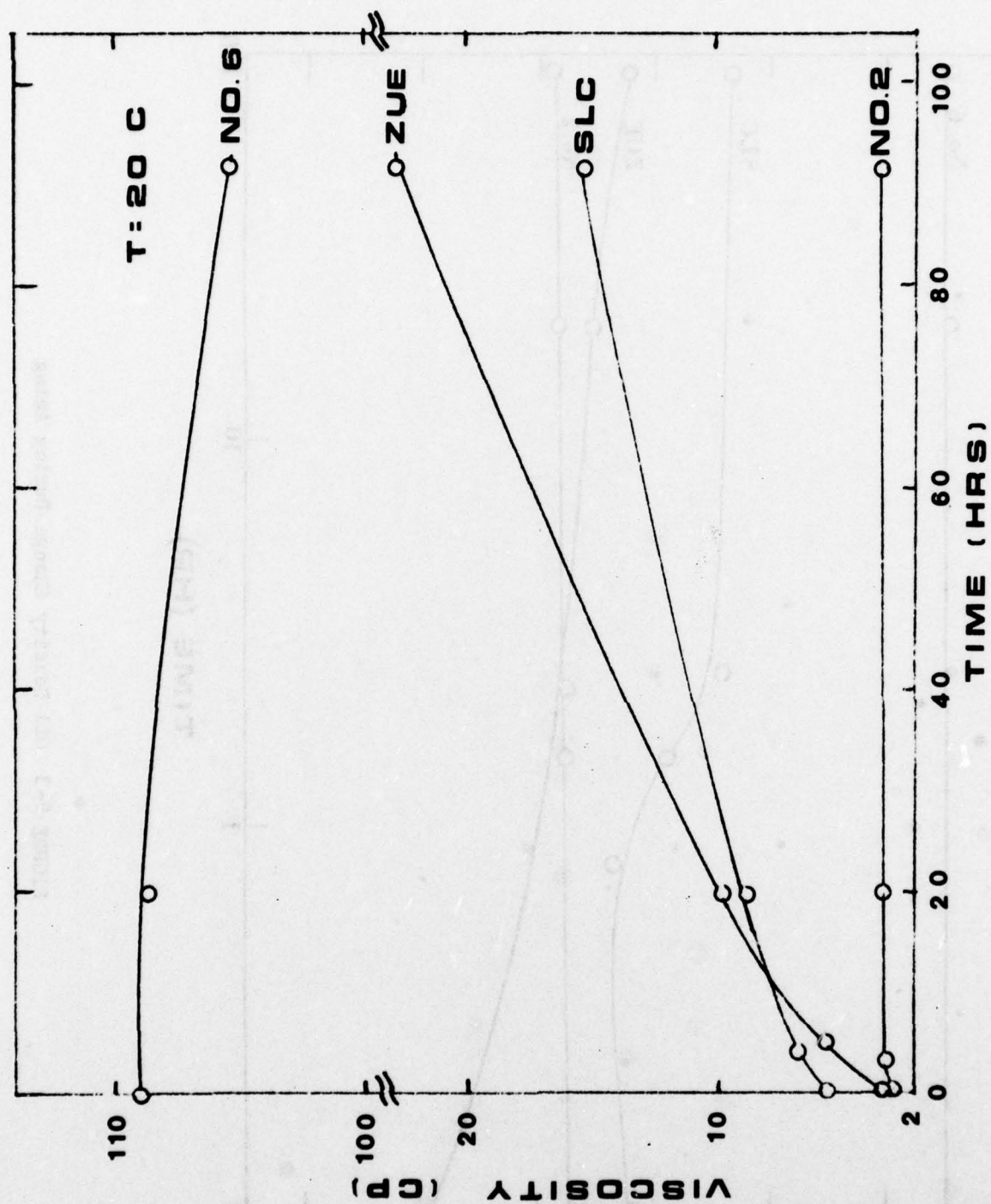
FIGURE 9-2. Oil Viscosity Variation During Aging
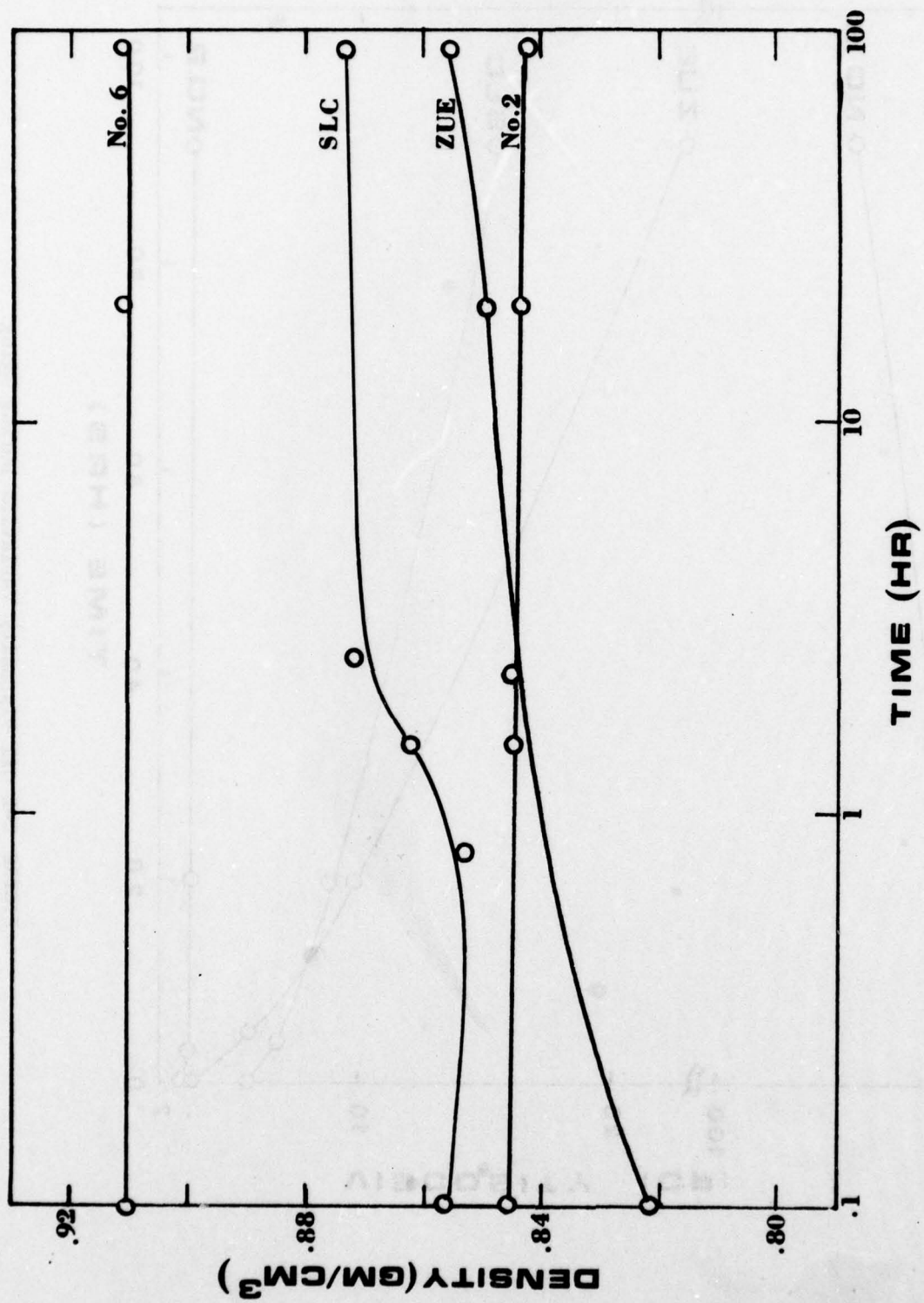
FIGURE 9-3 Oil Density Change During Aging
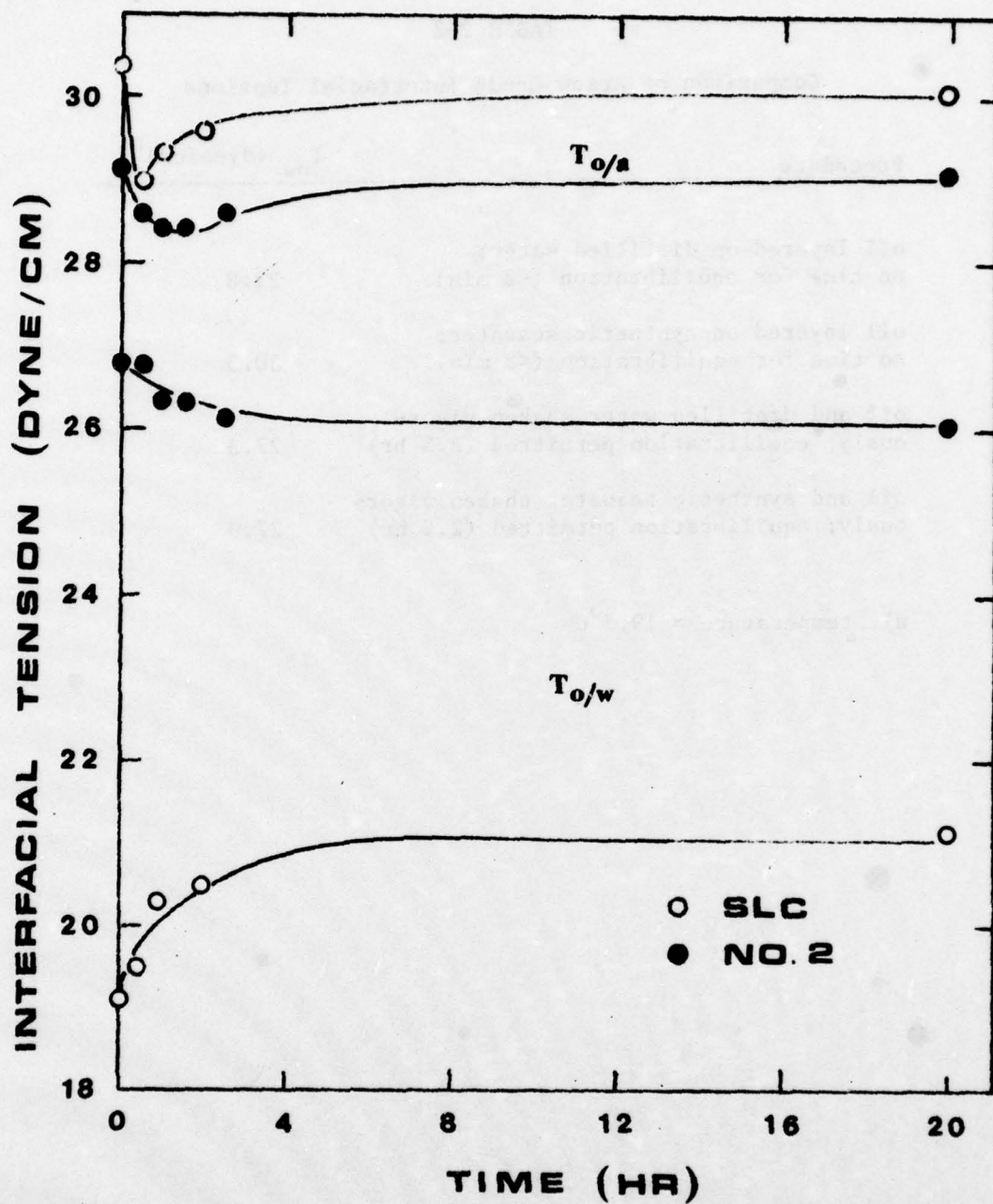
FIGURE 9-4 Oil Surface and Interfacial Tension Variation
During Aging

-253-

TABLE 9-2

Comparison of Arzew Crude Interfacial Tensions

Procedure	T_{ow} (dyne/cm)[a]
oil layered on distilled water; no time for equilibration (<2 min)	33.8
oil layered on synthetic seawater; no time for equilibration (<2 min)	30.5
oil and distilled water shaken vigorously; equilibration permitted (2.5 hr)	27.3
oil and synthetic seawater shaken vigorously; equilibration permitted (2.5 hr)	27.0

a) temperature = 19.5^{o}C

10.   SYNTHETIC CRUDE OIL FORMULATION

In order to assess the importance of the major physical properties
viscosity, density, surface tension and interfacial tension on the dis-
persion and recoalescence processes of crude oils it was originally felt
that the formulation of "synthetic crude oils" would be desirable. These
synthetic oils were to be well characterized materials that could be util-
ized in future experiments by other investigators. The four physical
properties mentioned above were to approximate those of crude oils. By
choosing from a sufficiently large number of available oils it was felt
that it would be possible to find two or more oils in which all properties
were constant except for one (e.g., viscosity). Then by carrying out
tests with these oils it would be possible to determine the effect of
variation of the single property.

10.1 Mineral Oils

After a thorough review of available relatively pure mineral oils,
we secured samples of several and measured their physical properties. These
are listed in Table 10-1, in which is also listed the properties of three
of the crude oils examined in our studies. It can be seen that the mineral
oils typically exhibit higher viscosity than do the crude oils at compar-
able density. This proved to be a very difficult problem in accurate
simulation of true crude oil properties. In fact, a substantial portion
of the research effort in synthetic oil formulation was devoted to attempt-
ing to raise the density of mineral oil mixtures to the levels more typically
exhibited by crude oils. Attempts to increase synthetic crude oil density
consisted of the following:

> (1) Attempting to suspend carbon black particles in the
>   mineral oils in such a way that the oil would remain
>   homogeneous for a period of time sufficiently long to
>   accomplish the water impingement dispersion tests and/or
>   the droplet-slick recoalescence tests. The carbon black
>   particulate material utilized as an additive has its
>   natural counterpart in the asphaltenic fraction of true
>   crude oils. Asphaltenics tend to raise crude oil density

TABLE 10-1

Physical Properties of Oils in Order
Of Increasing Viscosity[a]

Oil	Surface Tension	Interfacial Tension	Density	Viscosity
	(dyne/cm)	(dyne/cm)	(g/cm^3)	(cP)
Mineral Oils				
Penetek	27.2	27.2	0.800	3.91
Dratex 50	28.5	35.5	0.818	8.54
Drakeol 5	28.6	31.2	0.826	9.68
Drakeol 9	28.7	37.7	0.841	22.1
Fisher Light	29.6	31.1	0.847	39.3
Drakeol 21	31.1	36.5	0.862	81.8
Fisher Heavy	30.3	48.9	0.874	163.
Coray 150	32.2	-	0.906	>300.
Crude Oils				
South Louisiana	30.4	19.2	0.855	5.73
Arabian Light	25.0	27.2	0.860	8.91
Kuwait	27.2	17.9	0.866	12.60

a) recorded at 20±1°C

-256-

to levels between 0.9 and ~1.0 g/cm^3, depending upon
the amount present. We examined a number of sur-
factants for their suspending power for carbon black
in mineral oils, in part in consultation with the major
U.S. manufacturer of carbon black, and did succeed in
achieving a formulation which remained stable for per-
iods of 30 to 60 minutes. This was not sufficiently
long to permit satisfactory experiments of the disper-
sion or recoalescence types, however.

2) An alternative approach was to add varying amounts of
some higher density soluble compound. Among the hydro-
carbons, aromatics alone exhibit higher densities (~0.86),
while olefinic, naphthenic and of course paraffinic species
are comparable to the mineral oil densities (0.80-0.84) at
sufficiently low viscosities. Aromatics are volatile
materials, however, and though highly soluble in mineral
oils we found that they volatilize rapidly when oil
mixtures containing them are spread for the dispersion
or recoalescence experiments. This would lead to property
variation with time during the experiment and would
present toxicity problems as well. Thus, this approach
was abandoned.

3) A final alternative approach was to select various non-
paraffinic mineral oils, primarily the silicone oils.
These oils tend to exhibit natural densities from ~0.97
to >1.0. Few silcone oils of density <1.0 are available,
however, and these are exceedingly costly. For this
reason experimentation with silicone oils was not
attempted.

10.2 Mixture Properties

Although the physical properties of available mineral oils
would not span the range of properties of typical crudes, the objective
of utilizing these oils to demonstrate the effect on dispersion or re-
coalescence of variation of a single property remained valid. The sur-
face and interfacial tension variations were easily achievable by addi-

-257-

tion of suitable surfactants, as discussed in Section 10.3, below. Thus, it was density-viscosity pair properties which were of interest. As perusual of Table 10-1 indicates, viscosity and density do not vary independently for paraffinic mineral oils. The relationship is given in Figure 10-1, it which it can be seen that as density increases, viscosity increases. Both increase as molecular weight of the paraffin hydrocarbon increases. Thus, in order to achieve variation of viscosity while holding density fixed, we investigated the efficacy of making binary mixtures which might vary both in the two components selected and in the proportion of the components mixed.

The theory of prediction of mixture properties for complex materials such as mineral oils is not highly advanced. However, we applied the current accepted theory to enable us to estimate the composition of mixtures we should begin to investigate experimentally. The theory of mixture density (Reid, et al., 1977) is quite simple for systems in which volume change upon mixing is small, as would be expected for paraffinic oils. The molar volume of the mixture, $\underline{V}_m$:

$$\underline{V}_m = \sum_j x_j \underline{V}_j \tag{10-1}$$

where $\underline{V}_j$ = molar volume of pure liquid j (cm^3/gmol) and x_j = mole fraction of j. Liquid mixture viscosities follow somewhat more complex rules (Reid, et al., 1977). The mixture viscosity, μ_m, can often be predicted for a binary using:

$$\ln \mu_m = \sum_i x_i \ln \mu_i \tag{10-2}$$

where μ_i = absolute viscosity of liquid i (cP) and x_i = mole fraction of i.

We generated solutions of these equations for the entire range of mineral oils available to us. Details of these calculations are given in Appendix 8. Table 10-2 lists the binary combinations investigated. The curves corresponding to the mixing rules for several binaries are plotted in figure 10-1. It can be seen that the mixture density-viscosity pair properties follow the locus of the pair properties of the available pure mineral oils. It was not obvious that this would be the case at the outset of the study, and this finding
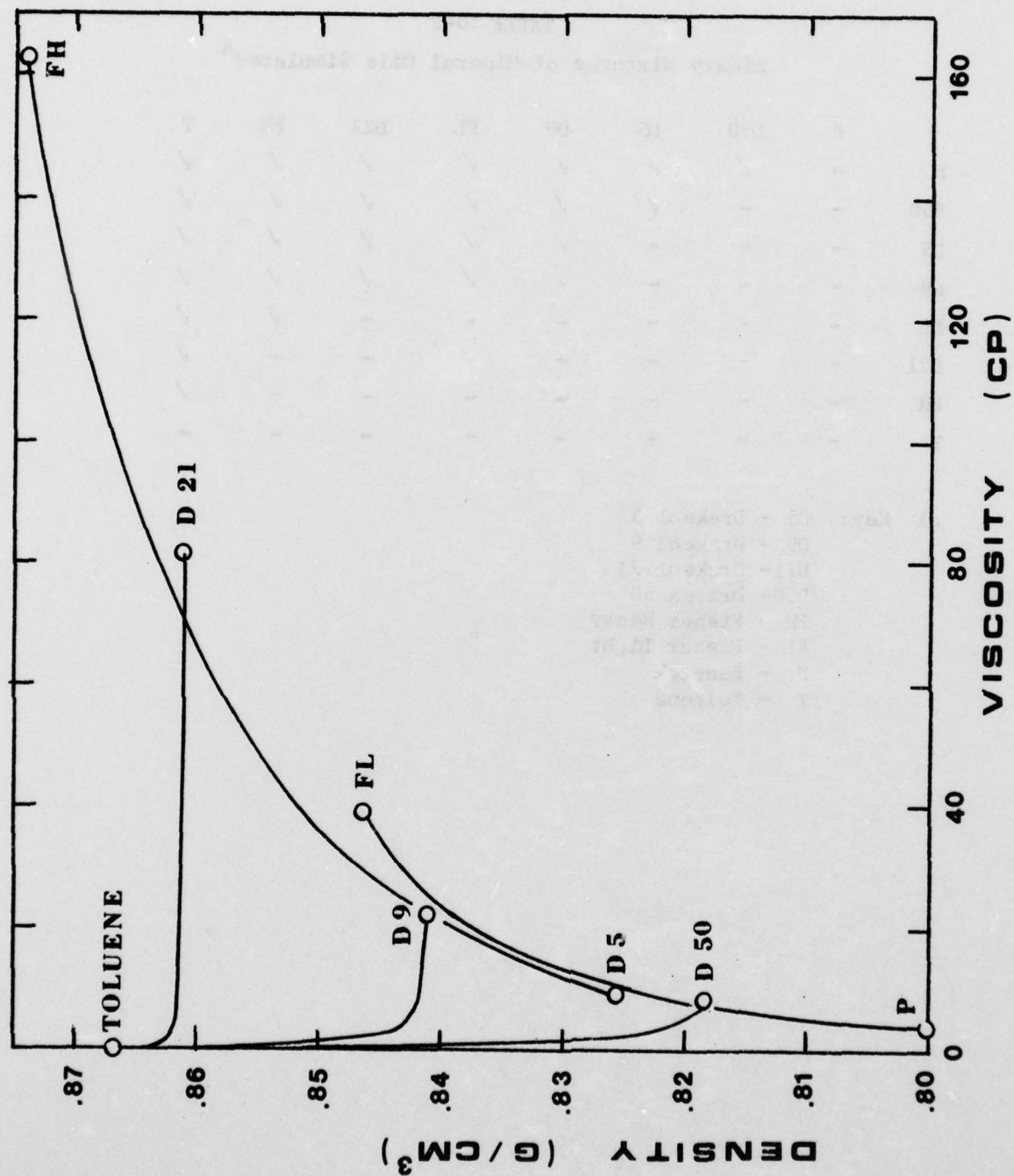
FIGURE 10-1 Density-Viscosity Relationship for Mineral Oils. Solid Curves
Illustrate Simulated Binary Mixture Properties According to
Equation (10-2)

TABLE 10-2
Binary Mixtures of Mineral Oils Simulated[a]

	P	D50	D5	D9	FL	D21	FH	T
P	-	✓	✓	✓	✓	✓	✓	✓
D50	-	-	✓	✓	✓	✓	✓	✓
D5	-	-	-	✓	✓	✓	✓	✓
D9	-	-	-	-	✓	✓	✓	✓
FL	-	-	-	-	-	-	✓	✓
D21	-	-	-	-	-	-	-	✓
FH	-	-	-	-	-	-	-	✓
T	-	-	-	-	-	-	-	-

a) Key: D5 – Drakeol 5
D9 – Drakeol 9
D21– Drakeol 21
D50– Dratex 50
FH – Fisher Heavy
FL – Fisher Light
P – Penetek
T – Toluene

was, needless to say, quite disheartening, for it meant that we could not formulate mineral oil mixtures which varied in only a single property. For purposes of illustration of the beneficial effect of adding one of the higher density aromatic components, we list the results of our theoretical work which indicate that by addition of toluene it should be possible to accomplish a variation in viscosity while holding density fixed and a variation in density while holding viscosity fixed. These data are given in Table 10-3.

10.3 Modification of Interfacial Tension

A final item of concern was the ability to influence interfacial tension freely while holding density, viscosity and surface tension fixed. We measured the surface tension and interfacial tension for a number of mixtures of mineral oils to determine whether surfactant addition would be necessary in order to attain interfacial tensions similar to those for crude oils. Data for several systems are listed in Table 10-4, in which it can be seen that binary mixtures of mineral oils generally exhibit surface tensions similar to those of pure mineral oils (i.e., somewhat higher than for crude oils). Accordingly, we investigated the effect of addition of surfactant.

In natural crude oils the surface active materials would, of course, be present initially in the organic phase. Thus we sought surfactants which were inherently soluble in mineral oils, namely those of low hydrophile-lipophile balance (HLB). A low HLB rating indicates that the major protion of the surfactant molecule is oil soluble and only a very small portion water soluble. Table 10-5 lists four surfactants (HLB ranging from 1.8 to 5.3), which we examined for their solubility in mineral oils, and indicates the results of these experiments.

The variation of interfacial tension with surfactant concentration for the two oil-soluble surfactants Atmos 300 and Span 85 was determined for the mineral oil Drakeol 5 as follows. Solutions of various surfactant concentrations were prepared using precision volumetric glassware. Every piece was cleaned, allowed to stand in chromic acid for several hours, then rinsed thoroughly with distilled water and allowed to dry.

The first solution was made in the largest flask (1 or 2 liters), usually to a concentration of 0.5%. From this, serial dilutions were made into several smaller flasks (50-250 ml). The surfactant concentrations

TABLE 10-3
Synthetic Oil Mixtures which give Target Properties

Target Density	Target Viscosity	System[a] A-B	Approx. Volume Fraction of A
(gm/cm^3)	(cP)		
0.8275	2.8	D50-T	0.91
0.8275	5.7	D5-T	0.04
0.8275	10.1	FH-P	0.33
0.8275	13.6	FL-D50	0.014
0.8095	5.7	D50-P	0.32
0.8120	5.7	FH-P	0.132
0.8200	5.7	D50-T	0.94
0.8275	5.7	D5-T	0.92
0.8445	5.7	D9-T	0.85
0.8635	5.7	D21-T	0.725

a) Key: D5 - Drakeol 5
         D9 - Drakeol 9
         D21- Drakeol 21
         D50- Dratex 50
         FH - Fisher Heavy
         FL - Fisher Light
         P - Penetek
         T - Toluene

TABLE 10-4

Surface and Interfacial Tensions of Synthetic Oil Mixtures

Mixture[a] Vol/Vol	Surface Tension	Interfacial Tension
	(dyne/cm)	(dyne/cm)
50/50 D5/D21	30.2	-
40/60 FH/D5	27.3	-
80/20 FL/D21	29.9	-
65/35 FL/FH	30.2	-
60/40 D50/P	28.0	31.0
65/35 D21/P	29.3	32.5
75/25 FL/FH	30.1	33.4
50/50 FL/FH	30.0	33.3
50/50 T/FH	29.0	32.2

a) Key: D5 - Drakeol 5
          D9 - Drakeol 9
          D21- Drakeol 21
          D50- Dratex 50
          FH - Fisher Heavy
          Fl - Fisher Light
          P - Penetek
          T - Toluene

TABLE 10-5

Surfactant/Mineral Oil Interactions

Surfactant	HLB	Solubility in Penetek[4]	Solubility in Drakeol-9[4]
Brij 52 [1]	5.3	I	I
Atmos 150 [2]	3.2	I	I
Atmos 300 [2]	2.8	S	S
Span 85 [3]	1.8	S	S

(1) Polyoxyethylene(2)cetylether

(2) Mono & Diglycerides

(3) Sorbitan Trioleate

(4) I = Insoluble, S = Soluble

ranged from the initial 0.5% to as low as 0.0005%. To bring about total dissolution, each flask was vigorously shaken (and heated if necessary). Solutions were allowed to cool back to room temperature before making surface and interfacial tension determinations. These measurements were all made with distilled water and oil at room temperature (20 to 21°C). The mineral oil investigated was Drakeol 5 (Howe-French). Two surfactants of suitably low hydrophilic nature, Span 85 and Atmos 300 (Atlas Chemical Co., ICI America) were studied. There was some difficulty in dissolving the surfactants in the Drakeol 5 at room temperature. However, slightly elevated temperatures led to rapid dissolution.

Even with the addition of very small amounts of surfactant (e.g., 0.0005 vol% Span 85) substantial changes in interfacial tensions were found. Interfacial tension data are given in Figure 10-2, which is a plot of interfacial tension versus log (vol.%) concentration for both Span 85 and Atmos 300. For each surfactant interfacial tension reached an approximate asymptote near 0.5 vol% surfactant. Surface tensions of the Drakeol 5 solutions were also measured and are given in Figure 10-2. These values dropped only about 1 percent for each surfactant over the entire concentration range. Values were measured at constant temperature (20° ± 1°C). At least two determinations were made for each sample (several where the tensions were less than 10 dynes/cm) to improve accuracy.

It was found possible to vary interfacial tension with virtually no effect on density, viscosity or surface tension by use of either Atmos 300 or Span 85. The failure of these surfactant additives to influence surface tension, while strongly influencing interfacial tension, is a consequence of the polar/nonpolar character of the water/oil interface and the polar/polar character of the oil/air interface. The surfactant molecules, while oil soluble, contain a small polar component which prefers the polar aqueous surroundings to the neutral vapor phase surroundings. It should be possible in the same manner to influence surface tension strongly while leaving interfacial tension approximately fixed. A surfactant molecule capable of accomplishing this would contain an oil soluble portion and a portion

To/a
To/w w. SPAN 85
To/w w. ATMOS 300

CONC. SURFACTANT (VOL %)

SURFACE TENSION (DYNE/CM)
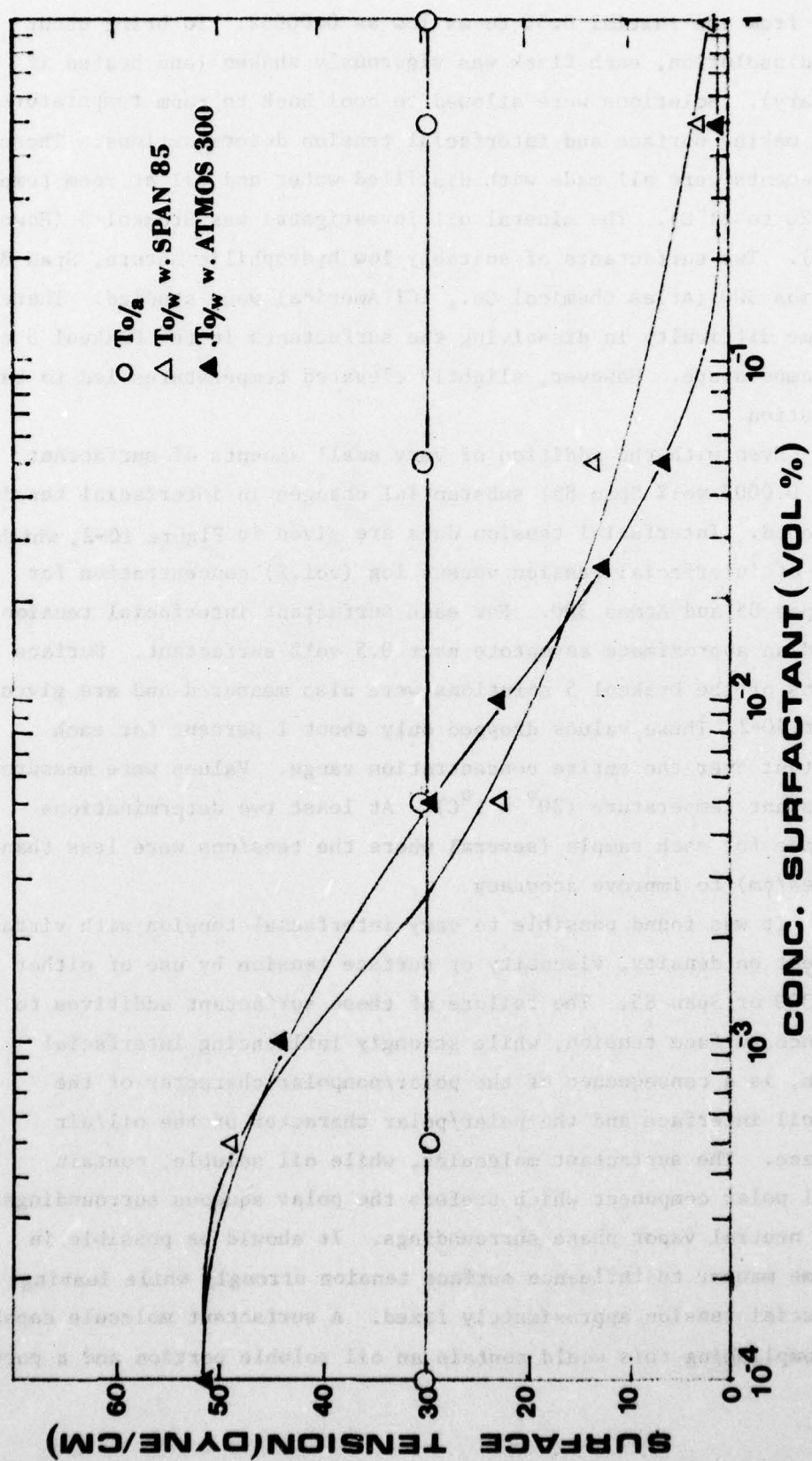
FIGURE 10-2 Surface and Interfacial Tensions of Drakeol 5 Surfactant Solutions

which was soluble in neither oil nor water -- for example, a silicone chain. We did not explore the effects of variation in surface tension alone in these studies.

We conclude from our attempts at synthetic crude oil formulation that the most promising route to determining the influence of the variation of individual physical properties is the selection of various pure natural and mineral oils, rather than mixtures of paraffinic mineral oils and/or mineral oils with density modifying additives. For example, vegetable oils range widely in properties (Weast, 1972) and should be amenable to study. In addition, small-scale tests using very expensive silicone oils may be worth the expense to determine unequivocally the effects of property variation. We do feel that a more exhaustive exploration of the possibility of suspending carbon black particles in mineral oils might be fruitful. Such experiments were beyond the scope of this study, however.

11. CONCLUDING SUMMARY

The conclusions stemming from this work can be divided into two groups: those resulting from our literature survey and theoretical studies, and those resulting from our experimental program. Certainly the most significant influence on the dispersion of oil into submerged droplets is that of breaking waves. Therefore, the ultimate generation of a capability for predicting the dispersion of oil into the sea will require knowledge about the distribution and intensity of breaking waves. It has been observed that the presence of spilled oil alters the distribution of breaking waves. For example, in many circumstances in which a large number of breaking waves in clean water exists, it is observed that hardly any breaking waves exist in oil covered regions. In these cases, the waves seem to enter an oil patch, disperse oil from the edge of the patch, and then stop breaking. It is known that the presence of oil has a wave damping effect, but the relative effects on breaking inhibition by this damping and by the possible reduction in wave generation by the oil are unknown. Observations at sea show that both the oil slick properties and the sea state are important variables related to whether or not waves can break in the interior of an oil slick. When wave breaking is weak, even thin layers of oil (about 0.5 millimeter thick) have been observed to inhibit breaking. In seas having a moderate breaking intensity, breaking has been observed to occur at a reduced rate within thin layers of oil, but breaking is inhibited in the thick layers (about 4 millimeters thick). In very severe breaking seas, breaking has even been observed to occur within thick layers of oil, but with a reduced intensity from that which is observed both in thin layers and in regions devoid of floating oil.

Although ultimate accurate prediction of dispersion rates will require knowledge of the breaking wave distribution within oil layers, it is important to indicate that our knowledge of breaking wave distributions on clean water at sea is inadequate, in spite of the fact that considerable research on the subject has taken place in the past, so our knowledge in this area will have to be augmented. The degree of our lack of knowledge can be demonstrated by an example. An important parameter with respect to breaking waves which must be known in order to be able to achieve a

predictive capability is the probability that a wave will break over some given length. The problem of establishing this probability has been addressed by several investigators, but their estimates for the breaking probability vary widely. For example, the breaking probability obtained from the mathematical model of Longuet-Higgins (1969a) differs from that obtained by Nath and Ramsey (1976) by a factor of about 10,000. Although we recognize that the breaking probability is the parameter with the largest discrepancies between various theories, it is a particularly important parameter for establishing just how many breakers an oil slick will encounter. In addition to inadequate knowledge about wave breaking probabilities, there is also inadequate knowledge about the spatial extent over which each wave breaks, not only in an oil slick, but also in clean water. These facts illustrate that much more information about the intricacies of wave breaking, both with and without oil present, will have to be obtained before an accurate quantitative model for oil dispersion can be generated. Our knowledge about the nature of the turbulence in the near-surface layers of the ocean is just as scanty as our knowledge of breaking waves. It is known that the largest source of turbulence is that of breaking waves when they are present. The only report of an accurate measurement of the turbulence at sea beneath breaking waves which we have found in the literature is that of Stewart and Grant (1962). Complete data was only reported for a single wave condition which had typical wave lengths of 5m and typical wave heights of 0.4m. The closest measurements to the surface presented were those taken at a distance of about two wave heights beneath the surface. In spite of the limited amount of data presented, some interesting and useful results can be derived from it. For example, the Kolmogorov microscale of the turbulence, based on the most intense turbulence,which was measured nearest to the free surface, is 0.08cm. This compares favorably with the typical diameters of oil droplets found in dispersions. Since the microscale is inversely proportional to the 1/4 power of the rate of energy dissipation, smaller microscale lengths would exist nearer the free surface than the positions measured by Stewart and Grant and in more intense breaking waves. This is consistent with the fact that smaller droplets in dispersed oil slicks have also been found (see, e.g., Forrester, 1971).

The initial breakup of oil into small droplets occurs in the near-surface zone so it is useful to obtain some measure of the turbulent velocities in that region. To obtain initial information about these turbulent intensities, we measured them beneath a breaking wave in the same apparatus we used for our experiments on the dispersion of oil by breaking waves. We found that near the surface typical turbulent velocities of about 20 percent of the wave particle velocities existed, but occasionally turbulent velocities as large as the wave particle velocities themselves were observed. Thus, as one might expect, a breaking wave contains particularly intense turbulence and, therefore, can split an oil spill into droplets. It will be necessary to learn the details of the oil droplet splitting process in the future in order to be able to generate an oil spill dispersion model. A reason why the droplet splitting effects are so important is that the rise velocity of an oil droplet depends on its size, smaller droplets rising much more slowly than larger ones, so the size of the droplets affects the mean time that they remain submerged beneath the slick. The breakup of droplets in turbulence has been considered by Kolmogorov (1949) and Hinze (1955) who showed that whether droplet breakup occurs or not depends on whether the pressure forces in the turbulence tending to break the droplet exceed the surface tension forces tending to hold the droplet together. The smallest length scale in the turbulence which could cause droplet breakup is the Kolmogorov microscale. Our theoretical analysis, presented in this report in §3 shows that in oceanic turbulence generated by breaking waves, the surface tension forces holding a droplet the size of this microscale together can often greatly exceed the turbulent pressure forces tending to tear it apart. Therefore, there will be some circumstances where the smallest oil droplets are considerably larger than the microscale length.

Our survey of the literature showed many theoretical derivations related to the rise of small buoyant droplets through a turbulent liquid. None of these were completely applicable to the dispersed oil problem, but they were found to have a common thread which would also be common to a correct and applicable treatment of the problem. This was the assumption that the instantaneous vertical velocity of an oil droplet was equal to the terminal rise velocity of that droplet plus the local vertical turbulent

velocity. Friedlander (1957) showed that this assumption was correct for droplets which were small in comparison to the microscale lengths. However, oil droplets are not always so small and ultimately a model for the dispersion of oil spills will have to consider how instantaneous droplet rise velocities depend on the turbulence. In §4 we presented a justification for using the additive assumption for vertical velocities for oil droplets much larger in diameter than the microscale length. To confirm our analysis and to extend this assumption to even larger droplets, we carried out an experiment in which we compared the measured variance of the rise times of small plastic spheres with the theoretical prediction for this variance using the assumption of additive vertical velocities. Spheres having diameters of 1.6 and 3.2mm were used. Spheres of each size were tested in three different velocity fields. The results, which are shown in Figure 4-3 indicate that the additive assumption is indeed justified. Therefore, when an accurate and appropriate model for the motion of oil droplets in a turbulent velocity field is made, it can be based on instantaneous droplet velocities being equal to the vector sum of the turbulent velocity and the terminal rise velocity.

As described by Shaw (1970) surfactant molecules, some of which are present in many types of oil, adsorb at interfaces. Since interfaces are present both on a floating slick and on oil droplets, the oil composition within the slicks and droplets will not be completely uniform. This lack of uniformity greatly complicates the phenomenon of recoalescence of oil droplets with the slick. The recoalescence time is an important parameter because oil droplets which are against the slick, but not recoalesced with it, can easily be torn away from the slick by weak turbulence; whereas the strong turbulence of a breaking wave is generally required to disperse oil which has recoalesced.

An accurate estimation of droplet recoalescence times based on theoretical grounds has not been possible, principally because of the multicomponent nature of most oils. Therefore, we carried out an experimental program to determine how various oil slick properties affect recoalescence time. In these experiments, an oil drop was allowed to rise to a slick and the time for recoalescence was measured. The independent variables in the experiment

AD-A062 693   COAST GUARD WASHINGTON D C OFFICE OF RESEARCH AND DE--ETC   F/G 11/8
EFFECTS OF OIL SLICK PROPERTIES ON THE DISPERSION OF FLOATING O--ETC(U)
AUG 78   J H MILGRAM, R G DONNELLY

UNCLASSIFIED   USCG-D-64-78   NL

4 OF 4
AD
A082693

END
DATE
FILMED
3-79
DDC

MICROCOPY RESOLUTION TEST CHART

NATIONAL BUREAU OF STANDARDS-1963-A
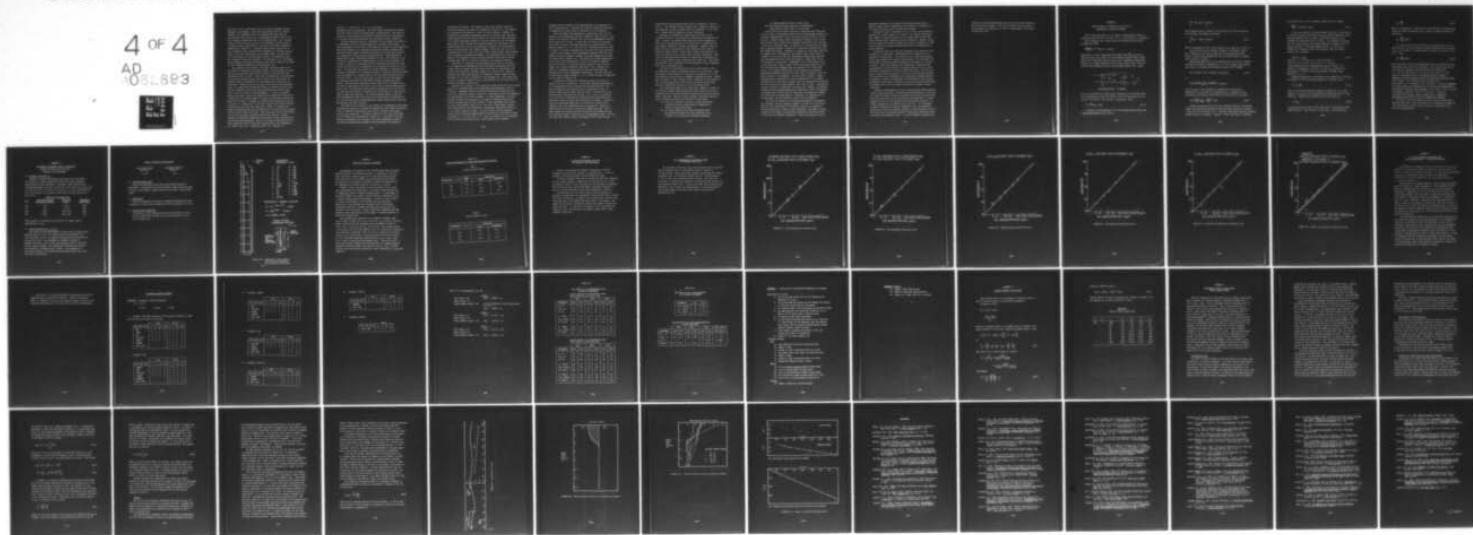
were the oil types, the droplet sizes, the slick thickness, and the atmospheric environment. Since the recoalescence time is a random variable, each experiment had to be repeated many times with the recoalescence time for each set of independent variables taken as the most probable recoalescence time for the distribution. For a certain range of droplet sizes for one oil, the coalescence time was found to be almost exactly proportional to the cube of the droplet diameter as exemplified in Figure 8-2. A general result shown by Figure 8-6 is that coalescence time increases with increasing oil viscosity and this effect can be very significant, as the figure shows. We also found that the thickness of the slick had an effect on recoalescence time, but no general trends were observed. For some types of oil increasing slick thickness increased recoalescence time, and for others an increase in slick thickness decreased the recoalescence time.

The comparative tests shown in the above referenced figures for the effects of viscosity and droplet diameter on recoalescence time were done with a sealed space above the oil slick so that this space was equilibrated with oil vapor. Under these circumstances, the composition of the droplet was more nearly equal to that of the slick except for possible slight differences due to the difference in opportunity for dissolution. When the top of the slick is left open to the atmosphere, there is a compositional difference between the droplets and the slick because evaporation occurs from the slick whereas the droplets came from a closed oil source in our experiments. In order to determine whether the change in the slick composition by evaporation could affect recoalescence, we compared results of tests with open and closed spaces above the oil slick. An example is shown for South Louisiana crude oil in Figure 8-5, showing that for this oil the open slick yields a smaller recoalescence time than the closed slick. There is a driving force toward recoalescence when the concentration of any surface active species differs between droplet and slick. This could occur for the open-topped case for the relatively volatile surface active species. Further evidence of surfactant evaporation was provided by direct observation of the recoalescence phenomenon. When an oil droplet recoalesced with the South Louisiana crude oil slick that had been open to the atmosphere, the region near the coalescence point was observed to

-273-

undergo a reduction in oil thickness
immediately after recoalescence. This thin region persisted for some min-
utes after which the slick thickness again became uniform. This could be
caused by a local increase in surfactant concentration upon recoalescence
if the slick itself had previously lost surfactant through evaporation.

The most extensive series of experiments in this program were those on
the dispersion of oil by breaking waves in a laboratory wave channel. In
these experiments, we were able to determine how varying oil slick properties
affected the amount of oil dispersed by generally similar breaking waves.
The waves varied somewhat in amplitude because of the differing effects of
oil properties on wave growth and breaking details. These experiments
showed that the most influential parameter, by far, on the fraction of the
floating oil dispersed by a breaking wave is the oil slick thickness. As
is shown in Table 5-8, increasing the slick thickness from 0.5mm to 5.5mm
reduced the fraction of oil dispersed by over 96 percent in four out of six
cases. For these cases the actual oil volume dispersed, as measured by an
average of the amount of oil beneath the water at times 2,5,10 and 20 seconds
after the passage of a breaking wave for the thin slick was more than for
the thick slick. In all six cases given in that table the percentage of
oil dispersed was reduced by more than 59 percent by making the slick
thicker. The reduced oil dispersion from a thick slick, as compared to a
thin slick, would appear to be due to one or both of the following reasons.
First of all, the turbulence which initially disperses the oil is that in
the white cap itself, and it is possible that the presence of a thick slick
tends to damp this turbulence. The second possible reason is that the
slick thickness may affect the droplet size distribution, as explained in
§3, with the thick slick yielding generally larger droplets which rise much
more quickly than small droplets.

The effect of oil viscosity on the amount of oil dispersed by the break-
ing waves was isolated by carrying out comparative tests using the same kind
of oil at different temperatures since the oil viscosity varied quite
strongly with temperature. As shown in Table 5-4, for a thin slick when
the oil viscosity was increased by a factor of 7, the amount of oil dis-
persed, as determined by an average of the amount dispersed at each of
the times following breaker passage at which dispersion was measured,

decreased by 80 percent. The results in this table indicate that for a thick slick when the viscosity is increased by a factor of 4, the volume of oil dispersed is decreased by a factor of only 10 percent. However, by examining the individual measurements made at the various times following breaker passage which are given in Table 5-3, we see that large reductions in the amount dispersed occurred for the more viscous oil for the measurements taken 2 and 5 seconds after breaker passage, but the amount of oil dispersed with the cold oil was drastically increased in the measurements made 10 and 20 seconds after breaker passage. These last two data are inconsistent with all of the other data in which viscous effects were measured and are therefore considered unreliable. The conclusion here is that the amount of oil dispersed is quite viscosity-sensitive with less oil being dispersed when the oil is viscous than when it is relatively inviscid.

The effect of variations in interfacial tension alone on the amount of oil dispersed by breaking waves was determined by comparing tests with a thick layer of mineral oil with tests of the same oil containing a surfactant that reduced its oil-water tension by a factor of 10. Table 5-6 indicates that this large decrease in interfacial tension roughly doubles the amount of oil that is dispersed by the breaking wave. Such large variations in interfacial tension are not found naturally but do occur when dispersants are added to spilled oil.

Because of the effects of oil properties on wave growth and wave breaking details, the breaking waves in the experiments described above were not identical. Experiments using an identical dispersing influence were carried out by spilling a sheet of water onto a floating oil slick and measuring the time history of the slick thickness. In these experiments, the water beneath the slick was flowing so as to remove all droplets that did not rise and coalesce with the slick quickly. These experiments were carried out with nine different types of oil. For five of these types, measurements were made with two different oil thicknesses, varying by a factor of 2. For each of these five cases, the rate at which oil was dispersed from the thick slick was slightly smaller than with the thin slick as shown in Figures 7-4, 7-6, and 7-10 to 7-12. Hence the fraction of oil dispersed with the thick slick was much less. These results are in complete

agreement with the results of the measurements of the dispersion of oil by breaking waves. Together they show the significant importance of keeping an oil slick thick if dispersion is to be minimized.

These experiments did demonstrate a significant effect of the severity of the dispersing influence, namely, the sheet of water. For three of the nine oils studied, water flow rate (impingement velocity) was varied by 40% or more. In each case, the effect of increasing water flow rate was to increase dispersion rate substantially, as is shown in Figures 7-4, 7-5, 7-10, and 7-11. Dispersion rate was found to exhibit a "critical" dependence on flow rate, flow rates less than a certain value leading to only negligible dispersion and flow rates greater than that leading to rapidly increasing dispersion, as shown for Arzew crude in Figure 7-14. This effect was further demonstrated in the case of the distillate No. 6 fuel oil in which a moderate flow rate led only to "chocolate mousse" formation and a rate 40% larger led to facile dispersion (see Figure 7-11). Finally, the effect of interfacial tension noted in the wave tank tests was continued in the water impingement experiments, a 10-fold reduction in interfacial tension leading to a 3- to 4-fold increase in dispersion rate, as shown in Figure 7-12.

Our work has provided some information about the effects of aging of the oil on dispersion. The two most important aging effects on the dispersion of oil are evaporation and emulsification. The most thorough work that has been done on evaporation is that of Blokker (1964), and this shows that the lighter fractions of oil are preferentially evaporated more quickly. As a result, the viscosity of an oil slick is increased by evaporation, and we have shown that dispersion rates are reduced when viscosity is increased. Figure 9-1 shows the percentage weight loss as a function of time for four different oils in an evaporation test we carried out. Figure 9-2 shows how the viscosities of these oils changed with time. Only a small weight loss occurred with the distillate and residual oil and the fractional change in viscosity was correspondingly small. For the two crude oils tested, however, approximately 15% of the oils was

-276-

evaporated, and the viscosities were found to increase by a factor of
about 5. The breaking wave tests showed that a change in viscosity of
this magnitude can have a marked effect on dispersion. In the tests
such a change reduced dispersion by about 80 percent.

Obviously the evaporation conditions for our test did not
correspond exactly to the evaporation conditions in any specific oil
spill. However, the general effect has been clearly demonstrated.
We do note in particular that in an actual spill a distillate oil
will undergo evaporation in many circumstances. However, since the
major fraction of the material in most distillate oils involves
molecular weights within a fairly narrow range, the evaporation of
these oils will have only a small effect on their viscosities. Thus,
it can be concluded that the effect of evaporation on dispersion of
the oil that remains is most influential for crude oils. This effect
was observed in our experiments on the dispersion of oil by breaking
waves and is explained in §5.

The effect of emulsification on the oil slick itself is the
incorporation of water, and possibly some air, into the slick. When
the amount of water present is a fraction of the amount of oil, the
slick generally acts like one of somewhat increased viscosity. However,
when the amount of water becomes large in comparison to the amount of
oil, the resulting material often called "chocolate mousse" has a
semi-solid consistency and does not act like liquid at all.

Our existing knowledge is not sufficiently complete to permit us
to be able to predict quantitatively the rate at which oil would be
dispersed from a slick with arbitrary properties by arbitrary environ-
mental conditions. However, we have learned a substantial amount of
useful information which can be divided into three areas:

    (1) We are in a position to be able to make qualitative
        estimates about the relative ease of dispersion of
        slicks of various properties;

    (2) The salient physical and chemical phenomena about
        the dispersion process have been identified and as
        a result we can evaluate the potential usefulness

of further studies in each of these areas;

(3) Our findings indicate important countermeasures
which should be taken after oil is spilled.

Thick slicks are far more resistant to dispersion than thin ones.
A direct result of the present study is that the dispersing influence of
a specific breaking wave on the thick slick is smaller than it is on a
thin one. Another result, which is explained in detail in §5, is that
thick slicks tend to inhibit wave breaking, especially if the viscosity
of the oil is relatively high. In addition, it is known that oil layers
have a damping influence on waves and it seems quite possible that they
may inhibit wave growth. Therefore, in addition to the direct reduction
in dispersion by a breaking wave that results from a thick slick as
compared to a thin one, there is considerable evidence that indicates
that the probability that a wave will break in a thick layer of oil
is less than in a thin layer. Furthermore, for a fixed volume of oil,
a thin slick will occupy a larger surface area than a thick one so it
will encounter more breaking waves just because of its larger area
alone. All of these effects point to the necessity of preventing
spreading and keeping a spilled oil layer thick if dispersion into the
water column is to be minimized. The only effect tending to reduce
dispersion from a thin slick is that the evaporation of the lighter
fractions from a thin slick is greater than the corresponding evaporation
from the thick one and tests indicate that crude oil aged by evaporation
is more resistant to dispersion than other oils. However, the physical
effects of slick thickness dominate the evaporative effect on dispersion
so strongly that the fact that the dispersion is minimized by keeping
the slick thick is unquestionable. Conversely, if dispersion is to
be encouraged, the slick should be made as thin as possible.

As far as the effects of oil properties themselves on dispersion
are concerned, the most important appears to be that of oil viscosity.
With all other properties held relatively constant, an increase in
viscosity was found to result in less dispersion. The effect is quite
strong over the range of viscosities encountered in the various kinds
of oils that are commonly transported. Since the viscosity is quite

temperature dependent, the results of this study indicate that a
specific product may be considerably more resistant to dispersion in
relatively cold water than in relatively warm water.

Although the ease of dispersion of an oil slick is increased by a
decrease in oil-water tension, the range of the tensions encountered
with commonly transported products is not large enough to make this
effect important when considering natural dispersion. However, disper-
sants can lower the oil-water tension by an order of magnitude or more,
so this effect is certainly important when the use of dispersants is
being considered.

The work we have done shows the importance of the details of wave
breaking on oil dispersion. Whitecaps initially disperse oil into
globules of various sizes. The turbulence in or under the whitecaps
splits these globules into smaller size droplets. The turbulence left
behind when a breaker has passed disperses the droplets to a variety
of depths. These facts indicate the importance of making detailed
measurements of the distribution of breaking waves at sea and of the
turbulence intensities in the water beneath the waves. We still have
much to learn about the details of the flow in the turbulence beneath
waves and much of this knowledge can be supplied by further laboratory
experiments. However, the magnitude of the turbulence itself should
be measured at sea, both to confirm any theoretical results which might
be obtained and to aid in scaling up laboratory findings to oceanic
conditions.

Similarly, measurements of actual oil dispersions beneath breaking
waves at sea must be made. The only reported measurements of this type
are those of Forrester (1971), who measured some droplet size distribu-
tions many days after the oil was initially dispersed, and it is quite
possible that the oil he found had been treated with dispersant. No
chemical analysis of the droplets was carried out. It is necessary
to measure dispersions during and immediately after the dispersing
process and to carry out chemical analyses on these droplets as well as
the parent slick to determine possible compositional differences which
could affect recoalescence times. It is both somewhat surprising and

unfortunate that such measurements have not been made even though oil
spills at sea are frequent. Since this frequency does not appear to
be decreasing, the opportunity to make the measurements still exists
and should be used.

APPENDIX 1

ENERGY BALANCE FOR BREAKING WAVES WITHIN AN
EXPONENTIALLY CONVERGING CHANNEL

The following derivation is the result of applying the results of
a previous study (Van Dorn and Pazan, 1975) to an exponential convergence.

For the general case, energy balance for surface waves is given
by (Phillips, 1969),

$$\frac{\partial E(x,t)}{\partial t} + \vec{\nabla} \cdot \vec{F}(x,y,t) = Q(x,t)$$

where $E(x,t)$ is total energy per unit surface area, $\vec{F}(x,y,t)$ is the
energy flux per crest length, $\vec{\nabla}$ is the gradient operator $\hat{i}\partial/\partial x + \hat{j}\partial/\partial y$
with $\hat{i}$ and $\hat{j}$ being unit vectors in the x and y directions respectively,
and $Q(x,t)$ is energy dissipation rate per unit surface area. The unit
surface areas referred to are in the horizontal plane, or dA = dxdy.
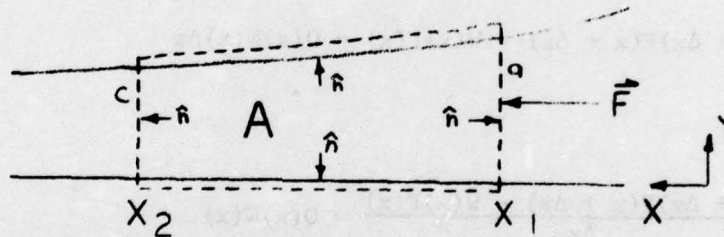
HORIZONTAL PLANE

In the oil dispersion by breaking wave experiments, the frequency band
of the breaking wave group was narrow so that time dependence near the
center of the group is weak and may be neglected. Then,

$$\vec{\nabla} \cdot \vec{F}(x,y) = Q(x) \qquad (A1.1)$$

Letting p be the perimeter of A for the control surface shown and
integrating Equation (A1.1) over A,

-281-

$$\int_A \vec{\nabla} \cdot \vec{F}(x,y)\,dA = \int_A Q(x)\,dA$$

Then, applying Green's theorem to the left side of the above equation, the following relationship is obtained:

$$\int_p \vec{F}(x,y) \cdot \hat{n}\,dp = \int_A Q(x)\,dA \qquad (A1.2)$$

where $\hat{n}$ represents the unit vectors normal to the sides of the region A.

Because energy flow is primarily parallel to the channel walls, the y component of the flux is small and may be neglected so that $\vec{F}(x,y) \simeq F_x(x,y)\hat{i}$, and assuming the flux is uniform across the channel width, $F_x(x,y)\hat{i} = F_x(x)\hat{i}$.

Applying Equation (A1.2) to an elemental slice so that $dA = W(x)dx$ and where the range of integration $x_2 - x_1 = \Delta x$ is small, while noting that there is no energy flux through the channel walls produces

$$W(x + \Delta x)F(x + \Delta x) - W(x)F(x) = Q(x)W(x)\Delta x \qquad (A1.3)$$

or

$$\frac{W(x + \Delta x)F(x + \Delta x) - W(x)F(x)}{\Delta x} = Q(x)W(x)$$

The left side of this equation is recognized as the derivative $\partial W(x)F(x)/\partial x$ in the limit as Δx approaches zero. Expansion of the derivative, and division of both sides of the equation by W, yields:

$$F(x)\,\frac{\partial W(x)}{\partial x}\,\frac{1}{W(x)} + \frac{\partial F(x)}{\partial x} = Q(x) \qquad (A1.4)$$

Energy dissipation may occur due to breaking, viscous or reflective losses, yet viscous and reflective losses are small relative to breaking losses (Van Dorn and Pazan, 1975). Therefore, $Q(x) \simeq Q_b(x)$ where Q_b represents energy loss due to breaking. Letting $G = \partial W/\partial x\; 1/W$, where G is defined

-282-

as the growth rate of the convergence, Equation (A1.4) becomes:

$$\frac{\partial F(x)}{\partial x} + F(x)G(x) = Q_b(x) \tag{A1.5}$$

It has been observed in previous studies (Van Dorn, 1975) that in a converging channel, wave height decreases slightly immediately after breaking commences and then remains essentially constant as the breaking wave progresses down the channel. This phenomenon indicates that the energy flux must also remain essentially constant after the initial decrease in flux when breaking starts. If, then, it is assumed that F remains constant over distance along the channel, Equation (A1.5) becomes:

$$F(x)G(x) = Q_b(x) \tag{A1.6}$$

Therefore, if the growth rate of the convergence is negative and is constant with respect to x, then the energy dissipated in wave breaking must also be constant. An exponential convergence, where $W(x) = B \exp(-Cx)$, satisfies this requirement if B and C are any real positive constants, since $\partial W(x)/\partial x \ 1/W = -C$.

Energy dissipated due to breaking may be estimated by calculating the energy flux from the energy equation for a periodic wave,

$$E = \frac{1}{2} \rho_w g A^2 \tag{A1.7}$$

where E is the wave energy per horizontal surface area, ρ_w is the density of the water, g is gravitational acceleration, and A is wave amplitude. Energy flux per surface area is then given by

$$F = EC_g \tag{A1.8}$$

C_g being the group velocity of the waves which is the speed at which energy travels. Group velocity for deep water waves is given by:

-283-

$$C_g = \frac{gT}{4\pi} \tag{A1.9}$$

where T is wave period. Combination of Equations (A1.6) through (A1.9) yields the energy dissipation rate in terms of parameters measured in this study,

$$Q_b = \frac{\rho_w T}{8\pi} (gA)^2 G$$

All energy terms in this derivation are average values per unit time and area. The total amount of energy dissipated per unit surface area by the passage of a single breaker is given by the product of Q_b and T. Thus,

$$DE = \frac{\rho_w G}{8\pi} (gTA)^2 \tag{A1.10}$$

gives the energy lost due to breaking, where DE is the energy lost per unit surface area within the observation. The parameters present in this study for standard conditions without an oil slick were G = -.299 1/m (.091 1/ft), A = 6.4 cm (2.5 in), and T = 1.0 sec, where G is determined from the convergence geometry equation (Appendix 2) and wave characteristics are taken from capacitance wave probe records. The resulting energy loss DE based on these values is 4.7 joules/m^2 or 0.33 ft-lb/ft^2. It must be remembered that these results are approximate due to theoretical assumptions and experimental tolerances, which together could cause DE to vary from its true absolute value by a factor of as much as 2. The valve calculated does, however, supply a useful order of magnitude approximation with which to view the breaking wave process.

As shown in §5.4, thick slicks of viscous oils had higher waves than did clean water. Thus the energy loss in breaking was larger for the thick slicks of viscous oils by a factor of the square of the ratio of wave amplitudes.

-284-

APPENDIX 2

MEASUREMENT INSTRUMENT AND WAVE GENERATION
APPARATUS SPECIFICATIONS FOR THE
BREAKING WAVE EXPERIMENTS

(1) Kinematic Viscosity (ν)

Kinematic viscosity measurements were carried out according to
the procedures of ASTM standards D445 and D2515, using calibrated
Cannon-Fenske Routine Viscometers. Viscometer sizes used and their
corresponding ranges are given in Table A2-1 below. The exact centistokes/
sec constant from the calibration certificate of a given instrument was
used for experimental measurements rather than the approximate value
shown below.

TABLE A2-1 Viscometer Data

SIZE	CENTISTOKES/SECOND APPROXIMATE CONSTANT	CENTISTOKES RANGE	PRECISION* (CENTISTOKES)
100	.015	3 to 15	.008
150	.035	7 to 35	.018
200	0.100	20 to 100	.050
300	0.250	50 to 250	.125

*This precision is dictated by the accuracy of timing, which is
approximately 0.5 sec.

(2) Surface Tension (T_{oa}, T_{ow}, T_{wa})

All surface tension measurements were made using a Fisher Surface
Tensiomat Model 21. This is a torsion balance which measures the
force required to pull a 6 centimeter platinum-iridium ring free from
a given test fluid. The instrument is equipped for manual or
automatic operation, both of which were generally used in this study
with the results averaged. All operational procedures were carried
out according to the manufacturer's manual. Dial readings, as
corrected according to the manufacturer's specifications, were used
for surface tension data.

SURFACE TENSIOMAT SPECIFICATIONS

Operational Range (dynes/cm)	Estimated Tolerance (dynes/cm)
0 to 90	.05

(3) Specific Gravity (SG)

Glass float hydrometers were used to make specific gravity measurements. Hydrometers with three different range scales were used to cover a total range of specific gravity from .700 to 1.000, within ±.0005.

(4) Temperature

Mercury thermometers calibrated for degrees Centigrade were used to measure all liquid and air temperatures with an accuracy of ±0.2 °C.

(5) Wave Generation Apparatus

A description of the wave generation apparatus appears in §5.2. Detailed dimensional information about the apparatus is given here in Figure A2-1.

-286-

PADDLE
AXIS

CONVERGENCE
DIMENSIONS (inches)

A	4 1/2	M	1 3/4
B	24	N	3 3/4
C	24	O	5 1/8
D	19	P	6 1/8
E	24	Q	7 1/8
F	26	U	8
G	28 1/2	R	8 11/16
H	26 1/2	S	9 1/4
I	24	T	9 3/8
J	22	U	9 15/16
K	32	V	10 5/8
L	30 9/16		

CONVERGENCE GEOMETRY EQUATION

$$W = 12e^{-7.58 \times 10^{-3}X} \quad (inches)$$

$$W = .305e^{-.299X} \quad (meters)$$

$$W = CHANNEL\ WIDTH$$

PADDLE STROKE
(DIMENSIONS IN INCHES)

← +X

WATER
SURFACE

INITIAL
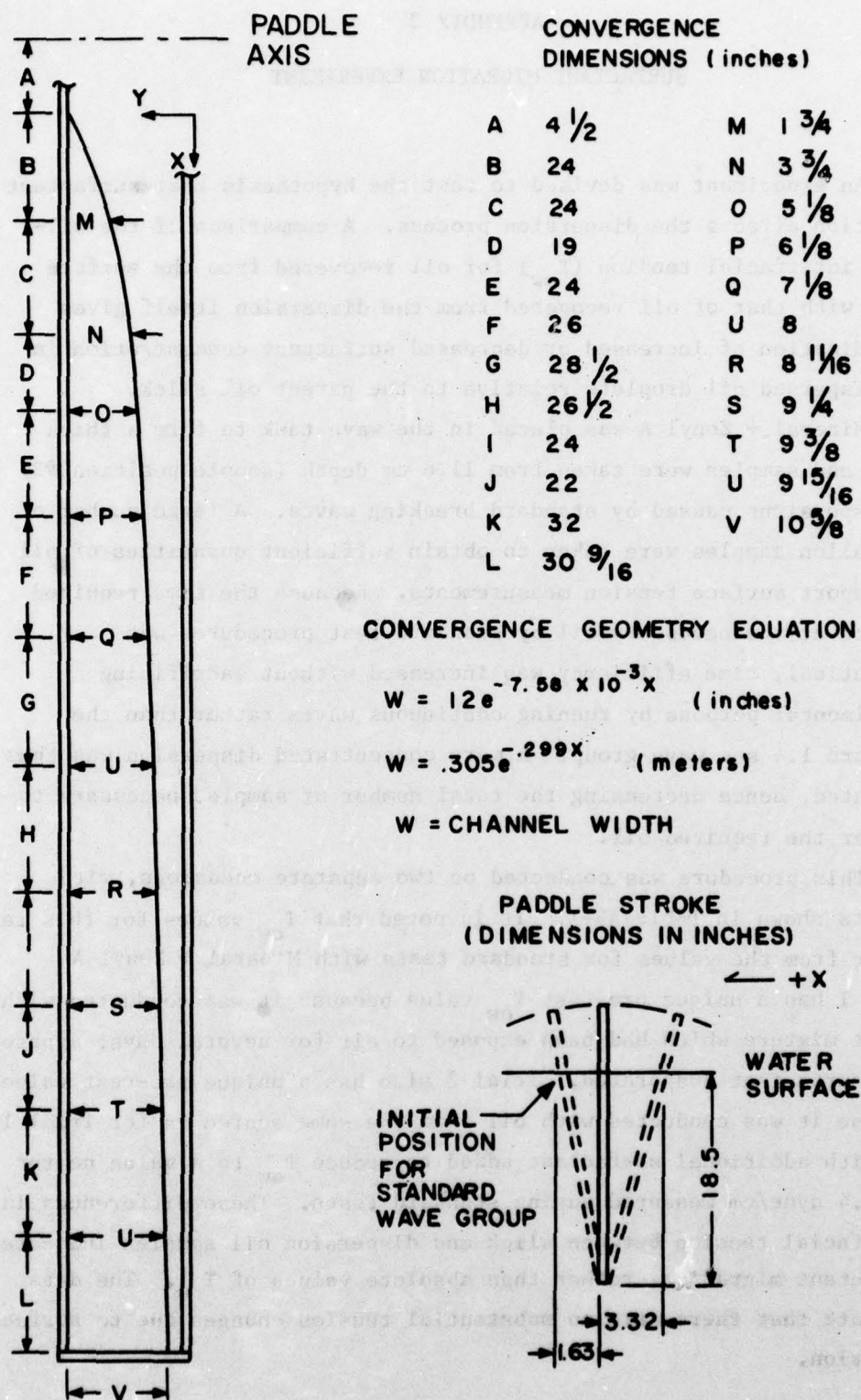POSITION
FOR
STANDARD
WAVE GROUP

18.5

3.32

1.63

FIGURE A2-1 Dimensions of Wave Channel,
Wave Generation Apparatus
and Horizontal Contractions.

-287-

APPENDIX 3

SURFACTANT MIGRATION EXPERIMENT

An experiment was devised to test the hypothesis that surfactant migration affects the dispersion process. A comparison of the oil-water interfacial tension (T_{ow}) for oil recovered from the surface slick with that of oil recovered from the dispersion itself gives an indication of increased or decreased surfactant concentration in the dispersed oil droplets relative to the parent oil slick.

Mineral + Zonyl A was placed in the wave tank to form a thick slick and samples were taken from 11.6 cm depth (sample position #2) of dispersions caused by standard breaking waves. A large number of one gallon samples were taken to obtain sufficient quantities of oil to support surface tension measurements. Because the time required to recover the necessary oil by standard test procedures was impractical, time efficiency was increased without sacrificing experimental purpose by running continuous waves rather than the standard 1.4 sec wave group. A more concentrated dispersion was thus generated, hence decreasing the total number of samples necessary to recover the required oil.

This procedure was conducted on two separate occasions, with results shown in Table A3-1. It is noted that T_{ow} values for this test differ from the values for standard tests with Mineral + Zonyl A. Trial 1 has a unique pre-test T_{ow} value because it was conducted with a test mixture which had been exposed to air for several days; apparently some surfactant evaporated. Trial 2 also has a unique pre-test value because it was conducted with oil from the same source as for Trial 1, but with additional surfactant added to reduce T_{ow} to a value nearer the 1.4 dyne/cm measured during standard tests. These differences in interfacial tension between slick and dispersion oil samples indicate surfactant migration, rather than absolute values of T_{ow}. The data indicate that there were no substantial tension changes due to surfactant migration.

TABLE A3-1

Tension Measurements in Surfactant Migration Experiment

TRIAL 1

Surface Tensions (d/cm)

TEMPERATURE = 21.0°C	BEFORE TEST	AFTER TEST	
		SLICK	DISPERSION
T_{wa}	67.8	67.9	68.4
T_{ow}	9.2	8.23	8.00
T_{oa}	33.8	34.0	34.5

TRIAL 2

Surface Tensions (d/cm)

TEMPERATURE = 24.5°C	AFTER TEST	
	SLICK	DISPERSION
T_{wa}	67.0	65.5
T_{ow}	5.4	4.6
T_{oa}	33.8	34.9

APPENDIX 4

AIR/WATER ENTRAINMENT TEST FOR
THE BREAKING WAVE EXPERIMENTS

Several oils exhibited an apparent entrainment of bubbles
throughout the slick after exposure to breaking waves. It was not
possible to discern the nature of these bubbles by sight.

In order to evaluate the fraction of aged oil which was comprised
of air or water bubbles, a simple test was carried out on oil from
the Mineral + Zonyl A slick, following the test described in Appendix 3.
This oil had the most concentrated bubble entrainment observed for
any oil, and thus provided a large bubble sampling for analysis.

Ten milliliters of oil from the aged slick were placed in a
graduated cylinder which was subsequently evacuated and held at vacuum
for about five minutes. No change in the liquid volume occurred, thus
indicating that no air bubbles had been present in the sample. The
sample was returned to atmospheric pressure and allowed to settle for
twenty-six hours. At the end of this period, the oil and water had
separated, and it was found that the sample of aged slick oil was
composed of 36% water.

APPENDIX 5

OIL CONCENTRATION CALIBRATION CURVES
FOR BREAKING WAVE TESTS

The following curves were taken from calibration plots that were used to determine the oil concentration found in samples of oil dispersions. These curves were prepared by plotting the infrared absorbance level of calibration samples with oil concentrations of 5, 20, 50, 200, 500, and 5000 parts per million. The curves are presented to illustrate the departure of calibration data points from the expected straight line. It may be seen that these departures are significant only at small oil concentrations, with the exception of the 200 ppm sample for #2 diesel fuel which is attributed to experimental error.

FIGURE A5-1   Arzew Absorbance Calibration Curve

⊙ CCL$_4$ SOLVENT WITH UNFILTERED H$_2$O
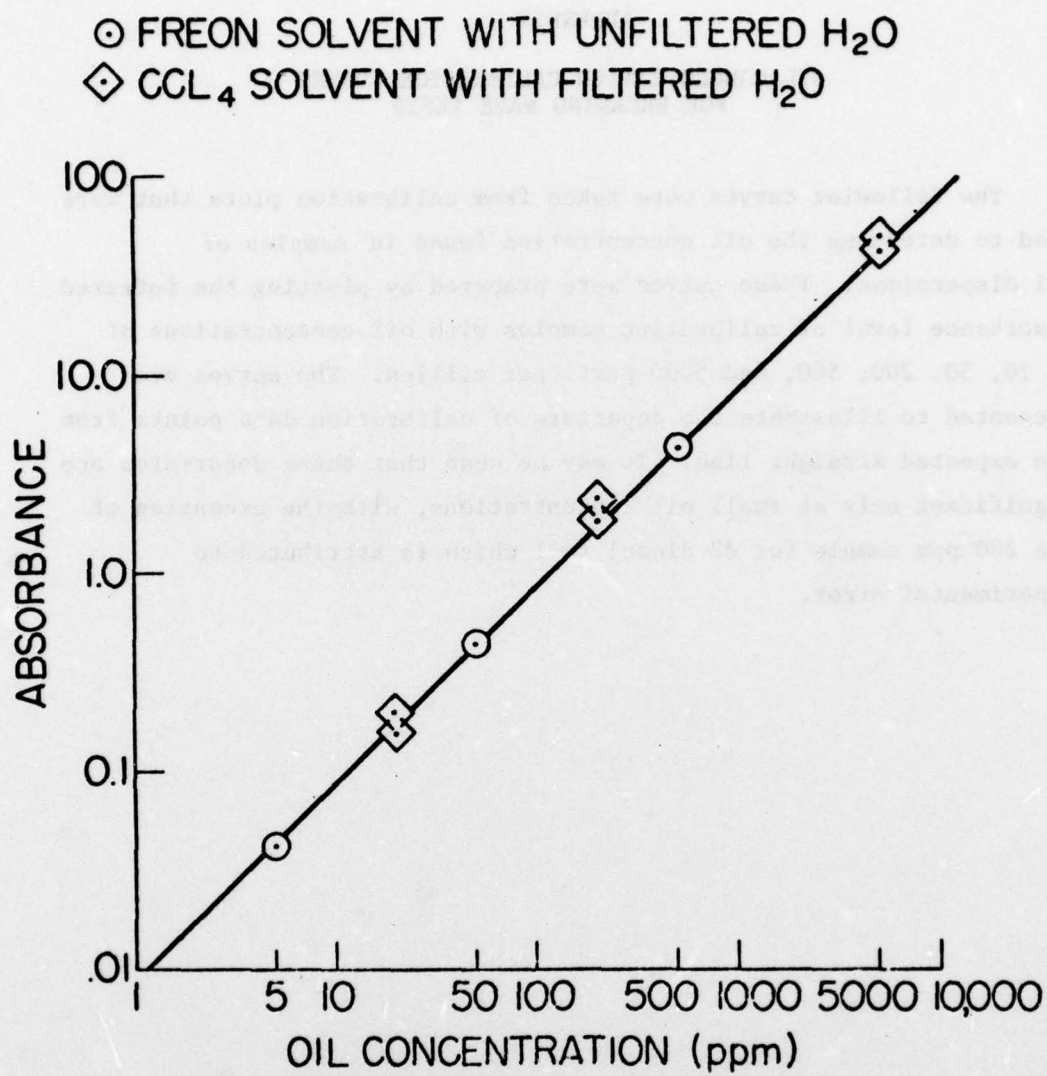◇ CCL$_4$ SOLVENT WITH FILTERED H$_2$O
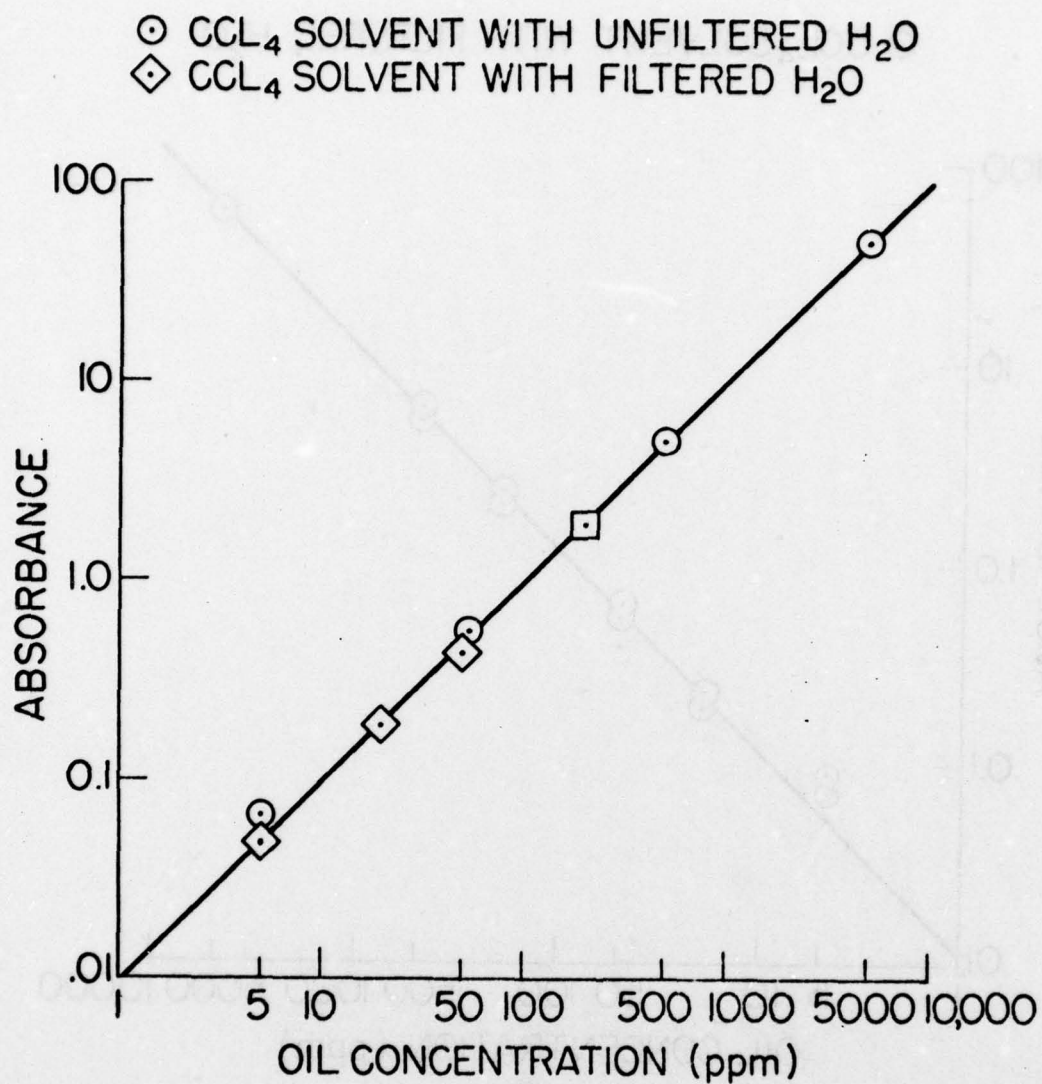
FIGURE A5-2 ABL Absorbance Calibration Curve
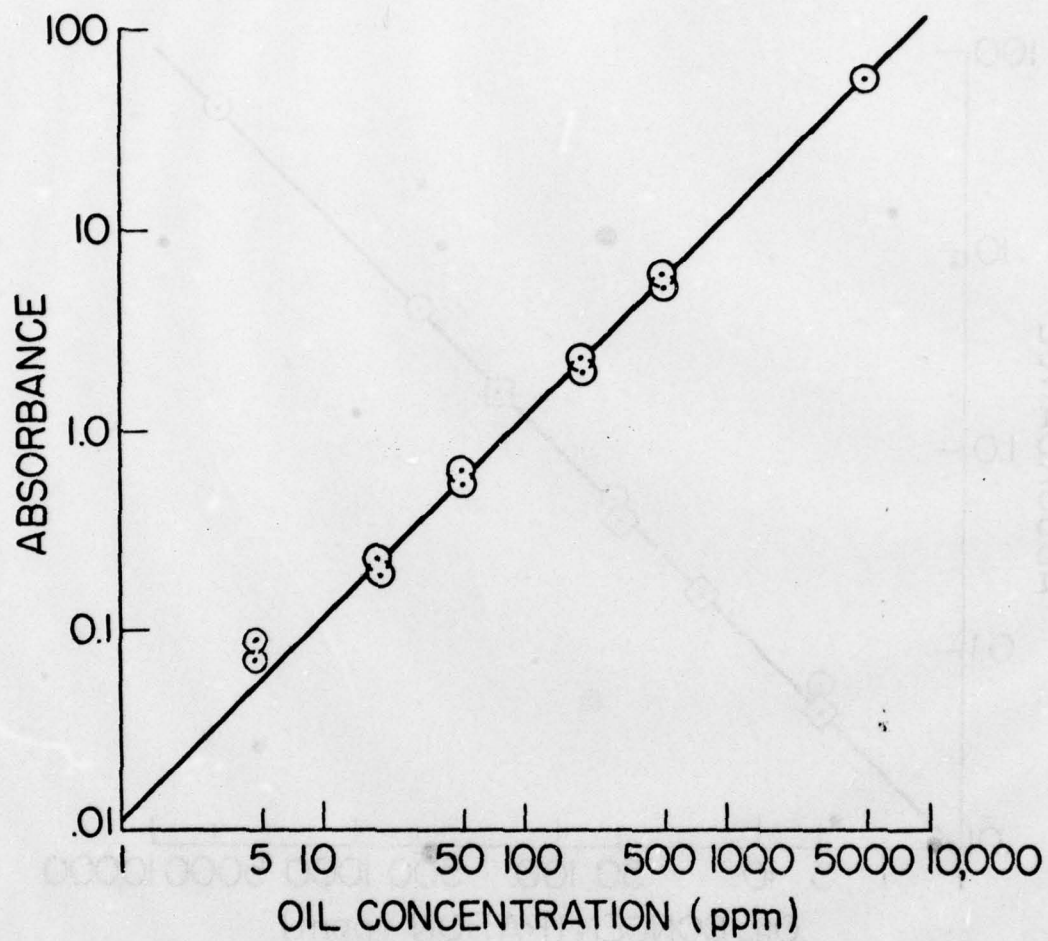
FIGURE A5-3 THUMS Absorbance Calibration Curve

⊙ CCL$_4$ SOLVENT WITH FILTERED H$_2$O
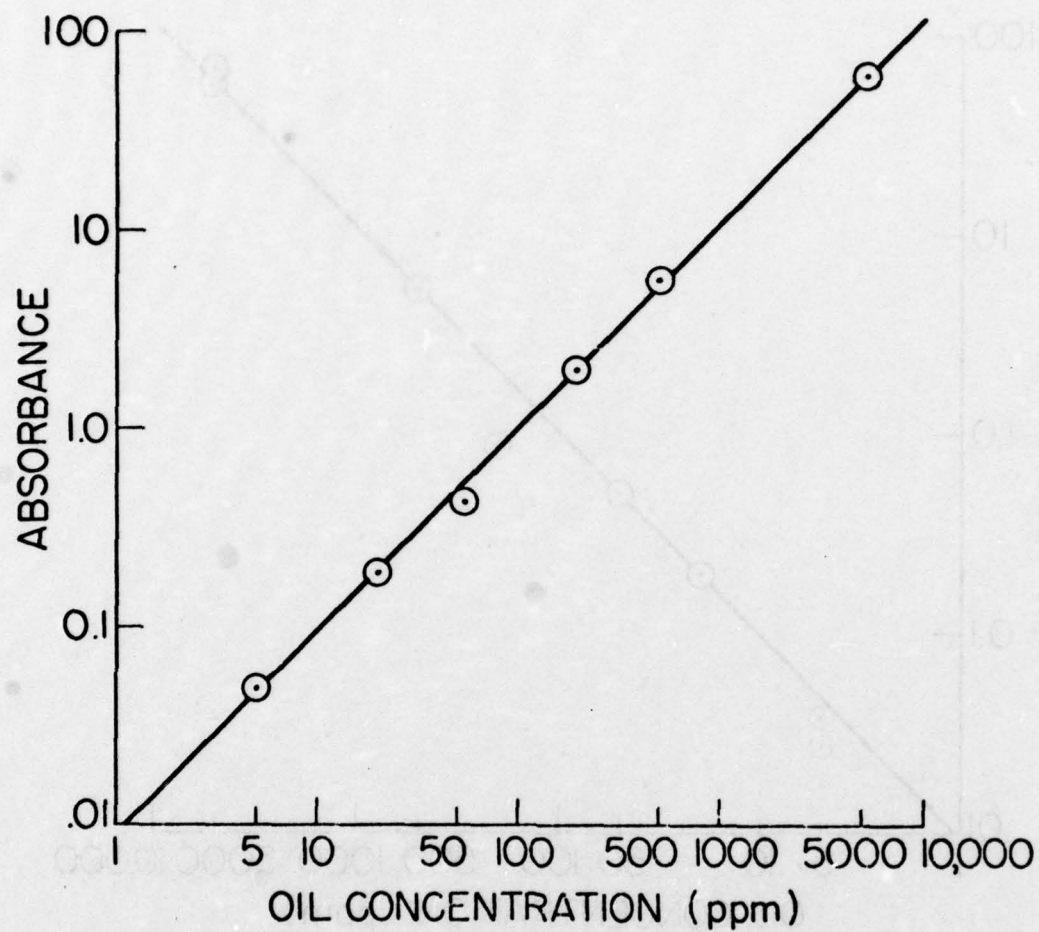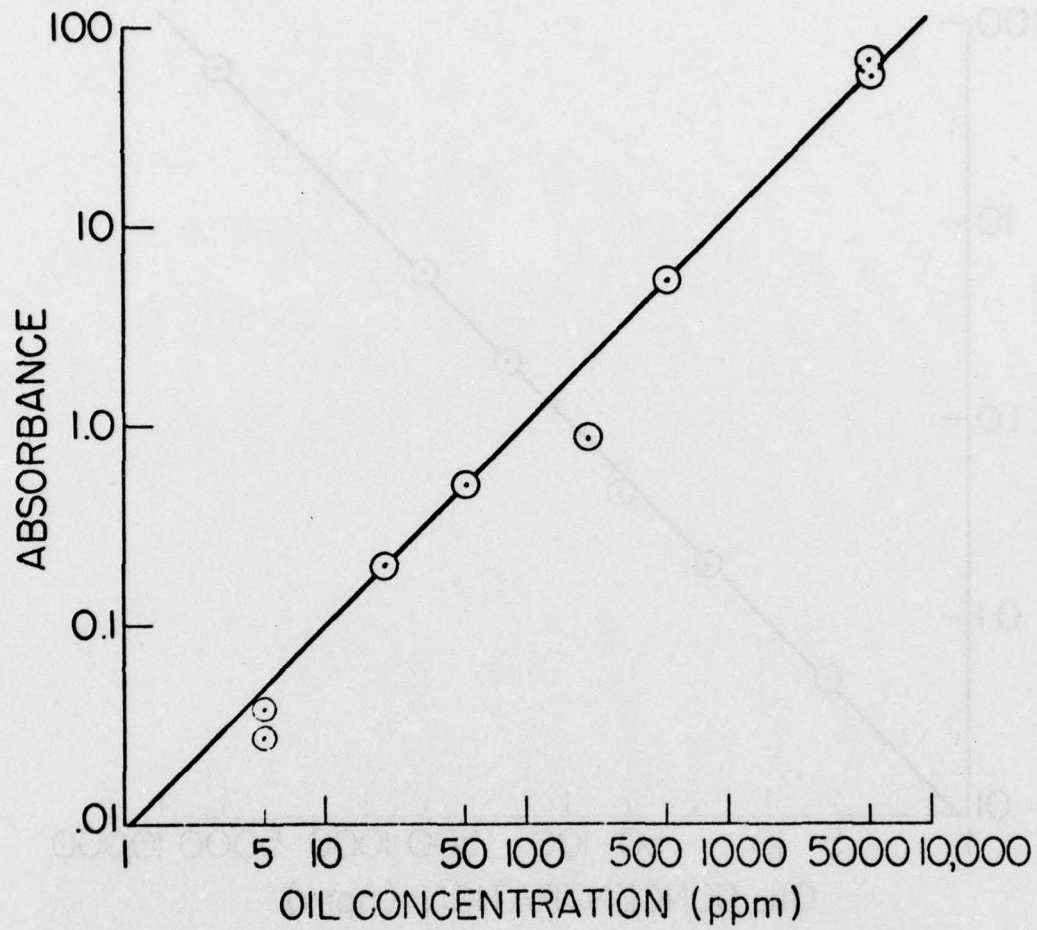
FIGURE A5-4   ZUE Absorbance Calibration Curve

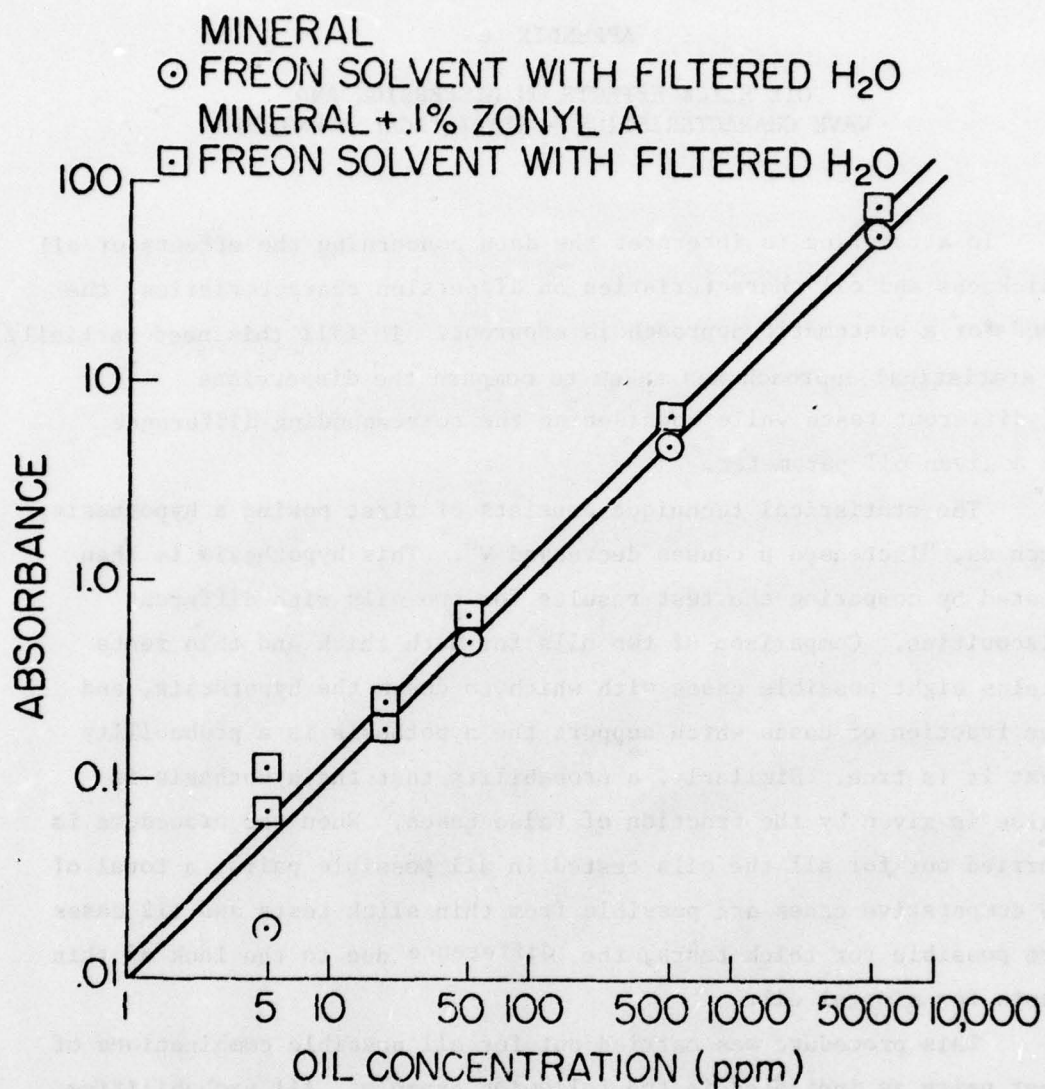FIGURE A5-5   #2 Diesel Fuel Absorbance Calibration Curve

FIGURE A5-6 Mineral Oil Absorbance Calibration Curves

APPENDIX 6

OIL SLICK EFFECTS ON DISPERSION AND
WAVE CHARACTERISTICS – STATISTICAL APPROACH

In attempting to interpret the data concerning the effects of oil thickness and oil characteristics on dispersion characteristics, the need for a systematic approach is apparent. To fill this need partially, a statistical approach was taken to compare the dispersions of different tests while considering the corresponding difference in a given oil parameter.

The statistical technique consists of first posing a hypothesis, such as, "Increased μ causes decreased Ψ". This hypothesis is then tested by comparing the test results for two oils with different viscosities. Comparison of two oils for both thick and thin tests yields eight possible cases with which to check the hypothesis, and the fraction of cases which support the hypothesis is a probability that it is true. Similarly, a probability that the hypothesis is false is given by the fraction of false cases. When the procedure is carried out for all the oils tested in all possible pairs, a total of 60 comparative cases are possible from thin slick tests and 112 cases are possible for thick tests, the difference due to the lack of thin tests for mineral oil.

This procedure was carried out for all possible combinations of test pairs as indicated in the following example. All probabilities listed for the effects of other oil parameters on Ψ and on other dispersion characteristics were calculated using the same technique. In addition, the effects of oil parameters were examined by this method based on measurements made both before and after the oil was exposed to breaking waves in order to observe aging effects. It must be remembered that the probabilities generated by this procedure ignore all effects due to characteristics other than the one stated in the hypothesis, hence these results only indicate the effect of a particular parameter if it outweighs all others.

The effects of oil characteristics on wave amplitude were also examined using the statistical technique. However, the limited number of comparative cases for this analysis reduces accuracy of the resulting probabilities so much that their validity is questionable.

HYPOTHESIS: Increased μ causes decreased ¥

    or: ↑μ, ↓¥

      T: True   F: False   S: Same

1.   Standard = ARZ (ARZ viscosity, and ¥ values are compared to other oils for each test shown in the table).

Test Time (sec)	Thin				Thick			
	2	5	10	20	2	5	10	20
ABL	T	F	F	F	T	F	T	S
THUMS	T	T	T	T	F	F	F	F
ZUE	T	T	F	F	T	T	T	S
COLD ZUE	T	T	T	T	T	T	F	F
DIESEL	T	T	F	F	T	T	F	F
MINERAL					T	T	F	F
MIN + ZON					T	F	T	F

2.   Standard = ABL

Test Time (sec)	Thin				Thick			
	2	5	10	20	2	5	10	20
THUMS	F	T	T	T	F	F	F	F
ZUE	T	F	F	T	F	F	S	S
COLD ZUE	T	T	T	T	T	T	F	F
DIESEL	F	F	F	F	F	F	T	T
MINERAL					T	T	F	F
MIN + ZON					F	T	T	F

3. Standard = THUMS

Test Time (sec)	Thin				Thick			
	2	5	10	20	2	5	10	20
ZUE	T	T	T	T	F	F	F	F
COLD ZUE	F	F	T	F	F	F	F	T
DIESEL	F	S	T	T	F	F	F	F
MINERAL					F	F	F	F
MIN + ZON					T	T	T	T

4. Standard = Zue

Test Time (sec)	Thin				Thick			
	2	5	10	20	2	5	10	20
COLD ZUE	T	T	T	T	T	T	F	F
DIESEL	F	F	T	F	T	F	T	T
MINERAL					F	T	F	F
MIN + ZON					F	F	T	F

5. Standard = Cold Zue

Test Time (sec)	Thin				Thick			
	2	5	10	20	2	5	10	20
DIESEL	T	T	T	T	T	T	T	F
MINERAL					F	T	F	T
MIN + ZON					F	F	T	T

6. Standard = Diesel

	Thin				Thick			
Test Time (sec)	2	5	10	20	2	5	10	20
MINERAL					F	T	F	T
MIN + ZON					F	F	T	F

7. Standard = Mineral

	Thick			
Test Time (sec)	2	5	10	20
MIN + ZON	F	F	T	F

Results for the Hypothesis: ↑μ, ↓∀

Thin

True values = 39 $P[T]$ = 39/60 = .65

False values = 20

Total possible values = 60   ($P[T]$= "Probability that the hypothesis is true")

                                $P[F]$ = 20/60 = .33

Thick

True values = 44 $P[T]$ = 44/112 = .39

False values = 64

Total possible values = 112 $P[F]$ = 64/112 = .57

Total

True values = 83 $P[T]$ = 83/172 = .48

False values = 84

Total possible values = 172 $P[F]$ = 84/172 = .49

-303-

THE EFFECT OF OIL CHARACTERISTICS ON DISPERSION PARAMETERS

Results Based on Oil Measurements made Before Exposure in the Wave Tank

HYPOTHESIS	Thin		Thick		Total	
	P[T]	P[F]	P[T]	P[F]	P[T]	P[F]
$\uparrow\mu$, $\uparrow\mathcal{V}$	.33	.65	.57	.39	.49	.48
$\uparrow T_{ow}$, $\uparrow\mathcal{V}$	.63	.35	.57	.43	.59	.40
$\uparrow\Delta$, $\uparrow\mathcal{V}$	.58	.42	.41	.56	.47	.51
$\uparrow\mu$, $\uparrow$AVG $\mathcal{Z}$	.37	.63	.56	.44	.49	.51
$\uparrow T_{ow}$, $\uparrow$AVG $\mathcal{Z}$	.67	.33	.51	.49	.57	.43
$\uparrow\Delta$, $\uparrow$AVG $\mathcal{Z}$	.63	.37	.43	.57	.50	.50
$\uparrow\mu$, $\uparrow$MAX $\mathcal{Z}$	.18	.65	.69	.28	.51	.41
$\uparrow T_{ow}$, $\uparrow$MAX $\mathcal{Z}$	.50	.35	.52	.46	.51	.42
$\uparrow\Delta$, $\uparrow$MAX $\mathcal{Z}$	.57	.27	.51	.44	.53	.38

Results Based on Oil Measurements made After Exposure in the Wave Tank

HYPOTHESIS	Thin		Thick		Total	
	P[T]	P[F]	P[T]	P[F]	P[T]	P[F]
$\uparrow\mu$, $\uparrow\mathcal{V}$	.32	.68	.54	.37	.52	.46
$\uparrow T_{ow}$, $\uparrow\mathcal{V}$	.43	.57	.57	.43	.52	.48
$\uparrow\Delta$, $\uparrow\mathcal{V}$	.55	.45	.40	.56	.46	.52
$\uparrow\mu$, $\uparrow$AVG $\mathcal{Z}$	.46	.54	.56	.44	.53	.47
$\uparrow T_{ow}$, $\uparrow$AVG $\mathcal{Z}$	.57	.43	.44	.56	.48	.52
$\uparrow\Delta$, $\uparrow$AVG $\mathcal{Z}$	.53	.47	.44	.56	.48	.52
$\uparrow\mu$, $\uparrow$MAX $\mathcal{Z}$	.21	.58	.71	.26	.56	.48
$\uparrow T_{ow}$, $\uparrow$MAX $\mathcal{Z}$	.27	.58	.41	.56	.36	.57
$\uparrow\Delta$, $\uparrow$MAX $\mathcal{Z}$	.58	.25	.53	.46	.55	.38

THE EFFECT OF OIL SLICK THICKNESS
ON DISPERSION PARAMETERS

HYPOTHESIS	P[T]	P[F]
↑h, ↑ % DISP	.02	.98
↑h, ↑ AVE $\bar{Z}$	.27	.73
↑h, ↑ MAX $\bar{Z}$	.36	.57

THE EFFECTS OF OIL SLICK CHARACTERISTICS
ON WAVE AMPLITUDE

HYPOTHESIS	Thin		Thick		Total		Total Cases	
	P[T]	P[F]	P[T]	P[F]	P[T]	P[F]	Thin	Thick
↑μ, ↑ A	1.0	0.0	.50	.50	.57	.43	2	12
↑T_{ow}, ↑ A	1.0	0.0	.83	.08	.86	.07	2	12
↑h, ↑ A					1.0	0.0	4 total	
↑Aging, ↑ A	1.0	0.0	1.0	0.0	1.0	0.0	2	4

APPENDIX 7   Droplet-Slick Recoalescence Experimental Procedures

Experimental Procedure

1) with the syringe filled with oil the apparatus was assembled as in Fig 1.

2) the syringe pump was started and one droplet was allowed to surface to remove any air from needle

3) the required amount of oil was placed on the water surface

4) the upper reservoir was filled with (25-X) ml of oil, where X is the amount used to form the slick

5) the apparatus vapor space was sealed

6) to form droplets syringe pump turned on at a flow rate of 0.0092 ml/min for the requisite time; the droplets were removed from the needle by moving needle rapildy downward; droplet rises to surface

7) after droplet coalesces with surface, 5 min. are allowed for surface to equilibrate

8) repeat "6" for second droplet, etc.

Cleaning Procedure

Tank

1) tank washed with Alconox and distilled water

2) rinsed 4 times

3) allowed to soak in distilled water for 15 min.

4) tank washed twice with Alonox and distilled water

5) rinsed 4 times

6) allowed to soak in distilled water for 15 min.

7) rinsed with distilled water 2 times

Needle

8) 10 ml of trichlororthylene passed through needle

9) 5 ml of acetone passed through needle

10) 10 ml of distilled water passed through needle

11) dry filtered air passed through needle for 5 min.

12) 5 ml of oil to be used passed through nee le

Syringe

13) washed 2 times with trichloroethylene

APPENDIX 7 (cont.)

14) washed 2 times with acetone

15) washed 2 times with distilled water

16) rinsed out 3 times with oil to be used.

APPENDIX 8

MIXTURE PROPERTY CALCULATIONS

The following details the development of Equations (A8-1) to (A8-3) which were solved to yield mixture properties.

By Equation (10-1):

$$\underline{V}_m = x_A \, \underline{V}_A + x_B \, \underline{V}_B$$

$$= \frac{x_A M_A + x_B M_B}{\rho_M}$$

where M_i = molecular weight of i (g/gmol) and ρ_M = density of the mixture (g/cm^3), if the volume change upon mixing is small. Then,

$$x_A \, \underline{V}_A + (1 - x_A)\underline{V}_B = x_A \frac{M_A}{\rho_M} + (1 - x_A) \frac{M_B}{\rho_M}$$

or

$$x_A = \left(\frac{M_B}{\rho_M} - \underline{V}_B\right) / \left[\left(\underline{V}_A - \underline{V}_B\right) - \left(\frac{M_A}{\rho_M} - \frac{M_B}{\rho_M}\right) \right] \tag{A8-1}$$

Now, also, if V_i = total volume of i present,

$$x_A = \frac{m_A}{m_A + m_B} = \frac{V_A/\underline{V}_A}{(V_A/\underline{V}_A) + (V_B/\underline{V}_B)}$$

$$= \frac{\phi_a/\underline{V}_A}{[(\phi_A/\underline{V}_A) + (1 - \phi_A)/\underline{V}_B]}$$

Rearranging,

$$\phi_A = \frac{x_A/\underline{V}_B}{\dfrac{1}{\underline{V}_A} - \dfrac{x_A}{\underline{V}_B}\left(\dfrac{\underline{V}_B}{\underline{V}_A} - 1\right)} \tag{A8-2}$$

Finally, by Equation (10-2):

$$\ell n \eta_M = x_A (\ell n \eta_A - \ell n \eta_B) + \ell n \eta_B \qquad (A8-3)$$

Typical results of these calculations for a mixture of Drakeol 21 (A)
and Penetek (B) are given in Table 8-1, below.

TABLE A8-1
Mixture Property Simulations

A	B	ρ	ϕ_A	η_M	ν_M	x_A
D21	P	.8001	0.0	3.91	4.89	0.0
		.81	.151	5.24	6.47	.096
		.82	.312	7.49	9.13	.214
		.83	.473	11.32	13.64	.350
		.84	.634	18.40	21.90	.509
		.85	.795	32.76	38.54	.699
		.86	.956	65.80	76.51	.928
		.862	1.000	81.80	94.89	1.000

APPENDIX 9

EXPERIMENTAL STUDY OF WAKE GROWTH
BEHIND BREAKING WAVES

While the preparation of this report was in progress, efforts were
made to measure the turbulence behind a stationary breaking wave in
the oil layer flume. Such an arrangement has two advantages over the
experiments described in Chapter 6. One is that the mean flow is
steady in time, so that one can measure the velocity as a function of
time at points fixed with respect to the wave, including points in
space above the trough level of the wave. This makes possible the
precise measurement of turbulence characteristics at various positions
around the breaker. When the flow is transient in nature, as was the
case in the experiments recorded in Chapter 6, such precision is only
possible after careful signal analysis, and only after repeating
experiments under identical conditions so as to obtain ensemble
averages of the various quantities of interest. The second advantage
is the fact that the phase speed of the wave is superimposed on the
orbital velocities, so that the velocity field is unidirectional.
This allows the use of hot film anemometry, which is simpler to use
than the laser anemometry which is required in the case of transient
waves. Furthermore, the hot film anemometer which was used in these
experiments has a far superior signal to noise ratio than the laser
system used in the earlier experiments.

Experimental Setup

In order to create a breaker in the test section of the flume, some
disturbance to the flow is necessary. In initial testing, solid objects
were placed under the free surface, spanning the test section at its
upstream end. It was found, however, that when the disturbance was
severe enough to create a breaker, flow separation would cause a turbulent
wake to be created behind the object, in addition to the wake behind the
breaker itself. These two wakes overlapped so that it was not possible

-310-

to measure the turbulence due solely to the breaker's wake. Longuet-Higgins (1974) avoided this problem by using a three-dimensional disturbance. The "bow wave" created by his ship model broke some distance abeam of the model so that the model wake and the breaker's wake did not overlap. This approach was not possible in the experiments reported here, since the flume is only eighteen inches (45.72 cm) wide.

After preliminary measurements indicated the importance of eliminating the viscous wake behind the disturbance, an attempt was made to impart a pressure disturbance to the free surface in such a way as to cause a breaking wave. The experimental setup included a blower whose outlet was led to a diffuser which was erected over the test section. In this way, the dynamic pressure in the outlet could be converted to a static pressure over an area 45.72 cm square. The diffuser was lowered until only a small gap existed between it and the water surface. It was hoped that the air flow through the gap would create only a minimal boundary layer on the water's surface. The results of this test were not completely conclusive. The 100 CFM blower which was available was of insufficient capacity to create a significant wave unless the gap was made very small. However, in this condition the inherent unsteadiness of the water's height would occasionally reduce the gap to zero, at which point the wave would increase in size dramatically. The replacement of the blower with a larger unit may have solved this problem, and would have been attempted had not another device been found to be superior.

The device which was found to be most successful in creating a two-dimensional breaking wave while introducing minimal vorticity into the flow was a "planing hydrofoil", as shown in Figure A9-1. This airfoil was placed in such a way that the free surface was almost tangent to the underside of the foil. At the point of contact, a miniature whitecap was formed, which entrained air and vorticity into the flow. The wake of this very turbulent region was eliminated by use of a suction slot which spanned the trailing edge of the foil. The suction was created by leading a three-inch hose from the hollow foil to the inlet of a pump which discharged into the test section

-311-

downstream of the measurements. The pump was rated at 60 gallons per minute against a 60' head, although in this application the head was a mere 6 feet or so. The position of the foil and operating condition of the flume were adjusted until a spilling breaker was created just downstream.

The flow configuration which existed when measurements were made is shown in Figure A9-1. The horizontal distance between the breaking crest and the crest downstream was 122 cm. The mean depth of the water after breaking was 36.2 cm, and the height of the wave after breaking was 5 cm. Small amplitude wave theory predicts a phase speed, C_p, of 136 cm/sec for this wave.

Measurement of Flow Velocities

Flow velocities were measured using the same hot film anemometer which was used in the experiments described in Chapter 4, but with a Model 1231W conical probe. RMS turbulent velocities were obtained by passing the linearized signal through a B&K Type 2416 voltmeter. The high pass filter built into this meter has a cutoff frequency of 2 Hz. It was assumed that lower frequencies made a negligible contribution to the total turbulent energy. Although the linearizer used was designed for velocities less than 3 ft/sec, the response appeared approximately linear well beyond this range.

Measurements of both the mean velocity and the RMS turbulent velocity were made on the test section centerplane roughly every 15 cms along the test section and at depth increments of 1.27 cm.

Estimation of Wake Growth Rate From Measurements

The presence of a surface wave complicates the measurement of the wake growth rate due to the fact that the vertical distance between any two streamlines varies along the length of the wave, the streamlines being farther apart under a wave crest than under a trough. This results in the wake's appearing to be relatively larger in the former location than in the latter. Although this does not affect the long-term growth rate, it can complicate the estimation of this growth rate from

-312-

data which is taken over a single wavelength or so. It is therefore
desirable to convert the wake depth in waves, b, to an equivalent wake
depth, b*, which would be measured in the absence of waves. Equating
the volume flux within the wake in the presence of waves to that flux
in the absence of waves, one gets:

$$Ub^* = Ub - \omega\eta \int_{\eta-b}^{\eta} e^{kz} dz \qquad (A9-1)$$

where η is the local wave height, ω is the wave frequency, k is the
wavenumber, z is the vertical dimension, and U is the free-stream
velocity, which is equal to the phase speed of the wave. This becomes

$$Ub^* = Ub - U\eta e^{k\eta} (1 - e^{-kb}) \qquad (A9-2)$$

$$b^* = b\left[1 - \eta e^{k\eta} \left(\frac{1 - e^{-kb}}{b}\right)\right] \qquad (A9-3)$$

In Chaper 3, the depth of dispersed oil is related to the growth
rate of the turbulent wake which lies behind the breaking wave. This
growth rate was given in Equation (3-27). The constant C in that
equation was presumed to be equal to that found in the case of circular
cylinders in an infinite fluid. One of the purposes of this experiment
was to verify the form of Equation (3-27), and to determine the value of
C for a spilling water wave. Identifying the corrected wake depth b*
as the b of Equation (3-27), we have

$$C^2 = \frac{\rho C_p^2}{\dot{M}} \frac{b^{*2}}{x} \qquad (A9-4)$$

where ρ is the water density, and $\dot{M}$ is the rate of momentum loss by the
breaker. Thus, the constant C is $\rho C_p^2/\dot{M}$ times the slope of the b^{*2}

versus x curve. The extent to which this curve follows a straight line is an indication of the correctness of Equation (3-27). In order to use Equation (A9-4), we must know C_p and $\dot{M}$. C_p can be gotten from velocity measurements or from the theoretical phase speed for a wave with the measured wavelength, amplitude, and water depth. $\dot{M}$ is more difficult to obtain. One method is to integrate the velocity defect of the wake in the flow behind the breaker. It can be shown that if the defect is small relative to the free-stream velocity, the momentum loss rate is given by:

$$\dot{M} = \rho C_p \int_{-\infty}^{\eta} u_d dz \qquad (A9-5)$$

where u_d is the velocity defect of the wake. The velocity defect can be measured directly at a position along the wave profile where the horizontal component of the orbital velocity is zero, say at a quarter of a wavelength behind the crest. If another position is chosen, the orbital velocities must be subtracted from the measured velocity defect to obtain the viscous wake defect.

Another technique for obtaining $\dot{M}$ is to measure the orbital velocity at some point upstream of the breaker, but still well downstream of the hydrofoil, and find the amplitude of the wave which would correspond to that velocity. The difference between the momentum flux of a wave of that amplitude and the momentum flux for the observed amplitude is just $\dot{M}$.

Results

Due to the time constraints under which this work was done, the results reported herein should be considered tentative. Although they demonstrate the feasibility of measuring breaking wave turbulence in a flume, a more exhaustive test program would be required in order to obtain dependable data.

The determination of momentum loss by the breaker was hindered by the fact that the anemometer used was not always calibrated correctly.

Of the methods discussed in the previous section, the only method which yielded a precise definition of momentum loss under these circumstances is that of integrating the velocity defect a quarter wavelength behind the breaking crest. The velocity profile there is shown in Figure A9-2. The area of the shaded region is found to be 15.7 cm^2/sec. From Equation (A9-5), we find that $\dot{M}$ is 2135 gm/sec^2. To put this momentum loss in perspective, the momentum flux in the wave after breaking is $\frac{1}{4} \rho gA^2$ = 1580 gm/sec^2. This wave has therefore lost about 60% of its momentum (and energy) in breaking.

The RMS turbulent velocities 30, 61, 91, 122, and 152 cm behind the breaking crest are plotted in Figure A9-3. An apparently anamolous result is that the turbulence intensity at the surface remains constant over the last half of the first wavelength downstream of the breaking crest. This is partially due to vortex stretching, which over this part of the wave tends to increase turbulence intensity. It is expected, however, that this contribution is a small one, and that some other factor is responsible.

For each section over which measurements were made, the maximum depth, b, of the wake was estimated to be that depth at which the RMS turbulence had decayed to 1% or so of its ambient value. These depths are plotted in Figure A9-1 and A9-4a. Figure A9-4a also shows values of corrected wake depths b*. It can be seen that b* grows much more regularly than does b. In order that the constant C in Equation (3-27) could be determined, b*^{2} was plotted against the distance behind the breaking crest, and a straight line fitted. The results are shown in Figure A9-4b. It can be seen that the data follows a straight line very well, confirming the functional form of Equation (3-27). The effective origin of x is found to be the location of the breaking crest. When the slope of the straight line and the previously computed value of $\dot{M}$ were substituted into Equation (A9-4), C was found to be 4.42, about four times that value obtained from experiments with circular cylinders in an infinite fluid. It should be pointed out that this value of C depends on the estimated value of $\dot{M}$, which in turn is based on three or four data points. A more careful analysis would involve a

-315-

number of wake surveys, and an estimate of the orbital velocity upstream of the breaking crest. However, a value of $\dot{M}$ fifteen times that measured in these experiments would be required to reduce C to the value obtained in the case of a circular cylinder in an infinite fluid.

One possible explanation for the very large apparent wake growth is the existence of secondary flows which can transport vorticity downward from the surface region. However, when these were measured in the flume without the wavemaker at velocities up to 2 ft/sec, they were found to be only about 1% of the free-stream velocity. If the secondary flows are of the same relative magnitude in the wake experiments, their effect on apparent wake growth would be negligible.

There are two possible explanations for the rapid growth rate of the wake behind the breaker as compared to that behind a circular cylinder. One is that the partition of energy between turbulence and the mean wake velocity field is quite different in the two cases. Increased turbulent energy in the case of the breaker could result in more rapid turbulent diffusion. The other explanation is that the presence of the free surface changes the structure of the wake. One obvious effect of the free surface is that turbulent eddies cannot extend beyond the free surface. The largest allowable eddies are only half as large as in the case of a wake in an infinite fluid.

The rapidity of the wake's growth is an important parameter in estimating the depth to which oil is dispersed. Equation (3-31) can be written as:

$$z_{o\ max} = \frac{C^2}{4} \frac{\dot{M}}{\rho C_p W} \tag{A9-6}$$

where W is the terminal velocity of the oil droplet. It can be seen that a factor of 4 in the value of C results in a factor of 16 in the maximum depth of dispersed oil.
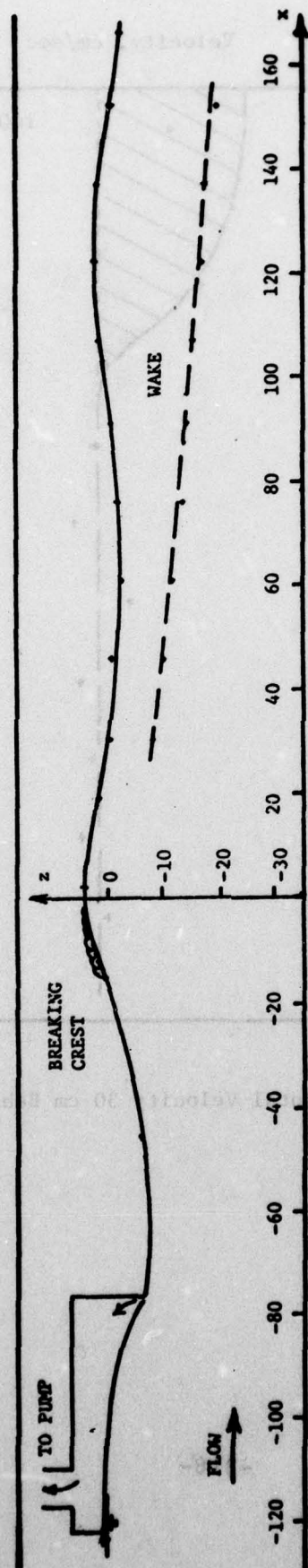
-316-

FIGURE A9-1. Breaking Wave in Flume

-317-
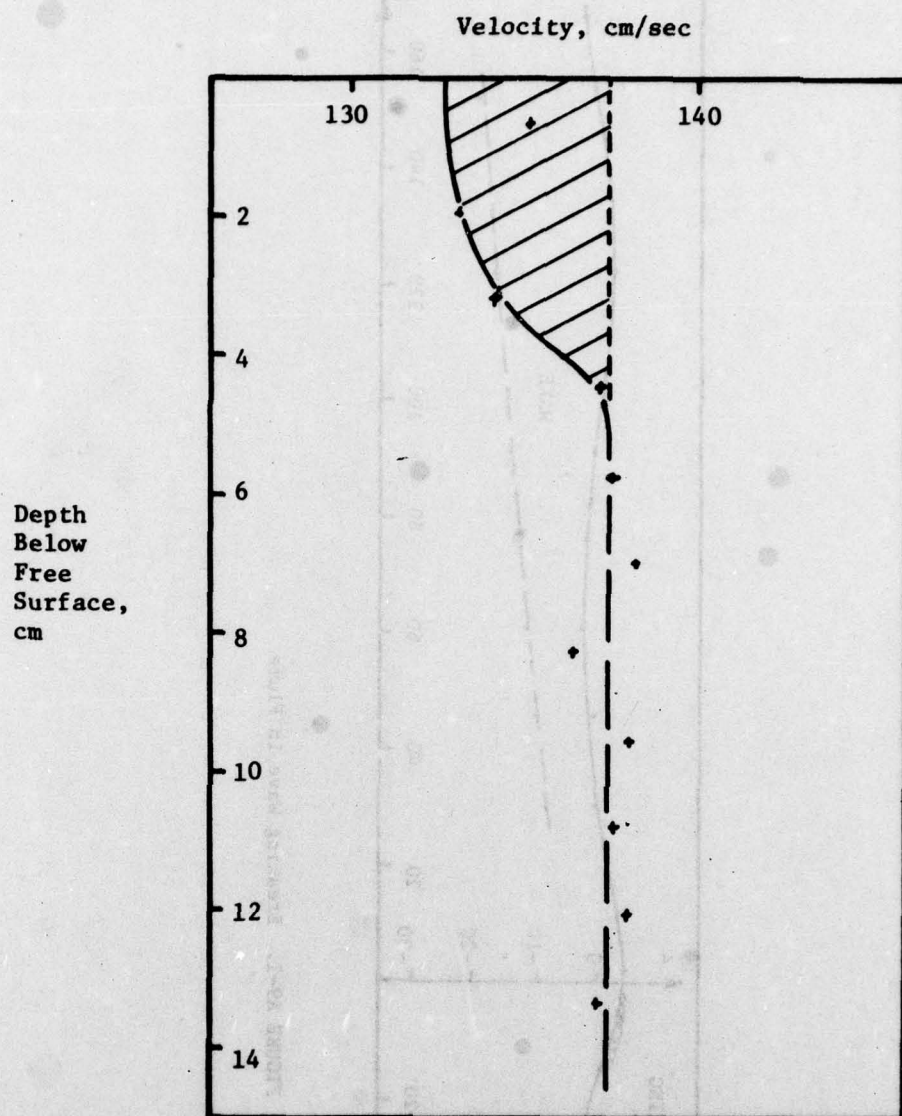
FIGURE A9-2. Mean Horizontal Velocity 30 cm Behind the Breaker

RMS Turbulent Velocity, cm/sec

Depth
Below
Free
Surface,
cm

DISTANCE BEHIND BREAKER

•	30	cm
+	61	cm
○	91	cm
✕	122	cm
□	152	cm

FIGURE A9-3. Turbulent Velocity Profiles Behind the Breaker

(a) Wake Depth versus Distance from Breaker

(b) Squared Corrected Wake Depth versus Distance from Breaker

FIGURE A9-4. Growth of Wake Behind Breaking Wave

REFERENCES

Banner, M.C. and O.M. Phillips, 1974, "On the Incipient Breaking of Small Scale Waves", J. Fluid Mechanics, 65, p. 647.

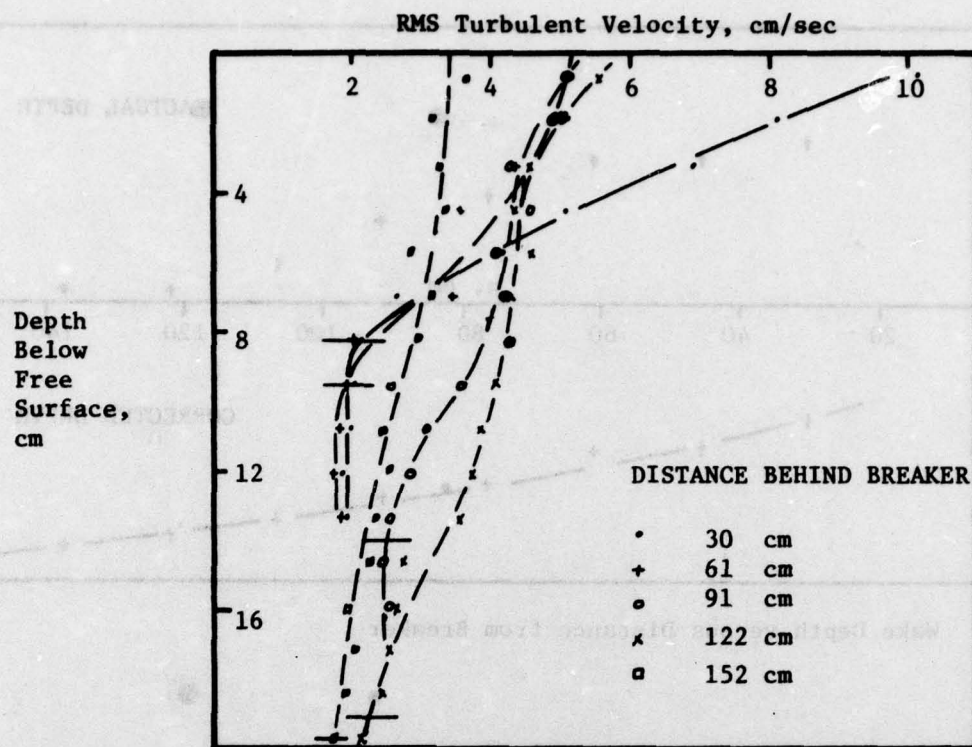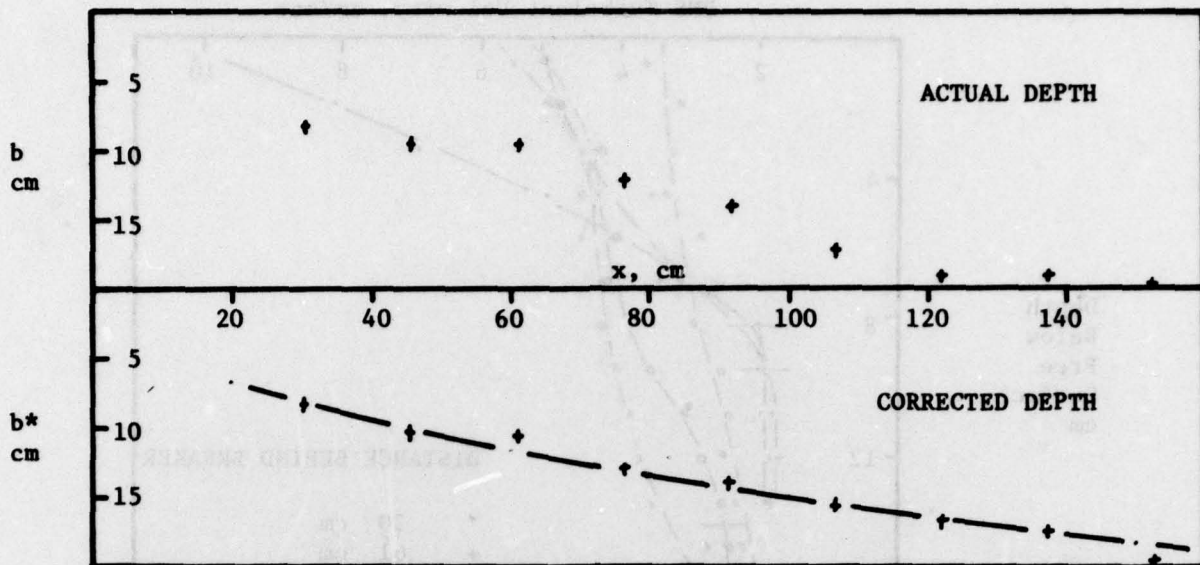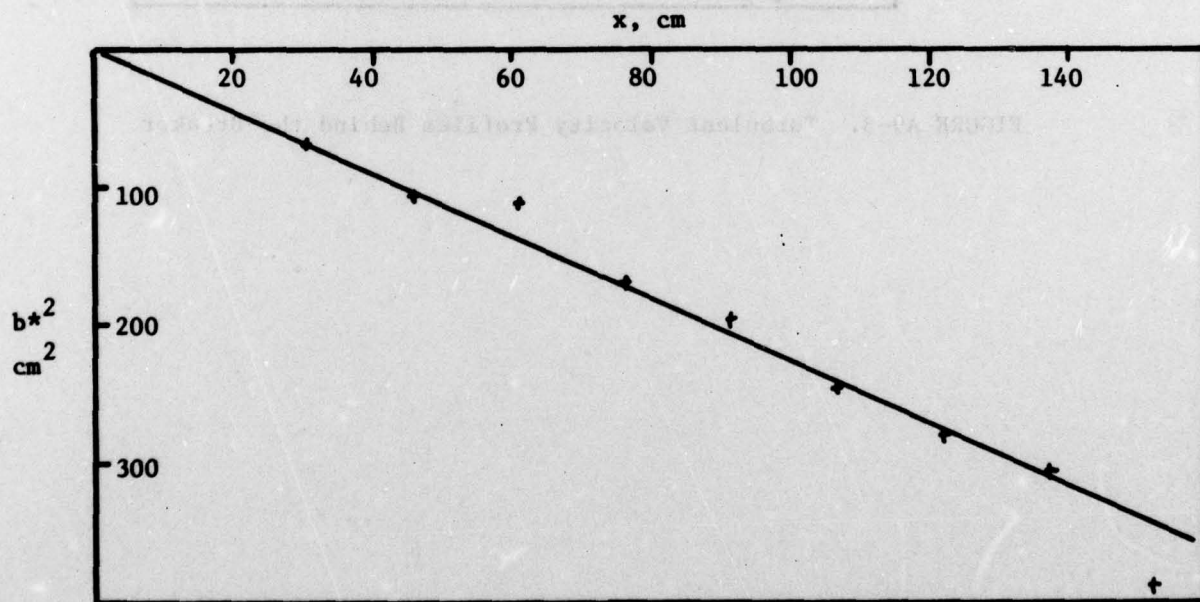Batchelor, G.K., 1951, Proc. Camb. Phil. Soc., Vol. 47, 359.

Batchelor, G.K., 1953, Theory of Homogeneous Turbulence, Cambridge University Press.

Belyaev, V.S., M.M. Lubimtzev, and R.V. Ozmipou, 1975, "The Rate of Dissipation of Turbulent Energy in the Upper Layer of the Ocean", J. Physical Oceanography, 5, p. 499.

Berridge, S.A., R.A. Dean, and R.G. Fallows, 1968a, "The Properties of Persistent Oils at Sea", Scientific Aspects of Pollution of the Sea by Oil, Hepple, P., ed., Elsevier Publishing Co., Ltd., London, p. 2.

Berridge, S.A., M.T. Thew, and A.G. Loriston-Clark, 1968b, "The Formation and Stability of Emulsions of Water in Crude Petroleum and Similar Stocks", Scientific Aspects of Pollution of the Sea by Oil, Hepple, P., ed., Elsevier Publishing Co., Ltd., London, p. 35.

Blacklaw, J.R., J.A. Strand, and P.C. Walkup, 1971, "Assessment of Oil Spill Treating Agent Test Methods", Proceedings of Joint Conference on Prevention and Control of Oil Spills, API/EPA/USCG, Washington, D.C., p. 253.

Blokker, P.C., 1964, "Spreading and Evaporation of Petroleum Products on Water", 4th International Harbor Conference, Antwerp, p. 911.

Bond, W.N., 1927, "Bubbles and Drops and Stokes' Law", Phil. Magazine (7), 4, p. 889.

Bond, W.N. and D.A. Newton, 1928, "Bubbles, Drops and Stokes' Law (Paper 2)", Phil. Magazine (7), 5, p. 794.

Canevari, G.P., 1969a, "The Role of Dispersants in Oil Cleanup", Oil on the Sea, D.P. Hoult, ed., Plenum Press, New York.

Canevari, G.P., 1969b, "General Dispersant Theory", Proceedings on Joint Conference on Prevention and Control of Oil Spills, API, New York, p. 171.

-321-

Canevari, G.P., 1971, "Oil Spill Dispersants - Current Status and
          Future Outlook", Proceedings of Joint Conference on Prevention
          and Control of Oil Spills, API/EPA/USCG, Washington, D.C.,
          p. 263.

Canevari, G.P., 1973, "Development of the 'Next Generation' Chemical
          Dispersants", Proceedings of Joint Conference on Prevention
          and Control of Oil Spills, API/EPA/USCG, Washington, D.C.,
          p. 231.

Charles, G.E. and S.G. Mason, 1960, J. Colloid Sci., 15, pp. 236-267.

Cleary, G.W., 1977, "Proposed Procedure for ASTM D19.06 Round Robin
          Test for Petroleum Hydrocarbons in Water", Atlantic Richfield
          Company Research and Development.

Davis, S.S. and A. Smith, 1976, Colloid and Polymer Science, 254,
          pp. 82-98.

Dean, R.G., 1965, "Stream Function Representation of Nonlinear Ocean
          Waves", J. Geophysical Research, 70, pp. 4561-4572.

Donelan, M., M.S. Longuet-Higgins, and J.S. Turner, 1972, Nature,
          239, p. 449.

Fay, J.A., 1971, "Physical Processes in the Spread of Oil on a Water
          Surface", Proceedings of Joint Conference on Prevention and
          Control of Oil Spills, API/EPA/USCG, Washington, D.C., p. 463.

Forrester, W.P., 1971, "Distribution of Suspended Oil Particles
          Following the Grounding of the Tanker ARROW", J. Marine
          Research, 29, p. 151.

Frankenfeld, J.W., 1973, "Factors Governing the Fate of Oil at Sea;
          Variations in the Amounts and Types of Dissolved or
          Dispersed Materials During the Weathering Process",
          Proceedings of the Joint Conference on Prevention and Control
          of Oil Spills, API/EPA/USCG, Washington, D.C., p. 485.

Friedlander, S.K., 1957, "Behavior of Suspended Particles in a
          Turbulent Fluid", A.I.Ch.E. Journal, 3, p. 381.

Garrett, W.D., 1969, "Confinement and Control of Oil Pollution on
          Water with Monomolecular Surface Films", Proceedings on Joint
          Conference on Prevention and Control of Oil Spills, API,
          New York, p. 257.

Garrett, W.D., and W.R. Barger, 1970, "Factors Affecting the Use of
          Monomolecular Surface Films to Control Oil Pollution on
          Water", Env. Sci. Tech., 4, p. 123-127.

Grant, H.L., R.W. Stewart, and A. Moilliet, 1962, "Turbulence Spectra From a Tidal Channel", J. Fluid Mechanics, 12, p. 241.

Hasselmann, K., 1962, "On the Nonlinear Energy Transfer in a Gravity-Wave Spectrum, Part I", J. Fluid Mechanics, 12, p. 481.

Hasselmann, K., 1963, "On the Nonlinear Energy Transfer in a Gravity-Wave Spectrum, Part II", J. Fluid Mechanics, 15, p. 273, Part III, ibid., p. 385.

Hasselmann, K., 1971, "On the Mass and Momentum Transfer Between Short Gravity Waves and Larger Scale Motions", J. Fluid Mechanics, 50, p. 189.

Hasselmann, K., T.P. Barnett, E. Boaws, H. Carlson, D.E. Cartwright, K. Enke, J.A. Ewing, H. Gienapp, D.E. Hasselmann, P. Kruseman, A. Meerburg, P. Muller, D.J. Olbers, K. Richter, W. Sell, and H. Walden, 1973, Measurements of Wind-Wave Growth and Swell Decay During the Joint North Sea Wave Project (JONSWAP), Deutsches Hydrographisches Institut, Hamburg.

Hasselmann, K., 1974, "On the Spectral Dissipation of Ocean Waves Due to Whitecapping", Boundary Layer Meteorology, 6, p. 107.

Hinze, J.O., 1955, "Fundamentals of the Hydrodynamic Mechanism of Splitting in Dispersion Processes", A.I.Ch.E. Journal, 1, p. 289.

Hoult, D.P., and W. Suchon, 1970, "The Spread of Oil in a Channel", Stop Oil Pollution, Report 2, MIT Department of Mechanical Engineering, Cambridge, Massachusetts.

Hoult, D.P., 1972, "Oil Spreading on the Sea", Ann. Rev. of Fluid Mech., 4, p. 341.

Houmb, O.G., and T. Overvik, 1976, "Parameterization of Wave Spectra and Long Term Joint Distribution of Wave Height and Period", BOSS '76, Trondheim.

Hu, S. and R.C. Kintner, 1955, "The Fall of Single Liquid Drops Through Water", A.I.Ch.E. Journal, 1, p. 42.

Ichiye, T., 1967, "Upper Ocean Boundary Layer Flow Determined by Dye Diffusion", Phys. Fluids Suppl., S270.

Jeffrey, P.G., 1971, "Large Scale Experiments on the Spreading of Oil at Sea and Its Disappearance by Natural Factors", Proceedings of the Joint Conference on Prevention and Control of Oil Spills, API/EPA/USCG, Washington, D.C., p. 469.

-323-

Kolmogorov, A.N., 1949, "On the Disintegration of Drops in Turbulent Flow", <u>Doklady Akad. Nauk S.S.S.R.</u>, <u>66</u>, p. 825.

Landau, L.D. and E.M. Lifshitz, 1959, <u>Fluid Mechanics</u>, Pergamon Press, London.

Leibovich, S., 1975, "A Natural Limit to the Containment and Removal of Oil Spills at Sea", <u>Ocean Engineering</u>, <u>3</u>, p. 29.

Levich, V.G., 1954, "Theory of Colloid Coagulation in a Turbulent Fluid Stream", <u>Doklady Akad. Nauk. S.S.S.R.</u>, <u>99</u>, p. 809.

Longuet-Higgins, M.S., 1969a, "On Wave Breaking and the Equilibrium Spectrum of Wind-Generated Waves", <u>Proc. Roy. Soc.</u>, <u>A</u>, <u>310</u>, p. 151.

Longuet-Higgins, M.S., 1969b, "A Nonlinear Mechanism for the Generation of Sea Waves", <u>Proc. Roy. Soc. A.</u>, <u>311</u>, p. 371.

Longuet-Higgins, M.S., 1973, "A Model of Flow Separation of a Free Surface", <u>J. Fluid Mechanics</u>, <u>57</u>, p. 129.

Longuet-Higgins, M.S., 1974, "Breaking Waves - In Deep or Shallow Water", 10th ONR Symposium, Cambridge, Massachusetts.

Longuet-Higgins, M.S., 1975, "On the Joint Distribution of the Periods and Amplitudes of Sea Waves", <u>J. Geophysical Research</u>, <u>80</u>, p. 2688.

Longuet-Higgins, M.S. and J.S. Turner, 1974, "An 'Entraining Plume' Model of a Spilling Breaker", <u>J. Fluid Mechanics</u>, <u>63</u>, p. 1.

MacIntyre, W.G., C.L. Smith, J.C. Munday, V.M. Gibson, J.L. Cake, J.G. Windsor, J.L. Dapuy, W. Harrison, and J.D. Oberholtzer, 1974, "Investigation of Surface Films - Chesapeake Bay Entrance", Report EPA-670/2-73-009, Office of R & D, U.S.E.P.A., Washington, D.C.

Milgram, H.J. and R.G. Donnelly, 1975, "Technical Proposal for United States Coast Guard Solicitation No. CG-61802-A, Public solicitation for "Study to Investigate the Effects of Oil Slick Properties on the Dispersion of an Oil Slick into the Sea Under the Action of Wind, Waves and Currents", M.I.T., Cambridge, Massachusetts.

Monaham, Edward C., 1971, "Oceanic Whitecaps", <u>J. Physical Oceanography</u>, <u>1</u>, p. 139.

Munk, W.H., 1947, "A Critical Wind Speed for Air-Sea Boundary Processes", <u>J. Marine Research</u>, <u>6</u>, p. 203.

Nath, J.H. and F.L. Ramsey, 1976, "Probability Distributions of Breaking Wave Heights Emphasizing the Utilization of the JONSWAP Spectrum", J. Physical Oceanography, 6, p. 316.

Nelson, W.L., 1958, Petroleum Refinery Engineering, Mc-Graw-Hill, New York.

Newman, J.N., 1977, Marine Hydrodynamics, MIT Press, Cambridge, Massachusetts.

Overbeek, J.Th.G., S.T. Mayr, and R.G. Donnelly, 1971, Surface Chemistry, MIT Press, Cambridge, Massachusetts.

Parker, C.A., M. Freegarde, and C.G. Hatchard, 1971, "The Effect of Some Chemical and Biological Factors on the Degradation of Crude Oil at Sea", Water Pollution by Oil, P. Hepple, ed., The Institute of Petroleum, London, p. 237.

Phillips, O.M., 1961, "A Note on the Turbulence Generated by Gravity Waves", J. Geophysical Research, 66, p. 2889.

Phillips, O.M., 1969, The Dynamics of the Upper Ocean, Cambridge University Press, London.

Phillips, O.M., 1963, "On the Attenuation of Long Gravity Waves by Short Breaking Waves", J. Fluid Mechanics, 16, p. 321.

Pierson, W.J., Jr., and L. Moskowitz, 1964, "A Proposed Spectral Form for Fully Developed Wind Seas Based on the Similarity Theory of S.A. Kitaigorodskii", J. Geophysical Research, 69, p. 5181.

Raj, P.K., 1977, Theoretical Study to Determine the Sea State Limit for the Survival of Oil Slicks on the Ocean, Arthur D. Little Report No. 79299.

Reid, R.C., J.M. Prausnitz, and T.K. Sherwood, 1977, Properties of Gases and Liquids, 3rd edition, McGraw-Hill, New York, p. 73-90.

Rouse, H., 1939, "Experiments on the Mechanics of Sediment Suspension", Proceedings of the Fifth International Congress of Applied Mechanics, New York: John Wiley & Sons.

Saffman, P.G. and J.S. Turner, 1956, "On the Collision of Drops in Turbulent Clouds", J. Fluid Mechanics, 1, p. 16.

Schlichting, H., 1968, Boundary Layer Theory, McGraw-Hill, New York.

Shaw, D.J., 1970, Introduction to Colloid and Surface Chemistry, 2nd edition, Butterworths, London.

Sherman, P., ed., 1968, *Emulsion Science*, Academic Press, London.

Sivadier, H.O. and P.G. Mikolaj, 1973, "Measurement of Evaporation Rates from Oil Slicks on the Open Sea", *Proceedings of Joint Conference on Prevention and Control of Oil Spills*, API/EPA/USCG, Washington, D.C., p. 475.

Sleicher, C.A., 1962, "Maximum Stable Drop Size in Turbulent Flow", *A.I.Ch.E. Journal*, 8, p. 471.

Smith, J.W., 1968, "Problems in Dealing with Oil Pollution on Sea and Land", *Scientific Aspects of Pollution of the Sea by Oil*, P. Hepple, ed., Elsevier Publishing Co., Ltd., London, p. 62.

Stewart, R.W. and H.L. Grant, 1962, "Determination of the Rate of Dissipation of Turbulent Energy Near the Sea Surface in the Presence of Waves", *J. Geophysical Research*, 67, p. 3177.

Sverdrup, H.V., M.W. Johnson, and R.H. Stein, 1942, *The Oceans*, Prentice-Hall, New York.

Townsend, A.A., 1976, *The Structure of Turbulent Shear Flow*, 2nd edition, Cambridge University Press.

Van Dorn, W.G. and S.P. Pazan, 1975, *Laboratory Investigation of Wave Breaking. Part II. Deep Water Waves*, Scripps Institution of Oceanography Report SIO 75-21, La Jolla, California.

Weast, R.C., ed., 1972, *Handbook of Chemistry and Physics*, 52nd edition, page D-178.

Wilkes Scientific Corporation, 1972, "MIRAN Application Report #1, Infrared Determination of Hydrocarbons in Water (After ASTM 733-58)".

Zobell, C.E., 1969, "Microbial Modification of Crude Oil in the Sea", *Proceedings of the Joint Conference on Prevention and Control of Oil Spills*, API, New York, p. 317.

Zuiderna and Waters, 1941, *Ind. Eng. Chem.*, 13, p. 312.